Elsevier Editorial System(tm) for Geomorphology

Manuscript Draft

Manuscript Number: GEOMOR-8685R1

Title: MIS 9 to MIS 5 terraces along the Tyrrhenian Sea coast of Latium (central Italy): assessing interplay between sea-level oscillations and tectonic movements

Article Type: Review Article

Keywords: paleo-surface; coastal terrace; glacio-eustasy; regional uplift

Corresponding Author: Dr. fabrizio marra,

Corresponding Author's Institution: Istituto Nazionale di Geofisica e Vulcanologia

First Author: fabrizio marra

Order of Authors: fabrizio marra; Mario Gaeta; Brian R Jicha; Cristiano Nicosia; Cristiano Tolomei; Piero Ceruleo; Fabio Florindo; Maurizio Gatta; Michelangelo La Rosa; Mario F Rolfo

Abstract: We present a review of the geomorphology of the Tyrrhenian Sea coast of central Italy integrated by a novel structural-geomorphological study coupled with statistical analysis of topographic culminations and comparison with a Digital Elevation Model, aimed at reconstructing a suite of paleo-surfaces corresponding to remnant portions of marine terraces. We performed geochronological, sedimentological, micromorphological and mineralogical investigations on the deposits forming the different paleo-surfaces between Civitavecchia and Anzio town, in order to provide chronostratigraphical, paleogeographical and paleoenvironmental constraints. Using the newly achieved dataset we correlate these paleo-surfaces with the coastal terraces formed during past sea-level highstands, as recognized by previous studies, and we refine their correlation with the Marine Isotope Stage (MIS) timescale. In particular, we have extended our geomorphological analyses landward in the area between the Tiber River mouth and Anzio, in order to include the oldest paleo-surface developed above the deposits of the last large explosive eruption at 365±4 ka in the Colli Albani Volcanic District. Results of this study allow us to recognize a set of higher paleo-surfaces at elevation ranging 108 thought 71 m a.s.l., which we interpret as one tectonically displaced, widespread coastal terrace originated during the MIS 9.1 highstand. We correlate the previously identified paleo-surfaces of 66-62 m and 56-52 m with the equivalent coastal terraces developed during the sea-level highstands of sub-stages 7.5 and 7.3/7.1. Moreover, based on data from literature on relative elevation of maximum sea level during the highstands of MIS 11 through MIS 5.1, we assess the regional uplift and the concurrent tectonic displacements that have occurred since 900 ka in this area.

REVIEWER #1

General points (all language related)

The use and/or omission of articles (definite and indefinite) differs significantly between Italian and English (I know this from a somewhat shaky experience of Italian from evening classes) and I think there are instances in this paper where such English usage is erroneous and requires attention or review. See my annotations but also look carefully at these throughout.

Word choice is often poor, ranging from words that are a bit strange but are understandable (marking the author(s) as writing English as non-first-language user(s)) to words that are simply erroneous. This includes a frequent poor choice of prepositions.

By way of examples, (1) 'superintended' is not a word to use; from the verb 'superintend', it means 'be responsible for the management or arrangement of' (it is commonly used only in the derivative 'superintendent', which is a rank in the police force) and can only be used with reference to people; (2) '…are constituted by …' is archaic and clumsy English and is a form of words that would be used very sparingly (if at all) by a first-language English writer. It should generally be replaced by 'consist of' or 'comprise'.

The word 'comprised' repeatedly appears in situations wehere it is superfluous – I have suggested deletion.

Your term 'silicoclastic' should be 'silciclastic', as Google will confirm. Unfortunately, there are several figures that will need correcting, in addition to the text.

We greatly apreciated the careful revision of the English and the precious suggestions provided by the Reviewer, that we have followed throughout.

There are several specialist soil terms used in this paper that may not be readily understood by the typical *Geomorphology* reader (e.g., vertic), although I suppose, like me, they can turn to Google.

The meaning of this word is explained (vertical turnover of soil material). For other specialist terms, see below.

The tenses of verbs are also non-optimal in many cases. I have suggested edited versions.

We thank the reviewer for these edits.

Points of detail:

Line 71 (also in one of the highlights). This is careless wording. The highstands are features of the sea-level record, not the marine-isotope record, as the authors know well enough. The attribution of highstands to particular isotope stages is by means of correlation, helped by the fact that the isotope record is also an archive (indirectly) of palaeoclimate. This passage and the highlight both need rewording.

Sure. We catch the point and agree with it. We have rephrased the sentence.

Line 85. I would query the use of 'the glacial termination IV'. Elsewhere MIS stages have been used, so it is not clear why this is different. Otherwise the system of numbered glacial terminations needs definition – perhaps a table correlating them with the MIS chronology. In terms of English language, I think the definite article (the) should be deleted here.

Ok for the article. We have kept the definition of glacial termination and specified the first time that we mention it that it represents "the onset of sea-level rise during the highstand". This concept is at the base of the methodological approach using the gravel-clay transition in the aggradational succession as a proxy of the sudden ice meltinng at the end of a glacial period.

Table 1 – some terms used in this table are not recognized and need checking. Please check 'limpid', 'typic', 'disorthic'.

Indeed, vertic, limpid, dishortic and typic are specific terms used in micromorphology. It is a scientific jargon: probably unpleasant, yet correct.

I presume that 'int.' is an abbreviation of 'interference', but this is by no means obvious and should be in full.

ok.

Fig. 13 is an important diagram but is over-reduced, making it difficult to see the subtly different colours (like a high proportion of the male population I have slightly defective colour vision. I would like to see this enlarged and published in landscape format.
We have rotated this figure at 90 degree, in order to have it fitting a full page.
Line 857. This is a rather cryptic statement that needs explanation if it is to mean anything. Do you really mean 'experiments'? This is not very scientific and you leave the reader to guess what the additional insight is. Please tighten this up.
We have rephrased this statement and eliminated the word "experiments". That's indeed a US jargon term for "analyses".

REVIEWER #2

My suggested edits are captured in detail by the numbered comments below.

1) Line 1209: "Facenna et al, 1994c" change with "Facenna et al, 1994"
ok.
2) Figure 1: I suggest adding a dot or a square for the location of Rome and the dash lines (faults) in the alluvial deposits.
ok.
3) Figure 2: the same observation regarding Rome of figure 1; insert also the "north" symbol.
ok.
4) Figure 3: on the contrary of figure 1 the faults are represented with dash line; are they inferred? I suggest to insert the dip for dip slip fault; insert the "north" symbol; draw a line to separate 3a with 3b.
ok.
5) Figs 5-6-7-9a: for a better comprehension I suggest to give a new layout to these figures because there are a lot of information (photo, scheme), but the comprehension is difficult.
We agree that these figures are a bit complicated, but we believe that they contain all the necessary information.
6) Figure 11: insert the graphic scale and "north" symbol.
ok.
9) Figure 16: I suggest to invert the "b^1" with "b" and "b" with "b^1".
ok.

***Highlights (for review)**

We reconstruct a suite of six paleo-surfaces along the central Tyrrhenian Sea coast
Paleoenvironmental data identify these paleo-surfaces as remnants of coastal terraces
We provide $^{40}Ar/^{39}Ar$ age constraints to the terraced sedimentary deposits
We correlate these terraces with the Marine Isotope Stage record
We identify previously unrecognized MIS 9 sea-level markers in this region
We assess regional uplift and tectonic displacements in the last 400 ka

We present a review of the geomorphology of the Tyrrhenian Sea coast of central Italy integrated by a novel structural-geomorphological study coupled with statistical analysis of topographic culminations and comparison with a Digital Elevation Model, aimed at reconstructing a suite of paleo-surfaces corresponding to remnant portions of marine terraces. We performed geochronological, sedimentological, micromorphological and mineralogical investigations on the deposits forming the different paleo-surfaces between Civitavecchia and Anzio town, in order to provide chronostratigraphical, paleogeographical and paleoenvironmental constraints. Using the newly achieved dataset we correlate these paleo-surfaces with the coastal terraces formed during past sea-level highstands, as recognized by previous studies, and we refine their correlation with the Marine Isotope Stage (MIS) timescale.

In particular, we have extended our geomorphological analyses landward in the area between the Tiber River mouth and Anzio, in order to include the oldest paleo-surface developed above the deposits of the last large explosive eruption at 365±4 ka in the Colli Albani Volcanic District. Results of this study allow us to recognize a set of higher paleo-surfaces at elevation ranging 108 thought 71 m a.s.l., which we interpret as one tectonically displaced, widespread coastal terrace originated during the MIS 9.1 highstand. We correlate the previously identified paleo-surfaces of 66-62 m and 56-52 m with the equivalent coastal terraces developed during the sea-level highstands of sub-stages 7.5 and 7.3/7.1. Moreover, based on data from literature on relative elevation of maximum sea level during the highstands of MIS 11 through MIS 5.1, we assess the regional uplift and the concurrent tectonic displacements that have occurred since 900 ka in this area.

MIS 9 to MIS 5 terraces along the Tyrrhenian Sea coast of Latium (central Italy): assessing interplay between sea-level oscillations and tectonic movements

Fabrizio Marra[1*], Mario Gaeta[2], Brian R. Jicha[3], Cristiano Nicosia[4], Cristiano Tolomei[1], Piero Ceruleo[5], Fabio Florindo[1], Maurizio Gatta[6,7], Michelangelo La Rosa[8], Mario F. Rolfo[7]

[1] Istituto Nazionale di Geofisica e Vulcanologia, Rome, Italy
[2] Dipartimento di Scienze della Terra, "Sapienza" Università di Roma, Italy
[3] Department of Geoscience, University of Wisconsin-Madison, USA
[4]Dipartimento dei Beni Culturali, Università di Padova, Italy
[5] Via Giotto 18, 00019 Tivoli (Roma), Italy
[6] University of York, Department of Archaeology, York YO1 7EP, UK
[7] Department of History, Culture and Society, University of Rome 'Tor Vergata', Italy
[8] Ecomuseo dell'Agro Pontino, via G.B. Vico 1, Latina, Italy

*correspondoing author: fabrizio.marra@ingv.it

Abstract

We present a review of the geomorphology of the Tyrrhenian Sea coast of central Italy integrated by a novel structural-geomorphological study coupled with statistical analysis of topographic culminations and comparison with a Digital Elevation Model, aimed at reconstructing a suite of paleo-surfaces corresponding to remnant portions of marine terraces. We performed geochronological, sedimentological, micromorphological and mineralogical investigations on the deposits forming the different paleo-surfaces between Civitavecchia and Anzio town, in order to provide chronostratigraphical, paleogeographical and paleoenvironmental constraints. Using the newly achieved dataset we correlate these paleo-surfaces with the coastal terraces formed during past sea-level highstands, as recognized by previous studies, and we refine their correlation with the Marine Isotope Stage (MIS) timescale.

In particular, we have extended our geomorphological analyses landward in the area between the Tiber River mouth and Anzio, in order to include the oldest paleo-surface developed above the deposits of the last large explosive eruption at 365±4 ka in the Colli Albani Volcanic District. Results of this study allow us to recognize a set of higher paleo-surfaces at elevation ranging 108 thought 71 m a.s.l., which we interpret as one tectonically displaced, widespread coastal terrace originated during the MIS 9.1 highstand. We correlate the previously identified paleo-surfaces of 66-62 m and 56-52 m with the equivalent coastal terraces developed during the sea-level highstands of sub-stages 7.5 and 7.3/7.1. Moreover, based on data from literature on relative elevation of maximum sea level during the highstands of MIS 11 through

MIS 5.1, we assess the regional uplift and the concurrent tectonic displacements that have occurred since 900 ka in this area.

Keywords: paleo-surface; coastal terrace; glacio-eustasy; regional uplift

Highlights:

We reconstruct a suite of six paleo-surfaces along the central Tyrrhenian Sea coast
Paleoenvironmental data identify these paleo-surfaces as remnants of coastal terraces
We provide $^{40}Ar/^{39}Ar$ age constraints to the terraced sedimentary deposits
We correlate these terraces with the Marine Isotope Stage record
We identify previously unrecognized MIS 9 sea-level markers in this region
We assess regional uplift and tectonic displacements in the last 400 ka

1. Introduction

The Tyrrhenian Sea coast of Latium (Figure 1) is part of a geodynamic domain characterized by back-arc extensional processes (Malinverno and Tayan, 1986; Patacca et al., 1990) that during Pleistocene times have led to the formation of an ultra-potassic chain of volcanic districts (Serri et al., 1993; Conticelli and Peccerillo, 1992; Peccerillo and Frezzotti, 2015). Concurrent with the volcanic processes, regional uplift has caused the progressive emergence of this area since the end of the Santernian (lower Calabrian), around 1.5 Ma, leading to widespread continentalization since ~1 Ma (Barberi et al., 1994; Marra et al., 2018a). The regional uplift along the Tyrrhenian coast of Latium has been interpreted as driven by the subduction process and uprising of metasomatized magma bodies on the Tyrrhenian Sea Margin of central Italy, superimposed on a smaller isostatic component of uplift (Marra et al., 2017, and references therein). Two major pulses of uplift are recognized: 0.86 through 0.5 Ma, and 0.25 Ma through the Present (Marra et al., 2016a); as a result of this overall uplifting regime, the continental, fluvial-lacustrine and coastal deposits in this area formed a widespread pattern of terraces that, similar to other regions in the world (e.g., Bridgland and Westaway, 2008), are organized in a staircase geometry, with the oldest surfaces at highest elevation.

Geographic extension and rates of the most recent phases of this uplift during Middle-Late Pleistocene have been assessed by a series of studies reconstructing a suite of coastal terraces and correlating them with the sea-level highstands identified by the Marine Isotope Stage (MIS) record (e.g., Karner et al., 2001a; Nisi et al., 2003; Ferranti et al., 2006). More recently, a re-evaluation of the geometry and the age of these terraces in the coastal area between the Argentario and Anzio promontories has been proposed by means of an original geomorphological approach and the integration of new geochronologic constraints provided by $^{40}Ar/^{39}Ar$ ages of volcanic layers intercalated within the glacio-eustatically forced aggradational successions forming the terraced deposits in this region (Marra et al., 2015; 2016a). Moreover, a new geomorphologic study coupled with biochronologic constraints allowed Marra et al. (2018b, 2019a) to extend the reconstruction of a complete suite of terraces in the coastal reach between Anzio and Circeo promontories, and to propose their correlation with MIS 7.5 through MIS 5.1. In contrast, only a poorly defined paleo-surface ranging 61-67 m a.s.l. has been dubiously assigned to the MIS 9 terrace (Marra et al., 2016a). Moreover, geochronologic constraints so far provided to the local MIS 9 aggradational succession (Aurelia Formation, Karner and Marra, 1998) evidenced a remarkable anomaly, significantly pre-dating glacial termination IV and the completion of MIS 9 highstand (Marra

et al., 2016b). Therefore, assessing the geometry and providing time constraint on the deposits of the MIS 9 coastal terrace in this region may have notable implications for understanding the response to the global paleo-climatic signal and on the tectonic process acting on the Tyrrhenian Sea margin of central Italy.

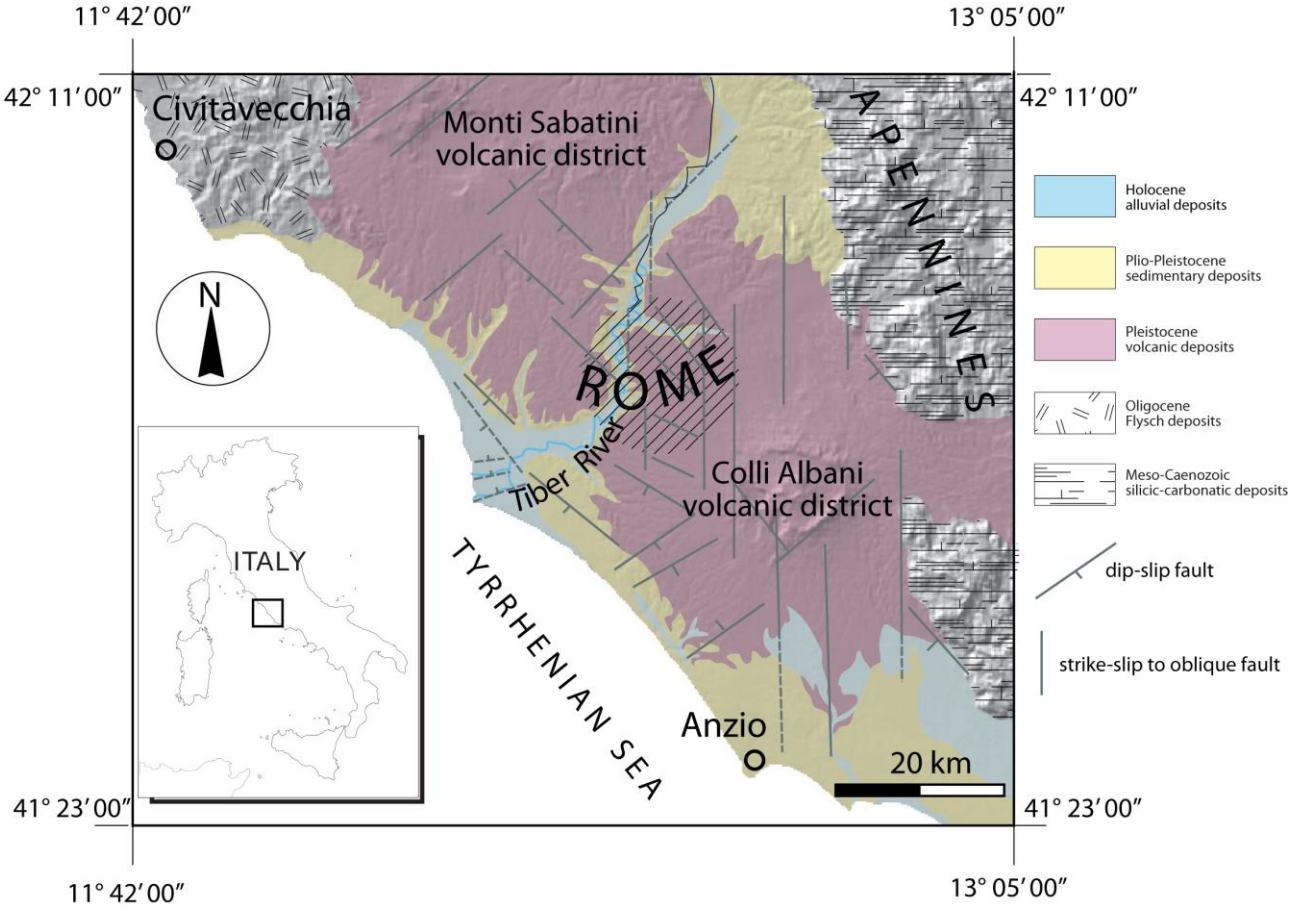

Figure 1 - DEM image of the Tyrrhenian Sea margin of central Italy showing the main structural features of the investigated area (after Acocella and Funiciello, 2006; Frepoli et al., 2010).

In the present paper we have refined the structural-geomorphological study in the previously investigated sector comprised between Civitavecchia and Anzio, and we have re-assessed the statistical analysis of the elevations of the paleo-surfaces correlated by Marra et al. (2016a, 2019a) with the MISs. In particular, we have extended the geomorphological analysis landward, in order to include the oldest paleo-surface affecting the deposits of the last large eruption in the Colli Albani Volcanic District (Villa Senni Eruption Cycle, 365±4 ka, Marra et al., 2009) in the area between the Tiber mouth and Anzio. Two huge pyroclastic-flow deposits emplaced during this eruption phase (Tufo Lionato and Pozzolanelle, Freda et al., 1995) mantle the surface with a volcanic cover spreading radially as far as 50 km from the vent and reaching up to 20 m in thickness, locally (De Rita et al., 1995; Giordano et al., 2006; Mariucci

et al., 2008). Due to this pyroclastic cover, the paleo-surfaces older than 365 ka are completely buried and no geomorphologic evidence is expected for them in this area.

We performed chronostratigraphical, sedimentological, micromorphological, mineralogical and petrographic investigations of the deposits forming the different paleo-surfaces in order to provide geochronological, paleogeographical and paleoenvironmental constraints. We used four $^{40}Ar/^{39}Ar$ age determinations on detrital sanidine crystals extracted from key deposits in order to provide post-quem ages on the paleo-surfaces and relative chronologic constraints for their correlation with the suite of coastal terraces recognized and geochronologically constrained by previous studies, refining their correlation with the MIS timescale.

2. Geological Setting

The study area is located on the Tyrrhenian Sea margin of central Italy (Figure 1).

Since the Middle Pleistocene the interplay between glacio-eustatic sea-level variations, tectonic processes, sedimentation and volcanic activity has built the geological framework of this area (Luberti et al., 2017, and references therein). During periods of sea-level fall, erosion occurred, whereas deposition took place during phases of sea-level rise, filling previously excavated incisions with a suite of aggradational successions (Karner and Marra, 1998; Marra et al., 2008). A thick succession of pyroclastic-flow deposits, from both the Colli Albani and Monti Sabatini volcanic districts, and subordinated Sabatinian air-fall deposits, interfingers with the continental sediments. After the last volcanic eruptions at 36 ka (Marra et al., 2016c), the volcanic plateau was deeply incised during the Last Glacial, partly as a consequence of the intervening regional uplift (Marra et al., 2016a). Eventually, the paleovalleys were filled by fluvial deposits as a consequence of the sea-level rise after the last glacial termination.

3. Methods

3.1 Geomorphological analysis

In the present study, paleo-surfaces have been mapped following the geomorphological approach described in Marra et al. (2016a; 2017), based on the identification of a set of flat surfaces characterized by topographic culminations with elevation ranging through a few meters around a mean value. Selected topographic culminations of the reconstructed paleo-surfaces were detected on Istituto Geografico Militare 1:25.000 topographic maps of Italy. They include all the hilltops (i.e., each elevation point within a closed, 5 m interval contour line, represented by upward triangles in the figures of this work) and other quasi-equivalent points within plateau-like sectors (downward triangles). The identification of the paleo-

surfaces is based on a combined approach that integrates statistically significant concentrations of elevations around a mean value, and the morphologic evidence for the concentration of these elevation points within a finite area, as detected in the maps (see Marra et al., 2016a for detailed methodology). The full dataset of topographic elevations is reported on the scanned 1:25.000 topographic maps and provided as Supplementary Material #1.

Distribution of the topographic culminations has been statistically analyzed in order to verify the occurrence of discrete elevation intervals corresponding to peaks of concentration, which can be assumed to be the mean level for each paleo-surface. Comparison between the complete dataset of elevation points (hilltops + plateaux) and that represented only by hilltop elevations has been also provided, to highlight possible subjective selection of the plateau-like culminations and to exclude biases.

Finally, a set of elevation ranges defining the principal paleo-surfaces identified using the described geomorphological method has been mapped through DEM analyses, to compare the results.

3.2 DEM analysis

Five classes of elevations highlighted by the geomorphological study have been mapped using an interferometric Digital Elevation Model (DEM) with a ground resolution of 30 meters (1 arcsec) derived from the NASA SRTM mission (http://www2.jpl.nasa.gov/srtm, Farr et al., 2000). When the overall topographic relief of the Italian peninsula is considered, the DEM shows an averaged altitude accuracy of ~15 meters, but in our case, considering areas quite close to the sea and showing low altitude ranges (i.e., 0 - 120 m), the accuracy is one order of magnitude better, and can be estimated in 1-2 m.

The analysis was performed entirily within a GIS environment. Initially, the DEM was delimited on the basis of the study area using a polygon shapefile, then the various classes were identified one by one, generating 5 different layers. Five queries were applied to the DEM, each time considering the maximum and minimum values of each class so as to isolate the desired altitude interval. Finally, the layers were merged into a single one and symbolized with 5 different colors, one for each class.

3.3 Micromorphological analyses

Three undisturbed soil samples (TML-CC, VDT, VOC) and three loose sand samples (TML-SA, PC-SA, CSR-SA) have been studied in thin sections for micromorphological analysis and for

sand mineralogy determination, respectively, aimed at investigating the pedological and/or sedimentological features, and to recognize the origin of the deposit forming the corresponding paleo-surface. One sediment sample collected from the paleo-surface ranging 60-67 m (CR1) in the northern sector was analyzed by Villa et al. (2018), and the results are reported here to integrate with the dataset above.

Descriptions of thin sections are summarized in Table 1, results of the petrographic determination of sand grains are reported in Table 2. Methods and microphotographs of thin sections for micromorphological analyses are provided in Supplementary File #2A.

3.4 Mineralogical analyses

Fifteen samples collected close to the top, and in some instances at increasing depth, on the different paleo-surfaces (VL-1, VL-2, MM, VCR-1, VCR-2, VCR-3, TB-1, TB-2, TB-3, VVL, TML-SA, TRIG, VDT, SPR, RUT), and three sediment samples (RSC, CDC, CR-1), have been analyzed by X-rays diffraction and with a scanning electron microprobe (SEM) in order to describe their mineralogy and texture.

Methods, microphotographs and full-resolution diffractograms are provided in Supplementary File #2B-C.

3.5 $^{40}Ar/^{39}Ar$ dating

Sanidine crystals were extracted from four samples of sediment to provide terminus post-quem ages to the time of deposition of the terrains and/or the accretionary soils forming the paleo-surfaces ranging 98-108 m (TML-SA), 71-79 m (RSC-SA), 60-67 m (CR-3), 51-57 m (CSR-SA) a.s.l., in the area between the Tiber mouth and Anzio. Sampling locations are shown in Figure 3.

Sanidine phenocrysts were co-irradiated with the 1.1864 Ma Alder Creek sanidine standard (Jicha et al., 2016; Rivera et al., 2013) at the Oregon State University TRIGA reactor in the Cadmium-Lined In-Core Irradiation Tube. Single crystal fusion analyses were performed at the WiscAr laboratory at the University of Wisconsin-Madison using a 60W CO_2 laser and a Noblesse multi-collector mass spectrometer following Jicha et al. (2016). Results are reported in Table 4. Full analytical data are reported in Supplementary Material #3.

4. Results

4.1 Geomorphological analysis

Results of the geomorphological study performed for the present work in the coastal area between Civitavecchia and Anzio are in good agreement with those previously obtained by Marra et al. (2016a, 2019a). We have statistically re-analyzed hilltops and plateaux elevations separately, in the two coastal sectors north and south of the Tiber mouth. Very similar statistical assessment for the elevation ranges of the detected paleo-surfaces have been obtained for the two sectors, which are reported in Figure 2 and 3, respectively. In these figures, all the topographic culminations identified on the 1:25.000 maps are indicated with triangles of different colors. In the northern sector, each color is associated with an elevation range defining a paleo-surface which, in turn, is established from the statistical analysis. Elevation ranges for the paleo-surfaces are represented by grey boxes of cumulative frequency above a threshold value of n=2 for a total number of data >20 (red horizontal line in Figure 2b), while continuous distributions are considered for classes of n <20. Open triangles are used for hilltops whose elevation is not statistically significant and are not associated with a paleo-surface. These elevations are interpreted as reflecting topographic culminations that represent eroded higher rank paleo-surfaces; for this reason, the same color used for the corresponding pristine paleo-surface is also used for these triangles.

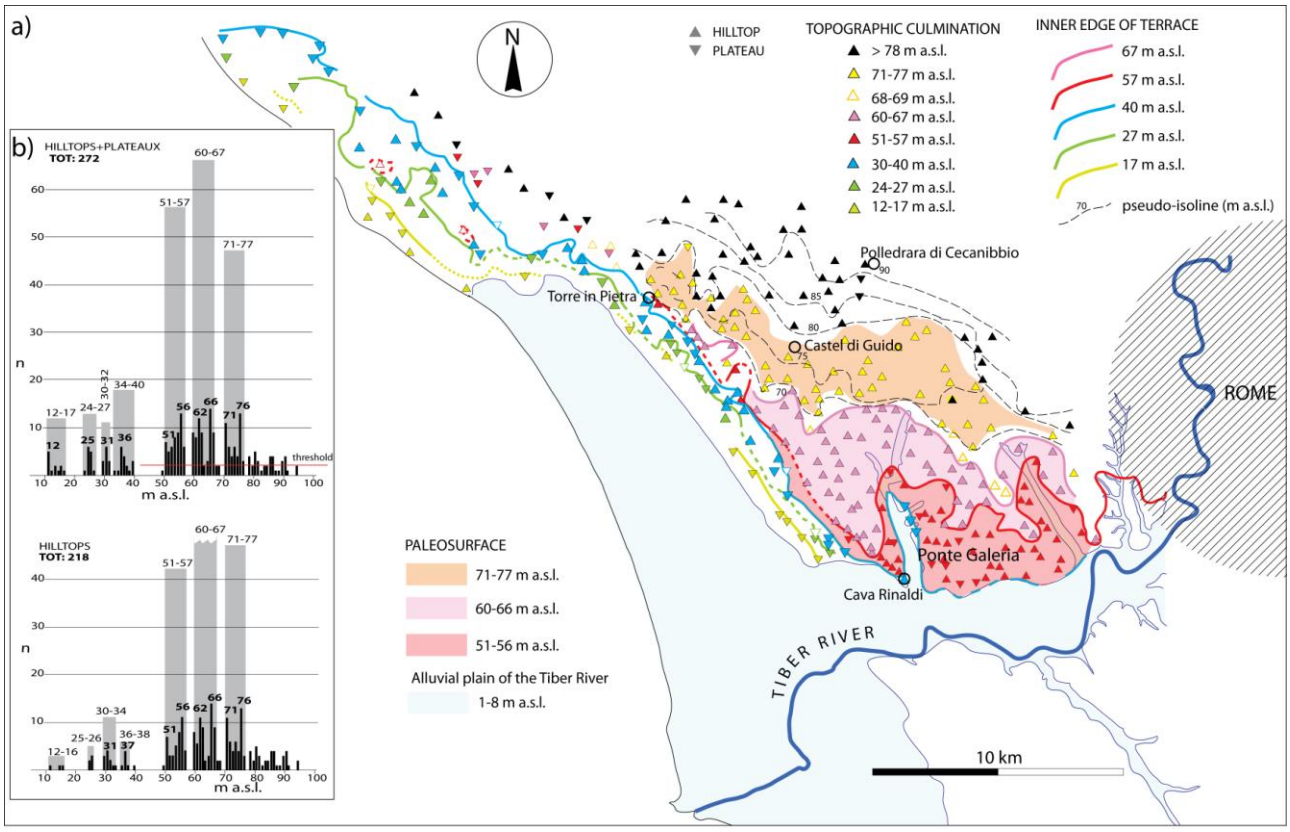

Figure 2 - Geomorphological map (a) and topographic culmination statistics (b) in the northern sector between Civitavecchia and the Tiber mouth. Elevations of topographic culmination are omitted for clarity in this figure and can be found in Suppl. Mat. #1A. See text for comments.

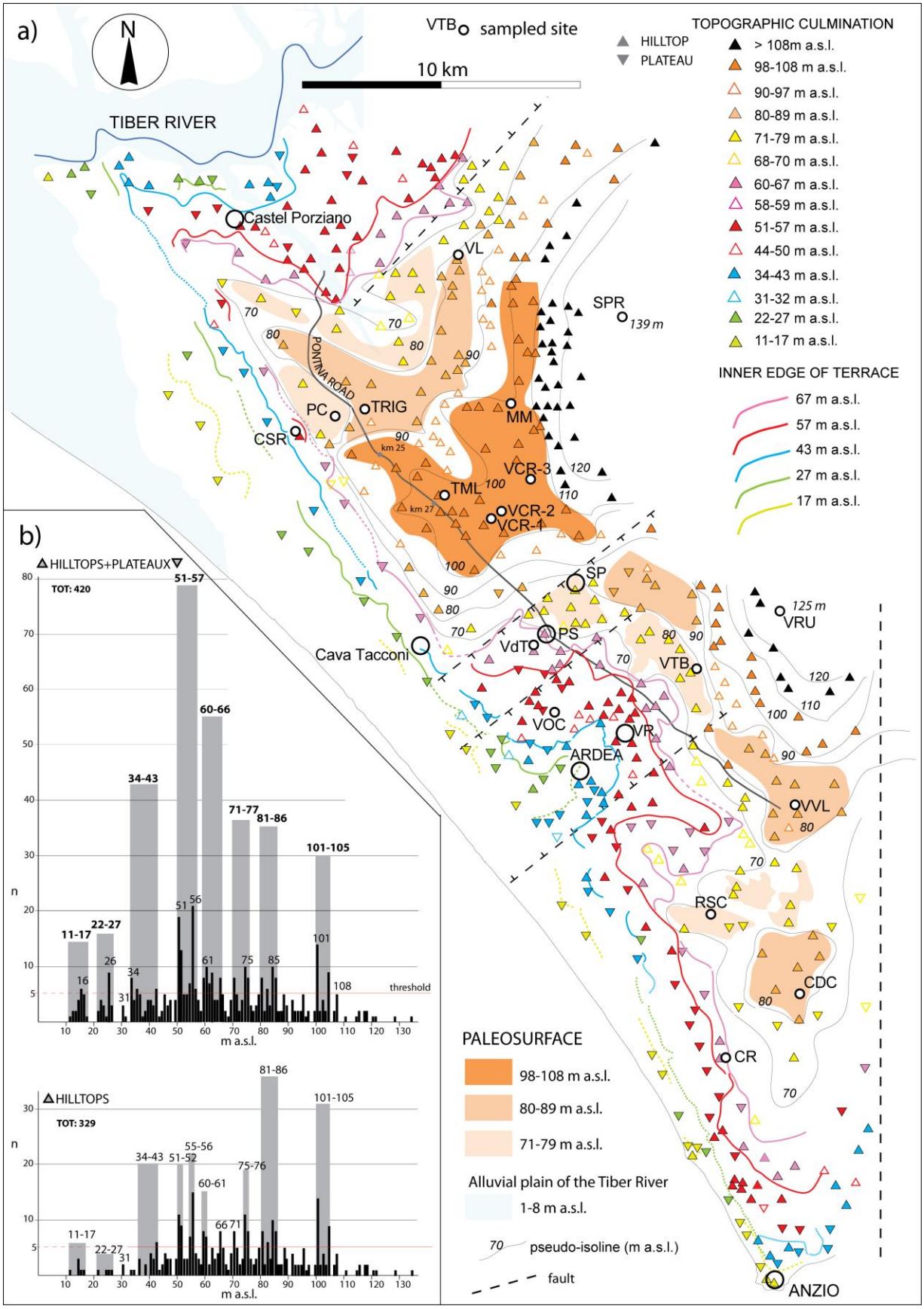
a)
N
VTB sampled site
10 km
TIBER RIVER
HILLTOP
PLATEAU
TOPOGRAPHIC CULMINATION
> 108m a.s.l.
98-108 m a.s.l.
90-97 m a.s.l.
80-89 m a.s.l.
71-79 m a.s.l.
68-70 m a.s.l.
60-67 m a.s.l.
58-59 m a.s.l.
51-57 m a.s.l.
44-50 m a.s.l.
34-43 m a.s.l.
31-32 m a.s.l.
22-27 m a.s.l.
11-17 m a.s.l.
INNER EDGE OF TERRACE
67 m a.s.l.
57 m a.s.l.
43 m a.s.l.
27 m a.s.l.
17 m a.s.l.
Castel Porziano
VL
SPR
139 m
PONTINA ROAD
PC
TRIG
CSR
MM
km 25
VCR-3
TML
km 27
VCR-2
VCR-1
SP
PS
VdT
Cava Tacconi
VTB
125 m
VRU
VOC
VR
ARDEA
VVL
RSC
CDC
CR
ANZIO
PALEOSURFACE
98-108 m a.s.l.
80-89 m a.s.l.
71-79 m a.s.l.
Alluvial plain of the Tiber River
1-8 m a.s.l.
pseudo-isoline (m a.s.l.)
fault
b)
HILLTOPS+PLATEAUX
TOT: 420
51-57
60-66
34-43
71-77
81-86
101-105
11-17
22-27
threshold
n
m a.s.l.
HILLTOPS
TOT: 329
81-86
101-105
55-56
34-43
51-52
75-76
60-61
66 71
11-17
22-27
31

Figure 3 - Geomorphological map (a) and topographic culmination statistics (b) in the southern sector between the Tiber mouth and the Anzio promontory. Elevations of topographic culmination are omitted for clarity in this figure and can be found in Suppl. Mat. #3. See text for comments.

A similar approach is used in the southern sector where, due to the larger number of data, a threshold value of n=5 is established to define the classes of elevation for all the paleo-surfaces except the lowest two (Figure 3b). Moreover, in a few cases the elevation range for each color is slightly larger than the mean elevation range (grey boxes) established for the paleo-surfaces based on histograms, in order to include all topographic points.

Color shading is used in Figure 2 for three oldest paleo-surfaces which have a wider extent and are located inland, while inner margins are represented by solid colored lines for the paleo-surfaces stretching along the coast, which are assumed to represent coastal terraces. Different shades of the orange color are used in Figure 3 to highlight the highest paleo-surfaces that are located inland which, according to discussion in the following sections, are interpreted as having the same age, whereas inner terrace margins are reported for the youngest paleo-surfaces along the coast.

In both sectors illustrated in Figures 2 and 3, three lowest orders of terrace are identified by a series of topographic culminations, each one providing well-clustered, distinct elevation ranges, which define three paleo-surfaces narrowly elongated parallel to the coast. The lowest paleo-surface ranges 12-17 m a.s.l., with a peak at 12 m (Figure 2b), and 12-18 m a.s.l., with a peak at 16 m (Figure 3b), in the northern and in the southern sector, respectively. A second paleo-surface has very narrow ranges of 24-27 and 22-27 m a.s.l., with peaks at 25 and 26 m, in the northern and in the southern sector, respectively.

A third, higher paleo-surface is characterized by a wider range of elevations, with a main concentrations between 34-40 and 34-43 m a.s.l. in the northern and southern sector, respectively, and with a minor peak at 31 m, in both sectors.

A fourth, wide paleo-surface is that ranging 51-57 m a.s.l. and characterized by two relative maxima at 51 and 56 m, in both sectors. Another two well-defined elevation ranges of 60-67 m, and of 71-77 m, are clearly identified in both sectors, and are associated with fifth and sixth paleo-surfaces, respectively.

Finally, two more concentrations of elevation values, peaking at 80-86 and 101-105 m a.s.l., define the two highest paleo-surfaces on the inland coastal sector south of the Tiber mouth, whereas in the northern sector topographic culminations show progressively increasing elevation inland, without any apparent clustering around a mean value.

Comparison of the results of the geomorphological study with the DEM of Figure 4 shows a very satisfactory match. In particular, we note the close correspondence between the geometrical patterns defined by the 51-57 m paleo-surface in the geomorphological maps of Figure 2 and 3, and in the DEM image of Figure 4 (represented by the red color in both representations), as well as, between those pertaining to the highest paleo-surface of 98-108 m (represented by the deep orange color in Figure 3 and by the deep blue color in Figure 4).

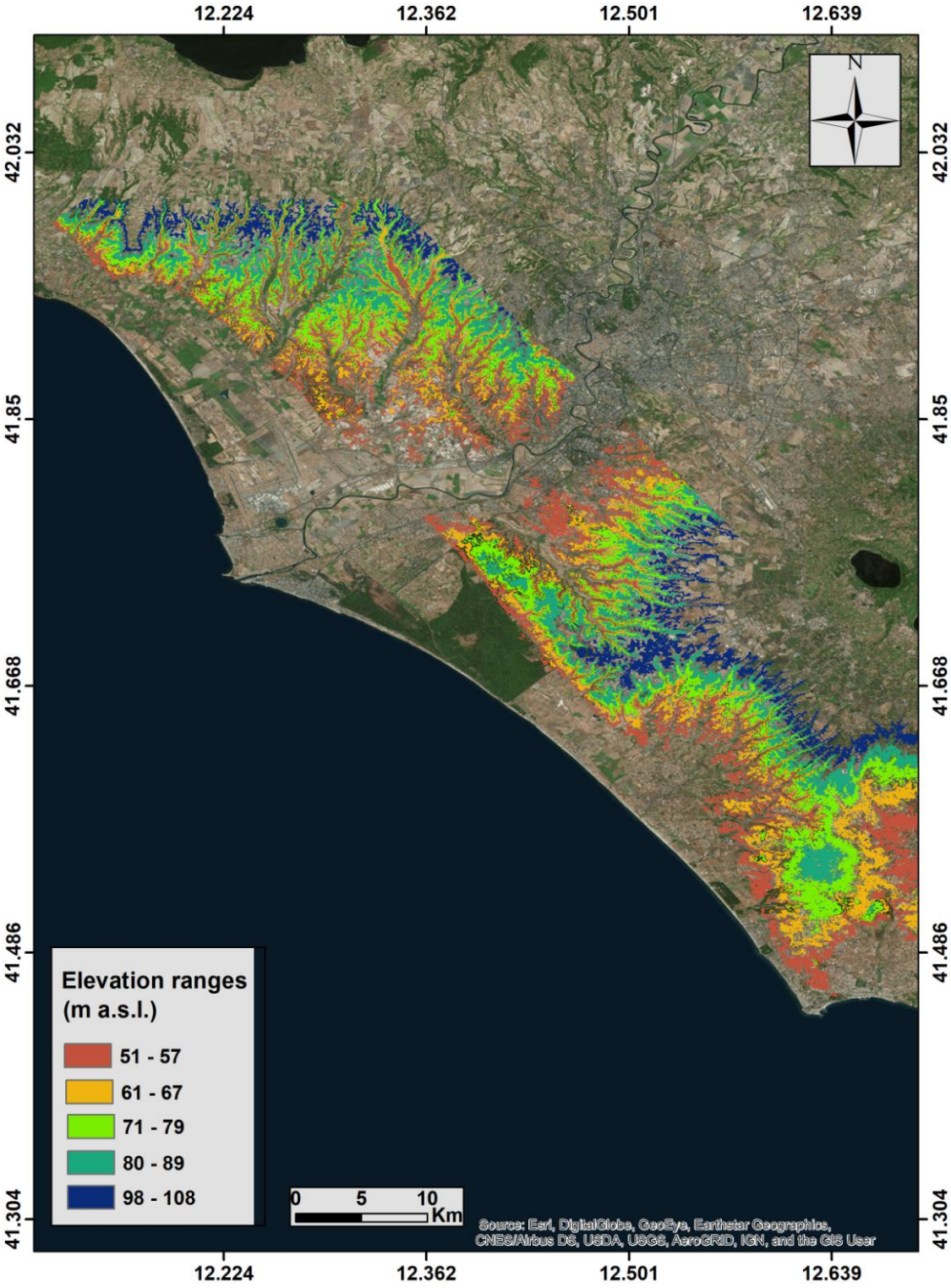

Figure 4 - Interferometric Digital Elevation Model (DEM) mapping of the five classes of elevations highlighted by the geomorphological study.

4.2 Stratigraphic investigations

4.2.1 Paleo-surface 98-108 m a.s.l.

Exposure of the sedimentary deposits forming the highest paleo-surface in the investigated area is provided by a road cut in Tenuta Monti di Leva (TML), at km 27 of Via Pontina (Figure 5a, see Figure 3 for location). Here, a pedogenically modified horizon occurs in the upper 100 cm and is constituted by fine to medium sized sand in silty-clayey matrix, orange in color (Figure 5a-a"). A 180 cm thick concretionary layer, constituted by aggregated, cm-sized Fe and Mn nodules within a sand matrix, occurs at the bottom of this horizon and overlies a red paleosol developed on top of the pyroclastic-flow deposit of Pozzolanelle (Villa Senni Eruption Cycle, 365±4 ka; Freda et al., 1997; Marra et al., 2009). A sample of the upper sand layer (TML-SA) and another from the concretionary layer (TML-CC) were analyzed for mineralogy and michromorphology, respectively. Forty-one sanidine crystals extracted from sample TML-SA were dated by the $^{40}Ar/^{39}Ar$ method.

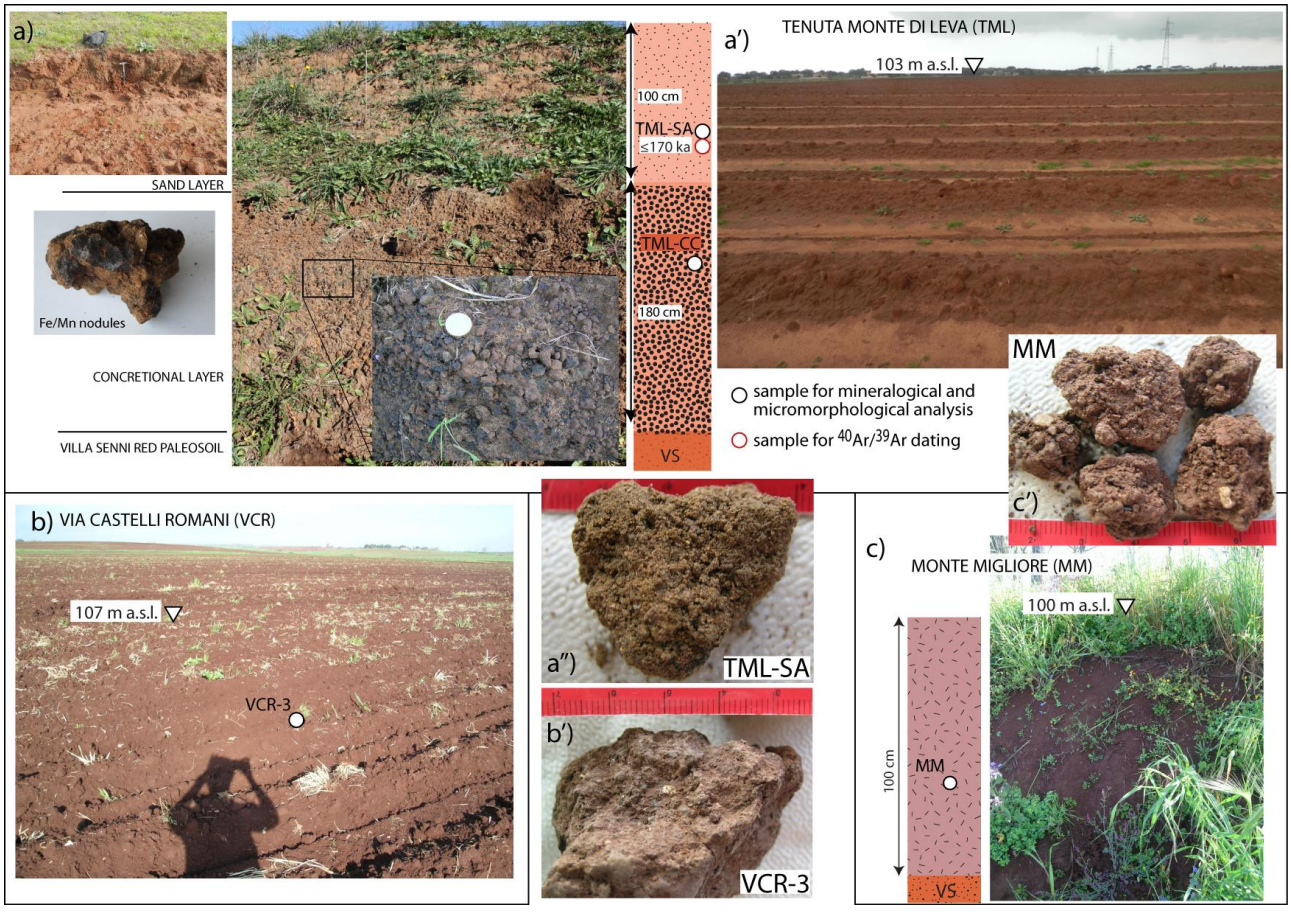

Figure 5 - Photographs and stratigraphic schemes showing the 98-108 m a.s.l. paleo-surface and the sections from which samples analyzed in the present study were collected. See text for comments.

The Tenuta Monte di Leva paleo-surface is affected by intensive ploughing which exposes shreds of the upper, orange sand layer, allowing recognition of the presence of this sedimentary deposit throughout the sector crossed by the Pontina Road between km 27 and km 25 (see Figure 3a). A similar in color, but finer sandy-clay deposit is exposed by plowing grooves on top of this highest paleo-surface, further inland. Four samples were collected along the Via dei Castelli Romani and Via Laurentina, at increasing distance inland, with respect to the Tenuta Monte di Leva site (Figure 3). Three samples (VCR 1-3) were collected at elevations between 105 and 107 m a.s.l. in the fields exposing clods of the sub soil (Figure 5b). Although the direct contact is not exposed in this flat sector, a geologic substrate represented by the Pozzolanelle pyroclastic-flow deposit (hereby PL) is visible in the scanty outcrops along the stream incisions at its margin. A fourth sample (MM) was collected at the Monte Migliore-La Selvotta locality, at 100 m a.s.l., from the middle of a 100 cm thick, dark red paleosol developed above the PL, exposed by a road cut (Figure 4c). A larger amount of clay matrix, dark red in color, characterizes the samples collected in these inland sectors of the 98-108 paleo-surface (VCR 1, 2, 3, MM, Figure 5b'-c'). Frequent pyroxene crystals and sparse, altered volcanic scoriae 1 to 5 mm in size, are embedded in the clay matrix of these soils, evidencing an at least partial origin from the directly underlying volcanic deposit.
Two more samples were collected in a later time at higher elevation, in the area inland with respect to that pertaining to the 98-108 paleosurface (SPR at 139 ma.s.l.) and with respect to the narrow alignment of topographic culminations ranging 100-110 m in the more southern sector (RUT at 125 m a.s.l.) (Figure 3), aimed at investigating the origin of the abundant silico-clastic fraction highlighted by micromorphologic and petrographic analyses in the soils developed above the volcanic substrate.

4.2.2 Paleo-surface 80-89 m a.s.l.

Different fragments of this paleo-surface are identified northwest and southeast of the highest sector corresponding to the 98-108 paleo-surface (Figure 3). As for the latter, the 80-89 paleo-surface is also developed above different geologic substrates as a function of the distance from the coastline: above the PL in the inland sectors, and above sedimentary sand deposits to the southwest. Five samples were collected in the different sectors of this paleo-surface. Two samples (VL-1, VL-2, Figure 6a) were collected in the middle and at the surface

of a thick paleosol developed above the PL in Via Laurentina, in the inland margin of the northernmost stretch of this paleo-surface. A further sample (TRIG, Figure 6b) was collected at its opposite, seaward extreme, on the ground surface in a sandy deposit (Figure 3).

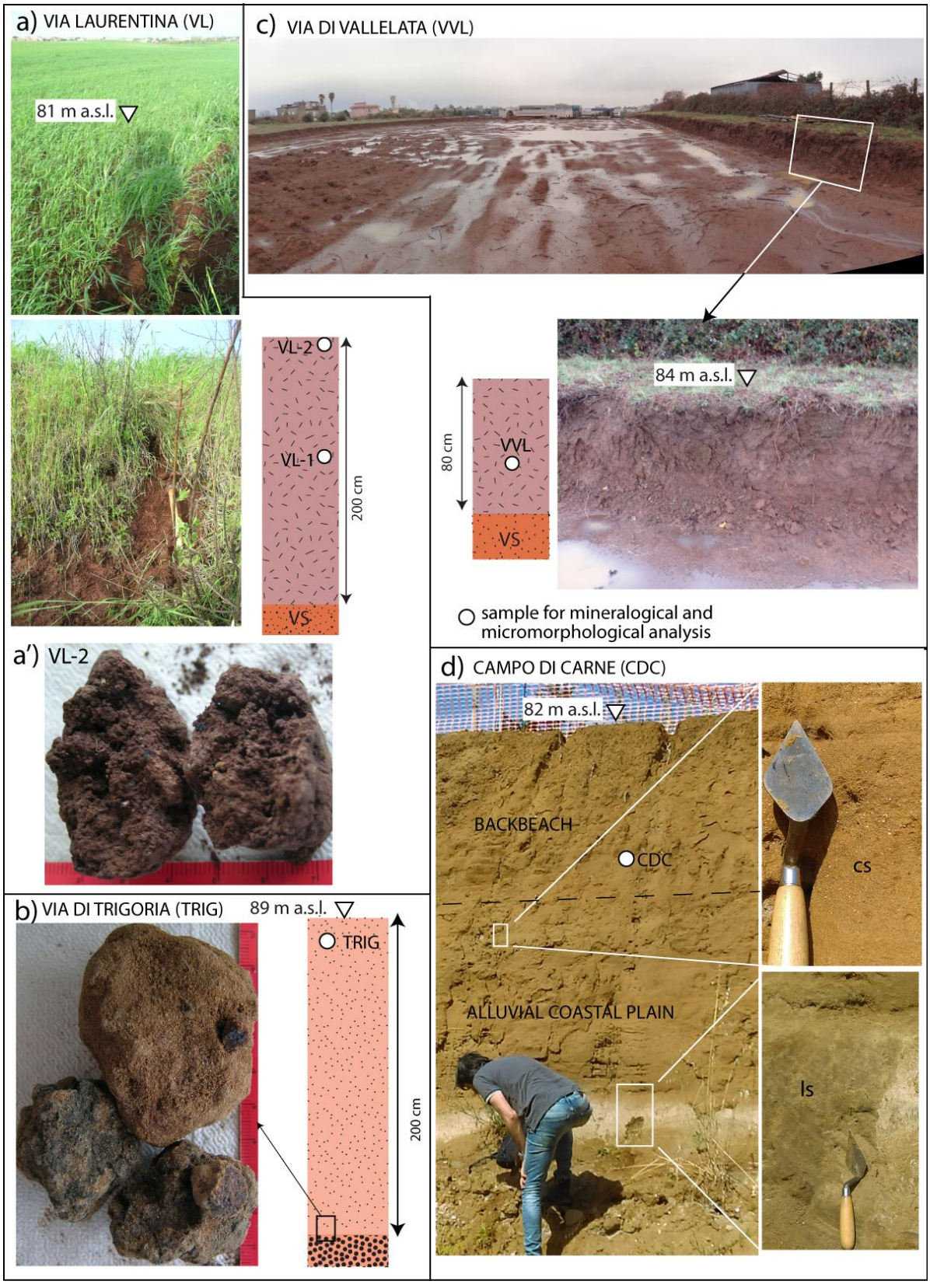

Figure 6 - Photographs and stratigraphic schemes showing the 80-89 m a.s.l. paleo-surface and the sections from which samples analyzed in the present study were collected. See text for comments.

This sedimentary deposit is quite similar to that cropping out in Tenuta Monte di Leva (TML): it is a medium-to-fine grained, orange sand in a sparse clay matrix, without sedimentary structures, ca. 3 m thick (Figure 6b). At the base of the exposed section a concretionary layer rich in Mn/Fe nodules, quite similar to that occurring in TML, is present.

A fourth sample (VVL, Figure 6c) was collected in the middle of an ca. 80 cm thick paleosol developed above the PL in Via Vallelata, in the inland margin of the southernmost stretch of the 80-89 m paleo-surface (Figure 3). This reddish soil, like the thicker soil sampled in Via Laurentina (Figure 6a'), constituts of very fine, clayey sediment containing abundant pyroxene crystals and altered volcanic scoriae, and appears quite similar to the other soils developed directly above the PL sampled for this study.

Finally, one sample (CDC) was collected in Campo di Carne in a road excavation exposing a ca. 3 m thick deposit constituting of fine, faintly bedded sand in a sparse clay matrix, with dm-thick layers of coarse sand (cs in Figure 6d), whose top at 82 m a.s.l. is part of the seaward portion of the 80-89 m a.s.l. paleo-surface. A layer of dark, greenish loamy fine sand, ca, 60 cm thick, occurs at the base of the exposed section in CDC (ls in Figure 6d).

4.2.3 Paleo-surface 71-79 m a.s.l.

Two particularly level, small sectors at elevations around 76 m a.s.l. can be detected in the northern and southern margins of the investigated area, in the Podere Carafa (PC) and Riserva Carpineto (RSC) estates (Figure 3). In the PC, an almost perfectly flat area (Figure 7a) is truncated by a sharp scarp to the southwest, dividing it from another level area at ca. 56 m a.s.l. (Castel Romano -CSR), while it connects more gently to a slightly higher sector, corresponding to the 80-89 paleo-surface, to the northeast. A marked fluvial incision dissecting the plateau exposes the terrains forming the 71-79 m paleo-surface, showing massive sand deposit of at least five meters thickness, where sample PC-SA analyzed during this study was collected (Figure 7a).

A remarkably similar geomorphologic and stratigraphic setting is observed at the RSC. Here a wide level area at elevations ranging 70-79 m is intensely dissected by steep stream valleys, and almost without geomorphologic break connects with another large area to the southeast, including the Campo di Carne (CDC) site, at an elevation between 80 and 85 m a.s.l. (Figure 3). A massive, medium to coarse sand deposit with sparse, well-rounded fine gravel (sample RSC,

Figure 7b) constitutes the geologic substrate in this area, and directly overlies the lower flow unit of the Villa Senni eruption cycle (Tufo Lionato).

Figure 7 - Photographs and stratigraphic schemes showing the 71-79 m a.s.l. paleo-surface and the sections from which samples analyzed in the present study were collected. See text for comments.

A portion of this 71-79 m a.s.l. paleo-surface also occurs within the structurally controlled sector of Ardea, bordered by the NE-SW trending normal faults of the Ardea Basin (Figure 3). This is a half-graben which originated as a transversal Tyrrhenian Sea basin in Lower Pleistocene times, as evidenced by off-shore seismic lines (Faccenna et al., 1994). The continued Middle Pleistocene activity of these faults is suggested by the marked control on the paleo-coastlines, testified by the geometry of the inner edges of the MIS 7 and MIS 5 terraces reconstructed in Marra et al. (2016a, 2019a) and shown by our refined study in Figure 3 and in Figure 4.

In contrast to the more seaward sectors, here the 71-79 paleo-surface is developed upon the PL (Figure 7c-d), and characterized by a shallow, 60-80 cm thick, dark brown paleosol. Three samples have been vertically sampled in this paleosol at the Via di Torre Bruna (VTB 1-3, Figure 7c).

Figure 2 shows a wide 71-77 m paleo-surface that we have reconstructed in the coastal sector north of the Tiber mouth (Ponte Galeria area), which in Marra et al. (2016a) was not highlighted. However, scanty sedimentary deposits occur at these elevations in this area, where the outcropping terrains are mostly represented by the Monti Sabatini volcanic succession. Notably, thin layers of calcareous lacustrine muds, ca. 50 m thick, crop out at 72 m a.s.l. in Castel di Guido, and are overlain by the pyroclastic-flow deposit of Tufo Giallo di Sacrofano (285±2 ka, Karner et al., 2001b; Sottili et al., 2010), which forms most of the hilltops of the 71-77 m paleo-surface (Marra et al., 2018c). We interpret these sedimentary strata as the remnants of an alluvial coastal plain, mantled by a thin cover of pyroclastic deposits.

4.2.4 Paleo-surface 61-67 m a.s.l.

No evident paleo-surface is associated with this class of elevations in the sector south of the Tiber mouth, except that pertaining to small, isolated plateaux, like at the Colle Rotondo locality (CR, Figure 8). The Colle Rotondo site is located on the flat surface of an E-W elongated hill, culminating 63.5 m a.s.l., bordered by the steep flanks of two convergent streams, 2.5 km east of the present coast, and 7.5 km north of Anzio (Figure 3). This is part of a series of hilltops ranging 61-67 m a.s.l., aligned along a narrow stripe of land defining a coastal terrace between Ardea and Anzio (pink triangles in Figure 3). This terrace is shifted inland, significantly, within the Ardea basin, paralleling the behavior of the inner edge of the 51-57 m terrace, as well as that of the two lower terraces of 34-43 m, and 22-27 m (Figure 3). Notably, in the coastal sector overlooking the most elevated area of TML, corresponding to the

98-108 m paleo-surface, only plateau points define the 60-67 m terrace, while almost no evidence of the 51-57 m terrace occurs in the coastal reach north of the Ardea basin, consistent with erosion due to tectonic uplift of this sector. In contrast, a well-defined 60-67 m terrace occurs at the northwestern margin of the lower area represented in Figure 3, facing the terminal reach of the Tiber Valley.

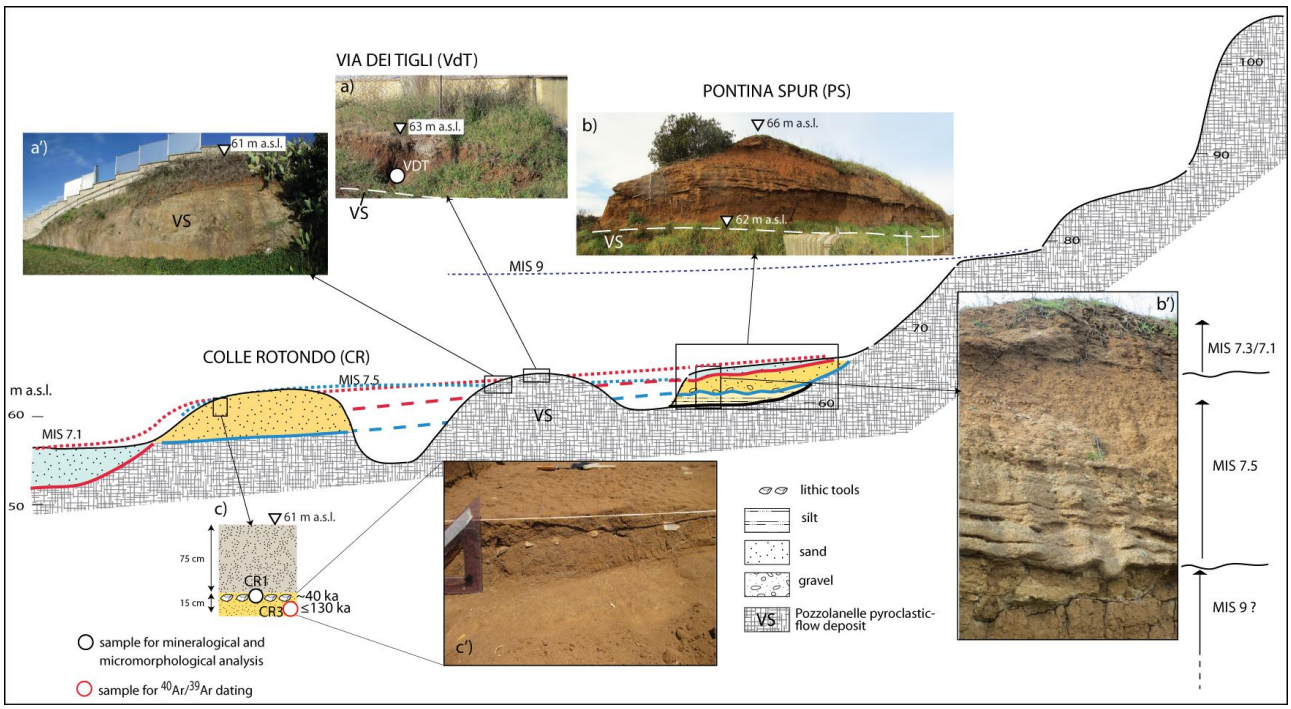

Figure 8 - Composite cross-section, constructed by projecting the Colle Rotondo (CR) site on an ideal profile passing by the Santa Procula (SP), Pontina Spur (PS), and Via dei Tigli (VdT) sites (see Figure 3 for location), aimed at showing the stratigraphic relationships between the sedimentary successions underlying the 60-67 m a.s.l. paleo-surface.

A pedogenized surface horizon constiting of brown sandy silt, heavily disturbed by ploughing, occurs in the upper 75 cm at CR (Figure 8c). It overlies a reddish-brown silty sand horizon, incorporating mm-sized Mn and/or Fe concretions (Figure 8c'). A large number of stone artifacts attributed to the Uluzzian culture (45-41 ka) was found within the upper portion of this sand layer, ranging in thickness from 6 to a maximum of 20 cm (Villa et al., 2018). One sand sample (CR1) collected within the archaeological layer was analyzed for michromorpholgy by Villa et al. (2016), while 39 sanidine crystals extracted from a sand sample (CR3) collected immediately below (see Figure 8c) have been dated as part of the present work.

A different geologic substrate characterizes the 60-67 m paleo-surface at two sites located in the northern portion of the Ardea Basin, Via dei Tigli (VdT) and Pontina Spur (PS) (Figure 3).

A ca. 80 cm thick, brown-reddish clayey paleosol overlies the PL at VdT (Figure 8a). Field surveys showed that the substrate of the 60-67 m paleo-surface in this area is represented by a pedogenized layer on top of the PL (e.g., Figure 8a'). One sample from this soil (VdT) has been analyzed for micromorphology.

A peculiar situation is observed at PS, where two fining-upwards successions overlie a third, faintly bedded fine sand deposit, which in turn overlies the PL (Figure 8b-b'). The two upper successions consist of a basal gravel layer, made up of reworked volcanic material with characteristic, large leucite crystals turned into analcime, suggesting provenance from the PL (Freda et al., 1997). The finer, upper part is also made up largely of volcanic sand. Both have evident fluvial origin. The lowest layer is a silty fine sand, of possible palustrine or alluvial origin. No sample was collected from this section, due to its very local significance, while a correlation with the other sections of the 60-67 m paleo-surface and a paleoenvironmental interpretation is provided in the cross-section of Figure 8.

The 60-67 m paleo-surface has a wide expression to the north of the Tiber (Figure 2). However, no sedimentary succession is apparently associated with this paleo-surface, its geologic substrate consisting of different, older volcanic deposits, ranging 561-400 ka (e.g., Karner and Marra, 1998; Marra et al., 2016b), which form the hilltops in this area. Consequently, the 60-67 paleo-surface in this area should be considered as a non-depositional terrace, possibly generated by uplift-induced erosional processes in the near-shore sector, similar to the higher level paleo-surface of 71-77 m in this sector.

4.2.5 Paleo-surface 51-57 m a.s.l.

This paleo-surface (red triangles in Figure 2 and 3) has a prominent expression in the Ponte Galeria area north of the Tiber mouth, where solid geochronologic constraints correlate it with MIS 7, as noted in Marra et al. (2016a). It is rather well preserved along the southeastern side of the Tiber Valley, south of the river mouth, and in the southernmost sector between Ardea and Anzio, while it disappears along the coastal reach facing the TML morpho-structural height (Figure 3). However, two fragments of coastal terrace are preserved immediately north of this sector, and one of these (Castel Romano -CSR) provides good exposure of the terrains underlying the paleo-surface. At CSR a large level area at elevations ranging 51-56 m a.s.l. is bordered to the west-northwest by a steep, 6 m high scarp (Figure 9a), separating it from the other wide level area of Podere Carafa, ranging 71-79 m a.s.l. (see Figure 3).

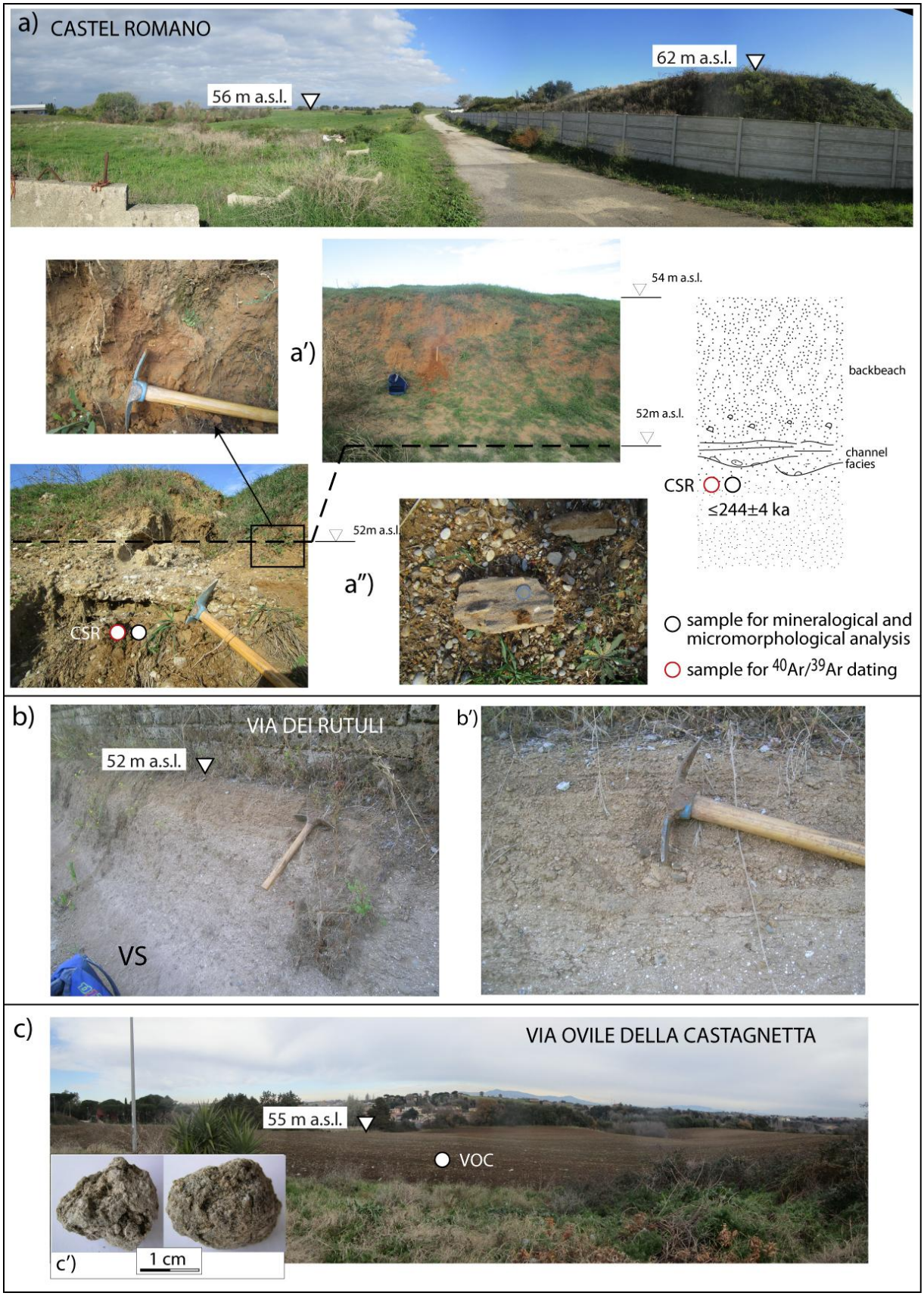

Figure 9 - Photographs and stratigraphic schemes showing the 51-57m a.s.l. paleo-surface and the sections from which samples analyzed in the present study were collected. See text for comments.

The 60-67 m terrace is not preserved between the two paleo-surfaces in this area, which are connected by a gentle incline degrading from ca. 70 m to 62 m a.s.l., behind the sub-vertical scarp. The 51-56 m paleo-surface at CSR is dissected by a gully exposing on its banks a reddened, massive sand deposit, 2 m thick (Figure 9a'), overlying a ca. 50 cm thick layer with gravel lenses and sandstone horizons with ripple marks (Figure 9a"). This braided channel facies overlies a massive sand deposit in which sample CSR for mineralogical analysis and $^{40}Ar/^{39}Ar$ dating was collected.

A different geologic substrate represented by the PL characterizes the 51-57 m paleo-surface within the Ardea Basin. However, exposure at Via dei Rutuli (VR, see Figure 3) provides evidence of a conglomeratic layer above the PL at 52 m a.s.l. (Figure 9b), which testifies the occurrence of a transgressive deposit that should be considered the coastal deposit associated with the 51-57 terrace in this area. It is a bedded, fining upward, 50 cm thick sand and gravel layer, containing well-rounded scoria clasts from the underlying pyroclastic deposit, which is erosionally truncated at the top (Figure 9b'). Evidence from another site within the Ardea basin (Via Ovile della Castagnetta -VOC, Figure 3) suggests that a fine-grained, lagoon deposit forms the upper portion of the 51-57 terrace in this area. Here, a wide paleo-surface around 55 m a.s.l. (Figure 9c) consits of a brown, mature paleosol in which one sample (VOC) was collected and analyzed for micromorphology. The occurrence of abundant, rounded calcareous concretions (Figure 9c'), which are uncommon in shallow soils developed directly upon the siliceous volcanic deposits, suggests the presence of a horizon of calcareous mud, as typically observed in the lagoon deposits of the MIS 7 Vitinia Formation (Karner and Marra, 1998) associated with the 51-57 paleo-surface in the northern coastal sector.

4.3 Micromorphological analyses

Results of thin section observations are summarized in Table 1.

TS[1]	Microstructure	Lithology	Groundmass[2]	c/f ratio	Rel Dist[3]	Pedofeatures
TML-CC	-	Matrix: 15 -20% fine sands (quartz; rare feldspar; chert; metamorphic rock fragments) Inside nodules: well sorted fine sands (±45%) (quartz; feldspar;	Orange (PPL) clay with SS and GS bfabric	20/80 (matrix) 50/50 (nodules)	OP (matr.) SSP (nod.)	Matrix: layered clay coatings and infillings, limpid and

		chert; metamorphic rock fragments; pyroxene)				silty clay, broad extinction lines, frequent.
CR1	Basic MS type: close porphyric	Fine sand (5%); Medium sand (60-65%) Lithology: quartz; feldspar; chert; pyroxene; metamorphic rock fragments; epidote. Sub-rounded and sub-angular grains.	Reddish (PPL) clays with SS and GS b-fabric	70/30	CP	Limpid clay coatings and infillings, 1st order yellow interference colors; broad extinction lines, occasional superimposed Fe coatings.
VDT	Subangular blocky, moderate	Very fine sand (5-10%); Fine sand (5%); Medium sand (5-10%) Lithology: quartz; chert; pyroxene (rare); Sub-rounded and sub-angular grains.	Orange (PPL) clay with CS and GS bfabric	20/80	OP	Limpid clay coatings, strongly deformed, frequent. Disorthic Fe/Mn nodules, typic and concentric, frequent, rounded.
VOC	Basic MS type: single-spaced porphyric	Very fine sand (±5%); Fine sand (15-20%); Medium sand (25-30%) Lithology: quartz; feldspar; chert; pyroxene; amphibole; volcanic scoria (rare); metamorphic rock fragments. Sub-rounded and sub-angular grains.	Yellowish (PPL) clays with GS bfabric	60/40	SSP	Limpid clay coatings, strongly deformed, frequent. Disorthic Fe/Mn nodules, typic and concentric, frequent, rounded.

Table 1 – Description of thin sections

[1] TS = Thin Section

[2] B-fabric: SS = Stipple speckled; PS = porostriated; GS = granostriated; CS = cross striated

[3] Rel Dist = Related distribution pattern: CP = close porphyric; SSP = single-spaced porphyric; OP = open porphyric

4.3.1 Concretionary layer from Tenuta Monte di Leva: sample TML-CC

Micromorophological analysis of this sample collected from the TML concretionary layer shows that the nodules are iron and manganese concretions that entrap sediments differing from those in the surrounding groundmass. The main differences between the sediments within the nodules and those in the matrix around them are as follows:

(a) The degree of sorting, which inside the nodules is good, with grains in the fine sand class, indicating that the nodules formed in aeolian or alluvial sands (e.g., channel facies).

(b) The lithology: the matrix consists only of weathering resistant species, whereas in the nodules some volcanic minerals (pyroxenes – Fig. S1) are preserved, and feldspar (e.g., microcline) is more abundant than in the surrounding matrix.

The matrix around the nodules shows the effects of marked pedogenesis. It is in fact very clay-rich and in the coarse fraction only weathering resistant material is preserved (quartz, chert,

metamorphic rock fragments – predominantly quartzite). Clay coatings, pertaining to several superimposed episodes of clay illuviation, are very strongly developed (Fig. S2). They occur as superimposed limpid and silty clay coatings or as coatings deformed due to shrink-swell phenomena.

Albeit that the nodules may be allochtonous (i.e., formed elsewhere and then transported and re-deposited after being eroded), observations attest that they contain remains of the former parent material on which pedogenesis has taken place, "preserving" it from successive weathering. Weathering and pedogenesis subsequently affected the groundmass but were impeded within the nodules.

4.3.2 Sand deposit from Colle Rotondo: sample CR-1

The sand fraction is composed of a mixture of siliciclastic and volcanoclastic (i.e. pyroxenes – augite) mineral species. The moderate sorting, the grainsize centered on the medium sand granulometric class, and the slight rounding of the grains are compatible with an aeolian (backbeach) sediment. There are no traces of reworking due to surface runoff or similar water and gravity-triggered slope processes. Pedogenesis is at an initial stage, especially compared to other samples from this study. Incipient reorganization of the groundmass, giving rise to a stipple-speckled b-fabric, is observed. Weak traces of incipient clay illuviation, such as thin clay coatings around skeletal grains, also point to an initial/moderate level of pedogenesis (Fig. S3). The weatherable minerals in the coarse fraction – especially pyroxenes – are abundant and do not show traces of weathering.

4.3.3 Paleosol from Via dei Tigli: sample VDT

This sample shows the highest degree of pedogenic weathering amongst the analyzed samples. The abundant clay in the groundmass shows orange-red colors resulting from the strong oxidation, and the clay are the outcome of repeated cycles of clay illuviation. Strong vertic processes (i.e.: internal turnover of soil material) led to the digestion of the illuvial clays in the fine mass and to the formation of strongly developed cross-striated and grano-striated b-fabric types (Fig. S4, S5). Also the nodules of iron and manganese owe their morphology to the strong shrink-swell phenomena in the sample (which led to the formation of concentric nodules with strong rounding). The coarse fraction is predominantly composed of weathering-resistant species (quartz and chert), albeit minor amounts of pyroxenes and unaltered volcanic glass are still present. The latter might derive from a 'fresher' or more recent input of volcaniclastic material into the soil during its formation. The poor sorting, sub-

552 angular morphology and medium-fine sand grain size of the siliciclastic fraction do not match
553 the expected characteristics of an aeolian input, strongly suggesting an alluvial/colluvial
554 origin.
555
556 **4.3.4 Paleosol from Via Ovile della Castagnetta: sample VOC**
557 The sorting of the coarse fraction is low. The sample has the highest percentage of volcanic
558 mineral grains (pyroxenes and amphiboles – see Fig. S6) in the studied set, included the loose
559 sand samples. The fine fraction derives from clay illuviation, which ultimately triggered vertic
560 processes and the digestion of clay coatings within the groundmass, the development of a
561 grano-striated b-fabric, and the formation of concentric iron and manganese nodules.
562 Grains are predominantly in the fine and medium sand fraction, and show subrounded and
563 rounded morphologies. The low sorting and the rounding of iron and manganese nodules
564 indicate reworking and redeposition of the material. The presence of rare calcite infillings
565 indicates re-carbonatation of the profile due to the effect of a dissolved carbonate-rich
566 groundwater table (Fig. S6). Abundant, large (1-2 cm) carbonatic nodules also occur in the
567 deposit.
568
569 **4.4 Mineralogical analyses in thin section**
570 **4.4.1 sample TML-SA**
571 Due to the granulometric bias introduced by sieving, it is not possible to ascertain the
572 sedimentary environment in which the deposit formed through thin section observation.
573 Nevertheless, it can be said that TML-SA is characterized by scanty medium and coarse sand
574 fraction, and by fine material possibly indicating pedogenesis. Indeed, the fine material was
575 observed before the sieving and also after it, especially in the form of "pseudosands" which
576 survived the sieving procedure. The nature of the sand grains is essentially siliciclastic (Table
577 2), with a very minor volcanoclastic fraction and lack of volcanic scoriae. Grains have a
578 subangular morphology.
579
580

Minerals	TML - SA	PC-SA	CSRM-SA
	%	%	%
Quartz	64	66	35
Metamporphic rock fragments	20	19	35
Chert	12	10	16
Feldspar	3	2	5
Pyroxene	1	3	8
Amphibole	1	0	0
Volcanic scoria	0	0	1

Total siliciclastic %	98	97	91
Total volcaniclastic %	2	3	9
Counted grains (n)	*152*	*156*	*154*

Table 2: results of petrographic determination of sands

Quartz, chert, metamorphic rock fragments (mainly quartzite with minor amounts of schist) and feldspar have been grouped under the "siliciclastic" category. Pyroxene (mostly augite and monocline pyroxene, diallagio), amphiboles (green and brown hornblende) and volcanic scoria belong to the "volcaniclastic" category.

4.4.2 Sand deposit at Podere Carafa: sample PC-SA

The sand displays strikingly similar grain composition (Table 1) and morphology as that of sample TML-SA.

4.4.3 Sand deposit at Castel Romano: sample CSR-SA

This sand sample is characterized by medium grain size with a subrounded morphology and no fine matrix. Mineralogical composition displays a higher percentage of volcanic species in comparison with the other sand samples (Table 1).

4.5 X-ray and SEM analysis

Results of diffractometric analyses are summarized in the diagrams of Figure 10.
Calcic clinopyroxene is ubiquitous in the pyroclastic rocks of the Colli Albani volcanic district. In addition, amorphous material derived from the weathering of volcanic glasses is typical of soils developed on pyroclastic rocks (generally, this soil component is identified in the RDX by the increase of counts in the region at lower 2Θ□□ Consequently, the height of clinopyroxene peak at 2Θ=29.85°, as well as that of amorphous material at 2Θ=4°, with respect to quartz peak at 2Θ=26.65° in the RDX can be assumed as an indicator of the abundance of volcanic components forming the soil. This provides an index (i.e. Qtz/(AM+Cpx) in Table 3) to distinguish the soils developed above a primary volcanic substrate (Index <6) from those overlying sedimentary deposits (Index >6).
Notably, quartz is present in all the soils developed above volcanic deposit and its abundance generally increases with decreasing depth as evidenced by magnitude of the peak at 2Θ=26.65° (Q1 Figure 10a). Quartz is practically absent closer to the base of the soil in VTB-1, and is scarce in the middle of the soil in VTB-2 and in Monte Migliore (MM). However, it is also abundant in the middle of VVL and VL, where the Q1 peak is comparable with that of all the surface samples. A marked quartz peak is present in sample VdT-2, from the soil developed

615 above the Villa Senni deposit on the 61-67 terrace, for which the siliciclastic fraction has been
616 investigated in thin section for micromorphology on sample VdT-1. However, excluding the
617 sample VCR-1, notably the closest one to the inferred sedimentary/volcanic transition in
618 Figure 11, all the soils developed above volcanic deposit show higher amount of AM+Cpx
619 (>12) in comparison with the others soils analyzed in this study (Table 3).

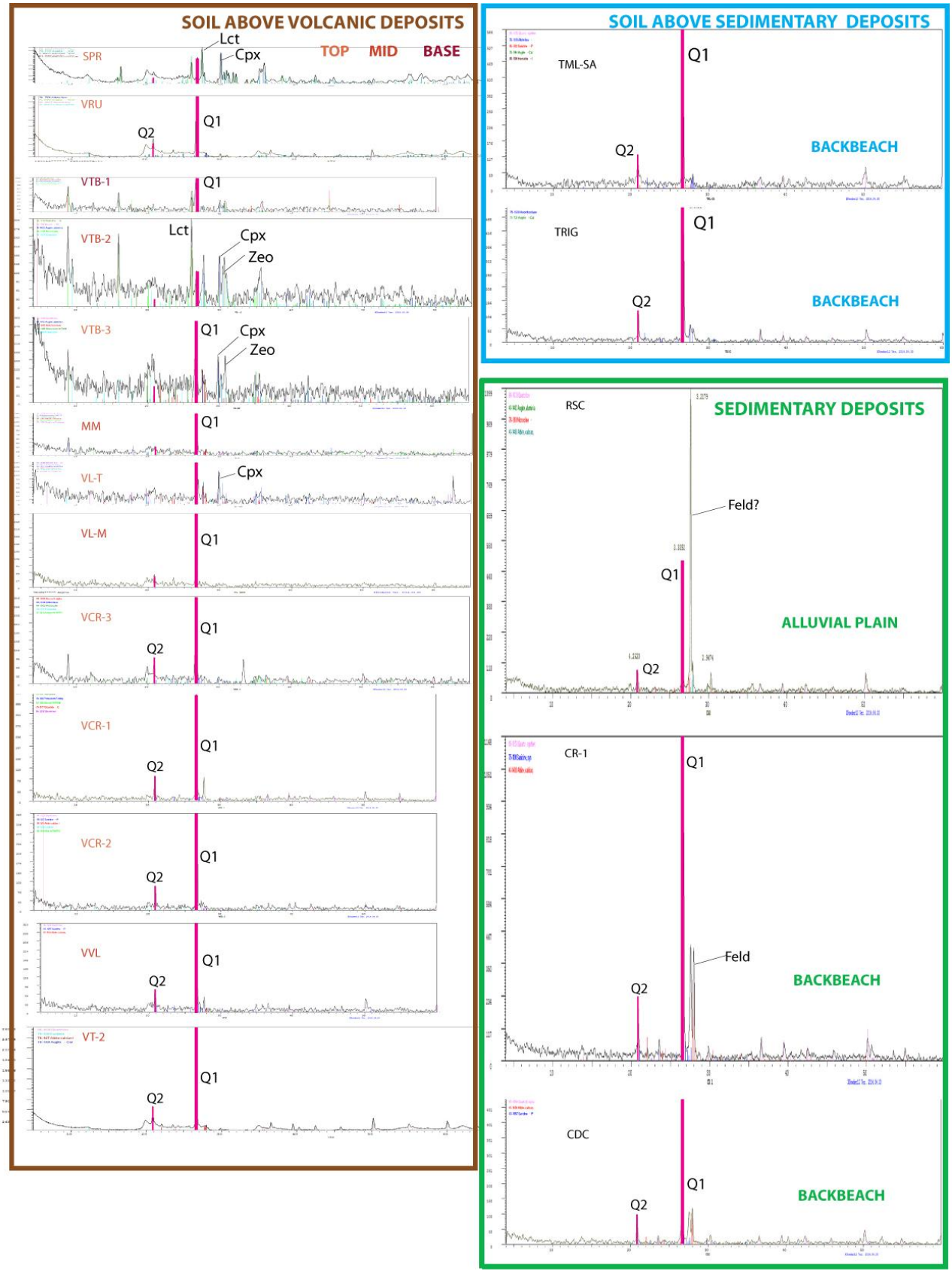

620

621 Figure 10 - Diffractograms of the soil and sediment samples. In inset a' diffractograms are...
622 Vertical axes are normalized to the same scale; full-resolution original diagrams are provided
623 in Suppl. Mat. #1B. See text for comments.
624

Moreover, quartz abundance decreases with the distance from the inferred paleo-shoreline in soils developed above the volcanic substrate. In order to verify this observation, we have collected two samples in the inland sector at the foot of the Colli Albani peri-caldera ring (SPR and RUT, Figure 11) and we have normalized results of diffractometric analyses peformed with a different equipment (see Methods in Supplementary Material #2) by re-analizing samples VTB-1 and VTB-3 with them (Table 3). As shown in Figure 10 and Tabkle 3, Q1 peaks and AM+Cpx/Qz are the highest one for thesec samples.

Apart for the discriminating AM+Cpx/Qz ratio, diffractograms of soils above sedimentary deposits differ from those above volcanic deposits only for the slightly larger magnitude of the main quartz peak Q1, and for the presence of a second quartz peak close to 10 (Q2). These peaks are much higher in the sediment samples which also display a remarkable peak corresponding to the pyroxene. Finally, the smaller magnitude of the quartz and pyroxene peaks in the fine sediment sample CDC suggests that magnitudes are also proportional to grainsize of the siliciclastic component.

Abundance, dimension and morphology of the Quartz and K-feldspar grains occurring in selected samples (VTB-1, TML-SA, VCR-1, CR1) have been analyzed at the SEM and discussed in section 5.1. Microphotographs are provided in Supplementaerty Material #2.

	SOILS ABOVE VOLCANIC DEPOSITS															SOILS ABOVE SEDIMEMNTARY DEPOSITS				
	VTB-1	VTB-2	VTB-1	VV	VL-M	VL-T	MM	VTB-1*	VTB-3*	VRU*	SPR*	VdT-2*	VCR-3	VCR-2	VCR-1	TRIG	TML-SA	RSC	CDC	CR-1
Amorphous	305	240	8000	58	54	121	45	68	9900	6100	8500	4750	80	70	30	52	59	55	45	110
Qtz	290	122	8000	320	270	147	150	0	20700	15977	6650	26343	316	349	394	520	586	1099	501	1168
Cpx	165	165	11500	0	10	118	15	40	9300	750	8000	550	25	0	10	20	20	40	20	0
TOT	760	527	27500	378	334	386	210	108	39900	22827	23150	31643	421	419	434	592	665	1194	566	1278
Amorphous	40	46	29	15	16	31	21	63	25	27	37	15	19	17	7	9	9	5	8	9
Qtz	38	23	29	85	81	38	71	0	52	70	29	83	75	83	91	88	88	92	89	91
Cpx	22	31	42	0	3	31	7	37	23	3	35	2	6	0	2	3	3	3	4	0
TOT	100	100	100	100	100	100	100	100	100	100	100	100	100	100	100	100	100	100	100	100
Qtz/Cpx+AM	0,6	0,3	0,4	5,5	4,2	0,6	2,5	0,0	1,1	2,3	0,4	5,0	3,0	5,0	9,9	7,2	7,4	11,6	7,7	10,6
Cpx+AM	62	77	71	15	19	62	29	100	48	30	71	17	25	17	9	12	12	8	11	9

Table 3 - X-ray powder diffraction (XRPD) data. Summary of absulte abundances of mineral phases in the analyzed samples (*samples analyzed with a different equipment, see Methods in Supplementary Material #2).

CR3	
Age (ka)	± 2σ (ka)
127,7	**± 11,3**
130,9	**± 11,2**
131,0	**± 9,6**
131,7	**± 9,7**
133,4	**± 13,7**
134,0	**± 14,3**
138,3	**± 6,3**
140,6	**± 12,5**
169,5	± 6,9
169,7	± 11,7
177,6	± 8,3
198,4	± 7,3
245,3	**± 6,6**
249,9	**± 7,2**
250,7	**± 6,5**
251,6	**± 6,6**
298,9	± 5,6
375,6	± 4,9
379,1	± 5,6
392,9	± 9,6
393,5	± 4,8
400,2	± 4,6
401,4	± 5,1
403,6	± 4,7
407,3	± 5,6
407,8	± 4,6
410,7	± 6,5
416,5	± 3,5
418,1	± 4,6
421,7	± 3,8
446,8	± 4,6
459,2	± 5,1
495,5	± 6,5
498,4	± 4,8
503,2	± 4,1
1289,3	± 6,5
1289,9	± 3,9
1293,0	± 6,9
1313,1	± 3,5
youngest population:	
134,2	**± 3,5**
249.3	**± 3.4**

TML-SA	
Age (ka)	± 2σ (ka)
151,1	**± 27,6**
165,5	**± 28,5**
166,6	**± 27,9**
171,0	**± 24,9**
181,7	**± 25,4**
189,3	**± 54,3**
216,5	± 6,0
239,9	± 4,7
246,2	± 17,8
250,0	± 6,6
252,3	± 7,1
257,6	± 5,1
262,8	± 22,7
266,0	± 20,0
287,5	*± 72,5*
316,8	± 18,7
329,8	± 20,8
335,5	± 96,7
351,5	± 15,7
361,0	± 40,6
368,2	± 32,7
369,5	± 20,0
371,2	± 21,5
372,6	± 18,7
382,2	± 23,2
389,6	± 23,0
398,9	± 16,2
409,6	± 5,9
422,9	± 63,3
430,5	± 10,9
435,7	± 8,7
446,4	± 5,6
504,4	± 5,6
541,7	± 5,0
549,4	± 5,4
551,8	± 4,3
557,0	± 40,2
589,3	± 4,4
600,0	± 6,4
1328,9	± 8,0
1339,3	± 15,9
youngest population:	
169	**± 11**

CSR-SA	
Age (ka)	± 2σ (ka)
232,3	**± 19,8**
240,9	**± 8,2**
244,5	**± 5,7**
246,8	**± 6,9**
263,1	± 4,6
263,7	± 29,1
310,1	± 16,3
395,5	± 5,0
407,9	± 4,4
476,6	± 7,1
488,3	± 5,3
494,5	± 4,7
500,8	± 6,8
508,5	± 3,5
542,1	± 17,2
552,1	± 9,0
563,1	± 6,2
597,3	± 3,7
625,7	± 6,7
805,2	± 9,7
youngest population:	
244.0	**± 3.8**

CAR-SA	
Age (ka)	±1σ (ka)
298,19	**± 3,50**
397,35	± 2,69
397,55	± 2,50
401,16	± 3,23
401,50	± 6,70
401,92	± 4,30
409,08	± 4,09
409,45	± 2,28
410,43	± 3,01
416,80	± 2,14
417,80	± 1,90
417,86	± 27,38
420,18	± 3,26
430,43	± 2,92
447,50	± 15,16
461,11	± 3,89
468,78	± 18,49
523,49	± 3,21
566,40	± 2,82
580,99	± 3,19

Table 4 - 40Ar/39Ar ages of dated samples

659 **4.6 $^{40}Ar/^{39}Ar$ data**

660 Single crystal age data for the three analyzed samples are reported in Table 4. Full analytical
661 data are proved in Supplementary Material #3.

662 **4.6.1 Sample CR3**

663 Thirty-nine sanidine crystals extracted from the sand sample collected ca. 90 cm below the
664 ground surface in Colle Rotondo provided a wide age spectrum, ranging 1.31 through 0.13 Ma.
665 A youngest population of eight crystals yielded a weighted mean age of 134±3.5 ka.

666 **4.6.2 Sample TML-SA**

667 Forty-one sanidine crystals extracted from the sand sample collected ca. 60 cm below the
668 ground surface in Tenuta Monte di Leva provided ages ranging 1.34 through 0.15 Ma. A
669 youngest population of six crystals yielded a weighted mean age of 169±11 ka.

670 **4.6.3 Sample CSR-SA**

671 Twenty sanidine crystals extracted from the sample collected in the fluvial sand cropping out
672 in Castel Romano provided ages ranging 0.80 through 0.23 Ma. A youngest population of four
673 crystals yielded a weighted mean age of 244±4 ka.

674 **4.6.4 Sample RSC-SA**

675 Twenty sanidine crystals extracted from the sample collected in the fluvial sand cropping out
676 in Riserva Carpineto provided one isolated, youngest crystal of 298±3.5 ka. The majority of
677 the crystal ages are spread in the interval 398-468 ka, with three oldest crystals ranging 523 -
678 581 ka.

679

680 **5. Discussion**

681 **5.1 Soils and paleo-surfaces**

682 Analysis of soil samples for the present study has been conducted aimed at identifying their
683 sedimentologic and petrographic features, in order to understand their origin and the
684 paleogeographic conditions in which they formed. Pedologic considerations and a complete
685 study of the processes involved the formation of these soils, as well as laboratory
686 granulometric analyses are beyond the scope of the present work. Our main scope is to verify
687 to what extent the present ground surfaces characterized by the same elevations range
688 represented in Figure 2 and 3 can be considered indicative of the original paleo-surfaces
689 representing the ancient coastal settings. In particular, we want to quantify the possible
690 amount of later deposition, or erosion, which may have increased or decreased, respectively,
691 the average elevation of these paleo-surfaces, therefore affecting our estimation of the sea-
692 level related with the corresponding coastal terrace.

When studying the composition of the soils developed above the reconstructed paleo-surfaces, some preliminary considerations are necessary. In particular, when the paleo-surfaces of highest order are considered (i.e. those ranging 98-108, 80-89, and 71-79 m a.s.l., Figure 3), we must realize that the sub-horizontal attitude of these isolated, plateau-like sectors precludes alluvial sedimentation, almost completely. Furthermore, the whole catchment area drained by these paleo-surfaces is developed above volcanic deposits. Therefore, the siliciclastic component of the soils above the paleo-surfaces of this sector, which in the X-ray diagrams is sometimes predominant, can only have the following two origins:

i. it can be a back-beach to coastal plain sediment originally deposited above the volcanic substrate when the paleogeographic conditions allowed (i.e.: before the regional uplift, when the paleo-surface represented a coastal environmental setting) (BB and AL in Figure 11a);

ii. it can be an aeolian sediment (i.e., loess-like) accumulated above the volcanic deposits through air-fall emplacement and successively diffused within the soil by vertic processes (i.e.: internal turnover of soil material originated by pedogenetic processes).

Recognizing the origin of this siliciclastic sediment is therefore fundamental in order to reconstruct the paleogeographic setting of these paleo-surfaces, correctly, as shown in Figure 11, in which the paleogeographic scenario is illustrated. The dashed green line in Figure 11 separates the sampling sites where field observation have shown that the present soil overlies sedimentary sand deposits (to the southwest), from those where the soil is developed above the volcanic deposit of Pozzolanelle (to the northeast), as reported also in the cross-section of Figure 12. The oblique green lines indicate the area where the siliciclastic fraction in the analyzed soils is predominant.

Composition of the analyzed soils overlying the volcanic deposit of Pozzolanelle, with abundant quartz and feldspar, combined with micromorphological and SEM analyses which confirm the sedimentary origin of the quartz grains but rule out an aeolian (loess-like) origin, at least for the larger fraction (>200 μm; Figure S7), demonstrate that these soils affect thin (≤ 1 m) layers of alluvial and backbeach, predominantly siliciclastic deposits. In keeping with this interpretation, quartz abundance strongly decreases in soil samples collected in more inland locations (SPR, RUT), far from the inferred paleo-coastline (Figure 10).

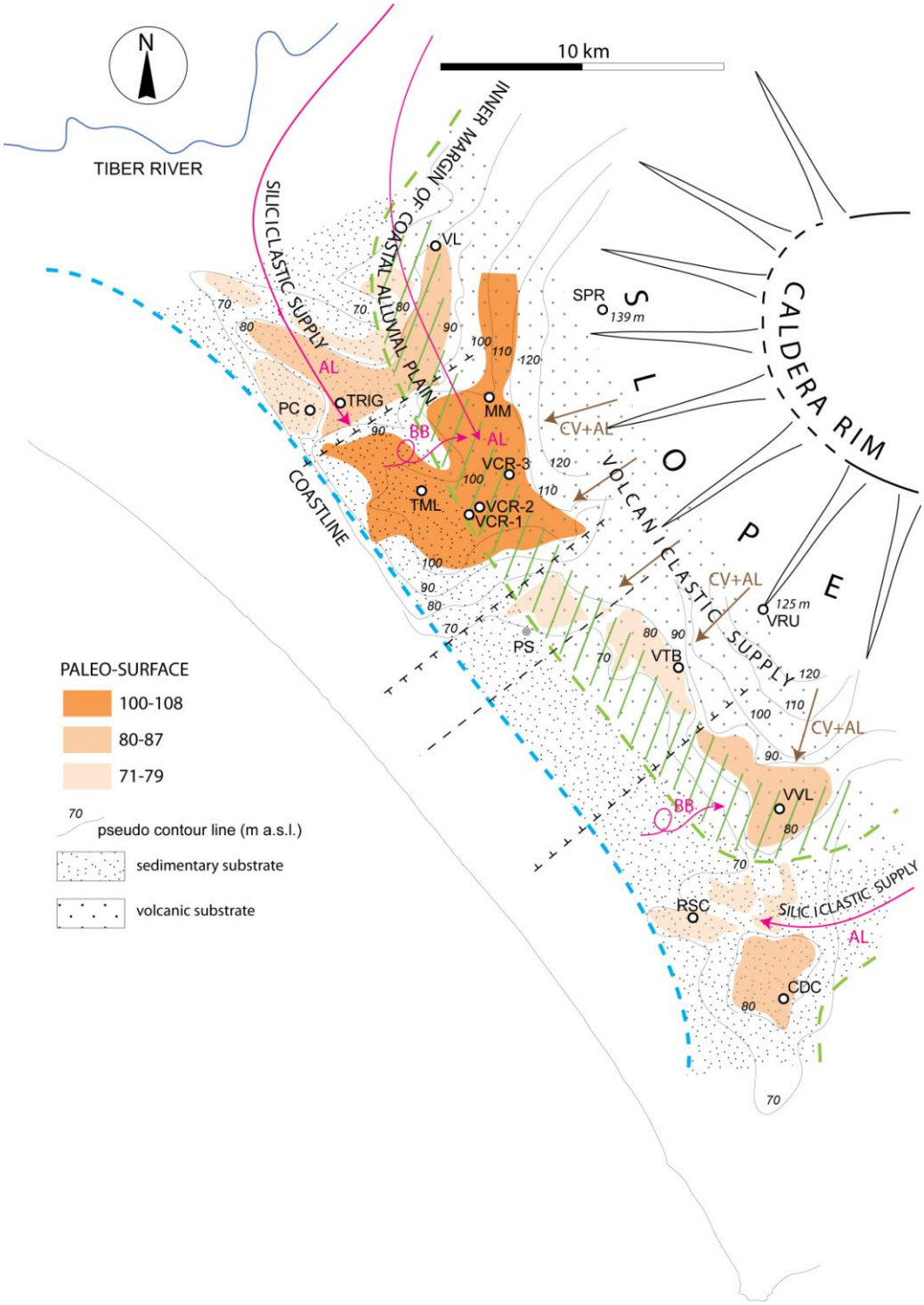

Figure 11- Paleogeographic reconstruction of the MIS 9 coastal setting. Stratigraphic investigations and sedimentologic, micromorphologic, mineralogic and petrographic analyses on sediment and soil samples have allowed to detect a transitional zone (oblique green dashes) corresponding with the inner margin of the coastal plain, where a thin horizon of backbeach to alluvial deposits overlaps the volcanic substrate. (see also cross-section in Figure 12a). This reconstruction evidences the occurrence of an original, homogeneous paleo-surface, subsequently disrupted and dislocated by tectonic movements, which gave rise to three main flat sectors at elevations ranging 100-108, 80-87, and 71-79 m a.s.l. (see text for comments).

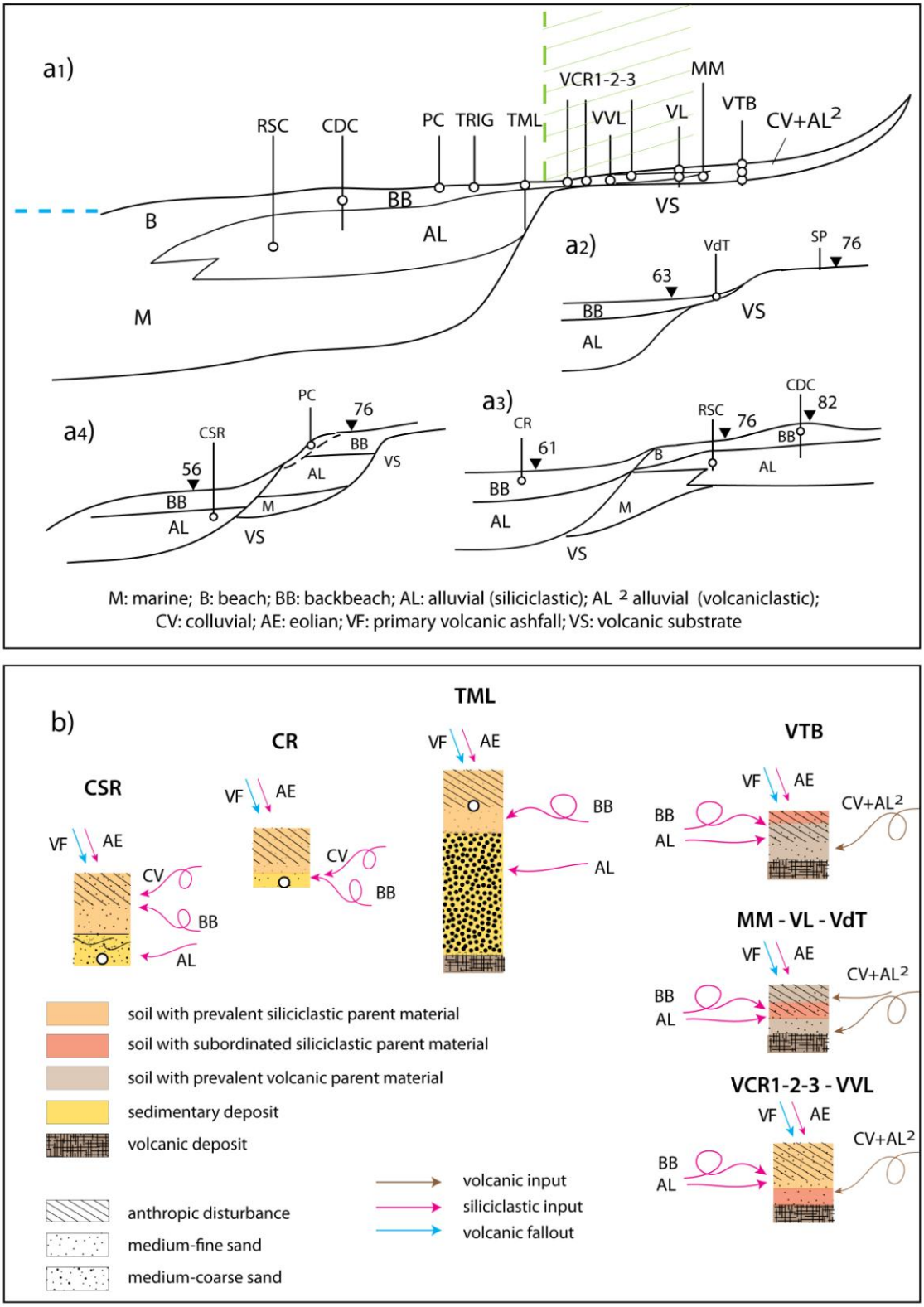

Figure 12 - a1-4) Cross-sections restored from tectonic dislocation showing the original paleogeographic and sedimentary settings reconstructed in the area where the soil and sediment samples were collected. b) Origin of the different sedimentary inputs contributing to the formation of the deposits and the related soils at the top of the paleo-surfaces reconstructed in the present study. See text for comments.

Alluvial/colluvial volcanic material (CV+AL in Figure 112b and 12), derived from the rocks cropping out at the inner margin of the coastal alluvial plain (green dashed area in Figure 11), were also continuously mixing with the alluvial and backbeach, predominantly siliciclastic deposits transported by the Tiber River and deposited in the coastal plain. Moreover, air-fall material including either loess-like sediment (AE in Figure 12b), or as primary air-fall volcanic ash (VF in Figure 12b), also progressively accumulated above this soils and was diffused by vertic processes into the sub-surface horizon. To this aeolian fraction must be ascribed part of the K-feldspar observed in this section and evidenced in the diffractograms, as well as part of the finest siliciclastic component.

Such an air-fall contribution must be extended to the soils developed above the sedimentary deposits, in which the volcanic component is also represented by re-deposited mineral species of the underlying sedimentary substrate, incorporated in the soil through colluviation, surface water and wind transport (CV in Figure 12b).

These mechanisms are envisaged in Figure 12, showing the different paleogeographic and sedimentary settings reconstructed in the area where the soil and sediment samples were collected. The age spectra provided by sanidine crystals extracted from the lowest portion (unaffected by agricultural disturbance) of the backbeach deposits above which the soils of the 98-108 and of the 61-67 paleo-surfaces have developed (TML-SA, CR3; Figure 13), compared to that of the "sealed" sedimentary deposit of the fluvial facies (RSC-SA, CSR-SA), provide further insights to the processes described above.

5.2 Age of the paleo-surfaces

Youngest crystal ages of 232±20 and 298±4 ka yielded by sedimentary samples collected in the alluvial facies (coastal plain) of the 51-57 m and of 71-79 m paleo-surfaces (CSR-SA and RSC-SA) support correlation with MIS 7 and MIS 9 for the corresponding coastal terraces, as discussed in the following sections.

Similarly, crystal ages of the samples collected from the backbeach facies at the top of the 98-108 m and 61-67 m paleo-surfaces provide time constraints on the sedimentary processes that acted in the time span following retreat of the coastline leading to progressive impoverishment of sediment supply.

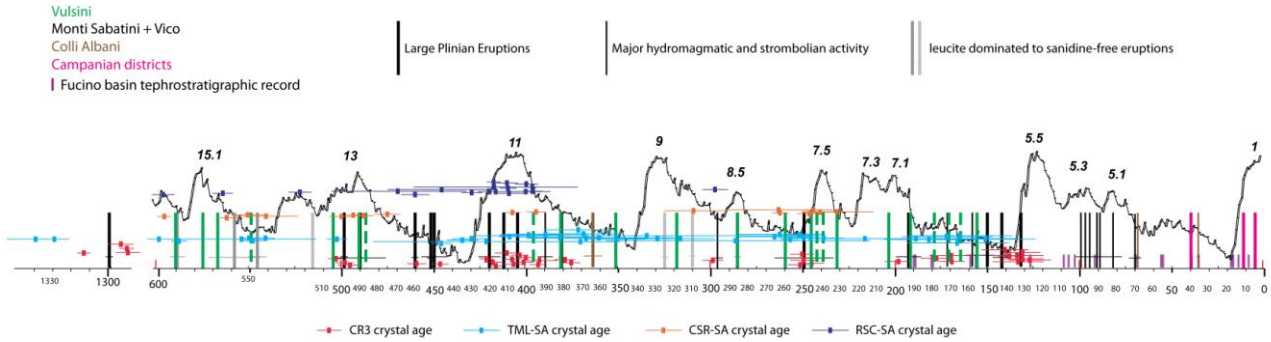

Figure 13 - Crystal age spectra for the four sedimentary samples dated in the present study. Each cross represents the age of one dated sanidine crystal with the associated analytical error at 2 σ. Comparison with the major eruptions occurred at the districts of the Roman Co-magmatic province is provided. Each bar represents one eruption age (see Suppl. Mat. for details and references). Comparison with the oxygen isotope curve (Lisiecki and Raymo, 2005) is also shown. See text for comments.

These age constraints are obtained by comparing the sample crystal ages with the eruptive histories of the volcanoes of the Latium Region, as provided in Figure 13. In considering the eruptive histories of the volcanic districts of Central Italy to compare age spectra yielded by the analyzed sedimentary samples reported in Figure 13, some preliminary considerations should be made.

i- These volcanoes are part of the "Roman Magmatic Province" (Conticelli and Peccerillo, 1992), characterized by a K-rich geochemistry which accounts for the diffuse presence of sanidine ($KAlSi_3O_8$) and leucite ($K[AlSi_2O_6]$) crystals, which also constitute the means of $^{40}Ar/^{39}Ar$ dating. However, while sanidine is a very resistant mineral species, leucite is highly sensible to weathering and easily alters to analcime ($NaAlSi_2O$): a process implying loose of K andcompromising $^{40}Ar/^{39}Ar$ dating. Indeed, fluvially transported and beach deposits of several hundred kyr lack pristine leucite crystals. Therefore, in Figure 13 we have not reported all the sanidine-free eruption units (i.e., most of those of the Colli Albani volcanic district, see Gaeta et al., 2016 and references therein), while we have indicated those dominated by leucite (for which a lesser statistical occurrence is expected).

ii- When incorporation of crystals derived from primary fallout deposits is considered, the overall eastward regional winds and a consequent dispersal axis should be considered, along with the distance from the source area. Therefore, the major source of fallout deposits are the MSVD and Vico, while deposits from the Colli Albani and the Campanian districts have a low probability of representation in the stratigraphic record. One exception is represented by the sanidine-bearing activity of the Albano Center spanning 70 through 36 ka (Giaccio et al., 2009, and ref.), for which the small vent distance should have led to a well-represented crystal population, as also evidenced by outcrops in the southeastern area of the CAVD (e.g., Cisterna

di Latina, Latina Plain; Gatta et al., 2018, Sevink et al., 2018). Moreover, huge explosive eruptions like the Campanian Ignimbrite (39 ka), Neapolitan Yellow Tuff (12 ka) and Avellino pumice (4 ka) have provided widespread tephrostratigraphic markers in Latium (e.g., Giaccio et al., 2017).

iii- The youngest eruptions should be better represented given the larger outcrop areas of the products in comparison with the older ones, which are buried under more recent cover. This reinforces the principle that a lack of crystals younger than the youngest population is evidence of deposition prior to the immediately following eruption.

Consistent with the considerations above, Figure 13 shows that the age spectra of sanidine crystals extracted from the four sand samples record a long eruptive history, ranging 0.60 - 0.13 Ma, plus one isolated cluster around 1.3 M. All crystal ages ≤0.6 Ma match known eruptions of the Monti Sabatini, Vico and Vulsini volcanoes (Palladino et al., 2010; Sottili et al., 2010; Marra et a., 2014, and ref. therein), while the oldest age matches that of early activity of the Cimini volcanic complex (Everdin and Curtis, 1965, Nicoletti, 1969), located in the upper Tiber Valley east of Vico. In contrast, all theeruption ages known from the literature that are missing in the dated crystal populations, besides the sanidine-free Colli Albani products, also correspond to sanidine-free or leucite-dominated products from Vico and Monti Sabatini volcanic districts (Cioni et al., 1987; Sottili et al., 2004; Perini et al., 2004; Masotta et al., 2010; Marra et al., 2014).

Based on these premises, in the following we discuss sample age implications on assessing the age of the related paleo-surfaces.

5.2.1 CSR-SA - 51-57 m paleo-surface

Based on the sedimentary features of the underlying deposits and the top elevation ranging 51-57 m a.s.l. (Figure 9a-a"), the Castel Romano paleo-surface is interpreted as a backbeach context, including the dune system superimposing the delta plain, developed during highstasnd of MIS 7.3/7.1. Loose sanidine crystals occurring in the sand deposit of the braided fluvial channel facies (Figure 9a'-a") yielded a youngest age of 232.3±19.8 ka, part of a statistically significant youngest population of 244.0±3.8 ka (Table 4). Such datum has to be considered a terminus post-quem which implies an age ≤ MIS 7.5 (Figure 13), excluding and age within MIS 9 and supporting correlation with highstand of the MIS 7.3/7.1.

5.2.2 RSC-SA - 71-79 m paleo-surface

The age spectrum of sample RSC-SA, collected within the alluvial plain deposit underlying the 71-79 paleo-surface at Riserva Carpineto, spans 581 - 398 ka, with a youngest crystal of 298±3.5 ka (Table 4). Most crystal ages are clustered between 460 and 390 ka, coincident with the large explosive phases emplacing sanidine-bearing products at Vico and Sabatini in this time span (Figure 13). In contrast, no crystal deriving from the Villa Senni eruption unit occurs in the dated sample, despite the sampled deposit overlies the Pozzolanelle eruption unit of 365±4 ka, consistent with the lack of sanidine phenocrystals in the Colli Albani products. The age of one single crystal yielding 298±3.5 ka has a poor statistical weight, and should be regarded as broadly indicative of the lack of crystals younger than 300 ka. However, it supports correlation with MIS 9 for the 71-79 m paleo-surface of Riserva Carpineto, suggesting that sedimentation in the alluvial plain was sealed in the late stages of the MIS 9 highstand, excluding an age within MIS 7, while an age within MIS 11 is also excluded by the fact that the sand deposit of Riserva Carpineto overlies the 365±5 ka Pozzolanelle pyroclastic-flow deposit.

5.2.3 CR3 - 61-67 m paleo-surface

Based on its sedimentologic features and the elevation ranging 61-67 m a.s.l., the Colle Rotondo paleo-surface is interpreted as a backbeach context, either part of a dune system or of a coastal alluvial plain, developed during highstasnd of MIS 7.5 (Figure 14a).

When the crystal ages from CR3 (red crosses in Figure 13) are compared to the eruptive histories of the volcanoes of the Latium Region, it is apparent that no eruption younger than 134±3.5 ka is recorded by the Colle Rotondo sand deposit. Indeed, given the large number of dated crystals (39) and the wide age spectrum observed, the lack of any crystal from the eruptive activity since 99 ka (see Figure 13) strongly suggests that the sample age should be constrained between 132 and 99 ka. In particular, a large hydromagmatic phase occurred in several volcanic centers of the MSVD, including Baccano, Stracciacappe, Le Cese, Acquarello, Piana dei Falliti and Martignano, 132±2 through 70±3 ka (Sottili et al., 2010; Marra et al., 2019b). While the earliest eruption that occurred at Baccano at 132±2 ka is evidently recorded by sample CR3, the lack of crystals from any later eruption strongly suggests a terminus ante-quem of ca. 99±3 ka (age of the products of the 2nd Baccano unit, erupted at the beginning of the multi-vented hydromagmatic activity that continued until 70±3 ka). Although this age boundary to the deposit is in conflict with the attribution to the Uluzzian for the lithic industry recovered at Colle Rotondo (Villa et al., 2018), we note that sample CR3 was not collected in the stratum in conjunction with the artifacts, but in a side excavation.

Therefore, its correspondence with the archaeological layer is not safely established and provenance may be from the immediately underlying older substrate. In this latter case, the occurrence of the Uluzzian lithic assemblage at ca. 80 cm depth suggests that the overlying package of sediment accumulated during the last 40 ky. Such an accelerated accumulation may be linked with recent anthropic activity (e.g., agriculture), triggering soil mobilization. In contrast, the apparent age of ~134 ka for the sand layer at 80 cm depth does not conflict with an inferred age of 250-200 ka within MIS 7 for the Colle Rotondo paleo-surface, as discussed hereby based on a detailed analysis of the $^{40}Ar/^{39}Ar$ dating results.

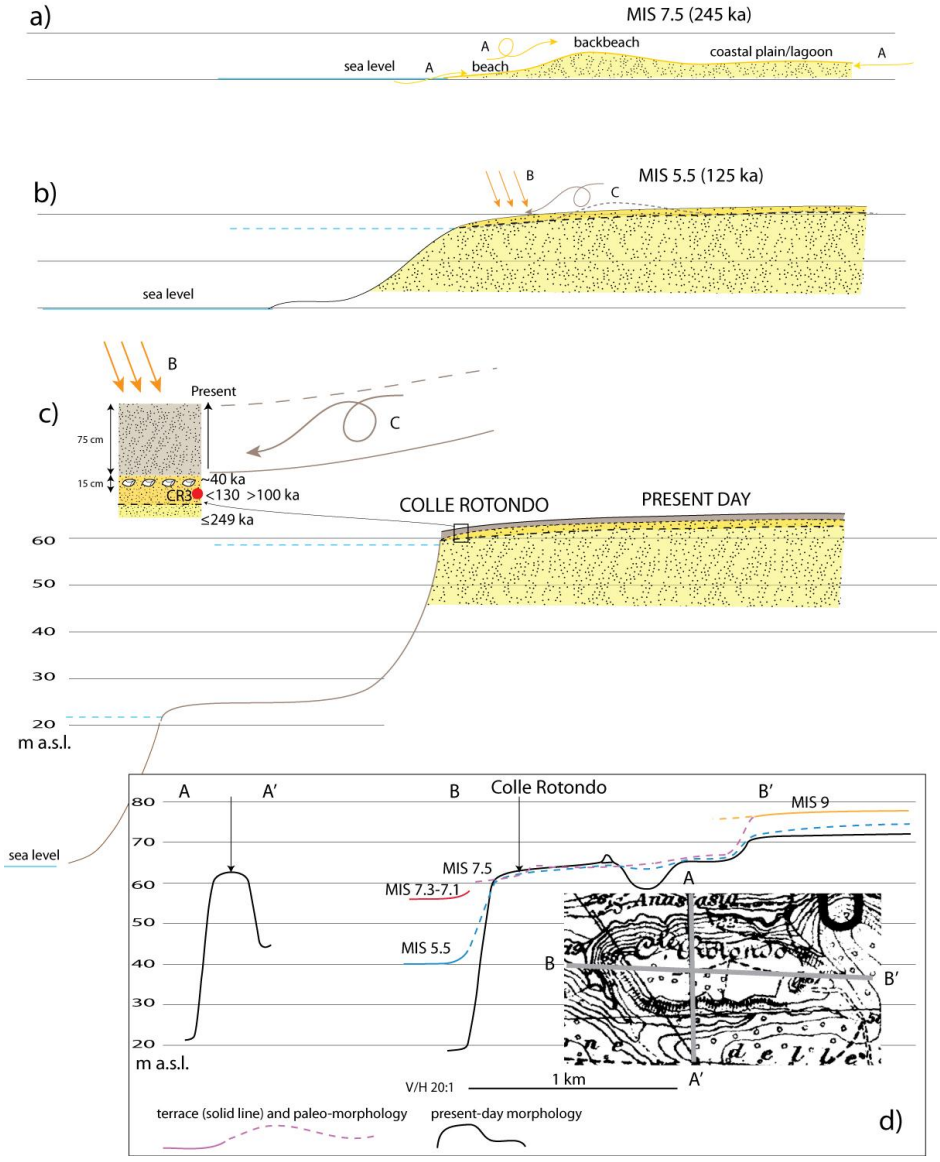

Figure 14 - Geomoprphological and paleogeographic evolution of the Collo Rotondo plateau (see text for step by step comment and explanation).

Like in the case of the sedimentary deposit sampled at Castel Romano which yielded a youngest crystal age of 232±20 ka, consistent with a deposition age corresponding to the highstand of MIS 7.3-7.1 (i.e. 220-200 ka), an age ≥245 ka is expected for the fluvial/beach

889 sedimentary deposit at Colle Rotondo (supply A in Figure 14a) incorporating crystals derived
890 from erosion and re-deposition of the volcanic rocks erupted before that time, corresponding
891 to highstand of MIS 7.5 (i.e., 245 ka, see Figure 13). However, a progressively younger age is
892 expected for the backbeach deposit deriving from mixing of wind-blown sediment previously
893 deposited (supply C in Figure 14b) with crystals deriving from primary eruptions occurring in
894 the following time span (supply B in Figure 14b). Sample CR3 from Colle Rotondo yielded a
895 statistically significant (8 crystals) youngest crystal population of 134.2±3.5 ka which is
896 characterized by significantly larger associated errors in comparison with the older
897 populations (see Table 5). In particular, these crystals yielded an average associated error of
898 ±11 ka (corresponding to 8.2% when an age of 134 ka is considered) in comparison with an
899 average associated error of ±5.4 ka for the 23 crystals yielding ages spanning 249.9 - 503.2 ka
900 (corresponding to 2.2% - 1.1%). These larger errors are due to the systematically smaller
901 dimensions of these crystals, evidencing their different means of transport in comparison
902 with that affecting the oldest ones, i.e.: wind vs. water. When this distinction is taken into
903 account, we find a second significant population age of 249.3±3.4 ka, along with a few crystal
904 ages ranging 200-170 ka (Table 4 and Figure 13), consistent with an age within MIS 7.5 for
905 the original beach/alluvial deposit. An age ≥134±3.5 ≤198.4±7.3 ka is established for the
906 sampled backbeach deposit, showing that it accumulated above the MIS 7.5 paleosurface
907 during ca. 110 ky (i.e., 245 through 134 ka). The lack of crystals deriving from the eruptions
908 between 132 and 70 ka at the MSVD (see Figure 13), strongly suggests that the sampled layer
909 cannot be younger. Indeed, accidental absence of crystal ages within this time span is
910 statistically unlikely, given the eastern dispersal axis of the MSVD eruption (e.g. Sottili et al.,
911 2004; Di Rita and Sottili, 2019) and the occurrence of large explosive eruptions 90 through 70
912 ka at a number of centers of the so-called "Hydromagmatic Phase" (De Rita et al., 1983; Sottili
913 et al., 2010; Marra et al., 2019b). This fact also testifies that the depositional context
914 progressively changed after 245 ka, consistent with continued uplift of the coast and isolation
915 of the Colle Rotondo remnant paleo-surface, which was unaffected by deposition of water
916 transported sediment, like that occurring in alluvial plain or beach contexts, while only eolian
917 fallout deposits were emplaced, from then on. Since sample CR-1 occurs 90 cm below the
918 present ground level (Figure 14c), we can infer that present elevation of 63 m is a close
919 approximation of the MIS 7.5 paleo-surface, which is overlain by a thin eolian deposit
920 accumulated since 245 ka (input B in Figure 14c). Indeed, it is likely that samples collected
921 closer to the surface would yield progressively younger ages, consistent with incorporation of
922 crystals deriving from the younger eruptions of 100 ka and 90 through 70 ka. However, the

strong anthropic disturbance of the upper 70 cm of sediment prevents any reliable analysis. Sample TML-SA from Tenuta Monte di Leva section provides further inferences on the formation process of this thin eolian cover of the paleo-surfaces.

927

928

CR3	
Age (ka)	± 2σ (ka)
134,0	**± 14,3**
133,4	**± 13,7**
140,6	**± 12,5**
169,7	± 11,7
127,7	**± 11,3**
130,9	**± 11,2**
131,7	**± 9,7**
131,0	**± 9,6**
392,9	± 9,6
177,6	± 8,3
198,4	± 7,3
249,9	± 7,2
169,5	± 6,9
1293,0	± 6,9
245,3	± 6,6
251,6	± 6,6
250,7	± 6,5
410,7	± 6,5
495,5	± 6,5
1289,3	± 6,5
138,3	**± 6,3**
298,9	± 5,6
379,1	± 5,6
407,3	± 5,6
401,4	± 5,1
459,2	± 5,1
375,6	± 4,9
393,5	± 4,8
498,4	± 4,8
403,6	± 4,7
400,2	± 4,6
407,8	± 4,6
418,1	± 4,6
446,8	± 4,6
503,2	± 4,1
1289,9	± 3,9
421,7	± 3,8
416,5	± 3,5
1313,1	± 3,5
youngest population:	
134,2	**±3,5**

929

930

TML-SA	
Age (ka)	± 2σ (ka)
335,5	± 96,7
287,5	± 72,5
422,9	± 63,3
189,3	**± 54,3**
361,0	± 40,6
557,0	± 40,2
368,2	± 32,7
165,5	**± 28,5**
166,6	**± 27,9**
151,1	**± 27,6**
181,7	**± 25,4**
171,0	**± 24,9**
382,2	± 23,2
389,6	± 23,0
262,8	± 22,7
371,2	± 21,5
329,8	± 20,8
266,0	± 20,0
369,5	± 20,0
316,8	± 18,7
372,6	± 18,7
246,2	± 17,8
398,9	± 16,2
1339,3	± 15,9
351,5	± 15,7
430,5	± 10,9
435,7	± 8,7
1328,9	± 8,0
252,3	± 7,1
250,0	± 6,6
600,0	± 6,4
216,5	± 6,0
409,6	± 5,9
446,4	± 5,6
504,4	± 5,6
549,4	± 5,4
257,6	± 5,1
541,7	± 5,0
239,9	± 4,7
589,3	± 4,4
551,8	± 4,3
youngest population:	
169	**±11**

931
932
933
934
935
936 Table 5
937
938
939

940

CSR-SA	
Age (ka)	± 2σ (ka)
263,7	± 29,1
232,3	**± 19,8**
542,1	± 17,2
310,1	± 16,3
805,2	± 9,7
552,1	± 9,0
240,9	**± 8,2**
476,6	± 7,1
246,8	**± 6,9**
500,8	± 6,8
625,7	± 6,7
563,1	± 6,2
244,5	**± 5,7**
488,3	± 5,3
395,5	± 5,0
494,5	± 4,7
263,1	± 4,6
407,9	± 4,4
597,3	± 3,7
508,5	± 3,5
youngest population:	
244	**±4**

941
942

5.2.4 TML-SA - 98-108 paleo-surface

Much caution should be used in interpreting results for the TML-SA sample because it was collected ca. 60 cm below the ground level within the soil horizon, in which both vertic processes and anthropic disturbance might have caused incorporation of younger crystals from the uppermost portion of the stratum.

However, the age spectrum of sample TML-SA, collected on the 98-108 paleosurface, is similar to that of CR3 but yields a youngest minimum age of 169±11 ka (Figure 13), evidencing a relative older age, with respect to the sample collected on the 61-67 paleosurface of Colle Rotondo.

These data suggest that the sampled sand deposit represents a sedimentary horizon that was sealed from air-fall input by 170 ka, supporting the notion that the uppermost portion of the reconstructed paleo-surfaces represents an accretionary horizon, built up mainly through accumulation of alluvially/colluvially transported and, subordinately, air-fallen material. Remarkably, also in this sample the youngest crystal population is characterized by larger associated errors (Table 5), supporting the different mean of transport for this sedimentary fraction which accumulated later, as an air-fall deposit above the underlying deposits of the alluvial plain.

The very low sedimentation rate and the limited thickness of these accretionary horizons overlying the "pristine" deposits forming the paleosurfaces, whose absolute age has been determined by $^{40}Ar/^{39}Ar$ dating on "in stratum" samples from Castel Romano and Riserva Carpineto, is consistent with the geomorphologic features of the TML and CR sectors, precluding significant alluvial/colluvial sedimentation.

5.3 The MIS 9 paleo-surface

Geomorphological, lithostratigraphic, paleo-environmental and geochronological constraints obtained for the deposits of the 71-79 m paleo-surface, and part of the 80-89 m and 98-108 m paleo-surfaces, allow the identification of these paleo-surfaces as the remnant coastal terrace of the MIS 9 highstand, tectonically dislocated (Figure 11 and 15). The subrounded morphology, the medium to coarse grain-size and the high degree of sorting of the sand deposits at Riserva Carpineto (RSC) clearly indicate that the flat sectors at elevations ranging 71-79 m a.s.l. represent remnant parts of an alluvial coastal plain, stretching NW to SE parallel to the present coastline (Figure 11 and 12a3). Crystal ages yielded by sample RSC-SA firmly constrain the formation of this coastal plain within MIS 9 (see also Figure 16). The bedded deposits of Campo di Carne (CDC), ranging from coarse sand to silty clay, are suggestive of a

coastal alluvial plain, overlain by a transgressive backbeach deposit forming a wide dune ridge system culminating at ca. 85 m a.s.l. in this area (Figure 11 and 12a3), and equivalent to that occurring in Trigoria (TRIG) at analogous elevations (Figure 11 and Figure 12a1). Evidence from the Tenuta Monte di Leva (TML) site shows that this backbeach setting homogeneously extends parallel to the paleo-coastline, but it is presently displaced to a ca. 20 m higher elevation in this sector (Figure 15). Micromorphological analysis of the concretionary layer observed in the TML indicates that this massive horizon formed in alluvial to backbeach environment characterized by a water table close to the surface, consistent with the reconstructed paleogeographic conditions, whichshow that it was part of the coastal plain. The geologic substrate at TML is indeed identical to that at TRIG, apart from the larger thickness of the upper, aeolian sand horizon above the concretionary layer at the latter location, consistent with a post-depositional tectonic displacement between these two sectors and limited erosion at TML.

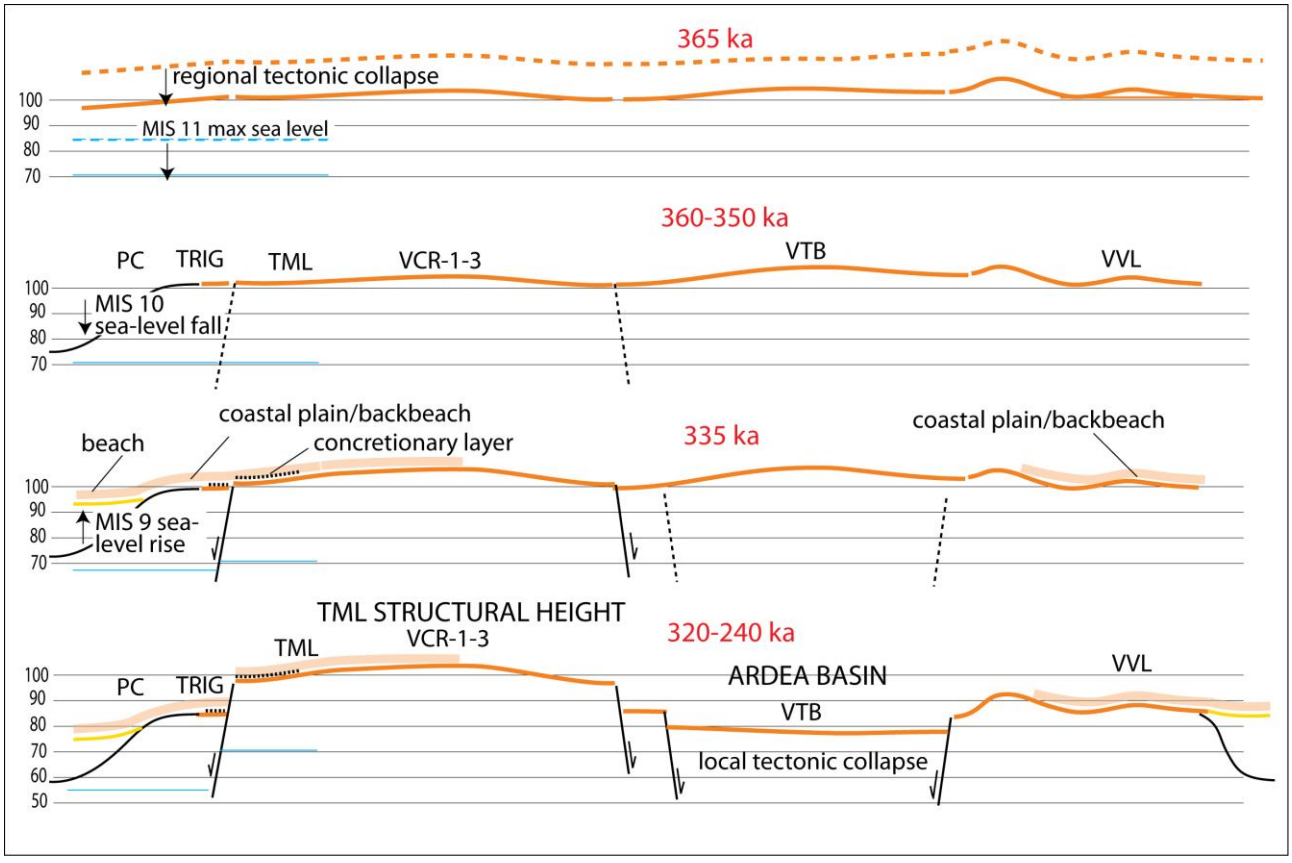

Figure 15 - Palinspastic reconstruction of the tectonic evolution of the coastal sector between the Tiber mouth and Anzio in the time span 365 ka (age of emplacement of the Villa Senni Eruption Unit during lowstand of MIS 10) and 240 ka (onset of MIS 7.5). a) A regional collapse immediately following emplacement of the pyroclastic flow-deposit is inferred from the elevation gain between the top surface of aggaddationasl successions of MIS 11 and MIS 9. MIS 11. b) Erosion of the original paleo-surface occurs during the lowstand of MIS 10, 360 through 350 ka. c) Fluvial and coastal incisions are filled by sediment-aggradation during glacial termination V (335 ka) at the onset of the sea-level rise during MIS 9, and a coastal

setting including a beach to backbeach and coastal plain environment forms during the MIS 9 highstand (325 ka). d) This homogeneous coastal setting is disrupted by fault displacement forming a structural heigh in the TML and a collapsed sector (Ardea basin) during the time span 320-240 ka (MIS 7.5 highstand) as indicated by the upper chrono-morphological constraint represented by the inner edges of MIS 7.5 coastal terrace (see text for further explanation).

On the other hand, the 98-108 paleo-surface represents a striking geomorphological anomaly bordering the Ardea Basin to the NW (see also Figure 4), and is clearly interpretable as the result of differential uplift at the footwall of a boundary fault of the half-graben structure (Figure 11 and 15). Also the different geologic substrate that characterizes the 71-79 m paleo-surface within the Ardea Basin (e.g., VTB), which is formed by volcanic deposits (i.e.: the same substrate as the inland portion of the 98-108 m paleo-surface in VCR 1-2), is suggestive of tectonic lowering following the formation of a homogeneous coastal platform during the highstand of MIS 9, throughout this region. In contrast, in the case of a pre-existing embayment in this area, the 71-79 m paleo-surface at VTB should have had the same sedimentary substrate as that occurring in PC and RSC, confirming a coastal environment. In particular, the tectonic collapse of the Ardea Basin is constrained between 320 ka (end of the MIS 9 highstand) and 240 ka (highstand of MIS 7.5) (Figure 15), as provided by the geometry of the 60-67 m and 51-57 m coastal terraces, indicating that an embayment formed by the time of establishment of the new coastline during MIS 7.5 through MIS 7.1 (see Figure 3 and 4). Remarkably, this time span is concident with the occurrence of the Monte delle Fate phase of activity at the Colli Albani Volcanic district (Gaeta et al., 2016, and references therein).

5.4 MIS 7.5 paleo-surface

The secure correlation with MIS 9 for the coastal plain deposits of the 71-79 m paleosurface, combined with previous geochronologic constraints that frame the 51-57m paleosurface within the broad MIS 7.5 - MIS 7.1 interval (Figure 16a), suggests that the intermediate 61-67 m surface should be correlated with the early interglacial 7.5, while the paleo-surface occurring a few meters below, at an elevation of 51-57 m, should be correlated with the later isotopic peaks 7.3/7.1 which are not separated by a marked sea-level fall (See Figure 16a), and can be regarded as a single eustatic event. Crystal age distribution yielded by sample CR3 from Colle Rotondo supports this correlation (Figure 16b). Based on the considerations reported above on the errors associated with the $^{40}Ar/^{39}Ar$ dating and their direct relation with grain-size, we can infer that an alluvial coastal plain formed by 249.3±3.4 ka, an age remarkably coincident with glacial termination III at the onset of MIS 7.5 (Figure 16b), at ca.

60 m a.s.l.. It was successively mantled by a wind-blown deposit derived from the nearby beach during the interval 200 - 170 ka, a time when the coastline rebounded to the elevation of 60 m a.s.l. during sea-level high stands linked with the double peak in the isotopes curve of MIS 7.3 and 7.1. Indeed, according to geomorphologic reconstruction, sedimentologic features, and micromorphologic analysis, the Colle Rotondo sand is a backbeach deposit. The sand grains originated mainly from very proximal aeolian transport from the beach, where the original sediment accumulated after being eroded and transported by the Tiber River and its tributaries (A in Figure 14a). Moreover, since formation of the dune ridge, more aeolian material, as well as primary, air-fallen volcanic deposits (including sanidine minerals, B in Figure 14a), accumulated above it. Eventually, this sector was isolated from the coastal environment by the continued uplift, and it was affected only by deposition of the syn-eruptive fallout deposit of the Baccano unit at 132±2 ka. If we consider the strong uplift of more than 50 m that occurred from 250 ka, the wind-blown depositional mechanism rapidly became ineffective, due to the increased elevation and distance from the coastline (e.g., by 125 ka, Figure 14b). The regional uplift, determining the deep incision of the coastal terrace through the action of fluvial erosion, also generated the canyon-like morphology that characterizes this area, isolating the Colle Rotondo plateau and preventing alluvial sedimentation on its top (Figure 14c-d). Therefore, it is reasonable to assume that a very limited thickness of sediment accumulated above the original paleo-surface representing the coastal terrace, mainly by the air-fall mechanism and only subordinately, as a consequence of re-mobilization of pre-existing sediment, through wind transport, or water run-off and colluviation from the upper part of the plateau towards the lower sectors (C in Figure 14b). If we consider that the elevation gain between the top and the margins of the Colle Rotondo plateau is less than 4 m (Figure 14d), the latter depositional mechanisms must have acted in a very limited way.

5.5 MIS 7.3-7.1 paleo-surface

The 51-57 m paleo-surface previously detected by Marra et al. (2016) has widespread expression at Ponte Galeria (Fig. 2), where chronostratigraphic constraints on the underlying aggradational deposits (Vitinia Formation, Luberti et al., 2017 and references therein) and their geometric/stratigraphic relationship with the 36 m terrace unambiguously provide correlation with the four-stepped sea-level rise that characterized MIS 7 (Marra et al., 2016b). In particular, an early aggradational phase of the Vitinia Formation around 269 ka matches the initial sea-level rise (A' in Fig. 16b) preceding the marked sea-level jump of glacial

termination III that occurred at 240 ka, with which in turn is associated the main aggradational succession of MIS 7.5, bracketed by post-quem ages of 253±8 ka and 248±4 ka (A in Fig. 16b).

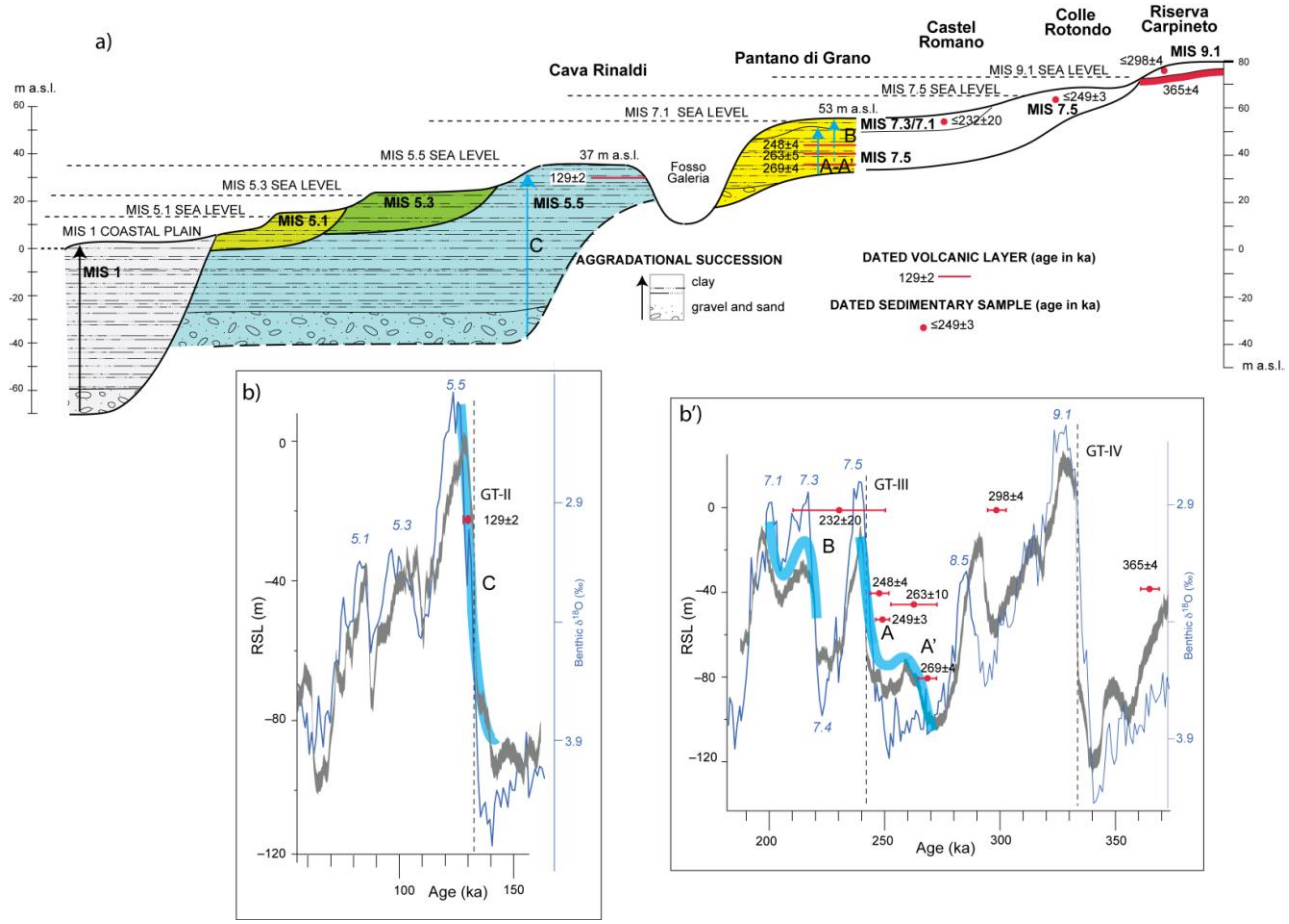

Figure 16 - a) Idealized cross-section reconstructing the terraced deposits and the corresponding aggradational successions in the investigated coastal sector, showing the geochronologic constraints providing correlation with MIS 9.1 through MIS 5.5. b-b') Ages of the dated volcanic deposits and reworked crystal populations (red dots, bars indicate the analytical error at 2σ) are compared with the Oxygen isotope curve (Lisiecki and Raymo, 2005) and the Relative Sea Level (RSL) curve (Grant et al., 2014). Correspondence of sediment aggradation with phases of rapid sea-level rise (thick blu lines) during glacial terminations (GT) is highlighted.

Finally, a marked unconformity cuts the deposits of MIS 7.5 aggradational succession and is overlain by a new aggradational succession that represents the deposit forming the flat top of the hills constituting the relict paleo-surface of 56-52 m a.s.l. The intervening erosional phase and the following sediment aggradation evidently match the sea-level fall of MIS 7.4 and the successive two-stepped sea-level rise of MIS 7.3 - MIS 7.1 (Marra et al., 2016b; B in Fig. 16b). This observation corroborates the new assessment of the 51-57 m paleo-surface, and its attribution to the later stages of MIS 7.3/7.1, rather than to MIS 7.5, as shown by correlation provided in cross-section of Figure 16a.

5.6 MIS 5.5 - 5.3 - 5.1 terraces

The occurrence of a suite of three lowest coastal terraces has been shown by geomorphologic reconstruction of their relict surfaces provided by Marra et al. (2016a, 2019a), who also demonstrated that three distinct successions of coastal plain sediments, corresponding to three coastlines at circa 34, 24 and 12 m a.s.l., are associated with these terraces (Figure 16a). The $^{40}Ar/^{39}Ar$ age of 129±1 ka on a pyroclastic-flow deposit intercalated within the aggradational succession forming the 36 m terrace at Cava Rinaldi (Epi-Tyrrhenian Formation, Marra et al., 2015) demonstrated correlation with the MIS 5.5 highstand of 125 ka (Figure 16b'). The two lower terraces at 26 and 16 m were therefore tentatively correlated with the sea-level highstands of MIS 5.3 and 5.1, respectively. However, an intervening tectonic collapse of ca. 10 around 100 ka, interrupting a steady uplift phase between 250 ka and the Holocene had to be invoked by Marra et al. (2016a), in order to reconcile elevation of the terrace at 26 m with absolute sea-level established for MIS 5.3 and 5.1 in the literature (e.g. Rohling t al., 2009). A discussion of the age of these terraces is beyond the scopes of the present paper, and further geochronologic and sedimentologic investigations of these youngest successions are in progress, aimed at verifying their exact correlation with the MIS timescale. However, in the present study we have found an excellent fit of the new geomorphological and statistical assessment of these paleo-surfaces with the previous results of Marra et al. (2016a, 2019a), and we maintain preliminary correlation with the three marine isotopes' sub-stages of MIS 5.5, 5.3, and 5.1 in the discussion of the tectonic uplift.

5.7 Tectonic implications

All the sea-level markers provided by the aggradational successions of the Paleo-Tiber River correlated with MIS 21 through MIS 1 from literature and from the present study are shown in Figure 17a. Differences in elevation among the different coastal deposits assumed as sea-level markers (green shading in Figure 17a) are the result of the intervening tectonic movement (uplift or collapse) combined with the difference in maximum sea-level at each interglacial (glacio-eustatic component). This latter element is estimated assuming a sea-level 10 m lower than present during MIS 21 through MIS 15 (blue crosses in Figure 17b') based on previous literature (Marra et al., 2016 and references therein), while values estimated in Rohling et al. (2009) are considered for MIS 13 through MIS 5.1 (green crosses).

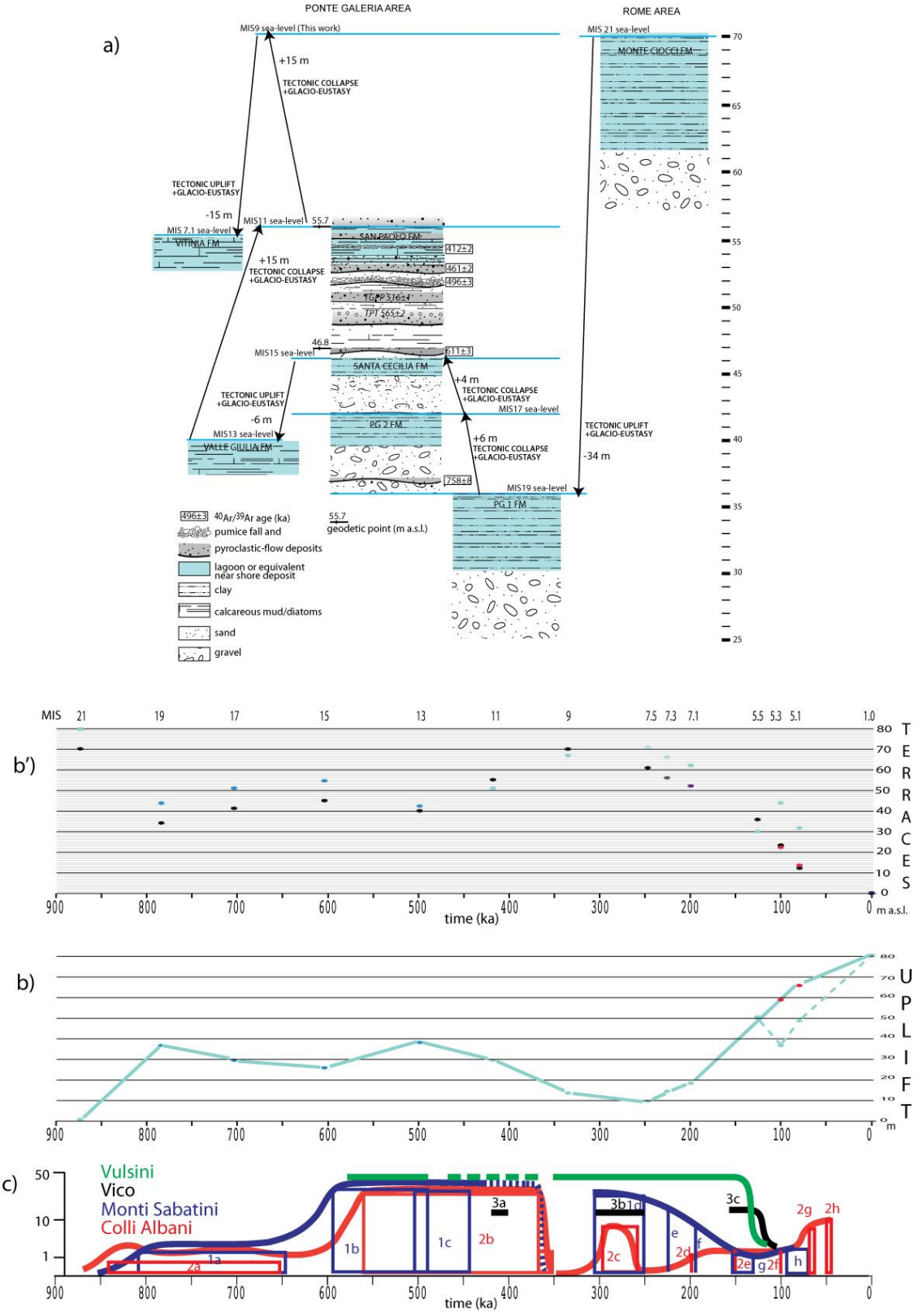

Figure 17 - a) Synoptic representation of the different sections from the Rome area indicating the aggradational successions and related sea-level indicators correlating with MIS 21 through MIS 7, integrating geochronologic and stratigraphic data from Karner and Renne, 1998; Karner and Marra, 1998; Karner et al., 2001b; Marra et al., 1998; 2016b; 2017a.

Alternative values for MIS 5.3 and 5.1 (red crosses) are also used to assess the uplift curve for the last 125 ka, based on the assumption of a more reliable uniform tectonic uplift in this time span, and on recently provided geochronologic and geomorphologic constraints on the related sea-level markers (Marra et al., 2016a, 2019a). Once the correction for the glacio-eustatic component is applied, the cumulative uplift curve of Figure 17b is obtained. Similar to previous work (Marra et al., 2016a, 2019b), comparison between the uplift curve and the eruptive histories of the volcanic districts of the Roman Province is also provided (Figure 17c). In comparison with previous reconstructions (e.g., Marra et al., 2016a) this refined uplift curve displays a marked subsidence phase between 500 and 300 ka, as provided by assessment of the MIS 9 sea-level markers at ca. 70 m a.s.l. established in the present work (Figure 17a). This fact reinforces the coupling already noted with the occurrence of two major phases of common volcanic activity at Colli Albani and Monti Sabatini 850 through 650 and 600 through 350 ka. In particular, uplift coincides with the onset of these phases, while subsidence characterizes the eruptive time spans. The subsidence phase continued until 250 ka and also encompasses the climax phase that, after a ca. 50 kyr dormancy, occurred at Vico, Monti Sabatini and Colli Albani, spanned the interval 320 - 250 ka, during which a rejuvenation of the volcanic activity occurred in all the districts of central Italy (Marra et al., 2004). The geochronologic constraints provided here for the MIS 7.5 and MIS 7.3/7.1 terraces allow a better definition of the beginning of the most recent uplift phase post-250 ka, which is characterized by an initial low gradient followed by a steady, steep increase 200 though 80 ka, and by a waning trend until the present (solid green curve in Figure 17b). As previously noted, this new uplift phase heralds and accompanies the latest volcanic phases during 90 - 70 ka at Monti Sabatini and 70-36 ka at Colli Albani, and it has been suggested to be related to the onset of a new magmatic phase extending from southern Latium to the Campanian districts of Phlegraean Fields and Vesuvius (Mara et al., 2016a). In contrast, volcanic activity seems to have been extinguished inthe districts of northern Latium (Vulsini, Vico) since 100 ka. However, Marra et al. (2019a) have shown that this recent uplift phase hs affected the whole coast of Latium homogeneously, in apparent conflict with the lack of a new magmatic phase at these volcanoes. In contrast, cessation of the activity at Vulsini and Vico matches the sudden tectonic collapse which is inferred when the current sea-level values for MIS 5.3 and 5.1 are assumed (dashed portion of the uplift curve in Figure 17c). However, a direct link between local volcanic activity in the northern sector and the global tectonic signal in this region is unlikely. Moreover, recent geochronologic and geomorphologic data strongly imply that anomalous sea-levels characterized the MIS 5.3 and MIS 5.1 highstands in the Mediterranean

region, suggesting the unforseen role played by Glacial Isostatic Adjustment (GIA) on regional tectonics during the the post-glacial period (Marra et al., 2019a).

Future investigation is needed in order to understand this complex framework of vertical movement, volcanic activity and glacio-eustasy affecting the Tyrrhenian Sea Margin during the last million years. Indeed, we note that beyond the common assumption of a interconnection between subduction, volcanism and regional uplift in the back-arc domain of the central Apennines (e.g., Conticelli and Peccerillo 1992), no dedicated study aimed at evaluating the geodynamic and isostatic forces responsible for the observed tectonic uplift has been undertaken so far.

6. Conclusions

Combined geomorphologic study and statistical analysis, together with review and re-analyses of previous published data, have allowed us to identify a set of paleo-surfaces defined by discrete classes of elevation for topographic culminations in the coastal Tyrrhenian Sea sector of central Latium.

We recognized eight such paleo-surfaces defined by the elevation ranges: 98-108, 80-89, 71-79, 61-67, 51-57, 30-43, 22-27, 11-17 m a.s.l..

The three lowest paleo-surfaces are narrowly elongated parallel to the coastline and were identified through definition of the corresponding sea-level markers and geochronologic constraints in previous studies as the marine terraces of MIS 5.5, 5.3 and 5.1, (Marra et al., 2016a, 2019a).

The highest five paleo-surfaces have been investigated here and their physical extension has been validated through DEM analyses, in order to compare the results of the geomorphological study on 1:25.000 topoghraphic maps.

The sedimentologic-stratigraphic features of the soils and of the sedimentary deposits forming these paleo-surfaces have been investigated in order to define their paleogeographic context and to identify the sea-level markers for those which have been interpreted as remnant portions of coastal terraces.

$^{40}Ar/^{39}Ar$ ages of detrital sanidine extracted from the sandy deposit of the recognized coastal terraces has allowed us to correlate the 71-79 m, the 61-67 m, and the 51-57 m paleo-surfaces with the coastal terraces formed during the MIS 9.1, MIS 7.5, and MIS 7.3/7.1 highstands, respectively.

Paleogeographic reconstrcution has allowed us to interpret the 71-79 m, 80-89 m, and 98-108 m paleo-surfaces as a sngle tectonically displaced, widespread coastal platform formed during the MIS 9.1 highstand.

Based on the combination of our refined dataset of terrace elevations with published data on relative elevation of maximum sea level during the highstands of MIS 21 through MIS 5.1, we assess the regional uplift curve in the last 900 ka and recognize the occurrence of a climactic extensional tectonic phase affecting this coastal sector between 320 and 240 ka, concident wirth occurrence of the Monte delle Fate phase of activity at the Colli albani Volcanic district.

Supplementary Material #1- 1:25.000 basemap with topographic culminations

Supplementary Material #2A: Micromorphology: Methods - Fig. S1-S6
#2B: X-Ray power diffraction methods **#2C**: SEM microphotographs - Fig. S7
Supplementary Material #2D - Diffractograms
Supplementary Material #3a, b: Full 40Ar/39Ar data.

REFERENCES

Barberi, F., Buonasorte, G., Cioni, R., Fiordelisi, A., Foresi, L., Iaccarino, S., Laurenzi, M.A., Sbrana, A., Vernia, L., Villa, I.M., 1994. Plio-Pleistocene geological evolution of the geothermal area of Tuscany and Latium. Mem. Descr. Carta Geol. d' It. 49, 77-134

Bridgland, D.R., Westaway, R., 2008. Climatically controlled river terrace staircases: a worldwide Quaternary phenomenon, Geomorphology 98, 285–315.

Cioni, R., Sbrana A., Bertagnini, A., Buonasorte G., Landi, P., Rossi, U., Salvati, L., 1987. Laurenzi, M.A., Tephrostratigraphic correlations in the Vulsini, Vico and Sabatini volcanic successions. Periodico di Mineralogia 56, 137-155.

Conticelli, S., Peccerilllo, A., 1992. Petrology and geochemistry of potassic and ultrapotassic volcanism in central Italy: petrogenesis and inferences on the evolution of the mantle sources, Lithos 28, 221-240.

De Rita, D., Funiciello, R., Rossi, U., Sposato, A., 1983. Structure and evolution of the Sacrofano-Baccano caldera, Sabatini Volcanic Complex, Rome: J. Volcanol. Geotherm. Res. 17, 219-236.

De Rita, D., Faccenna, C. Funiciello, R. Rosa, C., 1995. Stratigraphy and volcano-tectonics, in The Volcano of the Alban Hills, edited by R. Trigila, Università degli Studi di Roma "La Sapienza", Roma, 33–71.

Everdin, J.F., Curtis, G., 1965. The potassium-argon dating of Late Cenozoic rocks in East Africa and Italy. Current Anthrop., 6, 343-369.

Faccenna, C., Funiciello R., Bruni A., Mattei A., Sagnotti L., 1994. Evolution of a transfer-related basin: the Ardea Basin (Latium, Central Italy). Basin Research 5, 12-11.

Farr, T. G., Hensley, S., Rodriguez, E., Martin, J., Kobrick, M., 2000. The Shuttle Radar Topography Mission, Proceedings of a Conference held 26-29 October 1999, Toulouse, France. European Space Agency, 2000. ESA-SP vol. 450, ISBN: 9290926414, p.361.

Ferranti, L., Antonioli, F., Mauzc, B., Amorosi, A., Dai Pra, G., Mastronuzzi, G., Monaco, C., Orrù, P., Pappalardo, M., Radtke, U., Renda, P., Romano, P., Sansò, P., Verrubbi, V., 2006. Markers of the last interglacial sea-level high stand along the coast of Italy: Tectonic implications. Quaternay International 145/146, 30-54.

Freda, C., Gaeta, M., Palladino, D. M., Trigila, R., 1997. The Villa Senni Eruption (Alban Hills, Central Italy): the role of H_2O and CO_2 on the magma chamber evolution and on the eruptive scenario. Journal of Volcanology and Geothermal Research 78, 103-120.

Gaeta, M., Freda, C., Marra, F., Arienzo, I., Gozzi, F., Jicha, B., Di Rocco,T., 2016. Paleozoic metasomatism at the origin of Mediterranean ultrapotassic magmas: constraints inferred from time-dependent geochemistry of volcanic products from Colli Albani (Central Italy), Lithos, 244, 151-164. http://dx.doi.org/10.1016/j.lithos.2015.11.034

Gatta, M., Giaccio, B., Marra, F., Rolfo, M.F., 2017. Trace-element fingerprinting of the 69–36 ka Colli Albani eruptive units: A preliminary dataset for archaeological and tephra studies in central-southern Italy. Journal of Archaeological Science: Reports, 16, 330-340.

Giaccio, B., Marra, F., Hajdas, I., Karner D.B., Renne, P.R., Sposato A., 2009. $^{40}Ar/^{39}Ar$ and ^{14}C geochronology of the Albano maar deposits: implications for defining the age and eruptive style of the most recent explosive activity at the Alban Hills Volcanic District, Italy. Journal of Volcanology and Geothermal Research 185, 203-213.

Giaccio, B., Niespolo, E., Pereira, A., Nomade, S., Renne, P.R., Alber, P.G., Arienzo, I., Regattieri, Wagner, B., Zanchetta, G., Gaeta, M., Galli, P., Mannella, G., Peronace, E., Sottili , G., Florindo, F., Leicher, N., Marra, F., Tomlinson, E.L., 2017. First integrated tephrochronological record for the last ~190 kyr from the Fucino Quaternary lacustrine succession, central Italy. Quaternary Science Reviews 158, 211-234. http://dx.doi.org/10.1016/j.quascirev.2017.01.004

Giordano, G., De Benedetti, A.A., Diana, A., Diano, G., Gaudioso, F., Marasco, F., Miceli, M., Mollo, S., Cas, R.A.F., Funiciello, R., 2006. The Colli Albani mafic caldera (Roma, Italy): stratigraphy, structure and petrology, J. Volcanol. Geotherm. Res., 155, 49–80.

Grant, K.M., Rohling, E.J., Bronk Ramsey, C., Cheng, H., Edwards, R.L., Florindo, F., Heslop, D., Marra, F., Roberts, A.P., Tamisiea, M.E., Williams, F., 2014. Sea-level variability over five glacial cycles. Nature Communications 5, 5076. doi:10.1038/ncomms6076

Jicha, B.R., Singer, B.S., Sobol, P. 2016. Re-evaluation of the ages of 40Ar/39Ar sanidine standards and supereruptions in the western U.S. using a Noblesse multi-collector mass spectrometer. Chemical Geology 431, 54–66.

Karner, D.B., Marra, F., 1998. Correlation of fluviodeltaic aggradational sections with glacial climate history: A revision of the Pleistocene stratigraphy of Rome. Geological Society of America Bulletin 110, 748-758.

Karner, D.B., Marra, F., Florindo, F., Boschi, E., 2001a. Pulsed uplift estimated from terrace elevations in the coast of Rome: Evidence for a new phase of volcanic activity? Earth and Planetary Science Letters 188, 135-148.

Karner, D.B., Marra, F., Renne, P.R., 2001b. The history of the Monti Sabatini and Alban Hills volcanoes: groundwork for assessing volcanic-tectonic hazards for Rome. J. Volc. and Geoth. Res. 107: 185-215.

Lisiecki, L.E., Raymo, M.E., 2005. A Pliocene-Pleistocene stack of 57 globally distributed benthic $\delta^{18}O$ records. Paleoceanography 20, PA1003. doi:10.1029/2004PA001071.

Luberti, G.M., Marra, F., Florindo, F., 2017. A review of the stratigraphy of Rome (Italy) according to geochronologically and paleomagnetically constrained aggradational successions, glacio-eustatic forcing and volcano-tectonic processes. Quaternary International. http://dx.doi.org/10.1016/j.quaint.2017.01.044

Malinverno, A., Ryan, W.B.F., 1986. Extension in the Tyrrhenian sea and shortening in the Apennines as results of arc migration driven by sinking of the lithosphere. Tectonics 5, 227-245.

Mariucci, M.T., S. Pierdominici, F. Marra, P. Montone, L. Pizzino, 2008. Looking into a volcanic area: an overview on the 350m scientific drilling at Colli Albani (Rome, Italy). J. Volcanol. Geotherm. Res., doi:10.1016/j.jvolgeores.2008.04.007.

Marra, F., Florindo, F., Boschi E., 2008. The history of glacial terminations from the Tiber River (Rome): insights to glacial forcing mechanisms, Paleoceanography, 23, PA2205, doi:10.1029/2007PA001543.

Marra F., Karner, D.B., Freda, C., Gaeta, M., Renne, P.R., 2009. Large mafic eruptions at the Alban Hills Volcanic District (Central Italy): chronostratigraphy, petrography and eruptive behavior. Journ. of Volc. and Geoth. Res. 179, 217-232. doi:10.1016/j.jvolgeores.2008.11.009

Marra, F., Sottili, G., Gaeta, M., Giaccio, B., Jicha, B., Masotta, M., Palladino, D.M., Deocampo, D, 2014. Major explosive activity in the Sabatini Volcanic District (central Italy) over the 800-390 ka interval: geochronological - geochemical overview and tephrostratigraphic implications, Quaternary Science Reviews 94, 74-101.

Marra, F., Ceruleo, P., Jicha, B., Pandolfi, L. Petronio, Salari, L. , 2015. A new age within MIS 7 for the *Homo neanderthalensis* of Saccopastore in the glacio-eustatically forced sedimentary successions of the Aniene River Valley, Rome. Quaternary Science Reviews 129, 260–274. doi:10.1016/j.quascirev.2015.10.027

Marra, F., Florindo, F., Anzidei, M., Sepe, V., 2016a. Paleo-surfaces of glacio-eustatically forced aggradational successions in the coastal area of Rome: assessing interplay between tectonics and sea-level during the last ten interglacials. Quaternary Science Review, 148, 85-100. http://dx.doi.org/10.1016/j.quascirev.2016.07.003

Marra, F., Rohling, E.J., Florindo, F., Jicha, B., Nomade, S., Pereira, A., Renne., P.R., 2016b. Independent $^{40}Ar/^{39}Ar$ and 14C age constraints on the last five glacial terminations from the aggradational successions of the Tiber River, Rome (Italy). Earth Planet Sci Lett. in press.

Marra, F., Gaeta, M., Giaccio, B., Jicha, B., Palladino, D., Polcari, M., Sottili, G., Taddeucci, J., Florindo, F., Stramondo, S., 2016c. Assessing the volcanic hazard for Rome: $^{40}Ar/^{39}Ar$ and In-SAR constraints on the most recent eruptive activity and present-day uplift at Colli Albani Volcanic District, Geophys. Res. Lett. 43, 6898–6906. doi:10.1002/2016GL069518.

Marra, F., Florindo, F., Petronio, C., 2017. Quaternary fluvial terraces of the Tiber Valley: geochronologic and geometric constraints on the back-arc magmatism-related uplift in central Italy. Journal Scientific Reports 7: *2517*. DOI:10.1038/s41598-017-02437-1

Marra, F., Petronio, C., Salari, L., Florindo, F., Giaccio, B., Sottili, G., 2018a. A review of the Villafranchian fossiliferous sites of Latium in the framework of the geodynamic setting and paleogeographic evolution of the Tyrrhenian Sea margin of central Italy, Quaternary Science Reviews 191, 299-317. 10. 1016/ j. quascirev. 2018. 05. 011

Marra, F., Petronio, C., Ceruleo, P., Di Stefano, G., Florindo, F., Gatta, M., La Rosa, M., Rolfo, M.F., Salari, L., 2018b. The archaeological ensemble from Campoverde (Agro Pontino, central Italy): new constraints on the Last Interglacial sea level markers. Scientific Reports, SREP-18-23649, DOI : 10.1038/s41598-018-36111-x

Marra F., Nomade S., Pereira A., Petronio C., Salari L., Sottili G., Bahain J.J., Boschian G., Di Stefano G., Falgueres C., Florindo F., Gaeta M. Giaccio B., Masotta M., 2018c. A review of the geologic sections and the faunal assemblages of Aurelian Mammal Age of Latium (Italy) in the light of a new chronostratigraphic framework. Quaternary Science Reviews 181, 173-199. doi.org/10.1016/j.quascirev.2017.12.007

Marra, F., Bahain, J.-J., Jicha, B., Nomade, S., Palladino, D.M., Pereira, A., Tolomei, C., Voinchet, P., Anzidei, M., Aureli, D., Ceruleo, P., Falguères, C., Florindo, F., Gatta, M., Ghaleb, B., La Rosa, M., Peretto, C., Petronio, C., Rocca, R., Rolfo, M.F., Salari, L., Smedile, A., Tombret, O., 2019a. Reconstruction of the MIS 5.5, 5.3 and 5.1 coastal terraces in Latium (central Italy): a re-evaluation of the sea-level history in the Mediterranean Sea during the Last Interglacial, Quaternary International.

Marra, F., Florindo, F., Jicha, B.R., Nomade, S., Palladino, D.M., Pereira, A., Sottili, G., Tolomei, C., 2019b. Assessing volcano-tectonic hazard of the Monti Sabatini Volcanic District on the city of Rome (central Italy): evidence from new geochronologic constraints on the Tiber River MIS 5 terraces, Scientific Reports, in press.

Masotta, M., Gaeta, M., Gozzi, F., Marra, F., Palladino, D.M., Sottili, G., 2010. H_2O- and temperature-zoning in magma chambers: the example of the Tufo Giallo della Via Tiberina eruptions (Sabatini Volcanic District, central Italy). Lithos 118, 119-130.

Nicoletti, M., 1969. Datazioni argon-potassio di alcune vulcaniti dellew regioni vulcaniche Cimina e Vicana. Per. Mineral., 38, 1-20.

Nisi, M.F., Antonioli, F., Dai Pra, G., Leoni, G., Silenzi S., 2003. Coastal Deformation between the Versilia and the Garigliano plains (Italy) derived from the elevations of the Last Interglacial stage, Journal of Quaternary Science 18, 709-721.

Palladino, D, Simei, S., Sottili, G., and Trigila, R., 2010, Integrated approach for the reconstruction of stratigraphy and geology of Quaternary volcanic terrains: An application to the Vulsini Volcanoes (central Italy), in Stratigraphy and Geology of Volcanic Areas (eds. G. Groppelli, and L. Viereck-Goette), *The Geological Society of America Special Paper*, **464**, 63-84. doi: 10.1130/2010.2464(04).

Patacca, E., Sartori, R., Scandone, P., 1990. Tyrrhenian basin and apenninic arcs: kinematic relations since late Tortonian times. Mem. Soc. Geol. It. 45, 425-451.

Peccerillo, A., Frezzotti, M.L., 2015. Magmatism, mantle evolution and geodynamics at the converging plate margins of Italy. Journal of the Geological Society. http://dx.doi.org/10.1144/jgs2014-085

Pereira, A., Nomade, S., Falguères, C., Bahain, J-J., Tombret, O., Garcia, T., Voinchet, P., Bulgarelli, A.G., Anzidei, P., 2017. 40Ar/39Ar and ESR/U- series data for the La Polledrara di Cecanibbio archaeological site (Lazio, Italy). Journal of Archaeological Science: Reports, in press.

Perini, G., Francalanci, L., Davidson, J.P., and Conticelli, S., 2004, Evolution and genesis of magmas from Vico volcano, Central Italy: multiple differentiation pathways and variable parental magmas, *Journal of Petrology*, **45**, 139–182.

Rivera, T.A., Storey, M., Schmitz, M.D., Crowley, J.L., 2013. Age intercalibration of $^{40}Ar/^{39}Ar$ sanidine and chemically distinct U/Pb zircon populations from the Alder Creek Rhyolite Quaternary geochronology standard. Chemical Geology 345, 87-98.

Rohling E.J., Grant, K., Bolshaw, M., Roberts, A.P., Siddall, M. Hemleben, Ch., Kucera, M., 2009. Antarctic temperature and global sea level closely coupled over the past five glacial cycles. Nature Geoscience 2, 500-504. DOI: 10.1038/NGEO557

Serri, G., Innocenti, F., Manetti, P, 1993. Geochemical and Petrological evidence of the subduction of delaminated Adriatic continental lithosphere in the genesis of the Neogene-Quaternary magmatism of Central Italy, Tectonophysics 223, 117-147.

Sevink, J., Di Vito, M.A., Piochi, M., Mormone, A., Van Gorp, V., Bakels, C., 2018. A rare Mid-Würmian lithoid tuff in the Agro Pontino graben (Southern Lazio, Italy) and its identification as an Albano 5-7 related distal tephra deposit (41-36 kaBP): characteristics, provenance and palaeogeographical implications. Annals of Geophysics, 61, 1, S109. DOI: 10.4401/ag-7534

Sottili, G., Palladino, D.M., Marra, F., Jicha, B., Karner, D.B., Renne, P., 2010. Geochronology of the most recent activity in the Sabatini Volcanic District, Roman Province, central Italy, Journ. of Volc. and Geoth. Res. 196, 20-30. DOI:10.1016/j.jvolgeores.2010.07.003

Sottili G., Palladino D.M., Zanon V., 2004. Plinian activity during the early eruptive history of the Sabatini Volcanic District, Central Italy. J. Volcanol. Geotherm. Res. 135, 361-379.

Villa, P, Pollarolo, L., Conforti, I., Marra, F., Biagioni, C., Degano, I., Lucejko, J.J., Tozzi, C., Pennacchioni, M., Zanchetta, G., Nicosia, C., Panzeri, L., Martini, M., Sibilia, E., From Neandertals to modern humans: New data on the Uluzzian. Plos One 13(5): e0196786. https://doi.org/10.1371/journal.pone.0196786

MIS 9 to MIS 5 terraces along the Tyrrhenian Sea coast of Latium (central Italy): assessing interplay between sea-level oscillations and tectonic movements

Fabrizio Marra[1*], Mario Gaeta[2], Brian R. Jicha[3], Cristiano Nicosia[4], Cristiano Tolomei[1], Piero Ceruleo[5], Fabio Florindo[1], Maurizio Gatta[6,7], Michelangelo La Rosa[8], Mario F. Rolfo[7]

[1] Istituto Nazionale di Geofisica e Vulcanologia, Rome, Italy
[2] Dipartimento di Scienze della Terra, "Sapienza" Università di Roma, Italy
[3] Department of Geoscience, University of Wisconsin-Madison, USA
[4] Dipartimento dei Beni Culturali, Università di Padova, Italy
[5] Via Giotto 18, 00019 Tivoli (Roma), Italy
[6] University of York, Department of Archaeology, York YO1 7EP, UK
[7] Department of History, Culture and Society, University of Rome 'Tor Vergata', Italy
[8] Ecomuseo dell'Agro Pontino, via G.B. Vico 1, Latina, Italy

*correspondoing author: fabrizio.marra@ingv.it

Abstract

We present a review of the geomorphological studies performed ony of the Tyrrhenian Sea coast of central Italy integrated by a novel structural-geomorphological study coupled with statistical analysis of topographic culminations and comparison with a Digital Elevation Model of the ground surface, aimed at reconstructing a suite of paleo-surfaces corresponding to remnant portions of marine terraces. We performed geochronological, sedimentological, micromorphological and mineralogical investigations on the deposits forming the different paleo-surfaces in the coastal area of central Italy comprised between Civitavecchia and Anzio town, in order to provide chronostratigraphical, paleogeographical and paleoenvironmental constraints. Using the newly achieved dataset we correlate these paleo-surfaces with the coastal terraces formed during past sea-level highstands, as recognized by previous studies, and we refine their correlation with the Marine Isotope Stage (MIS) timescale.

In particular, we have extended our geomorphological analyses landward in the area between the Tiber River mouth and Anzio, in order to include the oldest paleo-surface developed above the deposits of the last large explosive eruption occurred at 365±4 ka at in the Colli Albani Volcanic District. Results of this study allow us to recognize a set of higher paleo-surfaces at elevation ranging 108 thought 71 m a.s.l., that which we interpret as one tectonically displaced, widespread coastal paleomorphological settingterrace originated during the MIS 9.1 highstand. We correlate the previously identified paleo-surfaces of 66-62 m and 56-52 m with the equivalent coastal setting terraces developed during the sea-level highstands of sub-stages 7.5 and 7.3/7.1. Moreover, based on data from literature data on

relative elevation of maximum sea level during the highstands of MIS 11 through MIS 5.1, we assess the regional uplift and the concurrent tectonic displacements that have occurred since 900 ka in this area.

Keywords: paleo-surface; coastal terrace; glacio-eustasy; regional uplift

Highlights:

- We reconstruct a suite of six paleo-surfaces ~~on~~ along the central Tyrrhenian Sea coast
- Paleoenvironmental data identify these paleo-surfaces as remnants of coastal terraces
- We provide $^{40}Ar/^{39}Ar$ age constraints to the terraced sedimentary deposits
- We correlate these terraces with ~~highstands of~~ the Marine Isotope Stage ~~timescale~~record
- We identify ~~the~~ previously unrecognized MIS 9 sea-level markers in this region
- We assess ~~the~~ regional uplift and ~~the~~ tectonic displacements in the last 400 ka

Formatted: Superscript

Formatted: Superscript

1. Introduction

The Tyrrhenian Sea coast of Latium (Figure 1) is part of a geodynamic domain characterized by back-arc extensional processes (Malinverno and Tayan, 1986; Patacca et al., 1990) that during Pleistocene times have lead to the origin formation of an ultra-potassic chain of volcanic districts (Serri et al., 1993; Conticelli and Peccerillo, 1992; Peccerillo and Frezzotti, 2015). Concurrent with the volcanic processes, regional uplift has caused the progressive emersion emergence of this area since the end of the Santernian (lower Calabrian), around 1.5 maMa, leading to widespread continentalization since ~1 ma Ma (Barberi et al., 1994; Marra et al., 2018a). The regional uplift along the Tyrrhenian coast of Latium has been interpreted as driven by the subduction process and uprising of metasomatized magma bodies on the Tyrrhenian Sea Margin of central Italy, superimposed on a smaller isostatic component of uplift (Marra et al., 2017, and references therein). Two major pulses of uplift are recognized: 0.86 through 0.5 Ma, and 0.25 Ma through the Present (Marra et al., 2016a); as a result of this overall uplifting regime, the continental, fluvial-lacustrine and coastal deposits in this area formed a widespread pattern of terraces that, similar to other regions in the world (e.g., Bridgland and Westaway, 2008), are organized in a staircase geometry, with the oldest surfaces at highest elevation.

Geographic extension and rates of the most recent phases of this uplift during Middle-Upper Late Pleistocene have been assessed by a series of studies reconstructing a suite of coastal terraces and correlating them with the sea-level highstands of identified by the Marine Isotope Stage (MIS) timescale record (e.g., Karner et al., 2001a; Nisi et al., 2003; Ferranti et al., 2006). More recently, a re-evaluation of the geometry and the age of these terraces in the coastal area comprised between the Argentario and Anzio promontories has been proposed by means of an original geomorphological approach and the integration of new geochronologic constraints provided by $^{40}Ar/^{39}Ar$ ages of volcanic layers intercalated within the glacio-eustatically forced aggradational successions forming the terraced deposits in this region (Marra et al., 2015; 2016a). Moreover, a new geomorphologic study coupled with biochronologic constraints allowed Marra et al. (2018b, 2019a) to extend the reconstruction of a complete suite of terraces in the coastal reach between Anzio and Circeo promontories, and to propose their correlation with MIS 7.5 through MIS 5.1. In contrast, only a poorly defined paleo-surface ranging 61-67 m a.s.l. has been dubitatively dubiously assigned to the MIS 9 terrace, so far (Marra et al., 2016a). Moreover, geochronologic constraints so far provided to the local MIS 9 aggradational succession (Aurelia Formation, Karner and Marra, 1998) evidenced a remarkable anomaly, significantly pre-dating the glacial termination IV

Formatted: Superscript

Formatted: Superscript

and the completion of MIS 9 highstand (Marra et al., 2016b). Therefore, assessing the geometry and providing time constraint ~~to~~ on the deposits of the MIS 9 coastal terrace in this region may have notable implications ~~on~~ for understanding the response to the global paleo-climatic signal and on the tectonic process acting on the Tyrrhenian Sea margin of central Italy.

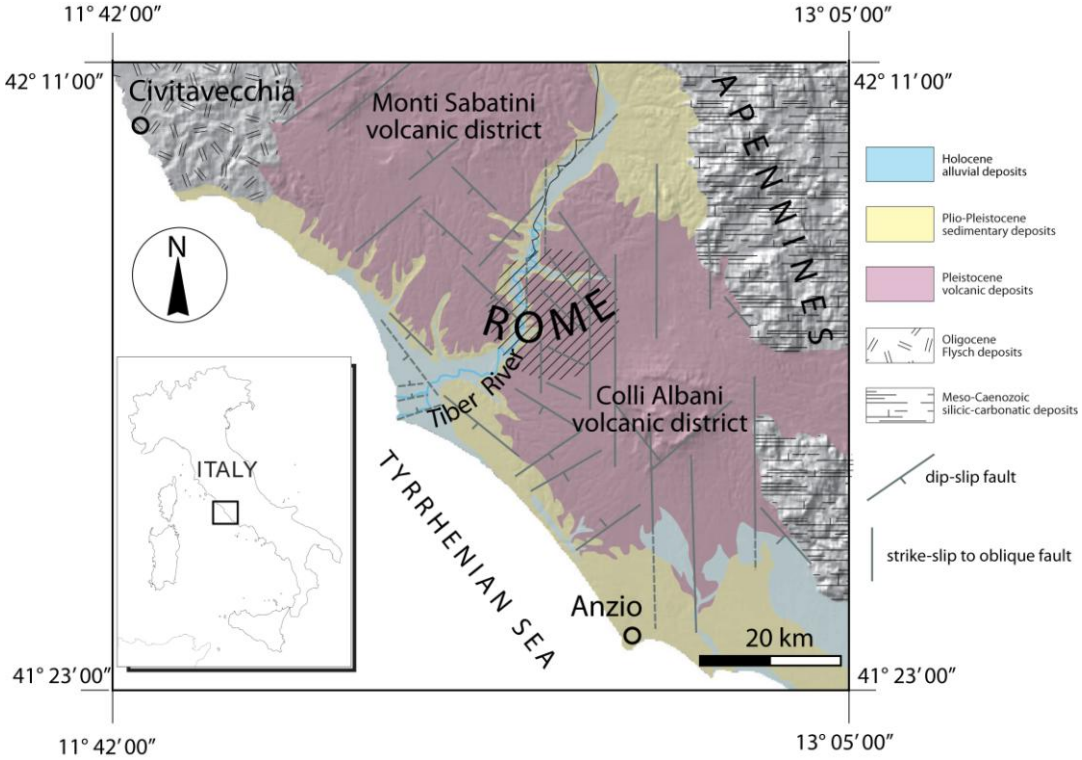

Figure 1 - DEM image of the Tyrrhenian Sea margin of central Italy showing the main structural features of the investigated area (after Acocella and Funiciello, 2006; Frepoli et al., 2010).

In the present paper we have refined the structural-geomorphological study in the previously investigated sector comprised between Civitavecchia and Anzio, and we have re-assessed the statistical analysis ~~on~~ of the elevations of the paleo-surfaces correlated by Marra et al. (2016a, 2019a) with the MISs. In particular, we have extended the geomorphological analysis landward, in order to include the oldest paleo-surface affecting the deposits of the last large eruption ~~occurred at~~in the Colli Albani Volcanic District (Villa Senni Eruption Cycle, 365±4 ka, Marra et al., 2009) in the area between the Tiber mouth and Anzio. Two huge pyroclastic-flow deposits emplaced during this eruption phase (Tufo Lionato and Pozzolanelle, Freda et al., 1995) ~~mantling~~ mantle the surface with a volcanic cover ~~radially~~ spreading radially as far as

50 km from the vent and reaching up to 20 m in thickness, locally (De Rita et al., 1995; Giordano et al., 2006; Mariucci et al., 2008). Due to this pyroclastic cover, the paleo-surfaces older than 365 ka are completely buried and no geomorphologic evidence is expected for them in this area.

We performed chronostratigraphical, sedimentological, micromorphological, mineralogical and petrographic investigations ~~on~~ of the deposits forming the different paleo-surfaces in order to provide geochronological, paleogeographical and paleoenvironmental constraints. We used four $^{40}Ar/^{39}Ar$ age determinations on detrital sanidine crystals extracted from key deposits in order to provide post-quem ages on the paleo-surfaces and relative chronologic constraints for their correlation with the suite of coastal terraces recognized and geochronologically constrained by previous studies, refining their correlation with the MIS timescale.

2. Geological Setting

The study area is located on the Tyrrhenian Sea margin of central Italy (Figure 1). Since the Middle Pleistocene the interplay between glacio-eustatic sea-level variations, tectonic processes, sedimentation and volcanic activity has built the geological framework of this area (Luberti et al., 2017, and references therein). During periods of sea-level fall, erosion occurred, ~~while~~ whereas deposition took place during phases of sea-level rise, filling previously excavated incisions with a suite of aggradational successions (Karner and Marra, 1998; Marra et al., 2008). A thick succession of pyroclastic-flow deposits, from both the Colli Albani and Monti Sabatini volcanic districts, and subordinated Sabatinian air-fall deposits, interfingers with the continental sediments. After the last volcanic eruptions at 36 ka (Marra et al., 2016c), the volcanic plateau was deeply incised during the Last Glacial, ~~also~~ partly as a consequence of the intervening regional uplift (Marra et al., 2016a). Eventually, the paleovalleys were filled by fluvial deposits as a consequence of the sea-level rise after the last glacial termination.

3. Methods

3.1 Geomorphological analysis

In the present study, paleo-surfaces have been mapped following the geomorphological approach described in Marra et al. (2016a; 2017), based on the identification of a set of flat surfaces characterized by topographic culminations with elevation ranging through a few meters around a mean value. Selected topographic culminations of the reconstructed paleo-

surfaces were detected on ~~the~~Istituto Geografico Militare 1:25.000 topographic maps of Italy ~~edited by Istituto Geografico Militare~~. They include all the hilltops (i.e., each elevation point within a closed, 5 m ~~spaced~~ interval contour line, represented by upward triangles in the figures of this work) and other quasi-equivalent points within plateau-like sectors (downward triangles). The identification of the paleo-surfaces ~~implies~~ is based on a combined approach that integrates statistically significant concentrations of elevations around a mean value, and the morphologic evidence for the concentration of these elevation points within a finite area, as detected in the maps (see Marra et al., 2016a for detailed methodology). The full dataset of topographic elevations is reported on the scanned 1:25.000 topographic maps and provided as Supplementary Material #1 ~~to this work~~.

Distribution of the topographic culminations has been statistically analyzed in order to verify the occurrence of discrete elevation intervals corresponding to peaks of concentration, which can be assumed ~~as~~ to be the mean ~~value~~ level for each paleo-surface. Comparison between the complete dataset of elevation points (hilltops + plateaux) and that represented only by hilltop elevations has been also provided, to highlight possible subjective selection of the plateau-like culminations and to exclude biases.

Finally, a set of elevation ranges defining the principal paleo-surfaces identified ~~through~~ using the described geomorphological method has been ~~elaborated~~ mapped through ~~by~~ DEM analyses, to compare the results.

3.2 DEM analysis

Five classes of elevations highlighted by the geomorphological study have been mapped using an interferometric Digital Elevation Model (DEM) with a ground resolution of 30 meters (1 arcsec) derived from the NASA SRTM mission (http://www2.jpl.nasa.gov/srtm, Farr et al., 2000). ~~In detail~~When the overall topographic relief of the Italian peninsula is considered, the DEM shows an averaged altitude accuracy of ~15 meters, but in our case, considering areas quite close to the sea and showing low altitude ~~values~~ranges (i.e., 0 - 120 m), the accuracy is ~~most likely~~one order of magnitude better, and can be estimated in 1-2 m.

The analysis was ~~totally~~ performed entirily within ~~into~~ a GIS environment. Initially, the DEM was ~~cut~~ delimited on the basis of the study area using a polygon shapefile, then the various classes were identified one by one, generating 5 different layers. ~~To this aim, 5~~ Five queries were applied to the DEM, each time considering the maximum and minimum values of each class so as to ~~only~~ isolate the desired altitude interval. Finally, the layers were merged into a single one and symbolized with 5 different colors, one for each class.

3.3 Micromorphological analyses

Three undisturbed soil samples (TML-CC, VDT, VOC) and three loose sand samples (TML-SA, PC-SA, CSR-SA) have been studied in thin sections for micromorphological analysis and for sand mineralogy determination, respectively, aimed at investigating the pedological and/or sedimentological features, and to recognize the origin of the deposit forming the corresponding paleo-surface. One sediment sample collected ~~in~~ from the paleo-surface ranging 60-67 m (CR1) in the northern sector was analyzed ~~for a work~~ by Villa et al. (2018), and the results are reported here to integrate with the dataset above.

Descriptions of thin sections are summarized in Table 1, results of the petrographic determination of sand grains are reported in Table 2. Methods and microphotographs of thin sections for micromorphological analyses are provided in Supplementary File #2A.

3.4 Mineralogical analyses

Fifteen ~~soil~~ samples collected close to the top, and in some instances at increasing depth, on the different paleo-surfaces (VL-1, VL-2, MM, VCR-1, VCR-2, VCR-3, TB-1, TB-2, TB-3, VVL, TML-SA, TRIG, VDT, SPR, RUT), and three sediment samples (RSC, CDC, CR-1), have been analyzed by X-rays diffraction and ~~at the scansion~~with a scanning electron microprobe (SEM) in order to describe their mineralogy and texture.

Methods, microphotographs and full-resolution diffractograms are provided in Supplementary File #2B-C.

3.5 $^{40}Ar/^{39}Ar$ dating

Sanidine crystals ~~have been~~were extracted from four samples of sediment to provide terminus post-quem ages to the time of deposition of the terrains and/or the accretionary soils forming the paleo-surfaces ranging 98-108 m (TML-SA), 71-79 m (RSC-SA), 60-67 m (CR-3), 51-57 m (CSR-SA) a.s.l., in the area ~~comprised~~ between the Tiber mouth and Anzio. Sampling locations ~~is provided~~are shown in Figure 3.

Sanidine phenocrysts were co-irradiated with the 1.1864 Ma Alder Creek sanidine standard (Jicha et al., 2016; Rivera et al., 2013) at the Oregon State University TRIGA reactor in the Cadmium-Lined In-Core Irradiation Tube. Single crystal fusion analyses were performed at the WiscAr laboratory at the University of Wisconsin-Madison using a 60W CO_2 laser and a Noblesse multi-collector mass spectrometer following Jicha et al. (2016). Results are reported in Table 4. Full analytical data are reported in Supplementary Material #3.

Formatted: Superscript

Formatted: Superscript

4. Results

4.1 Geomorphological analysis

Results of the geomorphological study performed for the present work in the coastal area between Civitavecchia and Anzio are in good agreement with those previously obtained by Marra et al. (2016a, 2019a). We have statistically re-analyzed hilltops and plateaux elevations separately, in the two coastal sectors north and south of the Tiber mouth. Very similar statistical assessment for the elevation ranges of the detected paleo-surfaces have been obtained for the two sectors, which are reported in Figure 2 and 3, respectively. In these figures, all the topographic culminations identified ~~in~~ on the 1:25.000 maps are ~~reported~~ indicated with triangles of different colors. In the northern sector, each color is associated with an elevation range defining a paleo-surface which, in turn, is established ~~based on~~from the statistical analysis. Elevation ranges for the paleo-surfaces are represented by grey boxes of ~~cumulated~~ cumulative frequency above a threshold value of n=2 for a total number of data >20 (red horizontal line in Figure 2b), while continuous distributions are considered for classes of n <20. Open triangles are used for hilltops whose elevation is not statistically significant and are not associated with a paleo-surface. These elevations are interpreted ~~to~~ as reflecting topographic culminations that represent~~ing~~ eroded higher rank paleo-surfaces; for this reason, the same color used for the corresponding pristine paleo-surface is also used ~~also~~ for these triangles.

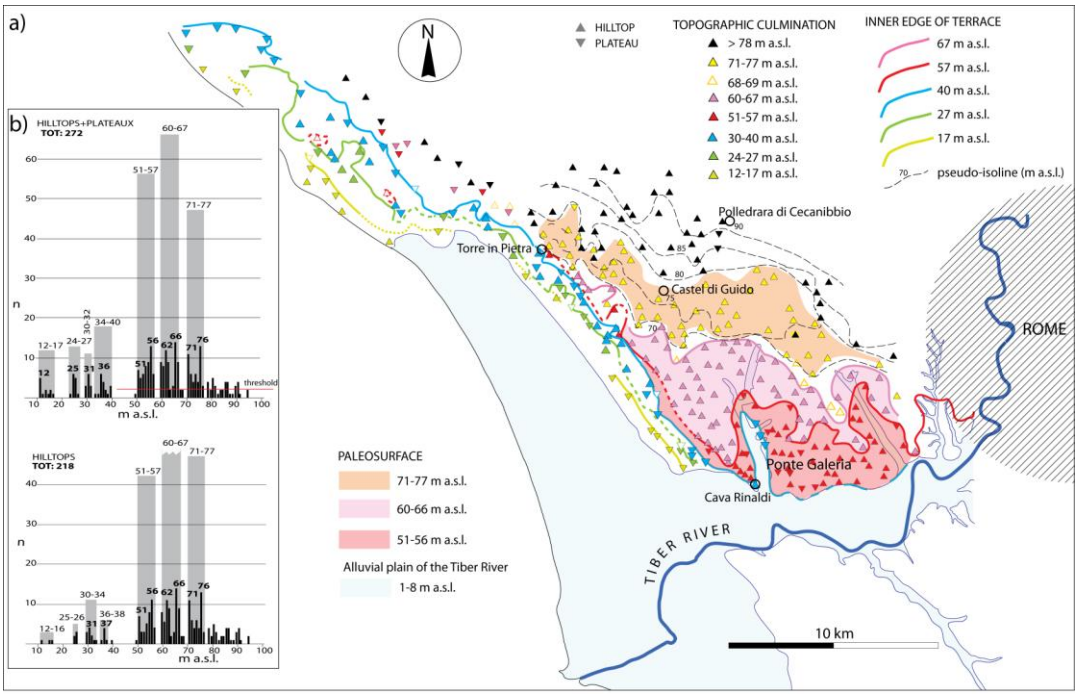

Figure 2 - Geomorphological map (a) and ~~statistics of~~ topographic culmination statistics (b) in the northern sector ~~comprised~~ between Civitavecchia and the Tiber mouth. Elevations of topographic culmination are omitted for clarity in this figure and can be found in Suppl. Mat. #1A. See text for comments.

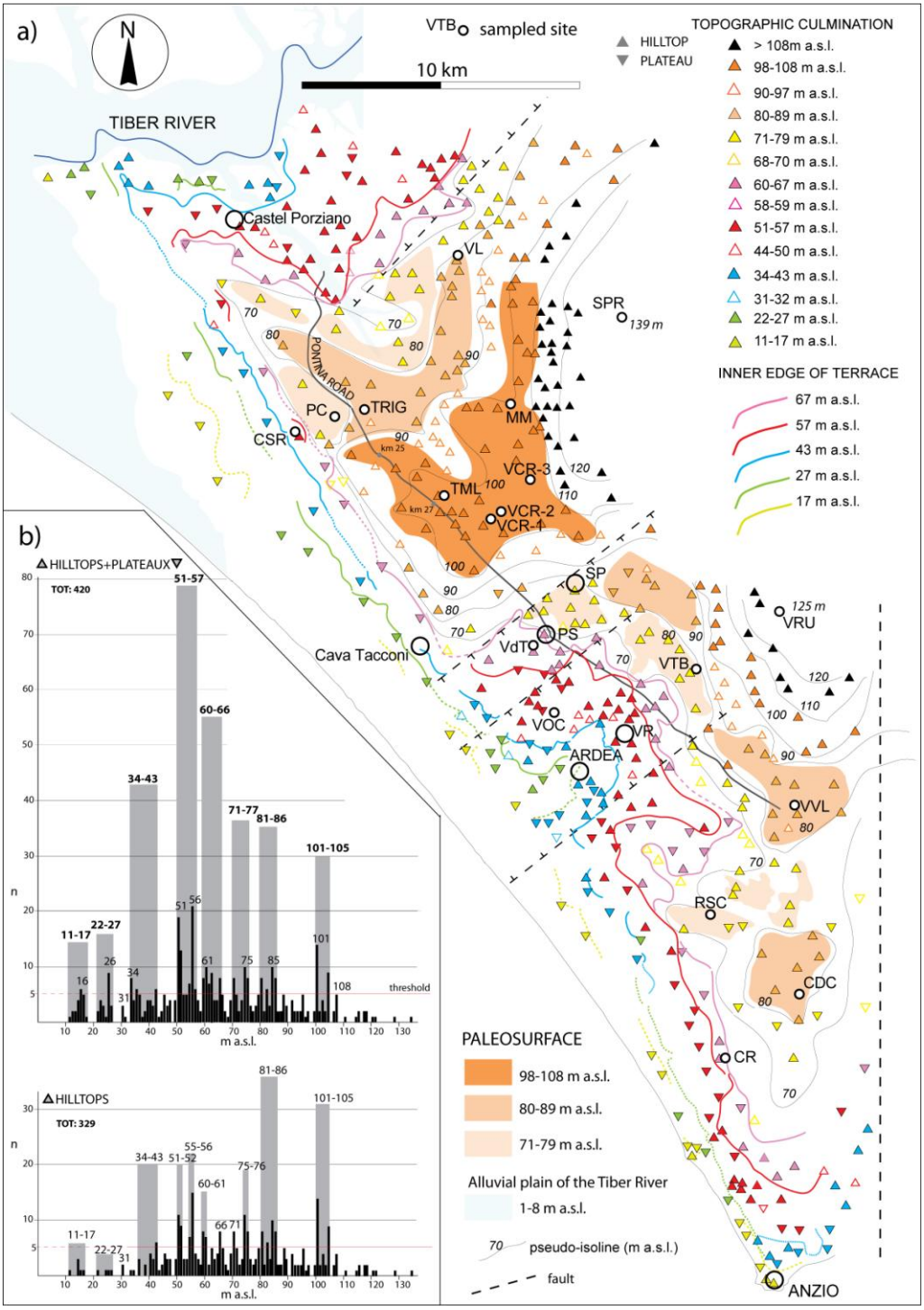

Figure 3 - Geomorphological map (a) and ~~statistics of~~ topographic culmination statistics (b) in the southern sector ~~comprised~~ between the Tiber mouth and the Anzio promontory. Elevations of topographic culmination are omitted for clarity in this figure and can be found in Suppl. Mat. #3. See text for comments.

A similar approach is used in the southern sector where, due to the larger number of data, a threshold value of n=5 is established to define the classes of elevation for all the paleo-surfaces ~~but~~ except the lowest two (Figure 3b). Moreover, in a few cases the elevation range for each color is slightly larger than the mean elevation range (grey boxes) established for the paleo-surfaces based on histograms, in order to include all topographic points.

Color shading is used in Figure 2 for three oldest paleo-surfaces which have ~~more~~ a wider ~~extension~~ extent and are located inland, while inner margins are represented by solid colored lines for the paleo-surfaces stretching along the coast, which are assumed to represent coastal terraces. Different shades of the orange color are used in Figure 3 to highlight the highest paleo-surfaces that are located inland which, according to discussion in the following sections, are interpreted as having the same age, whereas inner terrace margins ~~of terrace~~ are reported for the youngest paleo-surfaces along the coast.

In both sectors illustrated in Figures 2 and 3, three lowest orders of terrace are identified by a series of topographic culminations, each one providing well-clustered, distinct elevation ranges, which define three paleo-surfaces narrowly elongated parallel to the coast. The lowest paleo-surface ranges 12-17 m a.s.l., with a peak at 12 m (Figure 2b), and 12-18 m a.s.l., with a peak at 16 m (Figure 3b), in the northern and in the southern sector, respectively. A second paleo-surface has very narrow ranges of 24-27 and 22-27 m a.s.l., with peaks at 25 and 26 m, in the northern and in the southern sector, respectively.

A third, higher paleo-surface is characterized by a wider range of elevations, with a main concentrations between 34-40 and 34-43 m a.s.l. in the northern and southern sector, respectively, and with a minor peak at 31 m, in both sectors.

A fourth, wide paleo-surface is that ranging 51-57 m a.s.l. and characterized by two relative maxima at 51 and 56 m, in both sectors. Another two well-defined elevation ranges of 60-67 m, and of 71-77 m, are clearly identified in both sectors, and are associated with ~~a~~ fifth and ~~a~~ sixth paleo-surfaces, respectively.

Finally, two more concentrations of elevation values, ~~peaked~~ peaking at 80-86 and 101-105 m a.s.l., define the two highest paleo-surfaces ~~in~~ on the inland coastal sector south of the Tiber mouth, whereas in the northern sector topographic culminations show progressively increasing elevation inland, without any apparent clustering around a mean value.

Comparison of the results of the geomorphological study with the DEM of Figure 4 shows a very satisfactory match. In particular, we ~~remark~~ note the close correspondence between the geometrical patterns defined by the 51-57 m paleo-surface in the geomorphological maps of

Figure 2 and 3, and in the DEM image of Figure 4 (represented by the red color in both representations), as well as, between those pertaining to the highest paleo-surface of 98-108 m (represented by the deep orange color in Figure 3 and by the deep blue color in Figure 4).

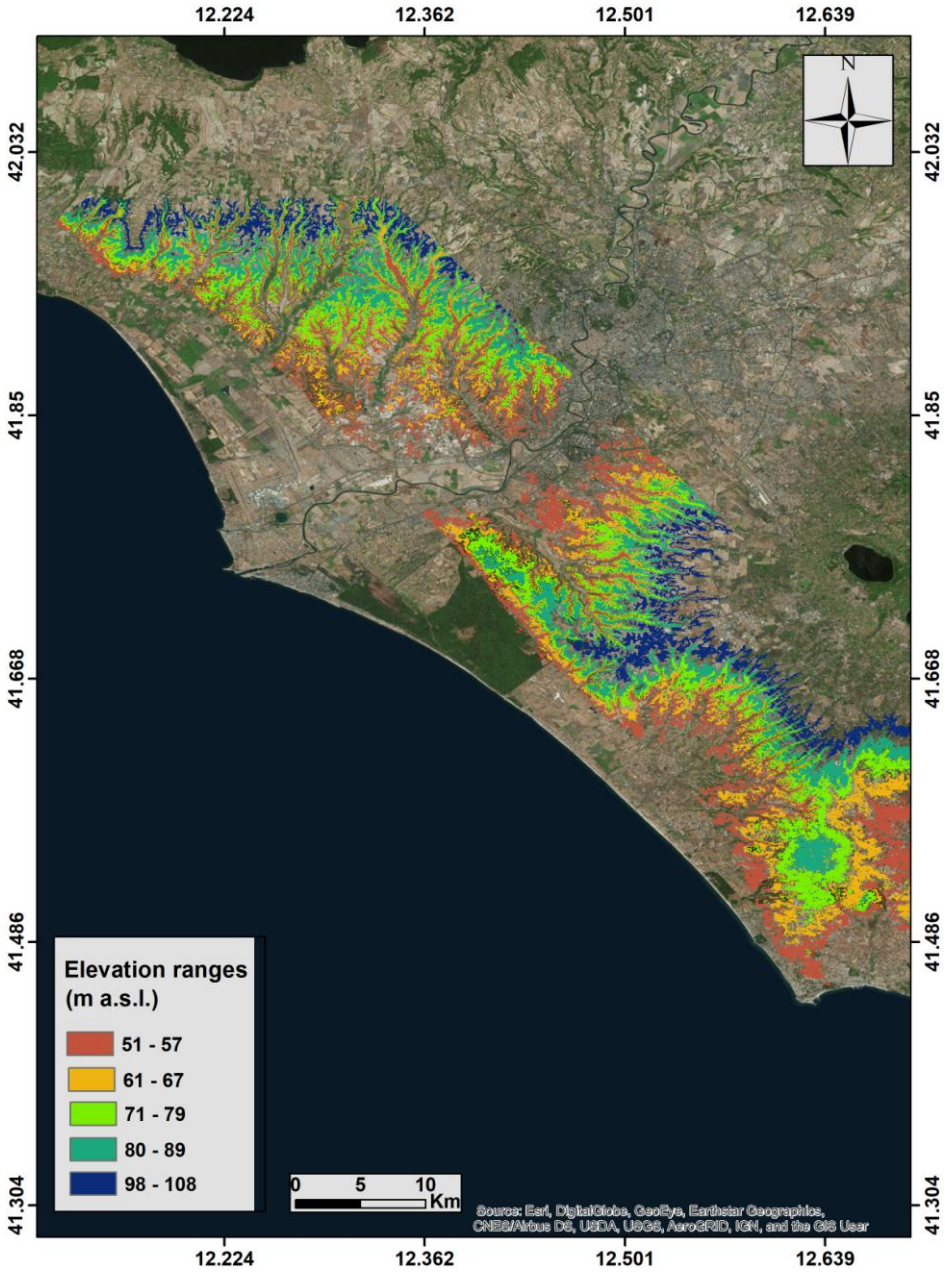

Figure 4 - Interferometric Digital Elevation Model (DEM) mapping of the five classes of elevations highlighted by the geomorphological study.

4.2 Stratigraphic investigations

4.2.1 Paleo-surface 98-108 m a.s.l.

Exposure of the sedimentary deposits forming the highest paleo-surface in the investigated area is provided by a road cut in Tenuta Monti di Leva (TML), at km 27 of Via Pontina (Figure 5a, see Figure 3 for location). Here, a~~n upper~~ pedogenically modified horizon~~pedogenized layer~~ occurs in the upper 100 cm and is constituted by fine to medium sized sand in silty-clayey matrix, orange in color (Figure 5a-a"). A 180 cm thick ~~concretional~~ concretionary layer, constituted by aggregated, cm-sized Fe and Mn nodules within a sand matrix, occurs at the bottom of this ~~layer~~ horizon and overlies a red paleoso~~i~~l developed on top of the pyroclastic-flow deposit of Pozzolanelle (Villa Senni Eruption Cycle, 365±4 ka; Freda et al., 1997; Marra et al., 2009). A sample of the upper sand layer (TML-SA) and another ~~one sample of~~from the ~~concretional~~ concretionary layer (TML-CC) ~~have been~~were analyzed for mineralogy and michromorphology, respectively. Forty-one sanidine crystals extracted from sample TML-SA ~~have been~~were dated by the $^{40}Ar/^{39}Ar$ method.

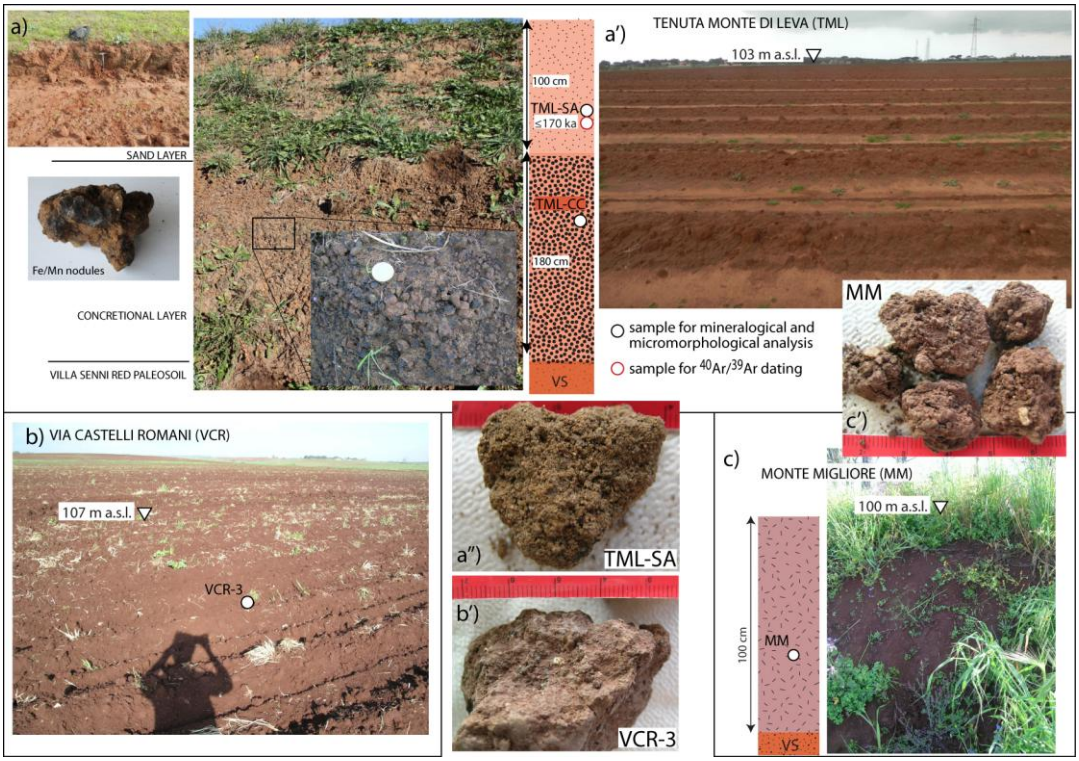

Figure 5 - Photographs and stratigraphic schemes showing the 98-108 m a.s.l. paleo-surface and the sections from which samples analyzed in the present study were collected. See text for comments.

The Tenuta Monte di Leva paleo-surface is affected by intensive ~~plowing~~ ploughing which exposes shreds of the upper, orange sand layer, allowing ~~to recognize~~recognition of the presence of this sedimentary deposit throughout the sector crossed by the Pontina Road between km 27 and km 25 (see Figure 3a). A similar in color, but finer sandy-clay deposit is exposed by plowing grooves on top of this highest paleo-surface, ~~more~~ further inland. Four samples were collected along the Via dei Castelli Romani and Via Laurentina, at increasing distance inland, with respect to the Tenuta Monte di Leva site (Figure 3). Three samples (VCR 1-3) were collected at elevations ~~comprised~~ between 105 and 107 m a.s.l. in the ~~plowed~~ fields exposing clods of the sub~~-surface portion of the~~ soil (Figure 5b). Although the direct contact is not exposed in this flat sector, a geologic substrate represented by the Pozzolanelle pyroclastic-flow deposit (hereby PL) is visible in the scanty outcrops along the stream incisions at its margin. A fourth sample (MM) was collected ~~in~~ at the Monte Migliore-La Selvotta locality, at 100 m a.s.l., from the middle of a 100 cm thick, dark red ~~paleosoil~~paleosol developed above the PL, exposed by a road cut (Figure 4c). A larger amount of clay matrix, dark red in color, characterizes the samples collected in these inland sectors of the 98-108 paleo-surface (VCR 1, 2, 3, MM, Figure 5b'-c'). Frequent pyroxene crystals and sparse, altered volcanic scoriae 1 to 5 mm in size, are embedded in the clay matrix of these soils, evidencing an at least partial origin from the directly underlying volcanic deposit.

Two more samples were collected in a later time at higher elevation, in the area inland with respect to that pertaining to the 98-108 paleosurface (SPR at 139 ma.s.l.) and with respect to the narrow alignment of topographic culminations ranging 100-110 m in the more southern sector (RUT at 125 m a.s.l.) (Figure 3), aimed at investigating the origin of the abundant silico-clastic fraction highlighted by micromorphologic and petrographic analyses in the soils developed above the volcanic substrate.

4.2.2 Paleo-surface 80-89 m a.s.l.

Different ~~shreds~~ fragments of this paleo-surface are identified northwest and southeast of the highest sector corresponding to the 98-108 paleo-surface (Figure 3). As ~~occurring~~ for the latter, ~~also~~ the 80-89 paleo-surface is also ~~develops~~ developed above different geologic substrates as a function of the distance from the coastline: above the PL in the inland sectors, and above sedimentary sand deposits to the southwest. Five samples were collected in the different sectors of this paleo-surface. Two samples (VL-1, VL-2, Figure 6a) were collected in the middle and at the surface of a thick ~~paleosoil~~paleosol developed above the PL in Via

Laurentina, in the inland margin of the northernmost stretch of this paleo-surface. ~~One more~~A further sample (TRIG, Figure 6b) was collected at its opposite, seaward extreme, on the ground surface in a sandy deposit (Figure 3).

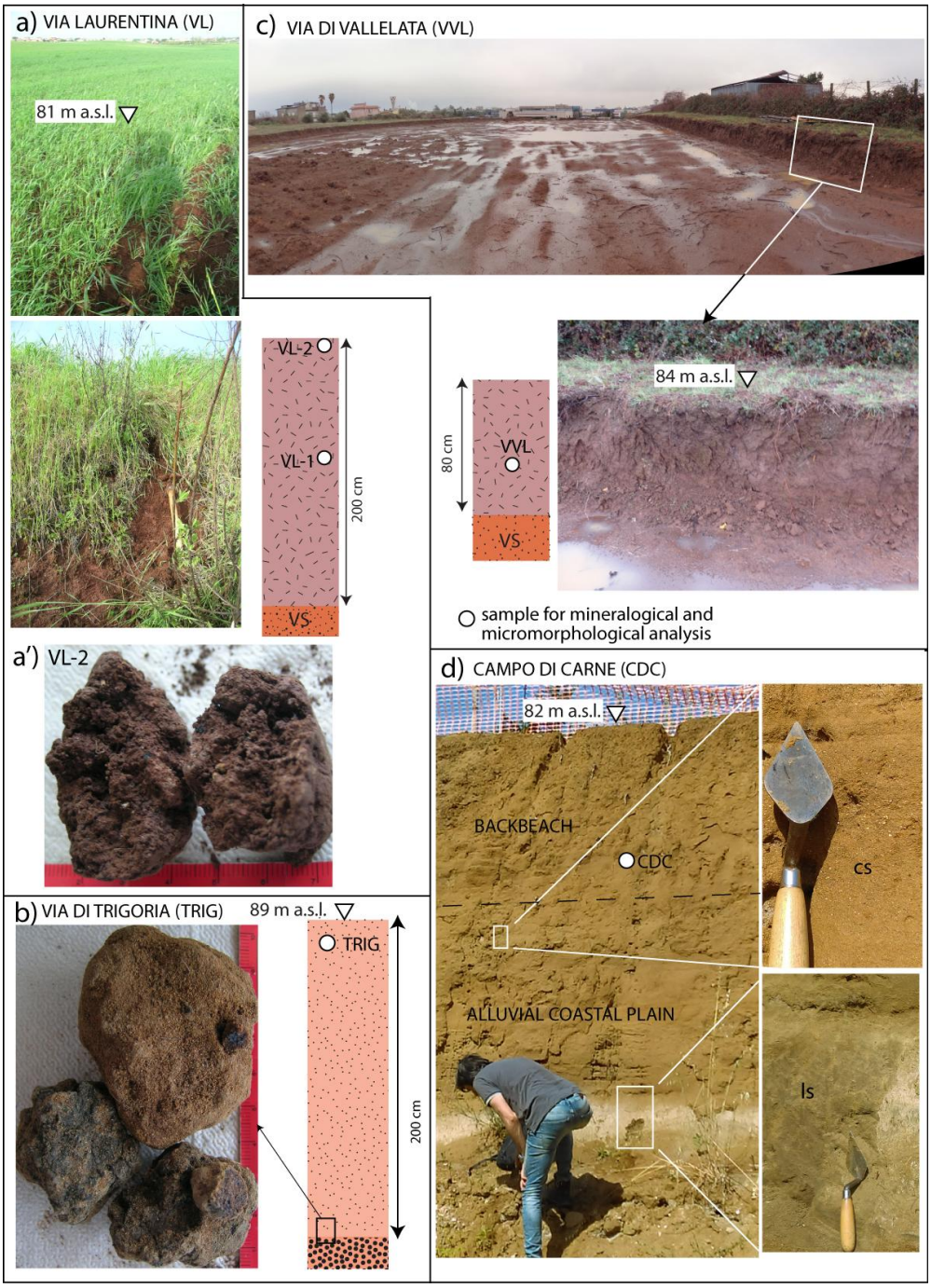

Figure 6 - Photographs and stratigraphic schemes showing the 80-89 m a.s.l. paleo-surface and the sections from which samples analyzed in the present study were collected. See text for comments.

This sedimentary deposit is quite similar to that cropping out in Tenuta Monte di Leva (TML): ~~it's~~ it is a ~~medium~~ medium-~~to~~ to-fine ~~sized~~grained, orange sand in a ~~scarce~~ sparse clay matrix, without sedimentary structures, ca. 3 m thick (Figure 6b). At the base of the exposed section a ~~concretional~~concretionary layer rich in Mn/Fe nodules, quite similar to that occurring in TML, is present.

A fourth sample (VVL, Figure 6c) was collected in the middle of an ca. 80 cm thick ~~paleosoil~~paleosol developed above the PL in Via Vallelata, in the inland margin of the southernmost stretch of the 80-89 m paleo-surface (Figure 3). This reddish soil, like the thicker soil sampled in Via Laurentina (Figure 6a'), ~~is~~ constitut~~ed by~~s of very fine, clayey sediment ~~conglobating~~ containing abundant pyroxene crystals and altered volcanic scoriae, and appears quite similar to the other soils developed directly above the PL sampled for this study.

Finally, one sample (CDC) was collected in Campo di Carne in a road excavation exposing a~~n~~ ca. 3 m thick ~~sedimentary~~ deposit constitut~~ed by~~ing of fine, faintly bedded sand in ~~scarce~~ a sparse clay matrix, with dm-thick layers of coarse sand (cs in Figure 6d), whose top at 82 m a.s.l. is part of the seaward portion of the 80-89 m a.s.l. paleo-surface. A layer of dark, greenish loamy fine sand, ca, 60 cm thick, occurs at the base of the exposed section in CDC (ls in Figure 6d).

4.2.3 Paleo-surface 71-79 m a.s.l.

Two particularly level, small sectors at elevations around 76 m a.s.l. ~~are~~ can be detected in the northern and southern margins of the investigated area, in the Podere Carafa (PC) and Riserva Carpineto (RSC) estates (Figure 3). In the PC, an almost perfectly flat area (Figure 7a) is truncated by a sharp scarp to the southwest, dividing it from another level area at ca. 56 m a.s.l. (Castel Romano -CSR), while it ~~more gently~~ connects more gently to a slightly higher sector, corresponding to the 80-89 paleo-surface, to the northeast. A marked fluvial incision dissecting the plateau exposes the terrains forming the 71-79 m paleo-surface, showing ~~an at least five meters thick,~~ massive sand deposit of at least five meters thickness, where sample PC-SA analyzed ~~in this work~~during this study was collected (Figure 7a).

A remarkably similar geomorphologic and stratigraphic setting is observed ~~in~~ at the RSC. Here a wide level area at elevations ranging 70-79 m is intensely dissected by steep stream valleys,

and almost without geomorphologic break connects with another large area to the southeast, including the Campo di Carne (CDC) site, at an elevation ~~comprised~~ between 80 and 85 m a.s.l. ~~to the southeast~~ (Figure 3). A massive, medium to coarse sand deposit with sparse, well-rounded fine gravel (sample RSC, Figure 7b) constitutes the geologic substrate in this area, and directly overlies the lower flow unit of the Villa Senni eruption cycle (Tufo Lionato).

Figure 7 - Photographs and stratigraphic schemes showing the 71-79 m a.s.l. paleo-surface and the sections from which samples analyzed in the present study were collected. See text for comments.

A portion of this 71-79 m a.s.l. paleo-surface also occurs within the structurally controlled sector of Ardea, bordered by the NE-SW trending normal faults of the Ardea Basin (Figure 3). This is a half-graben which originated as a transversal Tyrrhenian Sea basin in Lower Pleistocene times, as evidenced by off-shore seismic lines (Faccenna et al., 1994). The continued Middle Pleistocene activity of these faults is suggested by the marked control on the paleo-coastlines, testified by the geometry of the inner edges of the MIS 7 and MIS 5 terraces reconstructed in Marra et al. (2016a, 2019a) and shown by our refined study in Figure 3 and in Figure 4.

~~Differently than in~~In contrast to the more seaward sectors, here the 71-79 paleo-surface is developed upon the PL (Figure 7c-d), and characterized by a shallow, 60-80 cm thick, dark brown ~~paleosoil~~paleosol. Three samples have been vertically sampled in this ~~paleosoil~~paleosol ~~in~~ at the Via di Torre Bruna (VTB 1-3, Figure 7c).

Figure 2 shows a wide 71-77 m paleo-surface that we have reconstructed in the coastal sector north of the Tiber mouth (Ponte Galeria area), which in Marra et al. (2016a) was not highlighted. However, scanty sedimentary deposits occur at these elevations in this area, where the outcropping terrains are mostly represented by the Monti Sabatini volcanic succession. Notably, thin layers of calcareous lacustrine muds, ca. 50 m thick, crop~~s~~ out at ~~elevation of~~ 72 m a.s.l. in Castel di Guido, and are overlain by the pyroclastic-flow deposit of Tufo Giallo di Sacrofano (285±2 ka, Karner et al., 2001b; Sottili et al., 2010), which forms most of the hilltops of the 71-77 m paleo-surface (Marra et al., 2018c). We interpret these sedimentary strata as the remnants of an alluvial coastal plain, mantled by a thin cover of pyroclastic deposits.

4.2.4 Paleo-surface 61-67 m a.s.l.

No evident paleo-surface is associated with this class of elevations in the sector south of the Tiber mouth, except that pertaining to small, isolated plateaux, like ~~in~~ at the Colle Rotondo locality (CR, Figure 8). The Colle Rotondo site is located on the flat surface of an E-W elongated hill, culminating 63.5 m a.s.l., bordered by the steep flanks of two convergent streams, 2.5 km east of the present coast, and 7.5 km north of Anzio (Figure 3). This is part of a series of hilltops ranging 61-67 m a.s.l., aligned along a narrow stripe of land defining a coastal terrace between Ardea and Anzio (pink triangles in Figure 3). This terrace is shifted

inland, significantly, within the Ardea basin, paralleling the behavior of the inner edge of the 51-57 m terrace, as well as that of the two lower terraces of 34-43 m, and 22-27 m (Figure 3). Notably, in the coastal sector overlooking the most elevated area of TML, corresponding to the 98-108 m paleo-surface, only plateau points define the 60-67 m terrace, while almost no evidence of the 51-57 m terrace occurs in the coastal reach north of the Ardea basin, consistent with erosion due to tectonic uplift of this sector. In contrast, a well-defined 60-67 m terrace occurs at the northwestern margin of the lower area represented in Figure 3, facing the terminal reach of the Tiber Valley.

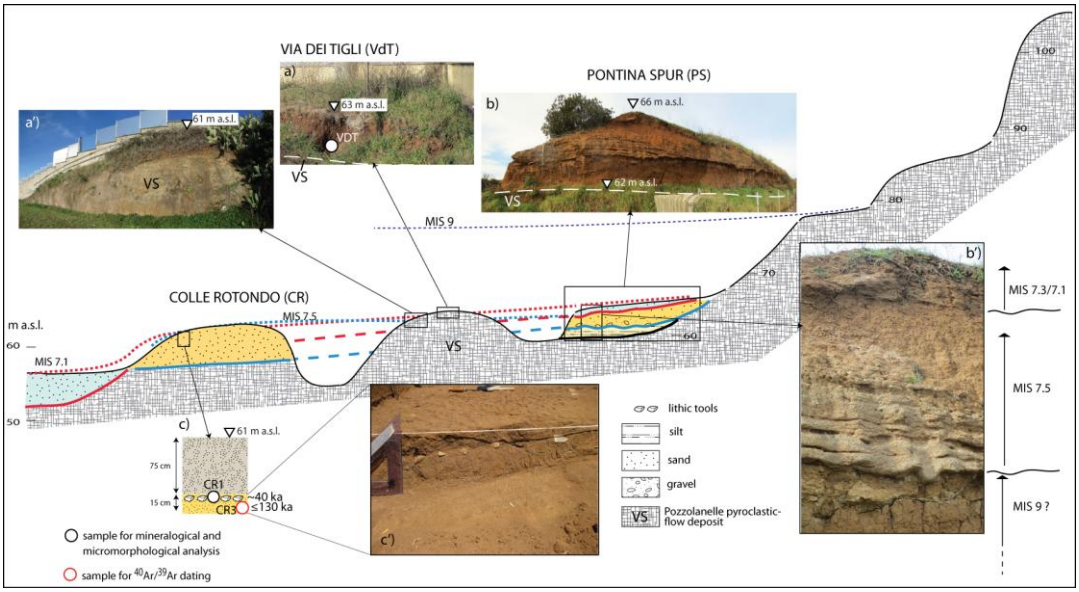

Figure 8 - Composite cross-section, constructed by projecting the Colle Rotondo (CR) site on an ideal profile passing by the Santa Procula (SP), Pontina Spur (PS), and Via dei Tigli (VdT) sites (see Figure 3 for location), aimed at showing the stratigraphic relationships between the sedimentary successions underlying the 60-67 m a.s.l. paleo-surface.

A pedogenized surface horizon constit~~uted by~~ing of brown sandy silt, heavily disturbed by ~~plowing~~ploughing, occurs in the upper 75 cm at CR (Figure 8c). It overlies a reddish-brown silty sand horizon, incorporating mm-sized Mn and/or Fe concretions (Figure 8c'). A large number of stone artifacts attributed to the Uluzzian culture (45-41 ka) was found within the upper portion of this sand layer, ranging in thickness from 6 to a maximum of 20 cm (Villa et al., 2018). One sand sample (CR1) collected within the archaeological layer was analyzed for michromorpholgy ~~in~~ by Villa et al. (2016), while 39 sanidine crystals extracted from a sand sample (CR3) collected immediately below (see Figure 8c) have been dated ~~in~~ as part of the present work.

A different geologic substrate characterizes the 60-67 m paleo-surface at two sites located in the northern portion of the Ardea Basin, Via dei Tigli (VdT) and Pontina Spur (PS) (Figure 3). A~~n~~ ca. 80 cm thick, brown-reddish clayey ~~paleosoil~~paleosol ~~overlays~~ overlies the PL ~~in~~ at VdT (Figure 8a). Field surveys ~~in this area~~ showed that the substrate of the 60-67 m paleo-surface in this area is ~~systematically constitu~~represented by a pedogenized layer on top of the PL (e.g., Figure 8a'). One sample ~~of~~ from this soil (VdT) has been analyzed for micromorphology.

A peculiar situation is observed at PS, where two fining-upwards successions overlie a third, faintly bedded fine sand deposit, which in turn overlies the PL (Figure 8b-b'). The two upper successions ~~are constituted by~~consist of a basal gravel layer, made up of reworked ~~volcanics~~ volcanic material with ~~idiosyncratic~~characteristic, large~~, analcimized~~ leucite crystals turned into analcime, suggesting provenance from the PL (Freda et al., 1997). The finer, upper part is also ~~prevalently~~ made up largely of volcanic sand. Both have evident fluvial origin. The lowest layer is a silty fine sand, of possible palustrine or alluvial origin. No sample was collected from this section, due to its very local significance, while a correlation with the other sections of the 60-67 m paleo-surface and a paleoenvironmental interpretation is provided in the cross-section of Figure 8.

The 60-67 m paleo-surface has a wide expression to the north of the Tiber ~~River~~ (Figure 2). However, no sedimentary succession is apparently associated with this paleo-surface, ~~where~~ its geologic substrate ~~is constituted by~~consisting of different, older volcanic deposits, ranging 561-400 ka (e.g., Karner and Marra, 1998; Marra et al., 2016b), which form the hilltops in this area. Consequently, the 60-67 paleo-surface in this area should be considered as a non-depositional terrace, possibly generated by uplift-induced erosional processes in the near-shore sector, similar to the ~~overlying~~ higher level paleo-surface of 71-77 m in this sector.

4.2.5 Paleo-surface 51-57 m a.s.l.

This paleo-surface (red triangles in Figure 2 and 3) has a prominent expression in the Ponte Galeria area north of the Tiber mouth, where solid geochronologic constraints correlate it with MIS 7, as ~~remarked~~ noted in Marra et al. (2016a). It is rather well preserved along the southeastern side of the Tiber Valley, south of the ~~River~~ river mouth, and in the southernmost sector between Ardea and Anzio, while it disappears along the coastal reach facing the TML morpho-structural height (Figure 3). However, two ~~shreds~~ fragments of coastal terrace are preserved immediately north of this sector, and one of these (Castel Romano -CSR) provides good exposure of the terrains underlying the paleo-surface. ~~In~~ At CSR a large level area at elevations ranging 51-56 m a.s.l. is bordered to the west-northwest by a steep, 6 m ~~tall~~ high

scarp (Figure 9a), separating it from the other wide level area of Podere Carafa, ranging 71-79 m a.s.l. (see Figure 3).

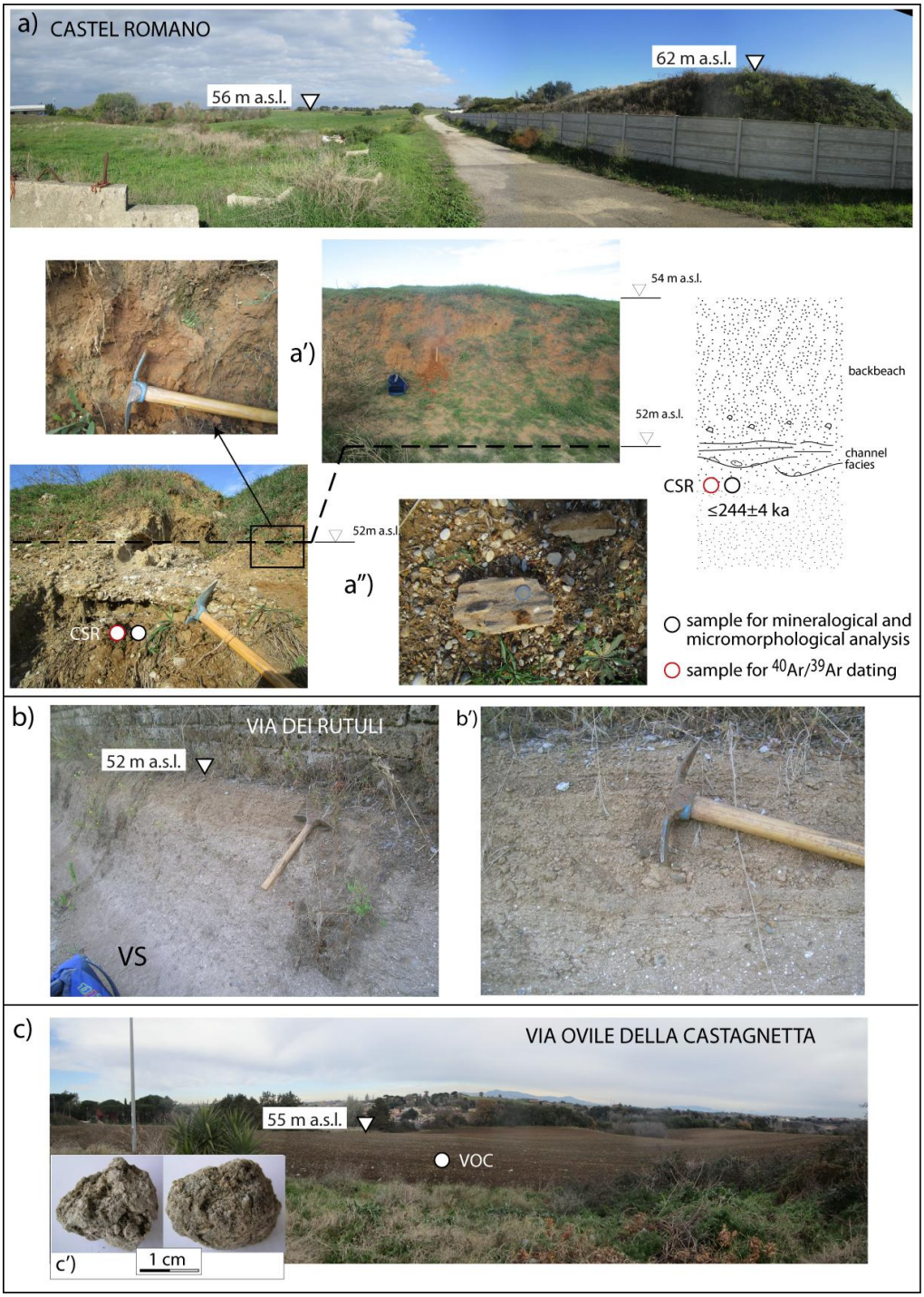

Figure 9 - Photographs and stratigraphic schemes showing the 51-57m a.s.l. paleo-surface and the sections from which samples analyzed in the present study were collected. See text for comments.

The 60-67 m terrace is not preserved between the two paleo-surfaces in this area, which are connected by a gentle incline degrading from ca. 70 m to 62 m a.s.l., behind the sub-vertical scarp. The 51-56 m paleo-surface ~~in~~ at CSR is dissected by a gully exposing on its banks a reddened, massive sand deposit, 2 m thick (Figure 9a'), overlying a ca. 50 cm thick layer with gravel lenses and sandstone horizons with ripple marks (Figure 9a"). This braided channel facies overlies a massive sand deposit in which sample CSR for mineralogical analysis and $^{40}Ar/^{39}Ar$ dating was collected.

A different geologic substrate represented by the PL characterizes the 51-57 m paleo-surface within the Ardea Basin. However, exposure ~~in~~ at Via dei Rutuli (VR, see Figure 3) provides evidence of a conglomeratic layer above the PL at 52 m a.s.l. (Figure 9b), which testifies the occurrence of a transgressive deposit that should be considered the coastal deposit associated with the 51-57 terrace in this area. It is a bedded, fining upward, 50 cm thick sand and gravel layer, ~~conglobating~~ containing well-rounded scoria clasts from the underlying pyroclastic deposit, which is erosionally truncated at the top (Figure 9b'). Evidence from another site within the Ardea basin (Via Ovile della Castagnetta -VOC, Figure 3) suggests that a fine-grained, lagoon deposit forms the upper portion of the 51-57 terrace in this area. Here, a wide paleo-surface around 55 m a.s.l. (Figure 9c) ~~is constituted by~~consits of a brown, mature ~~paleosoil~~paleosol in which one sample (VOC) was collected and analyzed for micromorphology. The occurrence of abundant, rounded calcareous concretions (Figure 9c'), which are uncommon in shallow soils developed directly upon the siliceous volcanic deposits, suggests the presence of a horizon of calcareous mud, as typically observed in the lagoon deposits of the MIS 7 Vitinia Formation (Karner and Marra, 1998) associated with the 51-57 paleo-surface in the northern coastal sector.

4.3 Micromorphological analyses

Results of thin section observations are summarized in Table 1.

TS[1]	Microstructure	Lithology	Groundmass[2]	c/f ratio	Rel Dist[3]	Pedofeatures
TML-CC	-	Matrix: 15 -20% fine sands (quartz; rare feldspar; chert; metamorphic rock fragments) Inside nodules: well sorted fine sands (±45%) (quartz; feldspar; chert; metamorphic rock fragments; pyroxene)	Orange (PPL) clay with SS and GS bfabric	20/80 (matrix) 50/50 (nodules)	OP (matr.) SSP (nod.)	Matrix: layered clay coatings and infillings, limpid and silty clay, broad extinction lines, frequent.
CR1	Basic MS type: close porphyric	Fine sand (5%); Medium sand (60-65%) Lithology: quartz; feldspar; chert; pyroxene; metamorphic rock fragments; epidote. Sub-rounded and sub-angular grains.	Reddish (PPL) clays with SS and GS b-fabric	70/30	CP	Limpid clay coatings and infillings, 1st order yellow interference colors; broad extinction lines, occasional superimposed Fe coatings.
VDT	Subangular blocky, moderate	Very fine sand (5-10%); Fine sand (5%); Medium sand (5-10%) Lithology: quartz; chert; pyroxene (rare); Sub-rounded and sub-angular grains.	Orange (PPL) clay with CS and GS bfabric	20/80	OP	Limpid clay coatings, strongly deformed, frequent. Disorthic Fe/Mn nodules, typic and concentric, frequent, rounded.
VOC	Basic MS type: single-spaced porphyric	Very fine sand (±5%); Fine sand (15-20%); Medium sand (25-30%) Lithology: quartz; feldspar; chert; pyroxene; amphibole; volcanic scoria (rare); metamorphic rock fragments. Sub-rounded and sub-angular grains.	Yellowish (PPL) clays with GS bfabric	60/40	SSP	Limpid clay coatings, strongly deformed, frequent. Disorthic Fe/Mn nodules, typic and concentric, frequent, rounded.

Table 1 – Description of thin sections

[1] TS = Thin Section

[2] B-fabric: SS = Stipple speckled; PS = porostriated; GS = granostriated; CS = cross striated

[3] Rel Dist = Related distribution pattern: CP = close porphyric; SSP = single-spaced porphyric; OP = open porphyric

4.3.1 ~~Concretional~~Concretionary layer from Tenuta Monte di Leva: sample TML-CC

Micromorophological analysis ~~on~~ of this sample collected ~~in~~ from the TML ~~concretional~~concretionary layer shows that the nodules are iron and manganese concretions that entrap sediments differing from those in the surrounding groundmass. The main differences between the sediments within the nodules and those in the matrix around them are as follows:

(a) The degree of sorting, which inside the nodules is good, with grains in the fine sand class, indicating that the nodules formed in aeolian or alluvial sands (e.g., channel facies).

(b) The lithology: the matrix ~~has~~ consists only of weathering resistant species, whereas in the nodules some volcanic minerals (pyroxenes – Fig. S1) are ~~still~~ preserved, and feldspar (e.g., microcline) is more abundant than in the surrounding matrix.

The matrix around the nodules shows the effects of marked pedogenesis. It is in fact very clay-rich and in the coarse fraction only weathering resistant ~~species are~~material is preserved (quartz, chert, metamorphic rock fragments – predominantly quartzite). Clay coatings, pertaining to several superimposed episodes of clay illuviation, are very strongly ~~attested~~ developed (Fig. S2). They occur as superimposed limpid and silty clay coatings or as coatings deformed due to shrink-swell phenomena.

~~Excluding~~ Albeit that the nodules may be allochtonous (i.e., formed elsewhere and then transported and re-deposited after being eroded), observations attest that they contain remains of the former parent material on which pedogenesis ~~took~~ has taken place, "preserving" it from successive weathering. Weathering and pedogenesis subsequently affected ~~then~~ the groundmass but were ~~hampered~~ impeded within the nodules.

4.3.2 Sand deposit from Colle Rotondo: sample CR-1

The sand fraction is composed of a mixture of s~~ilicoclastic~~iliciclastic and volcanoclastic (i.e. pyroxenes – augite) mineral species. The moderate sorting, the grainsize centered on the medium sand granulometric class, and the slight rounding of the grains are compatible with an aeolian (backbeach) sediment. There are no traces of reworking due to surface runoff or similar water and gravity-triggered slope processes. Pedogenesis is at an initial stage, especially compared to other samples from this study. Incipient reorganization of the groundmass, giving rise to a stipple-speckled b-fabric, is observed. Weak traces of incipient clay illuviation, such as thin clay coatings around skeletal grains, also point to an initial/moderate level of pedogenesis (Fig. S3). The weatherable minerals in the coarse fraction – especially pyroxenes – are abundant and do not show traces of weathering.

4.3.3 ~~Paleosoil~~Paleosol from Via dei Tigli: sample VDT

This sample shows the highest degree of pedogenic weathering ~~in~~ amongst the analyzed sample ~~lot~~s. The abundant clay in the groundmass shows orange-red colors resulting from the strong oxidation, and the clay ~~themselves~~ are the outcome of repeated cycles of clay illuviation. Strong vertic processes (i.e.: internal turnover of soil material) led to the digestion of the illuvial clays in the fine mass and to the formation of strongly developed cross-striated and grano-striated b-fabric types (Fig. S4, S5). Also the nodules of iron and manganese owe

their morphology to the strong shrink-swell phenomena in the sample (which led to the formation of concentric nodules with strong rounding). The coarse fraction is predominantly composed of weathering-resistant species (quartz and chert), albeit minor amounts of pyroxenes and unaltered volcanic glass are still present. The latter might derive from a 'fresher' or more recent input of volcaniclastic material into the soil during its formation. The poor sorting, sub-angular morphology and medium-fine sand grain size of the ~~silicoclastic~~ siliciclastic fraction do not match the expected characteristics of ~~account for~~ an aeolian input, strongly suggesting an alluvial/colluvial origin.

4.3.4 ~~Paleosoil~~Paleosol from Via Ovile della Castagnetta: sample VOC

The sorting of the coarse fraction is low. The sample has the highest percentage of volcanic mineral grains (pyroxenes and amphiboles – see Fig. S6) in the studied set, included the loose sand samples. The fine fraction derives from clay illuviation, which ultimately triggered vertic processes and the digestion of clay coatings within the groundmass, the development of a grano-striated b-fabric, and the formation of concentric iron and manganese nodules. Grains are predominantly in the fine and medium sand fraction, and show subrounded and rounded morphologies. The low sorting and the rounding of iron and manganese nodules indicate reworking and redeposition of the material. The presence of rare calcite infillings indicates re-carbonatation of the profile due to the effect of a dissolved carbonate-rich groundwater table (Fig. S6). Abundant, large (1-2 cm) carbonatic nodules also occur in the deposit.

4.4 Mineralogical analyses in thin section

4.4.1 sample TML-SA

Due to the granulometric bias introduced by sieving, it is not possible to ascertain the sedimentary environment in which the deposit formed through thin section observation. Nevertheless, it can be said that TML-SA is characterized by ~~scarce~~ scanty medium and coarse sand fraction, and by fine material possibly indicating pedogenesis. Indeed, the fine material was observed before the sieving and also after it, especially in the form of "pseudosands" which survived the sieving procedure. The nature of the sand grains is essentially ~~silicoclastic~~ siliciclastic (Table 2), with a very minor volcanoclastic fraction and lack of volcanic scoriae. Grains have a subangular morphology.

Minerals	TML - SA	PC-SA	CSRM-SA
	%	%	%
Quartz	64	66	35
Metamporphic rock fragments	20	19	35
Chert	12	10	16
Feldspar	3	2	5
Pyroxene	1	3	8
Amphibole	1	0	0
Volcanic scoria	0	0	1
Total siliciclastic %	98	97	91
Total volcaniclastic %	2	3	9
Counted grains (n)	*152*	*156*	*154*

Table 2: results of petrographic determination of sands

Quartz, chert, metamorphic rock fragments (mainly quartzite with minor amounts of schist) and feldspar have been grouped under the "s~~ilicoclastic~~iliciclastic" category. Pyroxene (mostly augite and monocline pyroxene, diallagio), amphiboles (green and brown hornblende) and volcanic scoria belong to the "volcaniclastic" category.

4.4.2 Sand deposit ~~from~~ at Podere Carafa: sample PC-SA

The sand displays strikingly similar grain composition (Table 1) and morphology as that of sample TML-SA.

4.4.3 Sand deposit ~~from~~ at Castel Romano: sample CSR-SA

This sand sample is characterized by medium grain size with a subrounded morphology and no fine matrix. Mineralogical composition displays a higher percentage of volcanic species ~~with respect~~in ~~to~~comparison with the other sand samples (Table 1).

4.5 X-ray and SEM analysis

Results of diffractometric analyses are summarized in the diagrams of Figure 10.

Calcic clinopyroxene is ubiquitous in the pyroclastic rocks of the Colli Albani volcanic district. In addition, amorphous material ~~deriving~~ derived from the weathering of volcanic glasses is typical of soils developed on pyroclastic rocks (generally, this soil component is identified in the RDX by the increase of counts in the region at lower 2Θ□□ Consequently, the height of clinopyroxene peak at 2Θ=29.85°, as well as that of amorphous material at 2Θ=4°, with respect to quartz peak at 2Θ=26.65° in the RDX can be assumed as an indicator of the abundance of volcanic components forming the soil. This provides an index (i.e. Qtz/(AM+Cpx) in Table 3) to distinguish the soils developed above a primary volcanic substrate (Index <6) from those overlying sedimentary deposits (Index >6).

Notably, quartz is present in all the soils developed above volcanic deposit and its abundance generally increases with decreasing depth as evidenced by magnitude of the peak at 2Θ=26.65° (Q1 Figure 10a). Quartz is practically absent closer to the base of the soil in VTB-1, and is scarce in the middle of the soil in VTB-2 and in Monte Migliore (MM). However, it is also abundant in the middle of VVL and VL, where the Q1 peak is comparable with that of all the surface samples. A marked quartz peak is present in sample VdT-2, from the soil developed above the Villa Senni deposit on the 61-67 terrace, for which the s~~ilicoclastic~~iliciclastic fraction has been investigated in thin section for micromorphology on sample VdT-1. However, excluding the sample VCR-1, notably the closest one to the inferred sedimentary/volcanic transition in Figure 11, all the soils developed above volcanic deposit show higher amount of AM+Cpx (>12) in comparison with ~~respect~~ the others soils analyzed in this study (Table 3).

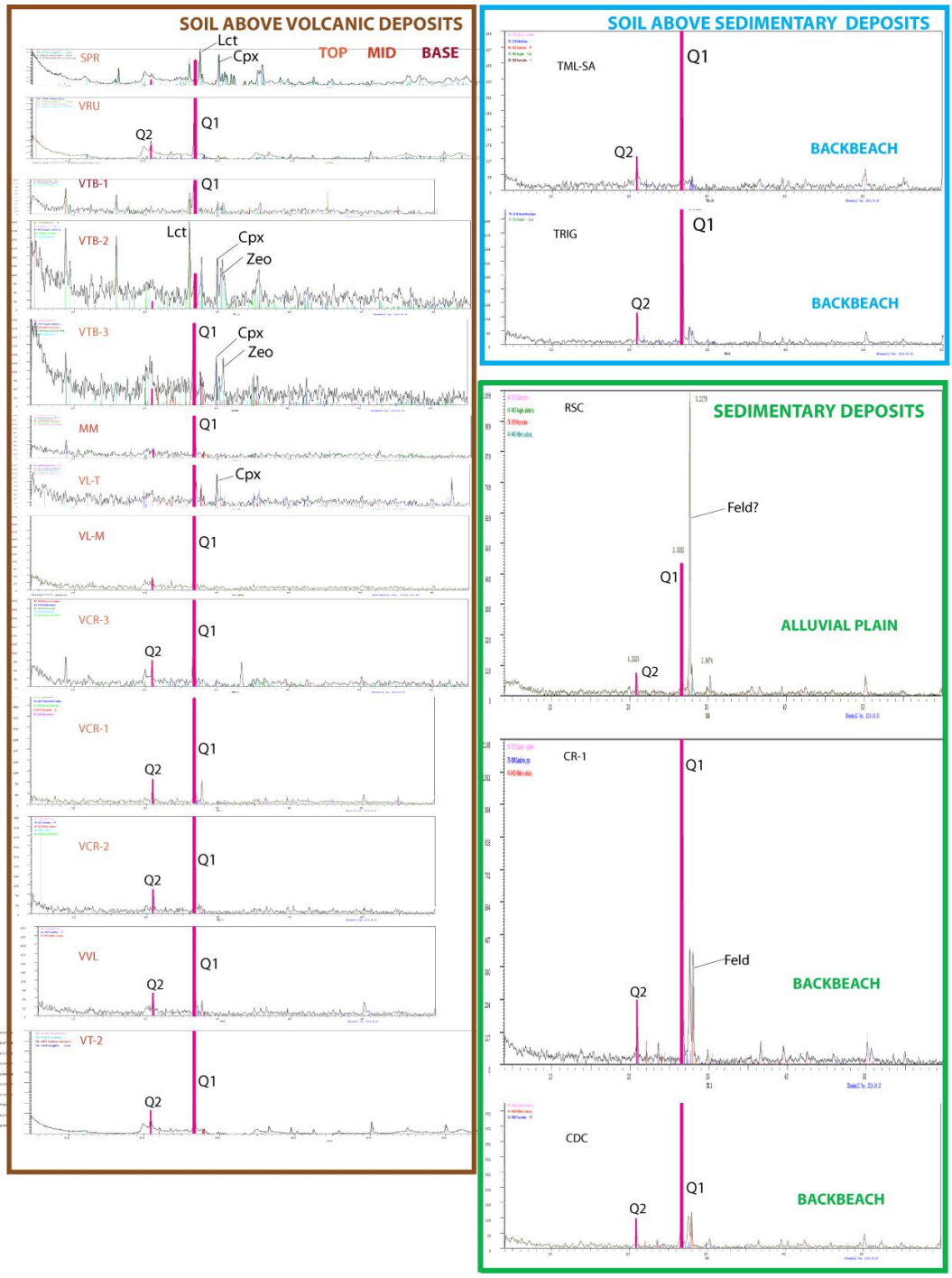

Figure 10 - Diffractograms of the soil and sediment samples. In inset a' diffractograms are... Vertical axes are normalized to the same scale; full-resolution original diagrams are provided in Suppl. Mat. #1B. See text for comments.

Moreover, quartz abundance decreases with the distance from the inferred paleo-shoreline in soils developed above the volcanic substrate. In order to verify this observation, we have collected two samples in the inland sector at the foot of the Colli Albani peri-~~calderig~~ caldera ring (SPR and RUT, Figure 11) and we have normalized results of diffractometric analyses peformed with a different equipment (see Methods in Supplementary Material #2) by re-analizing samples VTB-1 and VTB-3 with them (Table 3). As shown in Figure 10 and Tabkle 3, Q1 peaks and AM+Cpx/Qz are the highest one for thesec samples.

Apart for the discriminating AM+Cpx/Qz ratio, diffractograms of soils above sedimentary deposits differ from those above volcanic deposits only for the slightly larger magnitude of the main quartz peak Q1, and for the presence of a second quartz peak close to 10 (Q2). These peaks are much higher in the sediment samples which also display a remarkable peak corresponding to the pyroxene. Finally, the smaller magnitude of the quartz and pyroxene peaks in the fine sediment sample CDC suggests that magnitudes are also proportional to grainsize of the s~~ilicoclastic~~iliciclastic component.

Abundance, dimension and morphology of the Quartz and K-feldspar grains occurring in selected samples (VTB-1, TML-SA, VCR-1, CR1) have been analyzed at the SEM and discussed in section 5.1. Microphotographs are provided in Supplementaerty Material #2.

	SOILS ABOVE VOLCANIC DEPOSITS															SOILS ABOVE SEDIMEMNTARY DEPOSITS				
	VTB-1	VTB-2	VTB-1	VV	VL-M	VL-T	MM	VTB-1*	VTB-3*	VRU*	SPR*	VdT-2*	VCR-3	VCR-2	VCR-1	TRIG	TML-SA	RSC	CDC	CR-1
Amorphous	305	240	8000	58	54	121	45	68	9900	6100	8500	4750	80	70	30	52	59	55	45	110
Qtz	290	122	8000	320	270	147	150	0	20700	15977	6650	26343	316	349	394	520	586	1099	501	1168
Cpx	165	165	11500	0	10	118	15	40	9300	750	8000	550	25	0	10	20	20	40	20	0
TOT	760	527	27500	378	334	386	210	108	39900	22827	23150	31643	421	419	434	592	665	1194	566	1278
Amorphous	40	46	29	15	16	31	21	63	25	27	37	15	19	17	7	9	9	5	8	9
Qtz	38	23	29	85	81	38	71	0	52	70	29	83	75	83	91	88	88	92	89	91
Cpx	22	31	42	0	3	31	7	37	23	3	35	2	6	0	2	3	3	3	4	0
TOT	100	100	100	100	100	100	100	100	100	100	100	100	100	100	100	100	100	100	100	100
Qtz/Cpx+AM	0,6	0,3	0,4	5,5	4,2	0,6	2,5	0,0	1,1	2,3	0,4	5,0	3,0	5,0	9,9	7,2	7,4	11,6	7,7	10,6
Cpx+AM	62	77	71	15	19	62	29	100	48	30	71	17	25	17	9	12	12	8	11	9

Table 3 - X-ray powder diffraction (XRPD) data. Summary of absulte abundances of mineral phases in the analyzed samples (*samples analyzed with a different equipment, see Methods in Supplementary Material #2).

663

CR3

Age (ka)	± 2σ (ka)
127,7	**± 11,3**
130,9	**± 11,2**
131,0	**± 9,6**
131,7	**± 9,7**
133,4	**± 13,7**
134,0	**± 14,3**
138,3	**± 6,3**
140,6	**± 12,5**
169,5	± 6,9
169,7	± 11,7
177,6	± 8,3
198,4	± 7,3
245,3	**± 6,6**
249,9	**± 7,2**
250,7	**± 6,5**
251,6	**± 6,6**
298,9	± 5,6
375,6	± 4,9
379,1	± 5,6
392,9	± 9,6
393,5	± 4,8
400,2	± 4,6
401,4	± 5,1
403,6	± 4,7
407,3	± 5,6
407,8	± 4,6
410,7	± 6,5
416,5	± 3,5
418,1	± 4,6
421,7	± 3,8
446,8	± 4,6
459,2	± 5,1
495,5	± 6,5
498,4	± 4,8
503,2	± 4,1
1289,3	± 6,5
1289,9	± 3,9
1293,0	± 6,9
1313,1	± 3,5
youngest population:	
134,2	**± 3,5**
249.3	**± 3.4**

664

665

TML-SA

Age (ka)	± 2σ (ka)
151,1	**± 27,6**
165,5	**± 28,5**
166,6	**± 27,9**
171,0	**± 24,9**
181,7	**± 25,4**
189,3	**± 54,3**
216,5	± 6,0
239,9	± 4,7
246,2	± 17,8
250,0	± 6,6
252,3	± 7,1
257,6	± 5,1
262,8	± 22,7
266,0	± 20,0
287,5	*± 72,5*
316,8	± 18,7
329,8	± 20,8
335,5	± 96,7
351,5	± 15,7
361,0	± 40,6
368,2	± 32,7
369,5	± 20,0
371,2	± 21,5
372,6	± 18,7
382,2	± 23,2
389,6	± 23,0
398,9	± 16,2
409,6	± 5,9
422,9	± 63,3
430,5	± 10,9
435,7	± 8,7
446,4	± 5,6
504,4	± 5,6
541,7	± 5,0
549,4	± 5,4
551,8	± 4,3
557,0	± 40,2
589,3	± 4,4
600,0	± 6,4
1328,9	± 8,0
1339,3	± 15,9
youngest population:	
169	**± 11**

666

667

CSR-SA

Age (ka)	± 2σ (ka)
232,3	**± 19,8**
240,9	**± 8,2**
244,5	**± 5,7**
246,8	**± 6,9**
263,1	± 4,6
263,7	± 29,1
310,1	± 16,3
395,5	± 5,0
407,9	± 4,4
476,6	± 7,1
488,3	± 5,3
494,5	± 4,7
500,8	± 6,8
508,5	± 3,5
542,1	± 17,2
552,1	± 9,0
563,1	± 6,2
597,3	± 3,7
625,7	± 6,7
805,2	± 9,7
youngest population:	
244.0	**± 3.8**

668

CAR-SA

Age (ka)	±1σ (ka)
298,19	**± 3,50**
397,35	± 2,69
397,55	± 2,50
401,16	± 3,23
401,50	± 6,70
401,92	± 4,30
409,08	± 4,09
409,45	± 2,28
410,43	± 3,01
416,80	± 2,14
417,80	± 1,90
417,86	± 27,38
420,18	± 3,26
430,43	± 2,92
447,50	± 15,16
461,11	± 3,89
468,78	± 18,49
523,49	± 3,21
566,40	± 2,82
580,99	± 3,19

669

670

671

672 Table 4 - 40Ar/39Ar ages of dated samples
673

674

675 **4.6 $^{40}Ar/^{39}Ar$ data**

676 Single crystal age data for the three analyzed samples are reported in Table 4. Full analytical
677 data are proved in Supplementary Material #3.

678 **4.6.1 Sample CR3**

679 Thirty-nine sanidine crystals extracted from the sand sample collected ca. 90 cm below the
680 ground surface in Colle Rotondo provided a wide age spectrum, ranging 1.31 through 0.13 Ma.
681 A youngest population of eight crystals yielded a weighted mean age of 134±3.5 ka.

682 **4.6.2 Sample TML-SA**

683 Forty-one sanidine crystals extracted from the sand sample collected ca. 60 cm below the
684 ground surface in Tenuta Monte di Leva provided ages ranging 1.34 through 0.15 Ma. A
685 youngest population of six crystals yielded a weighted mean age of 169±11 ka.

686 **4.6.3 Sample CSR-SA**

687 Twenty sanidine crystals extracted from the sample collected in the fluvial sand cropping out
688 in Castel Romano provided ages ranging 0.80 through 0.23 Ma. A youngest population of four
689 crystals yielded a weighted mean age of 244±4 ka.

690 **4.6.4 Sample RSC-SA**

691 Twenty sanidine crystals extracted from the sample collected in the fluvial sand cropping out
692 in Riserva Carpineto provided one isolated, youngest crystal of 298±3.5 ka. The majority of
693 the crystal ages are spread in the interval 398-468 ka, with three oldest crystals ranging 523 -
694 581 ka.

695

696 **5. Discussion**

697 **5.1 Soils and paleo-surfaces**

698 Analysis of soil samples for the present study has been conducted aimed at identifying their
699 sedimentologic and petrographic features, in order to understand their origin and the
700 paleogeographic conditions in which they formed. Pedologic considerations and a complete
701 study of the processes ~~that superintended to~~involved the formation of these soils, as well as
702 laboratory granulometric analyses are beyond the scope of the present work. Our main scope
703 is to verify ~~at which~~to what extent the present ground surfaces characterized by the same
704 elevations range represented in Figure 2 and 3 can be considered indicative of the original
705 paleo-surfaces representing the ancient coastal settings. In particular, we want to quantify the
706 possible amount of later deposition, or erosion, which may have increased or decreased,
707 respectively, the average elevation of these paleo-surfaces, therefore affecting our estimation
708 of the sea-level related with the corresponding coastal terrace.

When studying the composition of the soils developed above the reconstructed paleo-surfaces, some preliminary considerations are necessary. In particular, when the paleo-surfaces of highest order are considered (i.e. those ranging 98-108, 80-89, and 71-79 m a.s.l., Figure 3), we must realize that the sub-horizontal attitude of these isolated, plateau-like sectors ~~prevents~~ precludes alluvial sedimentation, almost completely. ~~In second instance~~Furthermore, the whole catchment area drained by these paleo-surfaces is ~~develops~~ developed above volcanic deposits. Therefore, the s~~ilicoclastic~~iliciclastic component of the soils above the paleo-surfaces of this sector, which in the X-ray diagrams is sometimes predominant, can only have the following two origins:

i. it can be a back-beach to coastal plain sediment originally deposited above the volcanic substrate when the paleogeographic conditions allowed ~~it~~ (i.e.: before the regional uplift, when the paleo-surface represented a coastal environmental setting) (BB and AL in Figure 11a);

ii. it can be an aeolian sediment (i.e., loess-like) accumulated above the volcanic deposits through air-fall emplacement and successively diffused within the soil by vertic processes (i.e.: internal turnover of soil material originated by pedogenetic processes).

Recognizing the origin of this s~~ilicoclastic~~iliciclastic sediment is therefore fundamental in order to reconstruct the paleogeographic setting of these paleo-surfaces, correctly, as shown in Figure 11, ~~where~~ in which the paleogeographic scenario is illustrated. The dashed green line in Figure 11 separates the sampling sites where field observation have shown that the present soil overlies sedimentary sand deposits (to the southwest), from those where the soil is ~~develops~~ developed above the volcanic deposit of Pozzolanelle (to the northeast), as reported also in the cross-section of Figure 12. The oblique green lines indicate the area where the s~~ilicoclastic~~iliciclastic fraction in the analyzed soils ~~id~~ is predominant.

Composition of the analyzed soils overlying the volcanic deposit of Pozzolanelle, with abundant quartz and feldspar, combined with micromorphological and SEM analyses which confirm the sedimentary origin ~~for~~ of the quartz grains but rule out an aeolian (loess-like) origin, at least for the larger fraction (>200 μm; Figure S7), demonstrate that these soils affect thin (≤ 1 m) layers of alluvial and backbeach, ~~prevalently~~ predominantly s~~ilicoclastic~~iliciclastic deposits. ~~Consistent to~~In keeping with this interpretation, quartz abundance strongly decreases in soil samples collected in more inland locations (SPR, RUT), far from the inferred paleo-coastline (Figure 10).

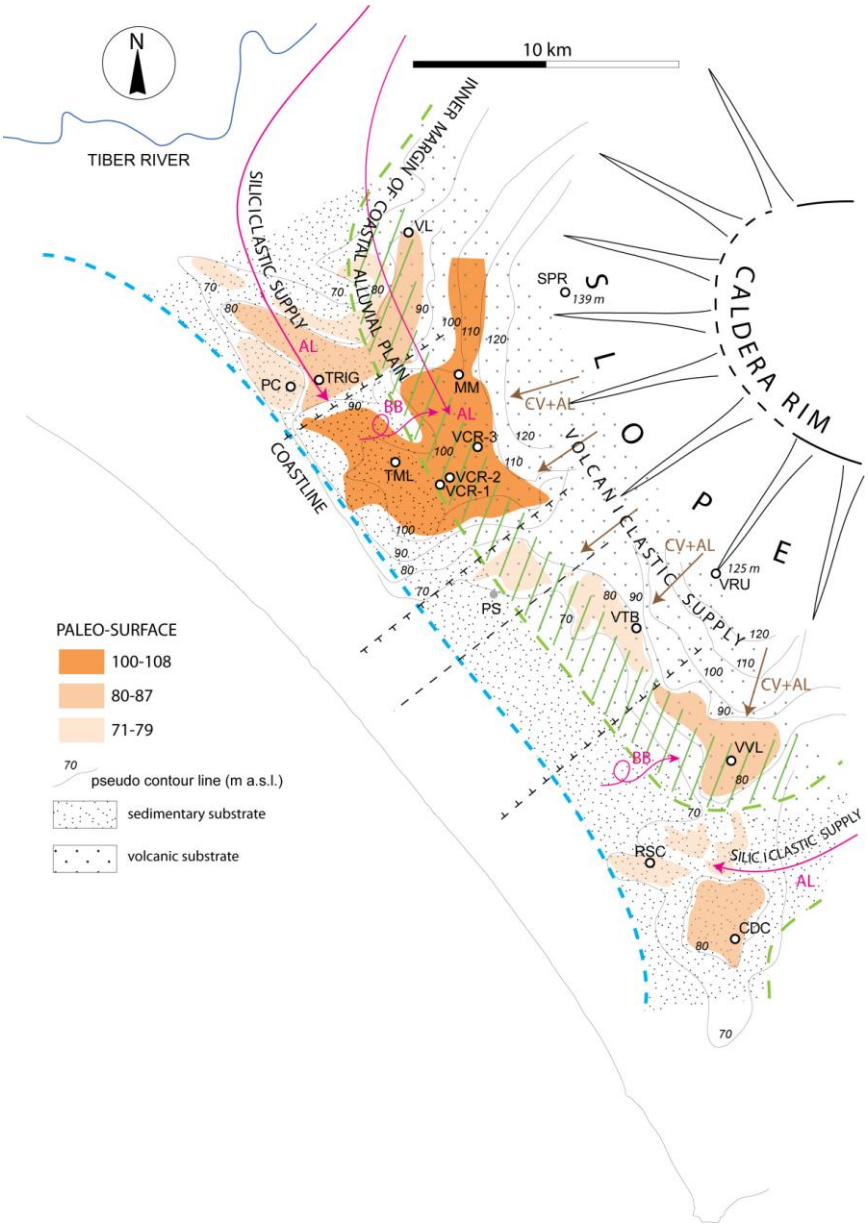

Figure 11- Paleogeographic reconstruction of the MIS 9 coastal setting. Stratigraphic investigations and sedimentologic~~-~~, micromorphologic, mineralogic and petrographic analyses on sediment and soil samples have allowed ~~at recognizing~~to detect a transitional zone (oblique green dashes) ~~in~~ correspond~~ence of~~ing with the inner margin of the coastal plain, where a thin horizon of backbeach to alluvial deposits overlaps the volcanic substrate. (see also cross-section in Figure 12a). This reconstruction evidences the occurrence of an original, homogeneous paleo-surface, subsequently disrupted and dislocated by tectonic movements, which ~~originated~~ gave rise to three main flat sectors at elevations ranging 100-108, 80-87, and 71-79 m a.s.l. (see text for comments).

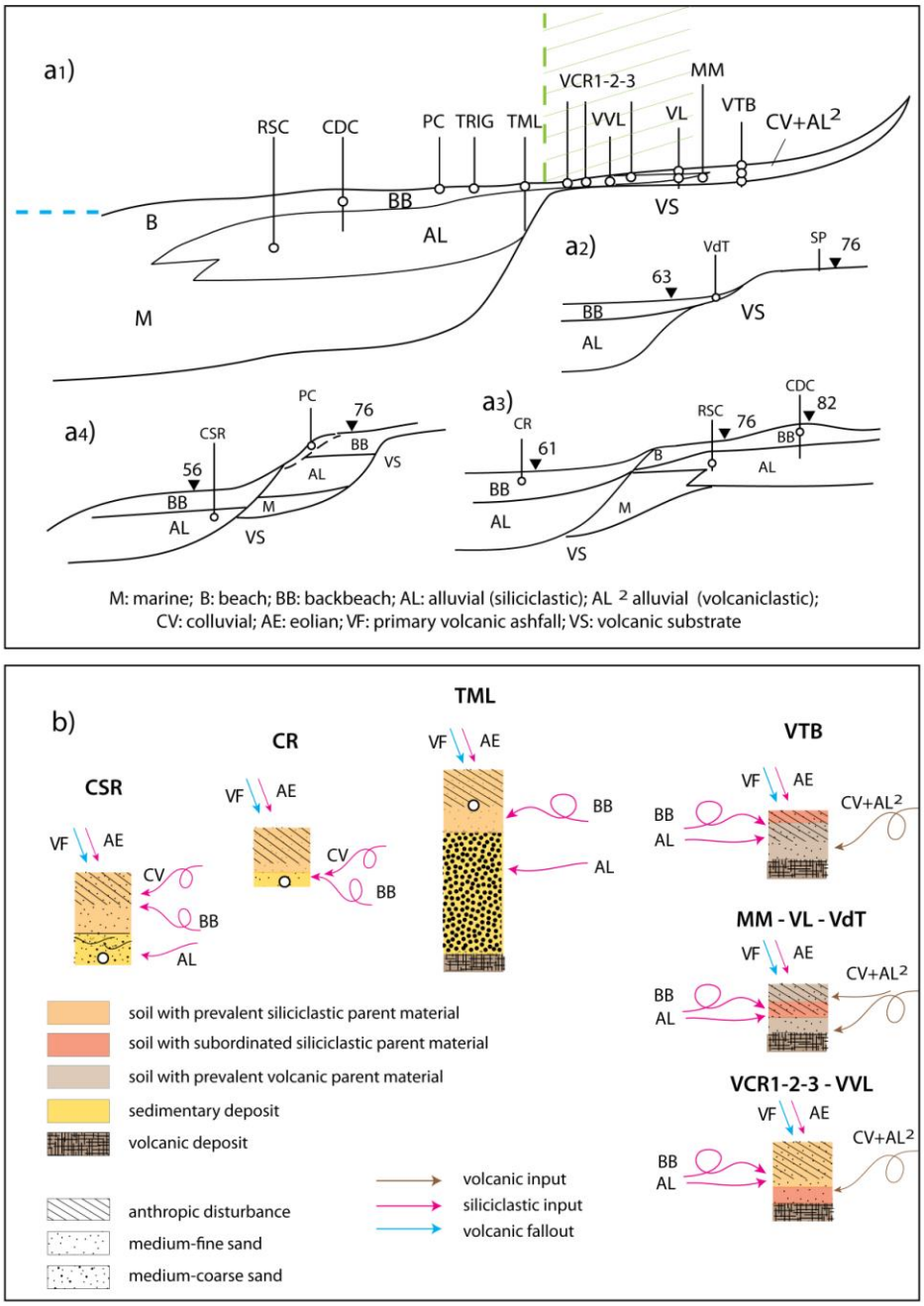

Figure 12 - a1-4) Cross-sections restored from tectonic dislocation showing the original paleogeographic and sedimentary settings reconstructed in the area where the soil and sediment samples were collected. b) Origin of the different sedimentary inputs contributing to the formation of the deposits and the related soils at the top of the paleo-surfaces reconstructed in the present study. See text for comments.

Alluvial/colluvial volcanic material (CV+AL in Figure 112b and 12), ~~deriving~~ derived from the rocks cropping out at the inner margin of the coastal alluvial plain (green dashed area in Figure 11), were also continuously mixing with the alluvial and backbeach, ~~prevalently~~ predominantly s~~ilicoclastic~~iliciclastic deposits transported by the Tiber River and deposited in the coastal plain. Moreover, air-fall~~en~~ material including either loess-like sediment (AE in Figure 12b), ~~as well~~or as primary air-fall~~en~~ volcanic ash (VF in Figure 12b), also progressively accumulated above this soils and ~~were~~ was diffused by vertic processes into the sub-surface horizon. To this aeolian fraction must be ascribed part of the K-feldspar observed in this section and evidenced in the diffractograms, as well as part of the finest silic~~o-~~iclastic component.

Such an air-fall contribution must be extended to the soils developed above the sedimentary deposits, in which the volcanic component is also represented by re-deposited mineral species of the underlying sedimentary substrate, incorporated in the soil through colluviation, surface water and wind transport (CV in Figure 12b).

These mechanisms are ~~resumed~~ envisaged in Figure 12, showing the different paleogeographic and sedimentary settings reconstructed in the area where the soil and sediment samples were collected. The age spectra provided by sanidine crystals extracted from the lowest portion (unaffected by agricultural disturbance) of the backbeach deposits above which the soils of the 98-108 and of the 61-67 paleo-surfaces have developed (TML-SA, CR3; Figure 13), compared to that of the "sealed" sedimentary deposit of the fluvial facies (RSC-SA, CSR-SA), provide further insights to the processes described above.

5.2 Age of the paleo-surfaces

Youngest crystal ages of 232±20 and 298±4 ka yielded by sedimentary samples collected in the alluvial facies (coastal plain) of the 51-57 m and of 71-79 m paleo-surfaces (CSR-SA and RSC-SA) support correlation with MIS 7 and MIS 9 for the corresponding coastal terraces~~, respectively~~, as discussed in the following sections.

Similarly, crystal ages of the samples collected ~~in~~ from the backbeach facies at the top of the 98-108 m and 61-67 m paleo-surfaces provide time constraints on the sedimentary processes that acted in the time span following retreat of the coastline leading to progressive ~~pauperization~~ impoverishment of sediment supply.

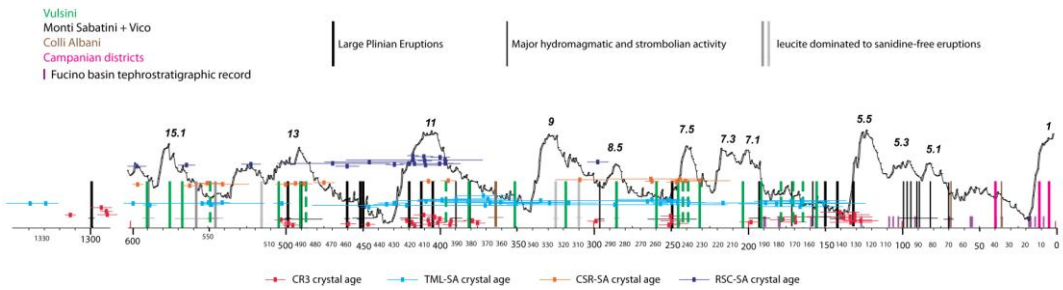

Figure 13 - Crystal age spectra for the four sedimentary samples dated in the present study. Each cross represents the age of one dated sanidine crystal with the associated analytical error at 2 σ. Comparison with the major eruptions occurred at the districts of the Roman Co-magmatic province is provided. Each bar represents one eruption age (see Suppl. Mat. for details and references). Comparison with the ~~Oxygen~~ oxygen isotope~~s~~ curve (Lisiecki and Raymo, 2005) is also shown. See text for comments.

These age constraints are obtained by comparing the sample crystal ages with the eruptive histories of the volcanoes of the Latium Region, as provided in Figure 13. In considering the eruptive histories of the volcanic districts of Central Italy to compare age spectra yielded by the analyzed sedimentary samples reported in Figure 13, some preliminary considerations should be made.

i- These volcanoes are part of the "Roman Magmatic Province" (Conticelli and Peccerillo, 1992), characterized by a K-rich geochemistry which accounts for the diffuse presence of sanidine ($KAlSi_3O_8$) and leucite ($K[AlSi_2O_6]$) crystals, which also constitute the means of $^{40}Ar/^{39}Ar$ dating. However, while sanidine is a very resistant mineral species, leucite is highly sensible to weathering and easily ~~turns out in~~alters to analcime ($NaAlSi_2O$): a~~n alteration~~ process implying loose of K and ~~hindering possibility of~~compromising $^{40}Ar/^{39}Ar$ dating. Indeed, fluvially transported and beach deposits of several hundred kyr lack ~~of~~ pristine leucite crystals. Therefore, in Figure 13 we have not reported all the sanidine-free eruption units (i.e., most of those of the Colli Albani volcanic district, see Gaeta et al., 2016 and references therein), while we have indicated those dominated by leucite (for which a lesser statistical occurrence is expected).

ii- When incorporation of crystals ~~deriving~~ derived from primary fallout deposits is considered, the overall eastward regional winds and a consequent dispersal axis should be considered, along with the ~~vent~~ distance from the source area. Therefore, the major source of fallout deposits are the MSVD and Vico, while deposits from the Colli Albani and the Campanian districts have a low probability ~~to be~~of ~~represented~~ representation in the stratigraphic record. ~~It makes exception t~~One exception is represented by the sanidine-bearing activity of the Albano Center spanning 70 through 36 ka (Giaccio et al., 2009, and ref.),

Formatted: Superscript
Formatted: Superscript
Formatted: Superscript
Formatted: Superscript

for which the small vent distance should ~~grant~~ have led to a well-represented crystal population, as also evidenced by outcrops in the southeastern area of the CAVD (e.g., Cisterna di Latina, Latina Plain; Gatta et al., 2018, Sevink et al., 2018). Moreover, huge explosive eruptions like the Campanian Ignimbrite (39 ka), Neapolitan Yellow Tuff (12 ka) and Avellino pumice (4 ka) have provided widespread tephrostratigraphic markers in Latium (e.g., Giaccio et al., 2017).

iii- ~~Youngest~~ The youngest eruptions should be ~~more~~ better represented given the ~~largest~~ larger outcrop~~ping~~ areas of the products ~~with respect~~ in ~~to~~comparison with the older ones, which are buried under more recent cover. ~~Thus~~ This ~~reinforcing~~ reinforces the principle that a lack of crystals younger than the youngest population is evidence of deposition prior to ~~evidences a deposition time preceding age of~~ the immediately following eruption.

Consistent with the considerations above, Figure 13 shows that the age spectra of sanidine crystals extracted from the four sand samples record a long eruptive history, ranging 0.60 - 0.13 Ma, plus one isolated cluster around 1.3 M. All crystal ages ≤0.6 Ma match known eruption ~~occurred at~~s of the Monti Sabatini, Vico and Vulsini volcanoes (Palladino et al., 2010; Sottili et al., 2010; Marra et a., 2014, and ref. therein), while the oldest age matches that of early activity ~~occurred at~~of the Cimini volcanic complex (Everdin and Curtis, 1965, Nicoletti, 1969), located in the upper Tiber Valley east of Vico. In contrast, all the ~~missing literature~~ eruption ages known from the literature that are missing in the dated crystal populations, besides the sanidine-free Colli Albani products, also correspond to sanidine-free or leucite-dominated products from Vico and Monti Sabatini volcanic districts (Cioni et al., 1987; Sottili et al., 2004; Perini et al., 2004; Masotta et al., 2010; Marra et al., 2014).

Based on these premises, in the following we discuss sample age implications on assessing the age of the related paleo-surfaces.

5.2.1 CSR-SA - 51-57 m paleo-surface

Based on the sedimentary features of the underlying deposits and the top elevation ranging 51-57 m a.s.l. (Figure 9a-a"), the Castel Romano paleo-surface is interpreted as a backbeach context, including the dune system superimposing the delta plain, developed during highstasnd of MIS 7.3/7.1. Loose sanidine crystals occurring in the sand deposit of the braided fluvial channel facies (Figure 9a'-a") yielded a youngest age of 232.3±19.8 ka, part of a statistically significant youngest population of 244.0±3.8 ka (Table 4). Such datum has to be considered a terminus post-quem ~~terminus~~ which implies an age ≤ MIS 7.5 (Figure 13), excluding and age within MIS 9 and supporting correlation with highstand of the MIS 7.3/7.1.

5.2.2 RSC-SA - 71-79 m paleo-surface

~~Age~~ The age spectrum of sample RSC-SA, collected within the alluvial plain deposit underlying the 71-79 paleo-surface ~~in~~ at Riserva Carpineto, spans 581 - 398 ka, with a youngest crystal of 298±3.5 ka (Table 4). Most crystal ages are clustered between 460 and 390 ka, coincident with the large explosive phases emplacing sanidine-bearing products at Vico and Sabatini in this time span (Figure 13). In contrast, no crystal deriving from the Villa Senni eruption unit occurs in the dated sample, despite the sampled deposit overlies the Pozzolanelle eruption unit of 365±4 ka, consistent with the lack of sanidine phenocrystals in the Colli Albani products. The age of one single crystal yielding 298±3.5 ka has a poor statistical weight, and should be regarded as broadly indicative of the lack of crystals younger than 300 ka. However, it supports correlation with MIS 9 for the 71-79 m paleo-surface of Riserva Carpineto, suggesting that sedimentation in the alluvial plain was sealed in the late stages of the MIS 9 highstand, excluding an age within MIS 7, while an age within MIS 11 is also excluded by the fact that the sand deposit of Riserva Carpineto overlies the 365±5 ka Pozzolanelle pyroclastic-flow deposit.

5.2.3 CR3 - 61-67 m paleo-surface

Based on its sedimentologic features and the elevation ranging 61-67 m a.s.l., the Colle Rotondo paleo-surface is interpreted as a backbeach context, either part of a dune system or of a coastal alluvial plain, developed during highstasnd of MIS 7.5 (Figure 14a).

When the crystal ages from CR3 (red crosses in Figure 13) are compared to the eruptive histories of the volcanoes of the Latium Region, it is apparent that no eruption younger than 134±3.5 ka is recorded by the Colle Rotondo sand deposit. Indeed, given the large number of dated crystals (39) and the wide age spectrum observed, the lack of any crystal from the eruptive activity since 99 ka (see Figure 13) strongly suggests that the sample age should be constrained between 132 and 99 ka. In particular, a large hydromagmatic phase occurred ~~at~~ in several volcanic centers ~~at~~ of the MSVD, including Baccano, Stracciacappe, Le Cese, Acquarello, Piana dei Falliti and Martignano, 132±2 through 70±3 ka (Sottili et al., 2010; Marra et al., 2019b). While the earliest eruption that occurred at Baccano at 132±2 ka is evidently recorded by sample CR3, the lack of crystals from any ~~other successive~~later eruption strongly suggests a~~n~~ terminus ante-quem ~~terminus~~ of ca. 99±3 ka (age of the products of the 2nd Baccano unit, erupted at the beginning of the multi-vented hydromagmatic activity ~~enduring~~ that continued until 70±3 ka). Although this age boundary

to the deposit is in conflict~~ing~~ with the attribution to the Uluzzian for the lithic industry recovered at Colle Rotondo (Villa et al., 2018), we ~~remark~~ note that sample CR3 was not collected in the stratum in conjunction with the artifacts, but in a side excavation. Therefore, its correspondence with the archaeological layer is not safely established and provenance may be from the immediately underlying older substrate. In this latter case, the occurrence of the Uluzzian lithic assemblage at ca. 80 cm depth suggests that the overlying package of sediment accumulated during the last 40 ky. Such an accelerated accumulation may be linked with recent anthropic activity (e.g., agriculture), triggering soil mobilization. In contrast, the apparent age of ~134 ka for the sand layer at 80 cm depth ~~is~~ does not conflict~~ing~~ with an inferred age of 250-200 ka within MIS 7 for the Colle Rotondo paleo-surface, as discussed hereby based on a detailed analysis of ~~and when results of~~the $^{40}Ar/^{39}Ar$ ~~experiments~~ dating ~~are examined in detail, they give insights on its actual age and on the sedimentary processes that superintended to its formation~~results.

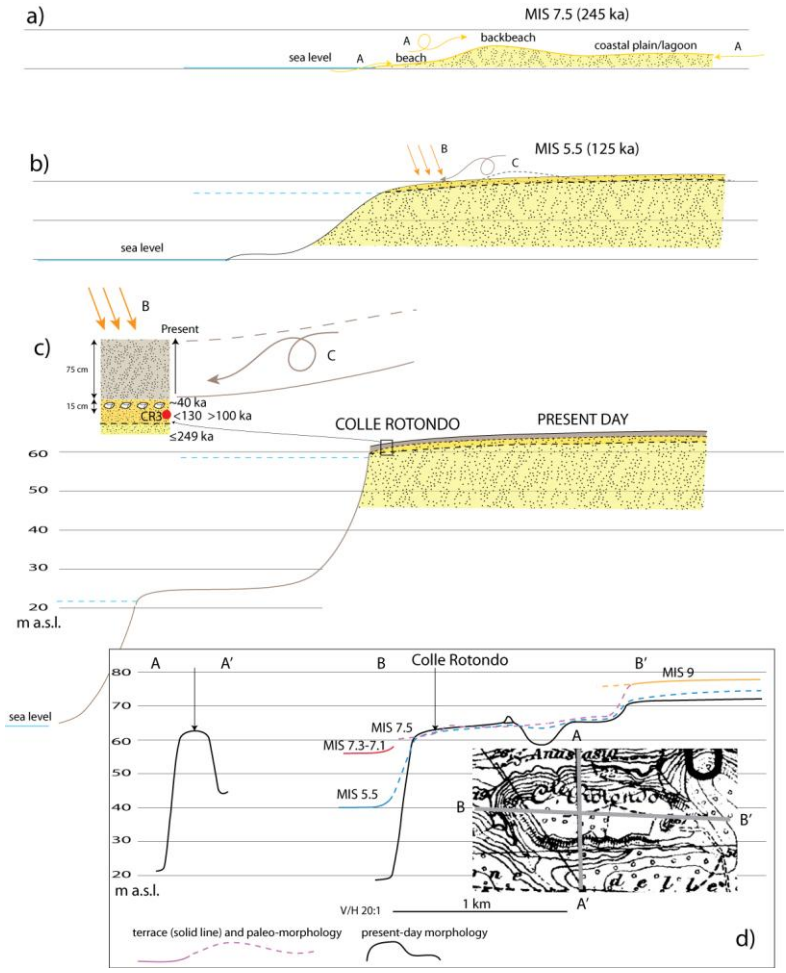

Formatted: Superscript

Formatted: Superscript

Figure 14 - Geomoprphological and paleogeographic evolution of the Collo Rotondo plateau (see text for step by step comment and explanation).

Like in the case of the sedimentary deposit sampled ~~in~~ at Castel Romano which yielded a youngest crystal age of 232±20 ka, consistent with a deposition age corresponding to the highstand of MIS 7.3-7.1 (i.e. 220-200 ka), an age ≥245 ka is expected for the fluvial/beach sedimentary deposit ~~from~~ at Colle Rotondo (supply A in Figure 14a) incorporating crystals ~~deriving~~ derived from erosion and re-deposition of the volcanic rocks erupted ~~until~~ before that time, corresponding to highstand of MIS 7.5 (i.e., 245 ka, see Figure 13). However, a progressively younger age is expected for the backbeach deposit deriving from mixing of wind-blown sediment previously deposited (supply C in Figure 14b) with crystals deriving from primary eruptions occurring in the following time span (supply B in Figure 14b). Sample CR3 from Colle Rotondo yielded a statistically significant (8 crystals) youngest crystal population of 134.2±3.5 ka which is characterized by significantly larger associated errors ~~with respect~~in ~~to~~comparison with the older populations (see Table 5). In particular, these crystals yielded an average associated error of ±11 ka (corresponding to 8.2% when an age of 134 ka is considered) ~~with respect~~in ~~to~~comparison with an average associated error of ±5.4 ka for the 23 crystals yielding ages spanning 249.9 - 503.2 ka (corresponding to 2.2% - 1.1%). These larger errors are due to the systematically smaller dimensions of these crystals, evidencing their different means of transport ~~with respect~~in ~~to~~comparison with that affecting the oldest ones, i.e.: wind vs. water. When this distinction is ~~noticed~~taken into account, we find a second significant population age of 249.3±3.4 ka, along with a few crystal ages ranging 200-170 ka (Table 4 and Figure 13), consistent with an age within MIS 7.5 for the original beach/alluvial deposit. An age ≥134±3.5 ≤198.4±7.3 ka is established for the sampled backbeach deposit, showing that it accumulated above the MIS 7.5 paleosurface ~~for~~ during ca. 110 ky (i.e., 245 through 134 ka). The lack of crystals deriving from the eruptions ~~occurred~~ between 132 ~~through~~ and 70 ka at the MSVD (see Figure 13), strongly suggests that the sampled layer cannot be younger. Indeed, accidental ~~lacking~~ absence of crystal ages within this time span is statistically unlikely, given the eastern dispersal axis of the MSVD eruption (e.g. Sottili et al., 2004; Di Rita and Sottili, 2019) and the occurrence of large explosive eruptions 90 through 70 ka at a number of centers of the so-called "Hydromagmatic Phase" (De Rita et al., 1983; Sottili et al., 2010; Marra et al., 2019b). This fact also testifies that the depositional context progressively changed after 245 ka, consistent with continued uplift of the coast and isolation of the Colle Rotondo remnant paleo-surface, which was unaffected by deposition of water transported sediment, like that occurring in alluvial plain or beach

943 contexts, while only eolian fallout deposits were emplaced, from then on. Since sample CR-1
944 occurs 90 cm below the present ground level (Figure 14c), we can infer that present elevation
945 of 63 m is a close approximation of the MIS 7.5 paleo-surface, which is overlain by a thin
946 eolian deposit accumulated since 245 ka ~~through the Present~~ (input B in Figure 14c). Indeed,
947 it is likely that samples collected closer to the surface would yield progressively younger ages,
948 consistent with incorporation of crystals deriving from the younger eruptions of 100 ka and
949 90 through 70 ka. However, the strong anthropic disturbance of the upper 70 cm of sediment
950 prevents any reliable analysis. Sample TML-SA from Tenuta Monte di Leva section provides
951 further inferences on the formation process of this thin eolian cover of the paleo-surfaces.
952

CR3	
Age (ka)	± 2σ (ka)
134,0	**± 14,3**
133,4	**± 13,7**
140,6	**± 12,5**
169,7	± 11,7
127,7	**± 11,3**
130,9	**± 11,2**
131,7	**± 9,7**
131,0	**± 9,6**
392,9	± 9,6
177,6	± 8,3
198,4	± 7,3
249,9	± 7,2
169,5	± 6,9
1293,0	± 6,9
245,3	± 6,6
251,6	± 6,6
250,7	± 6,5
410,7	± 6,5
495,5	± 6,5
1289,3	± 6,5
138,3	**± 6,3**
298,9	± 5,6
379,1	± 5,6
407,3	± 5,6
401,4	± 5,1
459,2	± 5,1
375,6	± 4,9
393,5	± 4,8
498,4	± 4,8
403,6	± 4,7
400,2	± 4,6
407,8	± 4,6
418,1	± 4,6
446,8	± 4,6
503,2	± 4,1
1289,9	± 3,9
421,7	± 3,8
416,5	± 3,5
1313,1	± 3,5
youngest population:	
134,2	**±3,5**

TML-SA	
Age (ka)	± 2σ (ka)
335,5	± 96,7
287,5	± 72,5
422,9	± 63,3
189,3	**± 54,3**
361,0	± 40,6
557,0	± 40,2
368,2	± 32,7
165,5	**± 28,5**
166,6	**± 27,9**
151,1	**± 27,6**
181,7	**± 25,4**
171,0	**± 24,9**
382,2	± 23,2
389,6	± 23,0
262,8	± 22,7
371,2	± 21,5
329,8	± 20,8
266,0	± 20,0
369,5	± 20,0
316,8	± 18,7
372,6	± 18,7
246,2	± 17,8
398,9	± 16,2
1339,3	± 15,9
351,5	± 15,7
430,5	± 10,9
435,7	± 8,7
1328,9	± 8,0
252,3	± 7,1
250,0	± 6,6
600,0	± 6,4
216,5	± 6,0
409,6	± 5,9
446,4	± 5,6
504,4	± 5,6
549,4	± 5,4
257,6	± 5,1
541,7	± 5,0
239,9	± 4,7
589,3	± 4,4
551,8	± 4,3
youngest population:	
169	**±11**

CSR-SA	
Age (ka)	± 2σ (ka)
263,7	± 29,1
232,3	**± 19,8**
542,1	± 17,2
310,1	± 16,3
805,2	± 9,7
552,1	± 9,0
240,9	**± 8,2**
476,6	± 7,1
246,8	**± 6,9**
500,8	± 6,8
625,7	± 6,7
563,1	± 6,2
244,5	**± 5,7**
488,3	± 5,3
395,5	± 5,0
494,5	± 4,7
263,1	± 4,6
407,9	± 4,4
597,3	± 3,7
508,5	± 3,5
youngest population:	
244	**±4**

Table 5

5.2.4 TML-SA - 98-108 paleo-surface

Much caution should be used in interpreting results for the TML-SA sample because it ~~is~~ was collected ca. 60 cm below the ground level within the soil horizon, in which both vertic processes and anthropic disturbance might have caused incorporation of younger crystals ~~coming~~ from the uppermost portion of the stratum.

However, the age spectrum of sample TML-SA, collected on the 98-108 paleosurface, is similar to that of CR3 but yields a youngest minimum age of 169±11 ka (Figure 13), evidencing a relative older age, with respect to the sample collected on the 61-67 paleosurface of Colle Rotondo.

These data suggest that the sampled sand deposit represents a sedimentary horizon that was sealed from air-fall input by 170 ka, supporting the notion that the uppermost portion of the reconstructed paleo-surfaces represents an accretionary horizon, built up mainly through accumulation of alluvially/colluvially transported and, subordinately, air-fallen material. Remarkably, also in this sample the youngest crystal population is characterized by larger associated errors (Table 5), supporting the different mean of transport for this sedimentary fraction which accumulated later, as an air-fall~~en~~ deposit above the underlying deposits of the alluvial plain.

The very low sedimentation rate and the limited thickness of these accretionary horizons overlying the "pristine" deposit ~~originat~~s forming the paleosurfaces, whose absolute age has been determined by $^{40}Ar/^{39}Ar$ dating on "in stratum" samples from Castel Romano and Riserva Carpineto, is consistent with the geomorphologic features of the TML and CR sectors, ~~preventing~~ precluding significant alluvial/colluvial sedimentation.

5.3 The MIS 9 paleo-surface

Geomorphological, lithostratigraphic, paleo-environmental and geochronological constraints ~~provided on~~obtained for the deposits of the 71-79 m paleo-surface, and part of the 80-89 m and 98-108 m paleo-surfaces, allow ~~at~~ the ~~identifying~~ identification of these paleo-surfaces as the remnant coastal terrace of the MIS 9 highstand, tectonically dislocated (Figure 11 and 15). The subrounded morphology, the medium to coarse grain-size and the ~~good~~ high degree of sorting of the sand deposits ~~of~~ at Riserva Carpineto (RSC) clearly indicate that the flat sectors at elevations ranging 71-79 m a.s.l. represent remnant ~~shreds~~ parts of an alluvial coastal plain, stretching NW to SE parallel to the present coastline (Figure 11 and 12a3). Crystal ages yielded by sample RSC-SA firmly constrain the formation of this coastal plain within MIS 9 (see also Figure 16). The bedded deposits of Campo di Carne (CDC), ranging from coarse sand

to silty clay, are suggestive of a coastal alluvial plain, overlain by a transgressive backbeach deposit forming a wide dune ridge system culminating at ca. 85 m a.s.l. in this area (Figure 11 and 12a3), and equivalent to that occurring in Trigoria (TRIG) at analogous elevations (Figure 11 and Figure 12a1). Evidence from the Tenuta Monte di Leva (TML) site shows that this backbeach setting homogeneously extends parallel to the paleo-coastline, but it is presently displaced ~~at~~ to a~~n~~ ca. 20 m higher elevation in this sector (Figure 15). Micromorphological analysis ~~on~~ of the ~~concretional~~concretionary layer observed in the TML ~~evidence~~ indicates that this massive horizon formed in alluvial to backbeach environment characterized by a water table close to the surface, consistent with the reconstructed paleogeographic conditions, which ~~indicate~~show that it was part of the coastal plain. The geologic substrate ~~in~~ at TML is indeed identical to that ~~in~~ at TRIG, apart from the larger thickness of the upper, aeolian sand horizon above the ~~concretional~~concretionary layer ~~in~~ at the latter location, consistent with a post-depositional tectonic displacement between these two sectors and limited erosion ~~occurred in~~at TML.

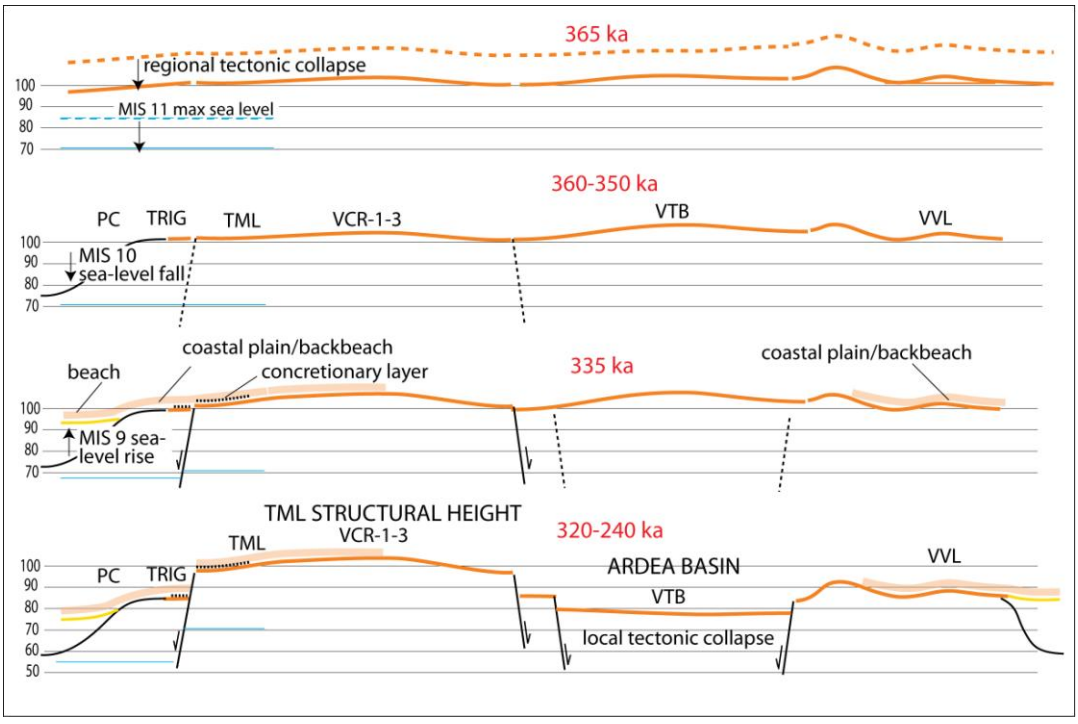

Figure 15 - Palinspastic reconstruction of the tectonic evolution of the coastal sector between the Tiber mouth and Anzio in the time span 365 ka (age of emplacement of the Villa Senni Eruption Unit during lowstand of MIS 10) and 240 ka (onset of MIS 7.5). a) A regional collapse immediately following emplacement of the pyroclastic flow-deposit is inferred ~~by~~ from the elevation gain between the top surface of aggaddationasl successions of MIS 11 and MIS 9. MIS 11. b) Erosion of the original paleo-surface occurs during the lowstand of MIS 10, 360

through 350 ka. c) Fluvial and coastal incisions are filled by sediment-aggradastion during glascial termination v V (335 ka) at the onset of the sea-level rise during MIS 9(335 ka), and as coastal setting including a beach to backbeach and coastal plain environment is formed forms during the MIS 9 highstand (325 ka). d) This homogeneous coastal setting is disrupted by faulyt displacement originating forming a structural heigh in the TML and a collapsed sector (Ardea basin) in during the time span 320--240 ka (MIS 7.5 highstand) as provided indicated by the upper chrono-morphological constraint represented by the inner edges of MIS 7.5 coastal terrace (see text for further explanation).

On the other hand, the 98-108 paleo-surface represents a striking geomorphological anomaly bordering the Ardea Basin to the NW (see also Figure 4), and is clearly interpretable as the result of differential uplift at the footwall of one a border boundary fault of the half-graben structure (Figure 11 and 15). Also the different geologic substrate that characterizes the 71-79 m paleo-surface within the Ardea Basin (e.g., VTB), which is formed by volcanic deposits (i.e.: the same substrate of as the inland portion of the 98-108 m paleo-surface in VCR 1-2), is suggestive of tectonic lowering following the formation of a homogeneous coastal setting platform during the highstand of MIS 9, throughout this region. DifferentlyIn contrast, in the case of a pre-existing gulf embayment in this area, the 71-79 m paleo-surface in at VTB should have had the same sedimentary substrate as that occurring in PC and RSC, testifying confirming a coastal environment. In particular, the tectonic collapse of the Ardea Basin is constrained between 320 ka (end of the MIS 9 highstand of MIS 9) and 240 ka (highstand of MIS 7.5) (Figure 15), as provided by the geometry of the 60-67 m and 51-57 m coastal terraces, evidencing indicating that a gulfn embayment formed by the time of establishment of the new coastline during MIS 7.5 through MIS 7.1 (see Figure 3 and 4). Remarkably, this time span is concident with the occurrence of the Monte delle Fate phase of activity at the Colli Albani Volcanic district (Gaeta et al., 2016, and references therein).

5.4 MIS 7.5 paleo-surface

The safe secure correlation with MIS 9 for the coastal plain deposits of the 71-79 m paleosurface, combined with previous geochronologic constraints that frame the 51-57m paleosurfaceon the 51-57 m paleosurface framing it within the broad MIS 7.5 - MIS 7.1 interval (Figure 16a), suggests that the intermediate 61-67 m surface should be correlated with the early interglacial 7.5, while the paleo-surface occurring a few meters below, at an elevation of 51-57 m, should be correlated with the latest later isotopic peaks 7.13-/7.3-1 which are not separated by a marked sea-level fall (See Figure 16a), and can be regarded as a single eustatic event. Crystal age distribution yielded by sample CR3 from Colle Rotondo

supports this correlation (Figure 16b). Based on the considerations reported above on the errors associated with the $^{40}Ar/^{39}Ar$ ~~experiment~~ dating and their direct relation with grain-size, we can infer that an alluvial coastal plain formed by 249.3±3.4 ka, an age remarkably coincident with glacial termination III at the onset of MIS 7.5 (Figure 16b), at ca. 60 m a.s.l.. It was successively mantled by a wind-blown deposit ~~coming~~ derived from the nearby beach ~~in~~ during the interval 200 - 170 ka, a time when the coastline re-~~approached~~bounded to the elevation of 60 m a.s.l. during sea-level high stands linked with the double peak in the isotopes curve of MIS 7.3 and 7.1. Indeed, according to geomorphologic reconstruction, sedimentologic features, and micromorphologic analysis, the Colle Rotondo sand is a backbeach deposit. The sand grains originated mainly from very ~~short~~ proximal aeolian transport from the beach, where the original sediment accumulated after being eroded and transported by the Tiber River and its tributaries (A in Figure 14a). Moreover, since formation of the dune ridge, more aeo~~a~~lian material, as well as primary, air-fallen volcanic deposits (including sanidine minerals, B in Figure 14a), accumulated above it. Eventually, this sector was isolated from the coastal environment by the continued uplift, and it was affected only by deposition of the syn-eruptive fallout deposit of the Baccano unit ~~occurred~~ at 132±2 ka. If we consider the strong uplift of more than 50 m that occurred ~~since~~ from 250 ka, the wind-blown depositional mechanism rapidly became ~~soon~~ ineffective, due to the increased elevation ~~gain~~ and distance from the coastline (e.g., by 125 ka, Figure 14b). The regional uplift, determining the deep ~~cutting~~ incision of the coastal terrace through the action of fluvial erosion, also ~~originated~~ generated the canyon-like morphology that characterizes this area, isolating the Colle Rotondo plateau and preventing alluvial sedimentation on its top (Figure 14c-d). Therefore, it is reasonable to assume that a very limited thickness of sediment accumulated above the original paleo-surface representing the coastal terrace, mainly by the air-fall mechanism and only subordinately, as a consequence of re-mobilization of pre-existing sediment, through wind transport, or water run-off and colluviation from the upper part of the plateau towards the lower sectors (C in Figure 14b). If we consider that the elevation gain between the top and the margins of the Colle Rotondo plateau is less than 4 m (Figure 14d), the latter depositional mechanisms must have acted in a very limited way.

5.5 MIS 7.3-7.1 paleo-surface

The 51-57 m paleo-surface previously detected ~~in~~ by Marra et al. (2016) has widespread expression ~~in~~ at Ponte Galeria (Fig. 2), where chronostratigraphic constraints on the underlying aggradational deposits (Vitinia Formation, Luberti et al., 2017 and references

Formatted: Superscript

Formatted: Superscript

therein) and their geometric/stratigraphic relationship with the 36 m terrace unambiguously provide correlation with the four-stepped sea-level rise that characterized MIS 7 (Marra et al., 2016b). In particular, an early aggradational phase of the Vitinia Formation around 269 ka matches ~~a first~~the initial sea-level rise (A' in Fig. 16b) preceding the marked sea-level jump of glacial termination III that occurred at 240 ka, ~~to~~ with which in turn is associated the main aggradational succession of MIS 7.5, bracketed by post-quem ages of 253±8 ka and 248±4 ka (A in Fig. 16b).

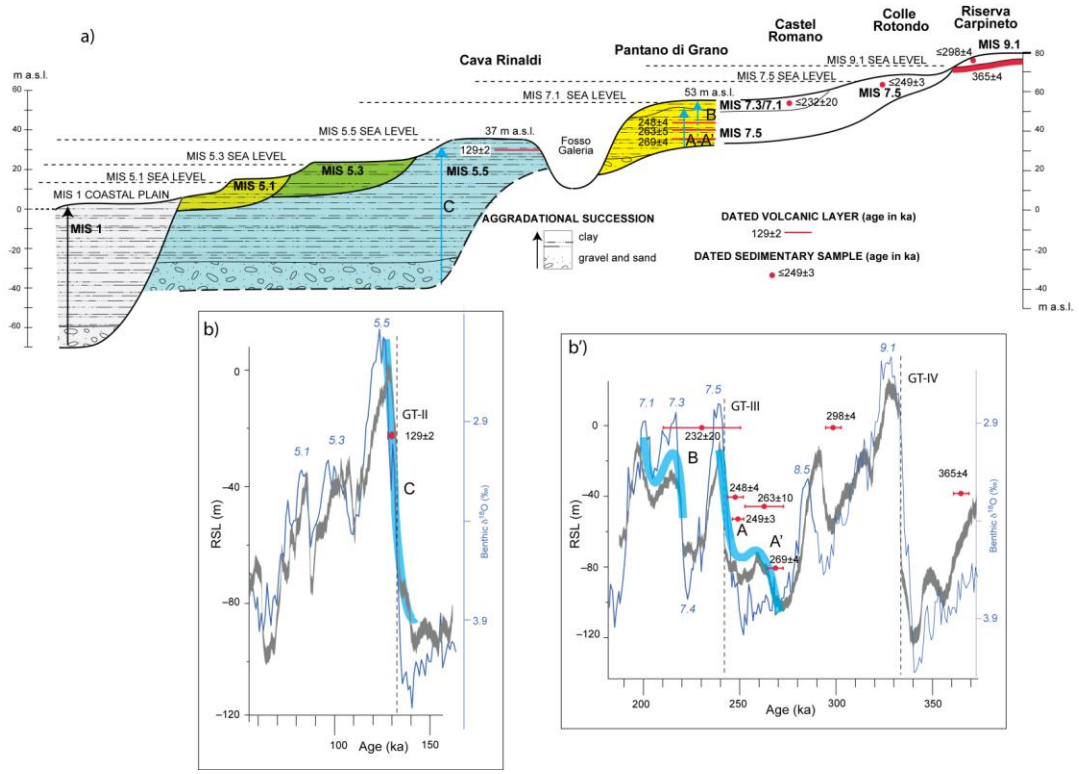

Figure 16 - a) Ideal~~ized~~ cross-section reconstructing the terraced deposits and the corresponding aggradational successions in the investigated coastal sector, showing the geochronologic constraints providing correlation with MIS 9.1 through MIS 5.5. b-b') Ages of the dated volcanic deposits and reworked crystal populations (red dots, bars indicate the analytical error at 2σ) are compared with the Oxygen isotope curve (Lisiecki and Raymo, 2005) and the Relative Sea Level (RSL) curve (Grant et al., 2014). Correspondence of sediment aggradation with ~~the~~ phases of ~~faast~~ rapid sea-level rise (thick blu lines) during ~~the~~ glacial terminations (GT) is highlighted.

Finally, a marked unconformity cuts the deposits of MIS 7.5 aggradational succession and is overlain by a new aggradational succession that represents the ~~sedimentary~~ deposit forming the flat top of the hills constituting the relict paleo-surface of 56-52 m a.s.l. The intervening erosional phase and the following sediment aggradation evidently match the sea-level fall of

MIS 7.4 and the successive two-stepped sea-level rise of MIS 7.3 - MIS 7.1 (Marra et al., 2016b; B in Fig. 16b). This observation corroborates the new assessment of the 51-57 m paleo-surface, and its attribution to the later stages of MIS 7.3/7.1, rather than to MIS 7.5, as shown by correlation provided in cross-section of Figure 16a.

5.6 MIS 5.5 - 5.3 - 5.1 terraces

The occurrence of a suite of three lowest ~~orders of~~ coastal terraces has been shown by geomorphologic reconstruction of their relict surfaces provided ~~in~~ by Marra et al. (2016a, 2019a), who also demonstrated that three distinct successions of coastal plain sediments, corresponding to three coastlines at circa 34, 24 and 12 m a.s.l., are associated with these terraces (Figure 16a). The $^{40}Ar/^{39}Ar$ age of 129±1 ka on a pyroclastic-flow deposit intercalated within the aggradational succession forming the 36 m terrace ~~in~~ at Cava Rinaldi (Epi-Tyrrhenian Formation, Marra et al., 2015) demonstrated correlation with the MIS 5.5 highstand of 125 ka (Figure 16b'). The two lower terraces at 26 and 16 m were therefore tentatively correlated with the sea-level highstands of MIS 5.3 and 5.1, respectively. However, an intervening tectonic collapse of ca. 10 around 100 ka, interrupting a steady uplift phase between 250 ka and the ~~Present~~ Holocene had to be invoked by Marra et al. (2016a), in order to reconcile elevation of the terrace at 26 m with absolute sea-level established for MIS 5.3 and 5.1 in the literature (e.g. Rohling t al., 2009). A discussion of the age of these terraces is beyond the scopes of the present paper, and further geochronologic and sedimentologic investigations of these youngest successions are in progress, aimed at verifying their exact correlation with the MIS timescale. However, in the present study we have found an excellent fit of the new geomorphological and statistical assessment of these paleo-surfaces with the previous results ~~in~~ of Marra et al. (2016a, 2019a), and we maintain preliminary correlation with the three marine isotopes' sub-stages of MIS 5.5, 5.3, and 5.1 in the discussion of the tectonic uplift.

Formatted: Superscript

Formatted: Superscript

5.7 Tectonic implications

All the sea-level markers provided by the aggradational successions of the Paleo-Tiber River correlated with MIS 21 through MIS 1 from literature and from the present study are shown in Figure 17a. Differences in elevation among the different coastal deposits assumed as sea-level markers (green shading in Figure 17a) ~~is~~ are the result of the intervening tectonic movement (uplift or collapse) combined with the difference in maximum sea-level at each interglacial (glacio-eustatic component). This latter element is estimated assuming a sea-level

10 m lower than ~~in the~~ present during MIS 21 through MIS 15 (blue crosses in Figure 17b') based on previous literature ~~data~~ (Marra et al., 2016 and references therein), while values estimated in Rohling et al. (2009) are considered for MIS 13 through MIS 5.1 (green crosses).

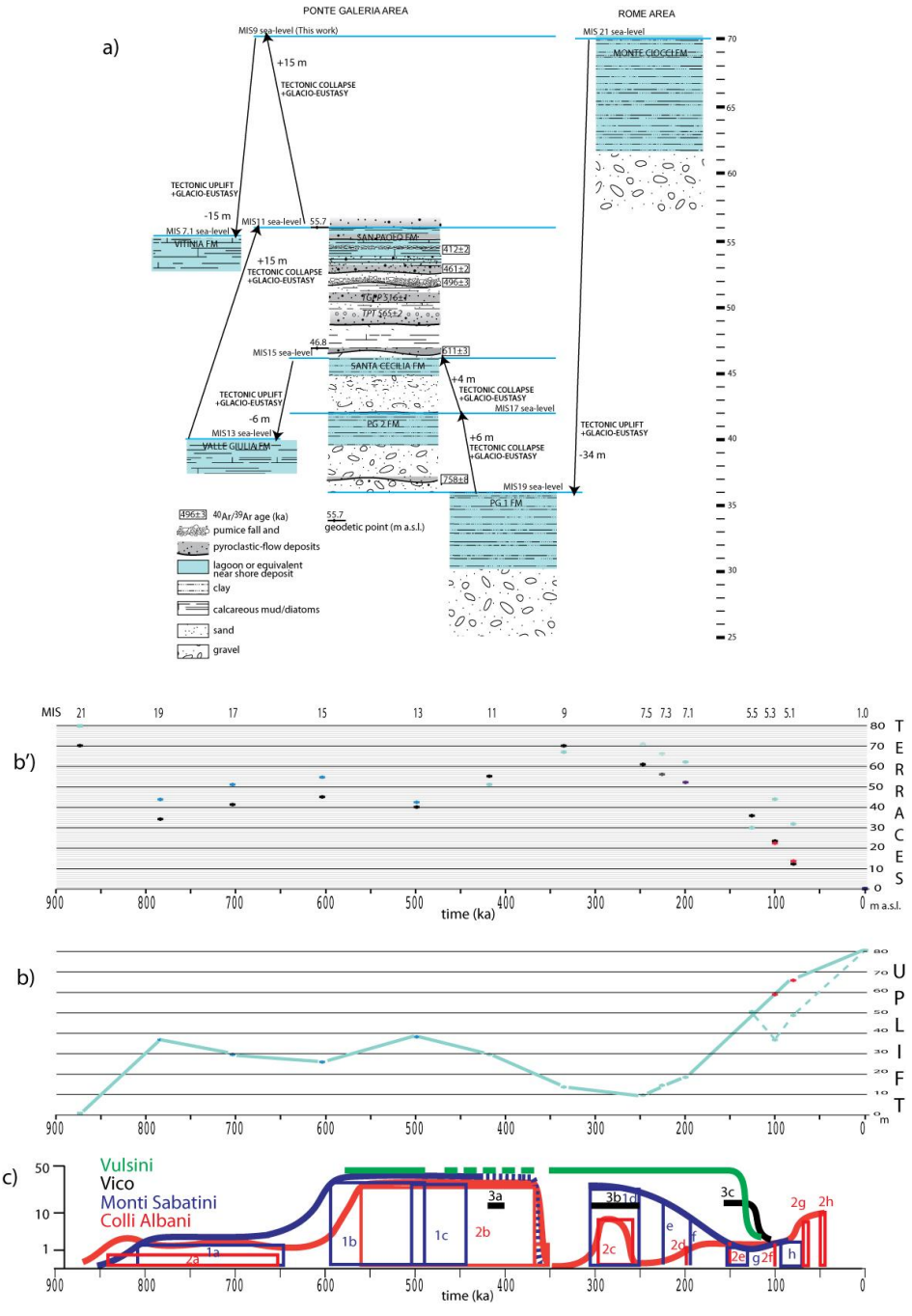

Figure 17 - a) Synoptic ~~picture~~ representation of the different sections from the Rome~~'s~~ area ~~exposing~~ indicating the aggradational successions and related sea-level indicators correlating with MIS 21 through MIS 7, integrating geochronologic and stratigraphic data from Karner and Renne, 1998; Karner and Marra, 1998; Karner et al., 2001b; Marra et al., 1998; 2016b; 2017a.

Alternative values for MIS 5.3 and 5.1 (red crosses) are also used to assess the uplift curve for the last 125 ka, based on the assumption of a more reliable uniform tectonic uplift in this time span, and on recently provided geochronologic and geomorphologic constraints ~~to~~ on the related sea-level markers (Marra et al., 2016a, 2019a). Once the correction for the glacio-eustatic component is applied, the cumulative uplift curve of Figure 17b is obtained. Similar to previous work (Marra et al., 2016a, 2019b), comparison between the uplift curve and the eruptive histories of the volcanic districts of the Roman Province is also provided (Figure 17c). ~~With respect~~In comparison ~~to~~ with previous reconstructions (e.g., Marra et al., 2016a) this refined uplift curve displays a marked subsidence phase between 500 and 300 ka, as provided by assessment of the MIS 9 sea-level markers at ca. 70 m a.s.l. ~~estabilshed~~ established in the present work (Figure 17a). This fact ~~enhances~~ reinforces the coupling already ~~remarked~~ noted with the occurrence of two major phases of common volcanic activity at Colli Albani and Monti Sabatini 850 through 650 and 600 through 350 ka. In particular, uplift coincides with the onset of these phases, while subsidence characterizes the eruptive time spans. The ~~subsiding~~ subsidence phase ~~endures~~ continued until 250 ka and also encompasses ~~also~~ the ~~climactic~~ climax phase that, after a ca. 50 kyr dormancy, occurred at Vico, Monti Sabatini and Colli Albani, spanned the interval 320 - 250 ka, during which a rejuvenation of the volcanic activity occur~~s at~~red in all the districts of central Italy (Marra et al., 2004). The geochronologic constraints provided here ~~to~~ for the MIS 7.5 and MIS 7.3/7.1 terraces allow~~s at defining~~ a better definition of the beginning of the most recent uplift phase ~~since~~ post-250 ka, which is characterized by an initial low gradient followed by a steady, steep increase 200 though 80 ka, and by a waning trend until the ~~Present~~ present (solid green curve in Figure 17b). As previously ~~remarked~~noted, this new uplift phase heralds and accompanies the latest volcanic phases ~~occurred~~ during 90 - 70 ka a~~s~~t Monti Sabatini and 70-36 ka at Colli Albani, and it has been suggested to be related ~~with~~ to the onset of a new magmatic phase extending from southern Latium to the Campanian districts of Phlegraean Fields and Vesuvius (Mara et al., 2016a). In contrast, volcanic activity seems to ~~be~~ have been ~~estinguished~~ extinguished ~~at~~ inthe districts of northern Latium (Vulsini, Vico) since 100 ka. However, Marra et al. (2019a) have shown that this recent uplift phase ~~homogeneously~~ hs ~~affects~~

affected the whole coast of Latium homogeneously, ~~comprising the northern sector facing the Vulsini and Vico districts,~~ in apparent conflict with the lack of a new magmatic phase at these volcanoes. In contrast, ~~estinguishment~~ cessation of the activity at Vulsini and Vico matches the sudden tectonic collapse which is inferred when the current sea-level values for MIS 5.3 and 5.1 are assumed (dashed portion of the uplift curve in Figure 17c). However, ~~hypothesizing~~ a direct link between local volcanic activity in the northern sector and the global tectonic signal in this region is unlikely. Moreover, recent geochronologic and geomorphologic data strongly ~~support~~ imply that anomalous sea-levels characterized the MIS 5.3 and MIS 5.1 highstands in the Mediterranean region, suggesting the unforseen role played by Glacial Isostatic Adjustment (GIA) on regional tectonics during the the post-glacial period (Marra et al., 2019a).

Future investigation~~s~~ is need~~s to be addresse~~d in order to understand this complex framework of vertical movement, volcanic activity and glacio-eustasy affecting the Tyrrhenian Sea Margin during the last million years. Indeed, we ~~remark~~ note that beyond the common assumption of a interconnection between subduction, volcanism and regional uplift in the back-arc domain of the central Apennines (e.g., Conticelli and Peccerillo 1992), no dedicated study aimed at ~~individuating~~ evaluating the geodynamic and isostatic forces responsible for the observed tectonic uplift has been ~~addressed~~ undertaken so far.

6. Conclusions

Combined geomorphologic study and statistical analysis, ~~and~~ together with review and re-analyses of previous ~~literature~~ published data, have allowed us to identify a set of paleo-surfaces defined by discrete classes of elevation for topographic culminations in the coastal Tyrrhenian Sea sector of central Latium.

We recognized eight such paleo-surfaces defined by the elevation ranges: 98-108, 80-89, 71-79, 61-67, 51-57, 30-43, 22-27, 11-17 m a.s.l..

The three lowest paleo-surfaces are narrowly elongated parallel to the coastline and were identified through definition of the corresponding sea-level markers and geochronologic constraints in previous studies as the marine terraces of MIS 5.5, 5.3 and 5.1, (Marra et al., 2016a, 2019a).

The highest five paleo-surfaces have been investigated here and their physical extension has been validated through DEM analyses, in order to compare the results of the geomorphological study on 1:25.000 topoghraphic maps.

The sedimentologic-stratigraphic features of the soils and of the sedimentary deposits forming these paleo-surfaces have been investigated ~~aimed~~ in order to define their paleogeographic context and to identify the sea-level markers for those which have been interpreted as remnant portions of coastal terraces.

$^{40}Ar/^{39}Ar$ ages of detrital sanidine extracted from the sandy deposit of the recognized coastal ~~plain setting~~terraces has allowed us to correlate the 71-79 m, the 61-67 m, and the 51-57 m paleo-surfaces with the coastal terraces formed during the MIS 9.1, MIS 7.5, and MIS 7.3/7.1 highstands, respectively.

~~The p~~Paleogeographic reconstrcution has allowed us to interpret the 71-79 m, ~~the~~ 80-89 m, and ~~the~~ 98-108 m paleo-surfaces as ~~one~~ a sngle tectonically displaced, widespread coastal ~~setting~~ platform ~~originated~~ formed during the MIS 9.1 highstand.

Based on the combination of our refined dataset of terrace elevations with ~~literature~~ published data on relative elevation of maximum sea level during the highstands of MIS 21 through MIS 5.1, we assess the regional uplift curve in the last 900 ka and ~~we~~ recognize the occurrence of a climactic extensional tectonic phase affecting this coastal sector between 320 and 240 ka, concident wirth occurrence of the Monte delle Fate phase of activity at the Colli albani Volcanic district.

Formatted: Superscript

Formatted: Superscript

Supplementary Material #1- 1:25.000 basemap with topographic culminations

Supplementary Material #2A: Micromorphology: Methods - Fig. S1-S6
#2B: X-Ray power diffraction methods **#2C**: SEM microphotographs - Fig. S7
Supplementary Material #2D - Diffractograms
Supplementary Material #3a, b: Full 40Ar/39Ar data.

REFERENCES

Barberi, F., Buonasorte, G., Cioni, R., Fiordelisi, A., Foresi, L., Iaccarino, S., Laurenzi, M.A., Sbrana, A., Vernia, L., Villa, I.M., 1994. Plio-Pleistocene geological evolution of the geothermal area of Tuscany and Latium. Mem. Descr. Carta Geol. d' It. 49, 77-134

Bridgland, D.R., Westaway, R., 2008. Climatically controlled river terrace staircases: a worldwide Quaternary phenomenon, Geomorphology 98, 285–315.

Cioni, R., Sbrana A., Bertagnini, A., Buonasorte G., Landi, P., Rossi, U., Salvati, L., 1987. Laurenzi, M.A., Tephrostratigraphic correlations in the Vulsini, Vico and Sabatini volcanic successions. Periodico di Mineralogia 56, 137-155.

Conticelli, S., Peccerilllo, A., 1992. Petrology and geochemistry of potassic and ultrapotassic volcanism in central Italy: petrogenesis and inferences on the evolution of the mantle sources, Lithos 28, 221-240.

De Rita, D., Funiciello, R., Rossi, U., Sposato, A., 1983. Structure and evolution of the Sacrofano-Baccano caldera, Sabatini Volcanic Complex, Rome: J. Volcanol. Geotherm. Res. 17, 219-236.

De Rita, D., Faccenna, C. Funiciello, R. Rosa, C., 1995. Stratigraphy and volcano-tectonics, in The Volcano of the Alban Hills, edited by R. Trigila, Università degli Studi di Roma "La Sapienza", Roma, 33–71.

Everdin, J.F., Curtis, G., 1965. The potassium-argon dating of Late Cenozoic rocks in East Africa and Italy. Current Anthrop., 6, 343-369.

Faccenna, C., Funiciello R., Bruni A., Mattei A., Sagnotti L., 1994c. Evolution of a transfer-related basin: the Ardea Basin (Latium, Central Italy). Basin Research 5, 12-11.

Farr, T. G., Hensley, S., Rodriguez, E., Martin, J., Kobrick, M., 2000. The Shuttle Radar Topography Mission, Proceedings of a Conference held 26-29 October 1999, Toulouse, France. European Space Agency, 2000. ESA-SP vol. 450, ISBN: 9290926414, p.361.

Ferranti, L., Antonioli, F., Mauzc, B., Amorosi, A., Dai Pra, G., Mastronuzzi, G., Monaco, C., Orrù, P., Pappalardo, M., Radtke, U., Renda, P., Romano, P., Sansò, P., Verrubbi, V., 2006. Markers of the last interglacial sea-level high stand along the coast of Italy: Tectonic implications. Quaternay International 145/146, 30-54.

Freda, C., Gaeta, M., Palladino, D. M., Trigila, R., 1997. The Villa Senni Eruption (Alban Hills, Central Italy): the role of H_2O and CO_2 on the magma chamber evolution and on the eruptive scenario. Journal of Volcanology and Geothermal Research 78, 103-120.

Gaeta, M., Freda, C., Marra, F., Arienzo, I., Gozzi, F., Jicha, B., Di Rocco,T., 2016. Paleozoic metasomatism at the origin of Mediterranean ultrapotassic magmas: constraints inferred from time-dependent geochemistry of volcanic products from Colli Albani (Central Italy), Lithos, 244, 151-164. http://dx.doi.org/10.1016/j.lithos.2015.11.034

Gatta, M., Giaccio, B., Marra, F., Rolfo, M.F., 2017. Trace-element fingerprinting of the 69–36 ka Colli Albani eruptive units: A preliminary dataset for archaeological and tephra studies in central-southern Italy. Journal of Archaeological Science: Reports, 16, 330-340.

Giaccio, B., Marra, F., Hajdas, I., Karner D.B., Renne, P.R., Sposato A., 2009. $^{40}Ar/^{39}Ar$ and ^{14}C geochronology of the Albano maar deposits: implications for defining the age and eruptive style of the most recent explosive activity at the Alban Hills Volcanic District, Italy. Journal of Volcanology and Geothermal Research 185, 203-213.

Giaccio, B., Niespolo, E., Pereira, A., Nomade, S., Renne, P.R., Alber, P.G., Arienzo, I., Regattieri, Wagner, B., Zanchetta, G., Gaeta, M., Galli, P., Mannella, G., Peronace, E., Sottili , G., Florindo, F., Leicher, N., Marra, F., Tomlinson, E.L., 2017. First integrated tephrochronological record for the last ~190 kyr from the Fucino Quaternary lacustrine succession, central Italy. Quaternary Science Reviews 158, 211-234. http://dx.doi.org/10.1016/j.quascirev.2017.01.004

Giordano, G., De Benedetti, A.A., Diana, A., Diano, G., Gaudioso, F., Marasco, F., Miceli, M., Mollo, S., Cas, R.A.F., Funiciello, R., 2006. The Colli Albani mafic caldera (Roma, Italy): stratigraphy, structure and petrology, J. Volcanol. Geotherm. Res., 155, 49–80.

Grant, K.M., Rohling, E.J., Bronk Ramsey, C., Cheng, H., Edwards, R.L., Florindo, F., Heslop, D., Marra, F., Roberts, A.P., Tamisiea, M.E., Williams, F., 2014. Sea-level variability over five glacial cycles. Nature Communications 5, 5076. doi:10.1038/ncomms6076

Jicha, B.R., Singer, B.S., Sobol, P. 2016. Re-evaluation of the ages of 40Ar/39Ar sanidine standards and supereruptions in the western U.S. using a Noblesse multi-collector mass spectrometer. Chemical Geology 431, 54–66.

Karner, D.B., Marra, F., 1998. Correlation of fluviodeltaic aggradational sections with glacial climate history: A revision of the Pleistocene stratigraphy of Rome. Geological Society of America Bulletin 110, 748-758.

Karner, D.B., Marra, F., Florindo, F., Boschi, E., 2001a. Pulsed uplift estimated from terrace elevations in the coast of Rome: Evidence for a new phase of volcanic activity? Earth and Planetary Science Letters 188, 135-148.

Karner, D.B., Marra, F., Renne, P.R., 2001b. The history of the Monti Sabatini and Alban Hills volcanoes: groundwork for assessing volcanic-tectonic hazards for Rome. J. Volc. and Geoth. Res. 107: 185-215.

Lisiecki, L.E., Raymo, M.E., 2005. A Pliocene-Pleistocene stack of 57 globally distributed benthic $\delta\,^{18}O$ records. Paleoceanography 20, PA1003. doi:10.1029/2004PA001071.

Luberti, G.M., Marra, F., Florindo, F., 2017. A review of the stratigraphy of Rome (Italy) according to geochronologically and paleomagnetically constrained aggradational successions, glacio-eustatic forcing and volcano-tectonic processes. Quaternary International. http://dx.doi.org/10.1016/j.quaint.2017.01.044

Malinverno, A., Ryan, W.B.F., 1986. Extension in the Tyrrhenian sea and shortening in the Apennines as results of arc migration driven by sinking of the lithosphere. Tectonics 5, 227-245.

Mariucci, M.T., S. Pierdominici, F. Marra, P. Montone, L. Pizzino, 2008. Looking into a volcanic area: an overview on the 350m scientific drilling at Colli Albani (Rome, Italy). J. Volcanol. Geotherm. Res., doi:10.1016/j.jvolgeores.2008.04.007.

Marra, F., Florindo, F., Boschi E., 2008. The history of glacial terminations from the Tiber River (Rome): insights to glacial forcing mechanisms, Paleoceanography, 23, PA2205, doi:10.1029/2007PA001543.

Marra F., Karner, D.B., Freda, C., Gaeta, M., Renne, P.R., 2009. Large mafic eruptions at the Alban Hills Volcanic District (Central Italy): chronostratigraphy, petrography and eruptive behavior. Journ. of Volc. and Geoth. Res. 179, 217-232. doi:10.1016/j.jvolgeores.2008.11.009

Marra, F., Sottili, G., Gaeta, M., Giaccio, B., Jicha, B., Masotta, M., Palladino, D.M., Deocampo, D, 2014. Major explosive activity in the Sabatini Volcanic District (central Italy) over the 800-390 ka interval: geochronological - geochemical overview and tephrostratigraphic implications, Quaternary Science Reviews 94, 74-101.

Marra, F., Ceruleo, P., Jicha, B., Pandolfi, L. Petronio, Salari, L. , 2015. A new age within MIS 7 for the *Homo neanderthalensis* of Saccopastore in the glacio-eustatically forced sedimentary successions of the Aniene River Valley, Rome. Quaternary Science Reviews 129, 260–274. doi:10.1016/j.quascirev.2015.10.027

Marra, F., Florindo, F., Anzidei, M., Sepe, V., 2016a. Paleo-surfaces of glacio-eustatically forced aggradational successions in the coastal area of Rome: assessing interplay between tectonics and sea-level during the last ten interglacials. Quaternary Science Review, 148, 85-100. http://dx.doi.org/10.1016/j.quascirev.2016.07.003

Marra, F., Rohling, E.J., Florindo, F., Jicha, B., Nomade, S., Pereira, A., Renne., P.R., 2016b. Independent $^{40}Ar/^{39}Ar$ and 14C age constraints on the last five glacial terminations from the aggradational successions of the Tiber River, Rome (Italy). Earth Planet Sci Lett. in press.

Marra, F., Gaeta, M., Giaccio, B., Jicha, B., Palladino, D., Polcari, M., Sottili, G., Taddeucci, J., Florindo, F., Stramondo, S., 2016c. Assessing the volcanic hazard for Rome: $^{40}Ar/^{39}Ar$ and In-SAR constraints on the most recent eruptive activity and present-day uplift at Colli Albani Volcanic District, Geophys. Res. Lett. 43, 6898–6906. doi:10.1002/2016GL069518.

Marra, F., Florindo, F., Petronio, C., 2017. Quaternary fluvial terraces of the Tiber Valley: geochronologic and geometric constraints on the back-arc magmatism-related uplift in central Italy. Journal Scientific Reports 7: *2517*. DOI:10.1038/s41598-017-02437-1

Marra, F., Petronio, C., Salari, L., Florindo, F., Giaccio, B., Sottili, G., 2018a. A review of the Villafranchian fossiliferous sites of Latium in the framework of the geodynamic setting and paleogeographic evolution of the Tyrrhenian Sea margin of central Italy, Quaternary Science Reviews 191, 299-317. 10. 1016/ j. quascirev. 2018. 05. 011

Marra, F., Petronio, C., Ceruleo, P., Di Stefano, G., Florindo, F., Gatta, M., La Rosa, M., Rolfo, M.F., Salari, L., 2018b. The archaeological ensemble from Campoverde (Agro Pontino, central Italy): new constraints on the Last Interglacial sea level markers. Scientific Reports, SREP-18-23649, DOI : 10.1038/s41598-018-36111-x

Marra F., Nomade S., Pereira A., Petronio C., Salari L., Sottili G., Bahain J.J., Boschian G., Di Stefano G., Falgueres C., Florindo F., Gaeta M. Giaccio B., Masotta M., 2018c. A review of the geologic sections and the faunal assemblages of Aurelian Mammal Age of Latium (Italy) in the light of a new chronostratigraphic framework. Quaternary Science Reviews 181, 173-199. doi.org/10.1016/j.quascirev.2017.12.007

Marra, F., Bahain, J.-J., Jicha, B., Nomade, S., Palladino, D.M., Pereira, A., Tolomei, C., Voinchet, P., Anzidei, M., Aureli, D., Ceruleo, P., Falguères, C., Florindo, F., Gatta, M., Ghaleb, B., La Rosa, M., Peretto, C., Petronio, C., Rocca, R., Rolfo, M.F., Salari, L., Smedile, A., Tombret, O., 2019a. Reconstruction of the MIS 5.5, 5.3 and 5.1 coastal terraces in Latium (central Italy): a re-evaluation of the sea-level history in the Mediterranean Sea during the Last Interglacial, Quaternary International.

Marra, F., Florindo, F., Jicha, B.R., Nomade, S., Palladino, D.M., Pereira, A., Sottili, G., Tolomei, C., 2019b. Assessing volcano-tectonic hazard of the Monti Sabatini Volcanic District on the city of Rome (central Italy): evidence from new geochronologic constraints on the Tiber River MIS 5 terraces, Scientific Reports, in press.

Masotta, M., Gaeta, M., Gozzi, F., Marra, F., Palladino, D.M., Sottili, G., 2010. H_2O- and temperature-zoning in magma chambers: the example of the Tufo Giallo della Via Tiberina eruptions (Sabatini Volcanic District, central Italy). Lithos 118, 119-130.

Nicoletti, M., 1969. Datazioni argon-potassio di alcune vulcaniti dellew regioni vulcaniche Cimina e Vicana. Per. Mineral., 38, 1-20.

Nisi, M.F., Antonioli, F., Dai Pra, G., Leoni, G., Silenzi S., 2003. Coastal Deformation between the Versilia and the Garigliano plains (Italy) derived from the elevations of the Last Interglacial stage, Journal of Quaternary Science 18, 709-721.

Palladino, D, Simei, S., Sottili, G., and Trigila, R., 2010, Integrated approach for the reconstruction of stratigraphy and geology of Quaternary volcanic terrains: An application to the Vulsini Volcanoes (central Italy), in Stratigraphy and Geology of Volcanic Areas (eds. G. Groppelli, and L. Viereck-Goette), *The Geological Society of America Special Paper*, **464**, 63-84. doi: 10.1130/2010.2464(04).

Patacca, E., Sartori, R., Scandone, P., 1990. Tyrrhenian basin and apenninic arcs: kinematic relations since late Tortonian times. Mem. Soc. Geol. It. 45, 425-451.

Peccerillo, A., Frezzotti, M.L., 2015. Magmatism, mantle evolution and geodynamics at the converging plate margins of Italy. Journal of the Geological Society. http://dx.doi.org/10.1144/jgs2014-085

Pereira, A., Nomade, S., Falguères, C., Bahain, J-J., Tombret, O., Garcia, T., Voinchet, P., Bulgarelli, A.G., Anzidei, P., 2017. 40Ar/39Ar and ESR/U- series data for the La Polledrara di Cecanibbio archaeological site (Lazio, Italy). Journal of Archaeological Science: Reports, in press.

Perini, G., Francalanci, L., Davidson, J.P., and Conticelli, S., 2004, Evolution and genesis of magmas from Vico volcano, Central Italy: multiple differentiation pathways and variable parental magmas, *Journal of Petrology*, **45**, 139–182.

Rivera, T.A., Storey, M., Schmitz, M.D., Crowley, J.L., 2013. Age intercalibration of $^{40}Ar/^{39}Ar$ sanidine and chemically distinct U/Pb zircon populations from the Alder Creek Rhyolite Quaternary geochronology standard. Chemical Geology 345, 87-98.

Rohling E.J., Grant, K., Bolshaw, M., Roberts, A.P., Siddall, M. Hemleben, Ch., Kucera, M., 2009. Antarctic temperature and global sea level closely coupled over the past five glacial cycles. Nature Geoscience 2, 500-504. DOI: 10.1038/NGEO557

Serri, G., Innocenti, F., Manetti, P, 1993. Geochemical and Petrological evidence of the subduction of delaminated Adriatic continental lithosphere in the genesis of the Neogene-Quaternary magmatism of Central Italy, Tectonophysics 223, 117-147.

Sevink, J., Di Vito, M.A., Piochi, M., Mormone, A., Van Gorp, V., Bakels, C., 2018. A rare Mid-Würmian lithoid tuff in the Agro Pontino graben (Southern Lazio, Italy) and its identification as an Albano 5-7 related distal tephra deposit (41-36 kaBP): characteristics, provenance and palaeogeographical implications. Annals of Geophysics, 61, 1, S109. DOI: 10.4401/ag-7534

Sottili, G., Palladino, D.M., Marra, F., Jicha, B., Karner, D.B., Renne, P., 2010. Geochronology of the most recent activity in the Sabatini Volcanic District, Roman Province, central Italy, Journ. of Volc. and Geoth. Res. 196, 20-30. DOI:10.1016/j.jvolgeores.2010.07.003

Sottili G., Palladino D.M., Zanon V., 2004. Plinian activity during the early eruptive history of the Sabatini Volcanic District, Central Italy. J. Volcanol. Geotherm. Res. 135, 361-379.

Villa, P, Pollarolo, L., Conforti, I., Marra, F., Biagioni, C., Degano, I., Lucejko, J.J., Tozzi, C., Pennacchioni, M., Zanchetta, G., Nicosia, C., Panzeri, L., Martini, M., Sibilia, E., From Neandertals to modern humans: New data on the Uluzzian. Plos One 13(5): e0196786. https://doi.org/10.1371/journal.pone.0196786

Formatted

MIS 9 to MIS 5 terraces along the Tyrrhenian Sea coast of Latium (central Italy): assessing interplay between sea-level oscillations and tectonic movements

Fabrizio Marra[1*], Mario Gaeta[2], Brian R. Jicha[3], Cristiano Nicosia[4], Cristiano Tolomei[1], Piero Ceruleo[5], Fabio Florindo[1], Maurizio Gatta[6,7], Michelangelo La Rosa[8], Mario F. Rolfo[7]

[1] Istituto Nazionale di Geofisica e Vulcanologia, Rome, Italy
[2] Dipartimento di Scienze della Terra, "Sapienza" Università di Roma, Italy
[3] Department of Geoscience, University of Wisconsin-Madison, USA
[4]Dipartimento dei Beni Culturali, Università di Padova, Italy
[5] Via Giotto 18, 00019 Tivoli (Roma), Italy
[6] University of York, Department of Archaeology, York YO1 7EP, UK
[7] Department of History, Culture and Society, University of Rome 'Tor Vergata', Italy
[8] Ecomuseo dell'Agro Pontino, via G.B. Vico 1, Latina, Italy

*correspondoing author: fabrizio.marra@ingv.it

Abstract

We present a review of the geomorphology of the Tyrrhenian Sea coast of central Italy integrated by a novel structural-geomorphological study coupled with statistical analysis of topographic culminations and comparison with a Digital Elevation Model, aimed at reconstructing a suite of paleo-surfaces corresponding to remnant portions of marine terraces. We performed geochronological, sedimentological, micromorphological and mineralogical investigations on the deposits forming the different paleo-surfaces between Civitavecchia and Anzio town, in order to provide chronostratigraphical, paleogeographical and paleoenvironmental constraints. Using the newly achieved dataset we correlate these paleo-surfaces with the coastal terraces formed during past sea-level highstands, as recognized by previous studies, and we refine their correlation with the Marine Isotope Stage (MIS) timescale.

In particular, we have extended our geomorphological analyses landward in the area between the Tiber River mouth and Anzio, in order to include the oldest paleo-surface developed above the deposits of the last large explosive eruption at 365±4 ka in the Colli Albani Volcanic District. Results of this study allow us to recognize a set of higher paleo-surfaces at elevation ranging 108 thought 71 m a.s.l., which we interpret as one tectonically displaced, widespread coastal terrace originated during the MIS 9.1 highstand. We correlate the previously identified paleo-surfaces of 66-62 m and 56-52 m with the equivalent coastal terraces developed during the sea-level highstands of sub-stages 7.5 and 7.3/7.1. Moreover, based on data from literature on relative elevation of maximum sea level during the highstands of MIS 11 through

MIS 5.1, we assess the regional uplift and the concurrent tectonic displacements that have occurred since 900 ka in this area.

Keywords: paleo-surface; coastal terrace; glacio-eustasy; regional uplift

Highlights:
We reconstruct a suite of six paleo-surfaces along the central Tyrrhenian Sea coast
Paleoenvironmental data identify these paleo-surfaces as remnants of coastal terraces
We provide $^{40}Ar/^{39}Ar$ age constraints to the terraced sedimentary deposits
We correlate these terraces with the Marine Isotope Stage record
We identify previously unrecognized MIS 9 sea-level markers in this region
We assess regional uplift and tectonic displacements in the last 400 ka

1. Introduction

The Tyrrhenian Sea coast of Latium (Figure 1) is part of a geodynamic domain characterized by back-arc extensional processes (Malinverno and Tayan, 1986; Patacca et al., 1990) that during Pleistocene times have led to the formation of an ultra-potassic chain of volcanic districts (Serri et al., 1993; Conticelli and Peccerillo, 1992; Peccerillo and Frezzotti, 2015). Concurrent with the volcanic processes, regional uplift has caused the progressive emergence of this area since the end of the Santernian (lower Calabrian), around 1.5 Ma, leading to widespread continentalization since ~1 Ma (Barberi et al., 1994; Marra et al., 2018a). The regional uplift along the Tyrrhenian coast of Latium has been interpreted as driven by the subduction process and uprising of metasomatized magma bodies on the Tyrrhenian Sea Margin of central Italy, superimposed on a smaller isostatic component of uplift (Marra et al., 2017, and references therein). Two major pulses of uplift are recognized: 0.86 through 0.5 Ma, and 0.25 Ma through the Present (Marra et al., 2016a); as a result of this overall uplifting regime, the continental, fluvial-lacustrine and coastal deposits in this area formed a widespread pattern of terraces that, similar to other regions in the world (e.g., Bridgland and Westaway, 2008), are organized in a staircase geometry, with the oldest surfaces at highest elevation.

Geographic extension and rates of the most recent phases of this uplift during Middle-Late Pleistocene have been assessed by a series of studies reconstructing a suite of coastal terraces and correlating them with the sea-level highstands identified by the Marine Isotope Stage (MIS) record (e.g., Karner et al., 2001a; Nisi et al., 2003; Ferranti et al., 2006). More recently, a re-evaluation of the geometry and the age of these terraces in the coastal area between the Argentario and Anzio promontories has been proposed by means of an original geomorphological approach and the integration of new geochronologic constraints provided by $^{40}Ar/^{39}Ar$ ages of volcanic layers intercalated within the glacio-eustatically forced aggradational successions forming the terraced deposits in this region (Marra et al., 2015; 2016a). Moreover, a new geomorphologic study coupled with biochronologic constraints allowed Marra et al. (2018b, 2019a) to extend the reconstruction of a complete suite of terraces in the coastal reach between Anzio and Circeo promontories, and to propose their correlation with MIS 7.5 through MIS 5.1. In contrast, only a poorly defined paleo-surface ranging 61-67 m a.s.l. has been dubiously assigned to the MIS 9 terrace (Marra et al., 2016a). Moreover, geochronologic constraints so far provided to the local MIS 9 aggradational succession (Aurelia Formation, Karner and Marra, 1998) evidenced a remarkable anomaly, significantly pre-dating glacial termination IV and the completion of MIS 9 highstand (Marra

et al., 2016b). Therefore, assessing the geometry and providing time constraint on the deposits of the MIS 9 coastal terrace in this region may have notable implications for understanding the response to the global paleo-climatic signal and on the tectonic process acting on the Tyrrhenian Sea margin of central Italy.

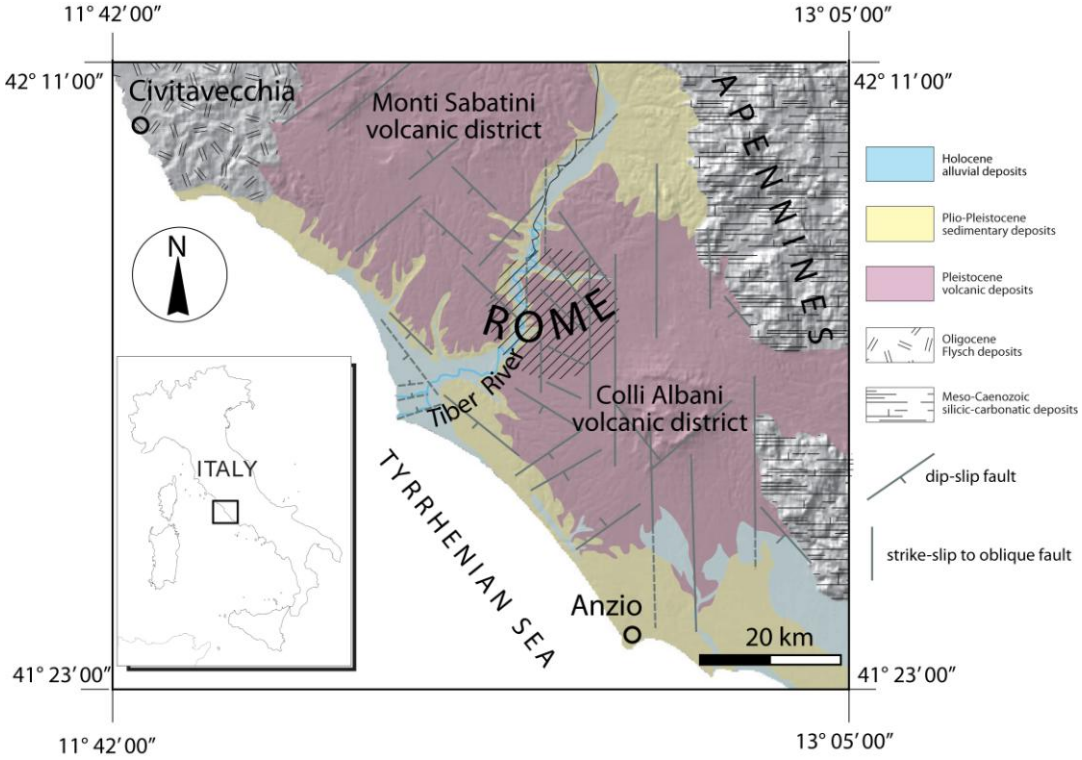

Figure 1 - DEM image of the Tyrrhenian Sea margin of central Italy showing the main structural features of the investigated area (after Acocella and Funiciello, 2006; Frepoli et al., 2010).

In the present paper we have refined the structural-geomorphological study in the previously investigated sector comprised between Civitavecchia and Anzio, and we have re-assessed the statistical analysis of the elevations of the paleo-surfaces correlated by Marra et al. (2016a, 2019a) with the MISs. In particular, we have extended the geomorphological analysis landward, in order to include the oldest paleo-surface affecting the deposits of the last large eruption in the Colli Albani Volcanic District (Villa Senni Eruption Cycle, 365±4 ka, Marra et al., 2009) in the area between the Tiber mouth and Anzio. Two huge pyroclastic-flow deposits emplaced during this eruption phase (Tufo Lionato and Pozzolanelle, Freda et al., 1995) mantle the surface with a volcanic cover spreading radially as far as 50 km from the vent and reaching up to 20 m in thickness, locally (De Rita et al., 1995; Giordano et al., 2006; Mariucci

et al., 2008). Due to this pyroclastic cover, the paleo-surfaces older than 365 ka are completely buried and no geomorphologic evidence is expected for them in this area.
We performed chronostratigraphical, sedimentological, micromorphological, mineralogical and petrographic investigations of the deposits forming the different paleo-surfaces in order to provide geochronological, paleogeographical and paleoenvironmental constraints. We used four $^{40}Ar/^{39}Ar$ age determinations on detrital sanidine crystals extracted from key deposits in order to provide post-quem ages on the paleo-surfaces and relative chronologic constraints for their correlation with the suite of coastal terraces recognized and geochronologically constrained by previous studies, refining their correlation with the MIS timescale.

2. Geological Setting

The study area is located on the Tyrrhenian Sea margin of central Italy (Figure 1).
Since the Middle Pleistocene the interplay between glacio-eustatic sea-level variations, tectonic processes, sedimentation and volcanic activity has built the geological framework of this area (Luberti et al., 2017, and references therein). During periods of sea-level fall, erosion occurred, whereas deposition took place during phases of sea-level rise, filling previously excavated incisions with a suite of aggradational successions (Karner and Marra, 1998; Marra et al., 2008). A thick succession of pyroclastic-flow deposits, from both the Colli Albani and Monti Sabatini volcanic districts, and subordinated Sabatinian air-fall deposits, interfingers with the continental sediments. After the last volcanic eruptions at 36 ka (Marra et al., 2016c), the volcanic plateau was deeply incised during the Last Glacial, partly as a consequence of the intervening regional uplift (Marra et al., 2016a). Eventually, the paleovalleys were filled by fluvial deposits as a consequence of the sea-level rise after the last glacial termination.

3. Methods

3.1 Geomorphological analysis

In the present study, paleo-surfaces have been mapped following the geomorphological approach described in Marra et al. (2016a; 2017), based on the identification of a set of flat surfaces characterized by topographic culminations with elevation ranging through a few meters around a mean value. Selected topographic culminations of the reconstructed paleo-surfaces were detected on Istituto Geografico Militare 1:25.000 topographic maps of Italy. They include all the hilltops (i.e., each elevation point within a closed, 5 m interval contour line, represented by upward triangles in the figures of this work) and other quasi-equivalent points within plateau-like sectors (downward triangles). The identification of the paleo-

surfaces is based on a combined approach that integrates statistically significant concentrations of elevations around a mean value, and the morphologic evidence for the concentration of these elevation points within a finite area, as detected in the maps (see Marra et al., 2016a for detailed methodology). The full dataset of topographic elevations is reported on the scanned 1:25.000 topographic maps and provided as Supplementary Material #1.

Distribution of the topographic culminations has been statistically analyzed in order to verify the occurrence of discrete elevation intervals corresponding to peaks of concentration, which can be assumed to be the mean level for each paleo-surface. Comparison between the complete dataset of elevation points (hilltops + plateaux) and that represented only by hilltop elevations has been also provided, to highlight possible subjective selection of the plateau-like culminations and to exclude biases.

Finally, a set of elevation ranges defining the principal paleo-surfaces identified using the described geomorphological method has been mapped through DEM analyses, to compare the results.

3.2 DEM analysis

Five classes of elevations highlighted by the geomorphological study have been mapped using an interferometric Digital Elevation Model (DEM) with a ground resolution of 30 meters (1 arcsec) derived from the NASA SRTM mission (http://www2.jpl.nasa.gov/srtm, Farr et al., 2000). When the overall topographic relief of the Italian peninsula is considered, the DEM shows an averaged altitude accuracy of ~15 meters, but in our case, considering areas quite close to the sea and showing low altitude ranges (i.e., 0 - 120 m), the accuracy is one order of magnitude better, and can be estimated in 1-2 m.

The analysis was performed entirily within a GIS environment. Initially, the DEM was delimited on the basis of the study area using a polygon shapefile, then the various classes were identified one by one, generating 5 different layers. Five queries were applied to the DEM, each time considering the maximum and minimum values of each class so as to isolate the desired altitude interval. Finally, the layers were merged into a single one and symbolized with 5 different colors, one for each class.

3.3 Micromorphological analyses

Three undisturbed soil samples (TML-CC, VDT, VOC) and three loose sand samples (TML-SA, PC-SA, CSR-SA) have been studied in thin sections for micromorphological analysis and for

sand mineralogy determination, respectively, aimed at investigating the pedological and/or sedimentological features, and to recognize the origin of the deposit forming the corresponding paleo-surface. One sediment sample collected from the paleo-surface ranging 60-67 m (CR1) in the northern sector was analyzed by Villa et al. (2018), and the results are reported here to integrate with the dataset above.
Descriptions of thin sections are summarized in Table 1, results of the petrographic determination of sand grains are reported in Table 2. Methods and microphotographs of thin sections for micromorphological analyses are provided in Supplementary File #2A.

3.4 Mineralogical analyses

Fifteen samples collected close to the top, and in some instances at increasing depth, on the different paleo-surfaces (VL-1, VL-2, MM, VCR-1, VCR-2, VCR-3, TB-1, TB-2, TB-3, VVL, TML-SA, TRIG, VDT, SPR, RUT), and three sediment samples (RSC, CDC, CR-1), have been analyzed by X-rays diffraction and with a scanning electron microprobe (SEM) in order to describe their mineralogy and texture.
Methods, microphotographs and full-resolution diffractograms are provided in Supplementary File #2B-C.

3.5 $^{40}Ar/^{39}Ar$ dating

Sanidine crystals were extracted from four samples of sediment to provide terminus post-quem ages to the time of deposition of the terrains and/or the accretionary soils forming the paleo-surfaces ranging 98-108 m (TML-SA), 71-79 m (RSC-SA), 60-67 m (CR-3), 51-57 m (CSR-SA) a.s.l., in the area between the Tiber mouth and Anzio. Sampling locations are shown in Figure 3.
Sanidine phenocrysts were co-irradiated with the 1.1864 Ma Alder Creek sanidine standard (Jicha et al., 2016; Rivera et al., 2013) at the Oregon State University TRIGA reactor in the Cadmium-Lined In-Core Irradiation Tube. Single crystal fusion analyses were performed at the WiscAr laboratory at the University of Wisconsin-Madison using a 60W CO_2 laser and a Noblesse multi-collector mass spectrometer following Jicha et al. (2016). Results are reported in Table 4. Full analytical data are reported in Supplementary Material #3.

4. Results

4.1 Geomorphological analysis

Results of the geomorphological study performed for the present work in the coastal area between Civitavecchia and Anzio are in good agreement with those previously obtained by Marra et al. (2016a, 2019a). We have statistically re-analyzed hilltops and plateaux elevations separately, in the two coastal sectors north and south of the Tiber mouth. Very similar statistical assessment for the elevation ranges of the detected paleo-surfaces have been obtained for the two sectors, which are reported in Figure 2 and 3, respectively. In these figures, all the topographic culminations identified on the 1:25.000 maps are indicated with triangles of different colors. In the northern sector, each color is associated with an elevation range defining a paleo-surface which, in turn, is established from the statistical analysis. Elevation ranges for the paleo-surfaces are represented by grey boxes of cumulative frequency above a threshold value of n=2 for a total number of data >20 (red horizontal line in Figure 2b), while continuous distributions are considered for classes of n <20. Open triangles are used for hilltops whose elevation is not statistically significant and are not associated with a paleo-surface. These elevations are interpreted as reflecting topographic culminations that represent eroded higher rank paleo-surfaces; for this reason, the same color used for the corresponding pristine paleo-surface is also used for these triangles.

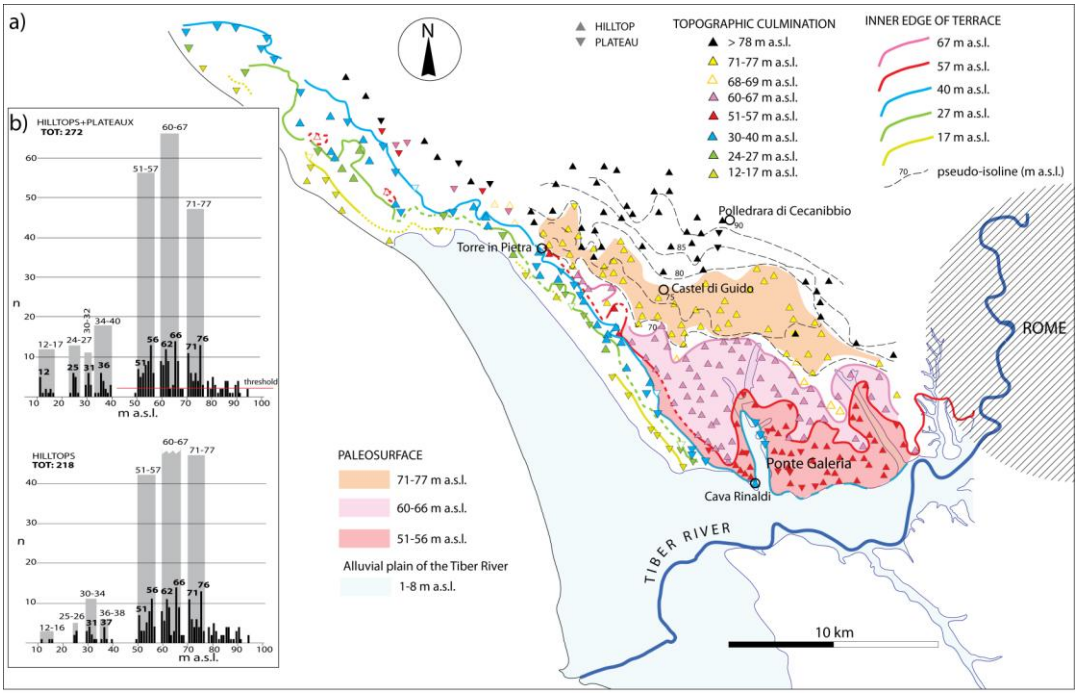

Figure 2 - Geomorphological map (a) and topographic culmination statistics (b) in the northern sector between Civitavecchia and the Tiber mouth. Elevations of topographic culmination are omitted for clarity in this figure and can be found in Suppl. Mat. #1A. See text for comments.

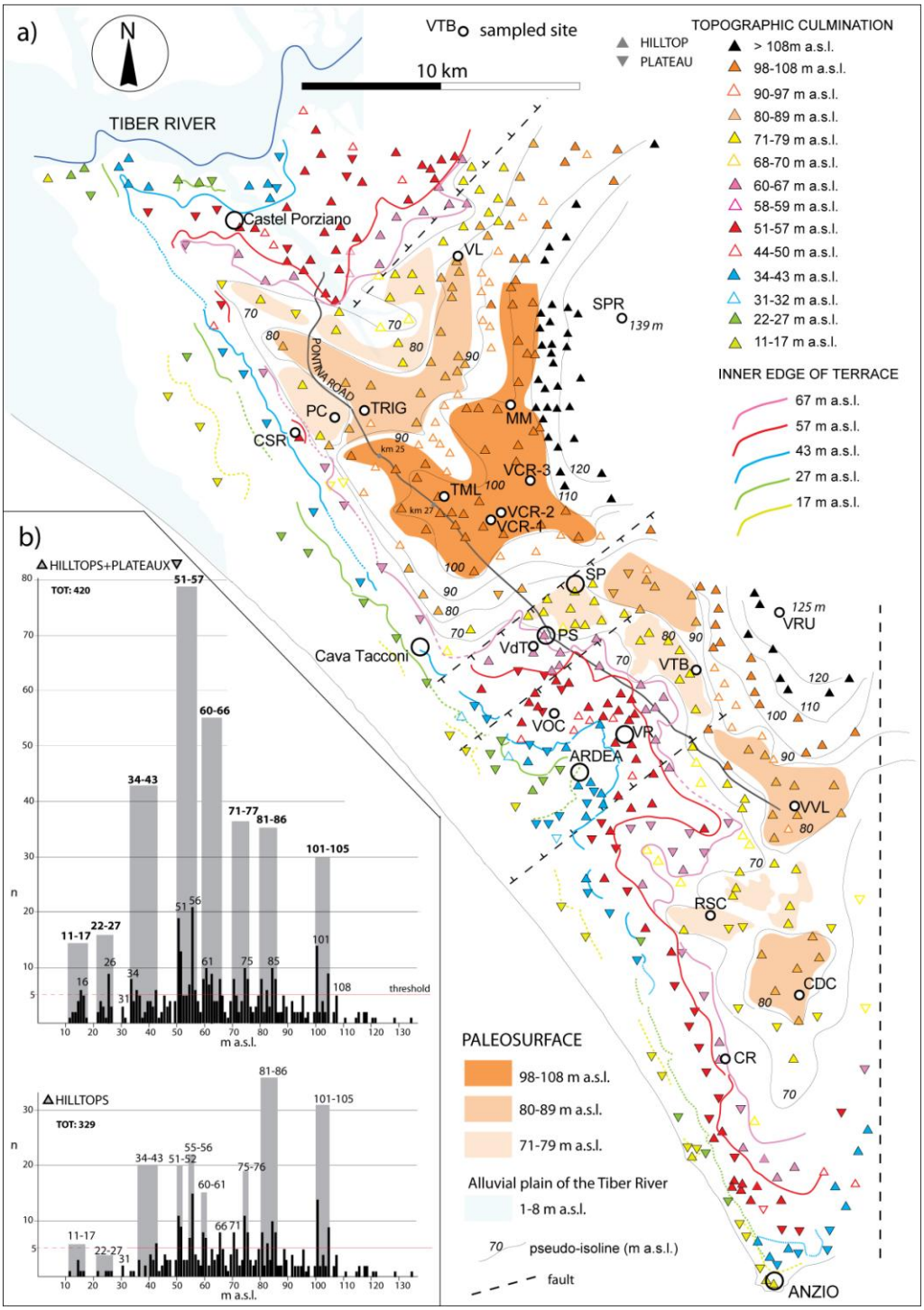
a)
N
VTB sampled site
HILLTOP
PLATEAU
10 km
TOPOGRAPHIC CULMINATION
> 108m a.s.l.
98-108 m a.s.l.
90-97 m a.s.l.
80-89 m a.s.l.
71-79 m a.s.l.
68-70 m a.s.l.
60-67 m a.s.l.
58-59 m a.s.l.
51-57 m a.s.l.
44-50 m a.s.l.
34-43 m a.s.l.
31-32 m a.s.l.
22-27 m a.s.l.
11-17 m a.s.l.
INNER EDGE OF TERRACE
67 m a.s.l.
57 m a.s.l.
43 m a.s.l.
27 m a.s.l.
17 m a.s.l.
TIBER RIVER
Castel Porziano
VL
SPR
139 m
PONTINA ROAD
PC
TRIG
CSR
MM
VCR-3
TML
VCR-2
VCR-1
km 25
km 27
SP
PS
VdT
Cava Tacconi
125 m
VRU
VTB
VOC
VR
ARDEA
VVL
RSC
CDC
CR
ANZIO
b)
HILLTOPS+PLATEAUX
TOT: 420
HILLTOPS
TOT: 329
n
m a.s.l.
threshold
PALEOSURFACE
98-108 m a.s.l.
80-89 m a.s.l.
71-79 m a.s.l.
Alluvial plain of the Tiber River
1-8 m a.s.l.
pseudo-isoline (m a.s.l.)
fault

Figure 3 - Geomorphological map (a) and topographic culmination statistics (b) in the southern sector between the Tiber mouth and the Anzio promontory. Elevations of topographic culmination are omitted for clarity in this figure and can be found in Suppl. Mat. #3. See text for comments.

A similar approach is used in the southern sector where, due to the larger number of data, a threshold value of n=5 is established to define the classes of elevation for all the paleo-surfaces except the lowest two (Figure 3b). Moreover, in a few cases the elevation range for each color is slightly larger than the mean elevation range (grey boxes) established for the paleo-surfaces based on histograms, in order to include all topographic points.

Color shading is used in Figure 2 for three oldest paleo-surfaces which have a wider extent and are located inland, while inner margins are represented by solid colored lines for the paleo-surfaces stretching along the coast, which are assumed to represent coastal terraces. Different shades of the orange color are used in Figure 3 to highlight the highest paleo-surfaces that are located inland which, according to discussion in the following sections, are interpreted as having the same age, whereas inner terrace margins are reported for the youngest paleo-surfaces along the coast.

In both sectors illustrated in Figures 2 and 3, three lowest orders of terrace are identified by a series of topographic culminations, each one providing well-clustered, distinct elevation ranges, which define three paleo-surfaces narrowly elongated parallel to the coast. The lowest paleo-surface ranges 12-17 m a.s.l., with a peak at 12 m (Figure 2b), and 12-18 m a.s.l., with a peak at 16 m (Figure 3b), in the northern and in the southern sector, respectively. A second paleo-surface has very narrow ranges of 24-27 and 22-27 m a.s.l., with peaks at 25 and 26 m, in the northern and in the southern sector, respectively.

A third, higher paleo-surface is characterized by a wider range of elevations, with a main concentrations between 34-40 and 34-43 m a.s.l. in the northern and southern sector, respectively, and with a minor peak at 31 m, in both sectors.

A fourth, wide paleo-surface is that ranging 51-57 m a.s.l. and characterized by two relative maxima at 51 and 56 m, in both sectors. Another two well-defined elevation ranges of 60-67 m, and of 71-77 m, are clearly identified in both sectors, and are associated with fifth and sixth paleo-surfaces, respectively.

Finally, two more concentrations of elevation values, peaking at 80-86 and 101-105 m a.s.l., define the two highest paleo-surfaces on the inland coastal sector south of the Tiber mouth, whereas in the northern sector topographic culminations show progressively increasing elevation inland, without any apparent clustering around a mean value.

Comparison of the results of the geomorphological study with the DEM of Figure 4 shows a very satisfactory match. In particular, we note the close correspondence between the geometrical patterns defined by the 51-57 m paleo-surface in the geomorphological maps of Figure 2 and 3, and in the DEM image of Figure 4 (represented by the red color in both representations), as well as, between those pertaining to the highest paleo-surface of 98-108 m (represented by the deep orange color in Figure 3 and by the deep blue color in Figure 4).

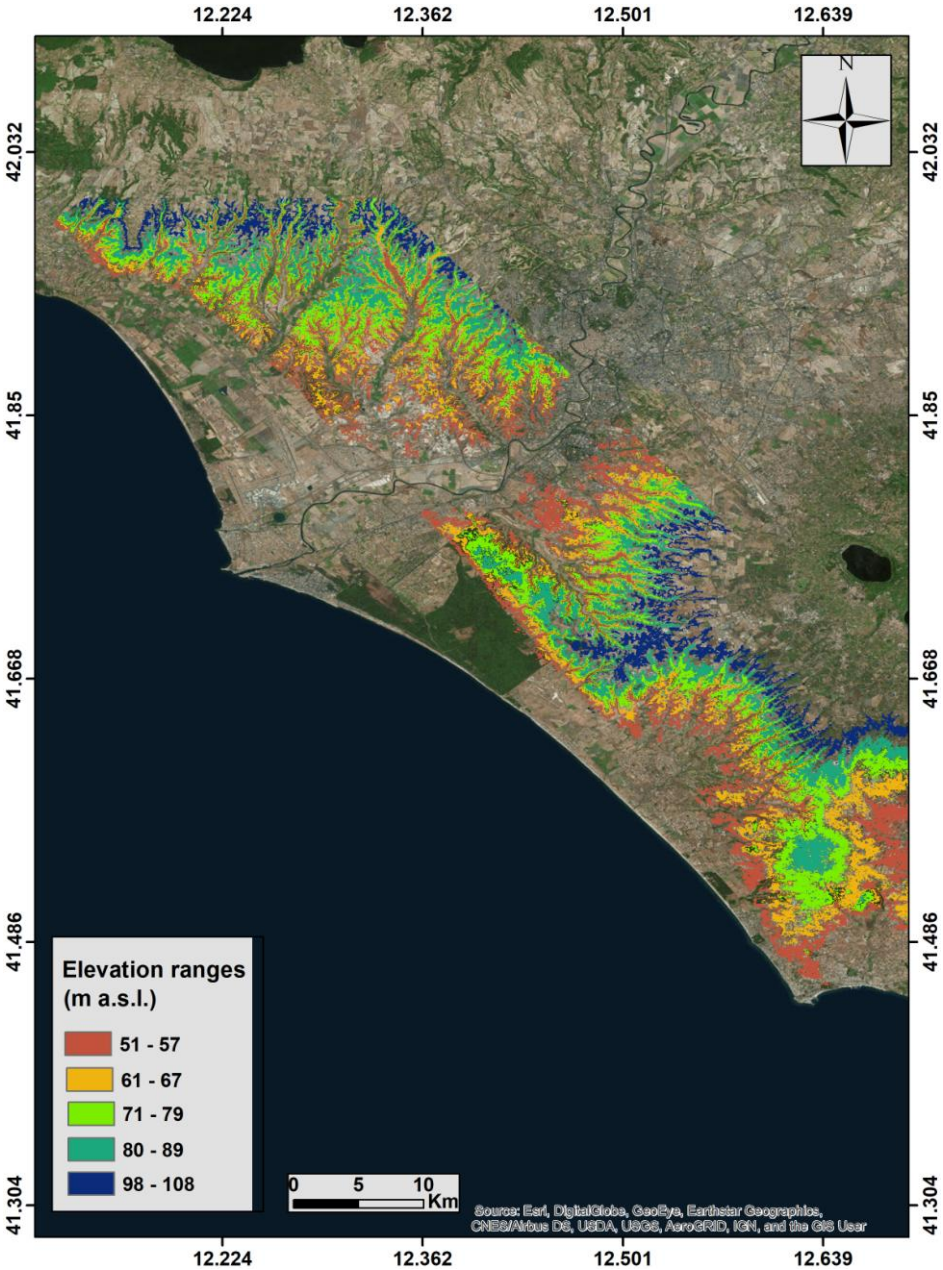

Figure 4 - Interferometric Digital Elevation Model (DEM) mapping of the five classes of elevations highlighted by the geomorphological study.

4.2 Stratigraphic investigations

4.2.1 Paleo-surface 98-108 m a.s.l.

Exposure of the sedimentary deposits forming the highest paleo-surface in the investigated area is provided by a road cut in Tenuta Monti di Leva (TML), at km 27 of Via Pontina (Figure 5a, see Figure 3 for location). Here, a pedogenically modified horizon occurs in the upper 100 cm and is constituted by fine to medium sized sand in silty-clayey matrix, orange in color (Figure 5a-a"). A 180 cm thick concretionary layer, constituted by aggregated, cm-sized Fe and Mn nodules within a sand matrix, occurs at the bottom of this horizon and overlies a red paleosol developed on top of the pyroclastic-flow deposit of Pozzolanelle (Villa Senni Eruption Cycle, 365±4 ka; Freda et al., 1997; Marra et al., 2009). A sample of the upper sand layer (TML-SA) and another from the concretionary layer (TML-CC) were analyzed for mineralogy and michromorphology, respectively. Forty-one sanidine crystals extracted from sample TML-SA were dated by the $^{40}Ar/^{39}Ar$ method.

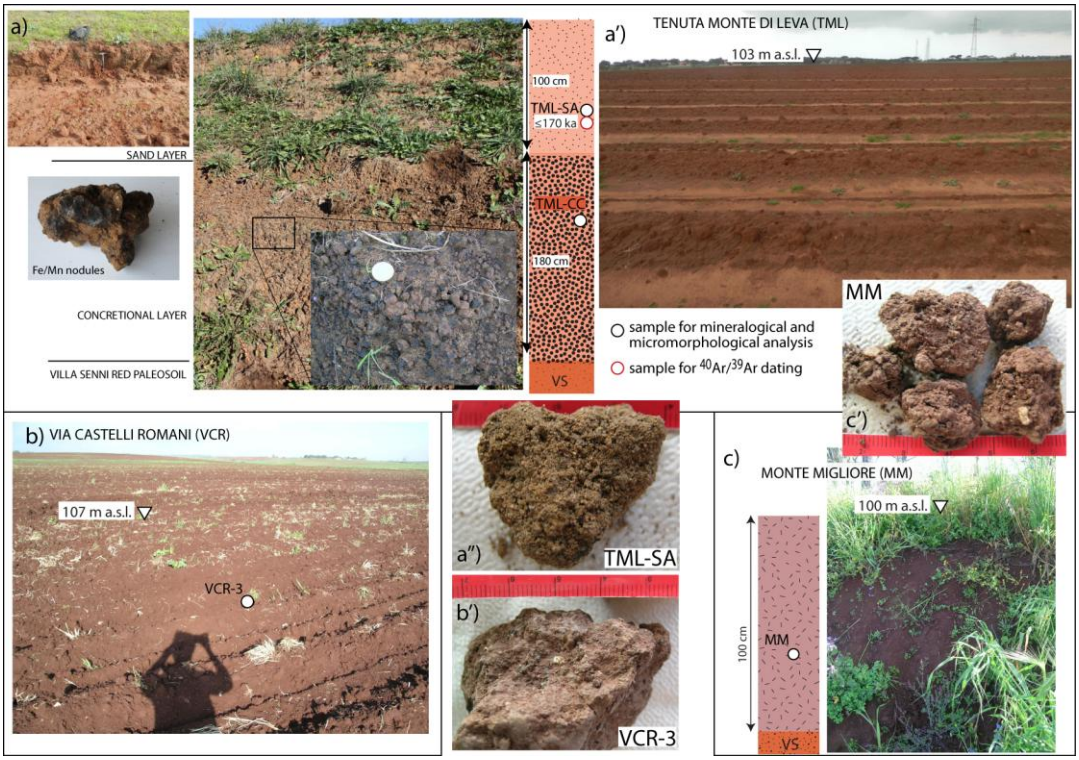

Figure 5 - Photographs and stratigraphic schemes showing the 98-108 m a.s.l. paleo-surface and the sections from which samples analyzed in the present study were collected. See text for comments.

The Tenuta Monte di Leva paleo-surface is affected by intensive ploughing which exposes shreds of the upper, orange sand layer, allowing recognition of the presence of this sedimentary deposit throughout the sector crossed by the Pontina Road between km 27 and km 25 (see Figure 3a). A similar in color, but finer sandy-clay deposit is exposed by plowing grooves on top of this highest paleo-surface, further inland. Four samples were collected along the Via dei Castelli Romani and Via Laurentina, at increasing distance inland, with respect to the Tenuta Monte di Leva site (Figure 3). Three samples (VCR 1-3) were collected at elevations between 105 and 107 m a.s.l. in the fields exposing clods of the sub soil (Figure 5b). Although the direct contact is not exposed in this flat sector, a geologic substrate represented by the Pozzolanelle pyroclastic-flow deposit (hereby PL) is visible in the scanty outcrops along the stream incisions at its margin. A fourth sample (MM) was collected at the Monte Migliore-La Selvotta locality, at 100 m a.s.l., from the middle of a 100 cm thick, dark red paleosol developed above the PL, exposed by a road cut (Figure 4c). A larger amount of clay matrix, dark red in color, characterizes the samples collected in these inland sectors of the 98-108 paleo-surface (VCR 1, 2, 3, MM, Figure 5b'-c'). Frequent pyroxene crystals and sparse, altered volcanic scoriae 1 to 5 mm in size, are embedded in the clay matrix of these soils, evidencing an at least partial origin from the directly underlying volcanic deposit.
Two more samples were collected in a later time at higher elevation, in the area inland with respect to that pertaining to the 98-108 paleosurface (SPR at 139 ma.s.l.) and with respect to the narrow alignment of topographic culminations ranging 100-110 m in the more southern sector (RUT at 125 m a.s.l.) (Figure 3), aimed at investigating the origin of the abundant silico-clastic fraction highlighted by micromorphologic and petrographic analyses in the soils developed above the volcanic substrate.

4.2.2 Paleo-surface 80-89 m a.s.l.

Different fragments of this paleo-surface are identified northwest and southeast of the highest sector corresponding to the 98-108 paleo-surface (Figure 3). As for the latter, the 80-89 paleo-surface is also developed above different geologic substrates as a function of the distance from the coastline: above the PL in the inland sectors, and above sedimentary sand deposits to the southwest. Five samples were collected in the different sectors of this paleo-surface. Two samples (VL-1, VL-2, Figure 6a) were collected in the middle and at the surface

of a thick paleosol developed above the PL in Via Laurentina, in the inland margin of the northernmost stretch of this paleo-surface. A further sample (TRIG, Figure 6b) was collected at its opposite, seaward extreme, on the ground surface in a sandy deposit (Figure 3).

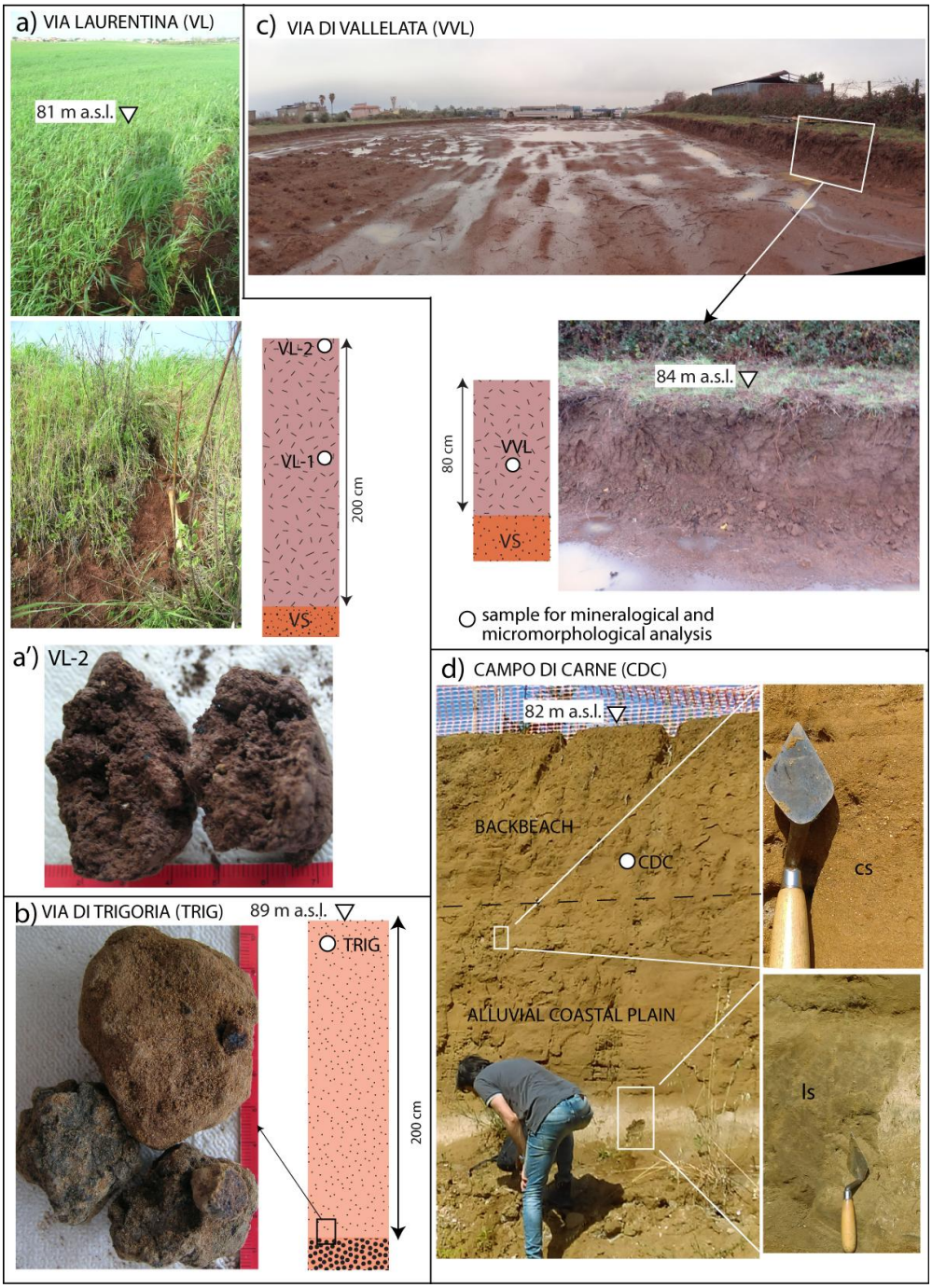

Figure 6 - Photographs and stratigraphic schemes showing the 80-89 m a.s.l. paleo-surface and the sections from which samples analyzed in the present study were collected. See text for comments.

This sedimentary deposit is quite similar to that cropping out in Tenuta Monte di Leva (TML): it is a medium-to-fine grained, orange sand in a sparse clay matrix, without sedimentary structures, ca. 3 m thick (Figure 6b). At the base of the exposed section a concretionary layer rich in Mn/Fe nodules, quite similar to that occurring in TML, is present.
A fourth sample (VVL, Figure 6c) was collected in the middle of an ca. 80 cm thick paleosol developed above the PL in Via Vallelata, in the inland margin of the southernmost stretch of the 80-89 m paleo-surface (Figure 3). This reddish soil, like the thicker soil sampled in Via Laurentina (Figure 6a'), constituts of very fine, clayey sediment containing abundant pyroxene crystals and altered volcanic scoriae, and appears quite similar to the other soils developed directly above the PL sampled for this study.
Finally, one sample (CDC) was collected in Campo di Carne in a road excavation exposing a ca. 3 m thick deposit constituting of fine, faintly bedded sand in a sparse clay matrix, with dm-thick layers of coarse sand (cs in Figure 6d), whose top at 82 m a.s.l. is part of the seaward portion of the 80-89 m a.s.l. paleo-surface. A layer of dark, greenish loamy fine sand, ca, 60 cm thick, occurs at the base of the exposed section in CDC (ls in Figure 6d).

4.2.3 Paleo-surface 71-79 m a.s.l.

Two particularly level, small sectors at elevations around 76 m a.s.l. can be detected in the northern and southern margins of the investigated area, in the Podere Carafa (PC) and Riserva Carpineto (RSC) estates (Figure 3). In the PC, an almost perfectly flat area (Figure 7a) is truncated by a sharp scarp to the southwest, dividing it from another level area at ca. 56 m a.s.l. (Castel Romano -CSR), while it connects more gently to a slightly higher sector, corresponding to the 80-89 paleo-surface, to the northeast. A marked fluvial incision dissecting the plateau exposes the terrains forming the 71-79 m paleo-surface, showing massive sand deposit of at least five meters thickness, where sample PC-SA analyzed during this study was collected (Figure 7a).
A remarkably similar geomorphologic and stratigraphic setting is observed at the RSC. Here a wide level area at elevations ranging 70-79 m is intensely dissected by steep stream valleys, and almost without geomorphologic break connects with another large area to the southeast, including the Campo di Carne (CDC) site, at an elevation between 80 and 85 m a.s.l. (Figure 3). A massive, medium to coarse sand deposit with sparse, well-rounded fine gravel (sample RSC,

Figure 7b) constitutes the geologic substrate in this area, and directly overlies the lower flow unit of the Villa Senni eruption cycle (Tufo Lionato).

Figure 7 - Photographs and stratigraphic schemes showing the 71-79 m a.s.l. paleo-surface and the sections from which samples analyzed in the present study were collected. See text for comments.

A portion of this 71-79 m a.s.l. paleo-surface also occurs within the structurally controlled sector of Ardea, bordered by the NE-SW trending normal faults of the Ardea Basin (Figure 3). This is a half-graben which originated as a transversal Tyrrhenian Sea basin in Lower Pleistocene times, as evidenced by off-shore seismic lines (Faccenna et al., 1994). The continued Middle Pleistocene activity of these faults is suggested by the marked control on the paleo-coastlines, testified by the geometry of the inner edges of the MIS 7 and MIS 5 terraces reconstructed in Marra et al. (2016a, 2019a) and shown by our refined study in Figure 3 and in Figure 4.

In contrast to the more seaward sectors, here the 71-79 paleo-surface is developed upon the PL (Figure 7c-d), and characterized by a shallow, 60-80 cm thick, dark brown paleosol. Three samples have been vertically sampled in this paleosol at the Via di Torre Bruna (VTB 1-3, Figure 7c).

Figure 2 shows a wide 71-77 m paleo-surface that we have reconstructed in the coastal sector north of the Tiber mouth (Ponte Galeria area), which in Marra et al. (2016a) was not highlighted. However, scanty sedimentary deposits occur at these elevations in this area, where the outcropping terrains are mostly represented by the Monti Sabatini volcanic succession. Notably, thin layers of calcareous lacustrine muds, ca. 50 m thick, crop out at 72 m a.s.l. in Castel di Guido, and are overlain by the pyroclastic-flow deposit of Tufo Giallo di Sacrofano (285±2 ka, Karner et al., 2001b; Sottili et al., 2010), which forms most of the hilltops of the 71-77 m paleo-surface (Marra et al., 2018c). We interpret these sedimentary strata as the remnants of an alluvial coastal plain, mantled by a thin cover of pyroclastic deposits.

4.2.4 Paleo-surface 61-67 m a.s.l.

No evident paleo-surface is associated with this class of elevations in the sector south of the Tiber mouth, except that pertaining to small, isolated plateaux, like at the Colle Rotondo locality (CR, Figure 8). The Colle Rotondo site is located on the flat surface of an E-W elongated hill, culminating 63.5 m a.s.l., bordered by the steep flanks of two convergent streams, 2.5 km east of the present coast, and 7.5 km north of Anzio (Figure 3). This is part of a series of hilltops ranging 61-67 m a.s.l., aligned along a narrow stripe of land defining a coastal terrace between Ardea and Anzio (pink triangles in Figure 3). This terrace is shifted inland, significantly, within the Ardea basin, paralleling the behavior of the inner edge of the 51-57 m terrace, as well as that of the two lower terraces of 34-43 m, and 22-27 m (Figure 3). Notably, in the coastal sector overlooking the most elevated area of TML, corresponding to the

98-108 m paleo-surface, only plateau points define the 60-67 m terrace, while almost no evidence of the 51-57 m terrace occurs in the coastal reach north of the Ardea basin, consistent with erosion due to tectonic uplift of this sector. In contrast, a well-defined 60-67 m terrace occurs at the northwestern margin of the lower area represented in Figure 3, facing the terminal reach of the Tiber Valley.

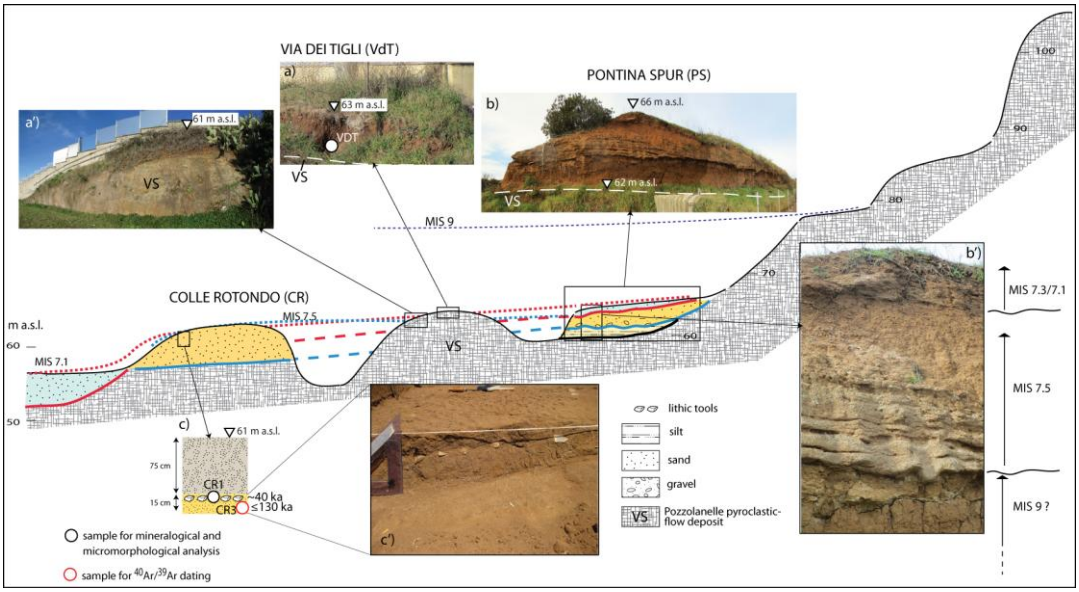

Figure 8 - Composite cross-section, constructed by projecting the Colle Rotondo (CR) site on an ideal profile passing by the Santa Procula (SP), Pontina Spur (PS), and Via dei Tigli (VdT) sites (see Figure 3 for location), aimed at showing the stratigraphic relationships between the sedimentary successions underlying the 60-67 m a.s.l. paleo-surface.

A pedogenized surface horizon consiting of brown sandy silt, heavily disturbed by ploughing, occurs in the upper 75 cm at CR (Figure 8c). It overlies a reddish-brown silty sand horizon, incorporating mm-sized Mn and/or Fe concretions (Figure 8c'). A large number of stone artifacts attributed to the Uluzzian culture (45-41 ka) was found within the upper portion of this sand layer, ranging in thickness from 6 to a maximum of 20 cm (Villa et al., 2018). One sand sample (CR1) collected within the archaeological layer was analyzed for michromorpholgy by Villa et al. (2016), while 39 sanidine crystals extracted from a sand sample (CR3) collected immediately below (see Figure 8c) have been dated as part of the present work.

A different geologic substrate characterizes the 60-67 m paleo-surface at two sites located in the northern portion of the Ardea Basin, Via dei Tigli (VdT) and Pontina Spur (PS) (Figure 3).

A ca. 80 cm thick, brown-reddish clayey paleosol overlies the PL at VdT (Figure 8a). Field surveys showed that the substrate of the 60-67 m paleo-surface in this area is represented by a pedogenized layer on top of the PL (e.g., Figure 8a'). One sample from this soil (VdT) has been analyzed for micromorphology.

A peculiar situation is observed at PS, where two fining-upwards successions overlie a third, faintly bedded fine sand deposit, which in turn overlies the PL (Figure 8b-b'). The two upper successions consist of a basal gravel layer, made up of reworked volcanic material with characteristic, large leucite crystals turned into analcime, suggesting provenance from the PL (Freda et al., 1997). The finer, upper part is also made up largely of volcanic sand. Both have evident fluvial origin. The lowest layer is a silty fine sand, of possible palustrine or alluvial origin. No sample was collected from this section, due to its very local significance, while a correlation with the other sections of the 60-67 m paleo-surface and a paleoenvironmental interpretation is provided in the cross-section of Figure 8.

The 60-67 m paleo-surface has a wide expression to the north of the Tiber (Figure 2). However, no sedimentary succession is apparently associated with this paleo-surface, its geologic substrate consisting of different, older volcanic deposits, ranging 561-400 ka (e.g., Karner and Marra, 1998; Marra et al., 2016b), which form the hilltops in this area. Consequently, the 60-67 paleo-surface in this area should be considered as a non-depositional terrace, possibly generated by uplift-induced erosional processes in the near-shore sector, similar to the higher level paleo-surface of 71-77 m in this sector.

4.2.5 Paleo-surface 51-57 m a.s.l.

This paleo-surface (red triangles in Figure 2 and 3) has a prominent expression in the Ponte Galeria area north of the Tiber mouth, where solid geochronologic constraints correlate it with MIS 7, as noted in Marra et al. (2016a). It is rather well preserved along the southeastern side of the Tiber Valley, south of the river mouth, and in the southernmost sector between Ardea and Anzio, while it disappears along the coastal reach facing the TML morpho-structural height (Figure 3). However, two fragments of coastal terrace are preserved immediately north of this sector, and one of these (Castel Romano -CSR) provides good exposure of the terrains underlying the paleo-surface. At CSR a large level area at elevations ranging 51-56 m a.s.l. is bordered to the west-northwest by a steep, 6 m high scarp (Figure 9a), separating it from the other wide level area of Podere Carafa, ranging 71-79 m a.s.l. (see Figure 3).

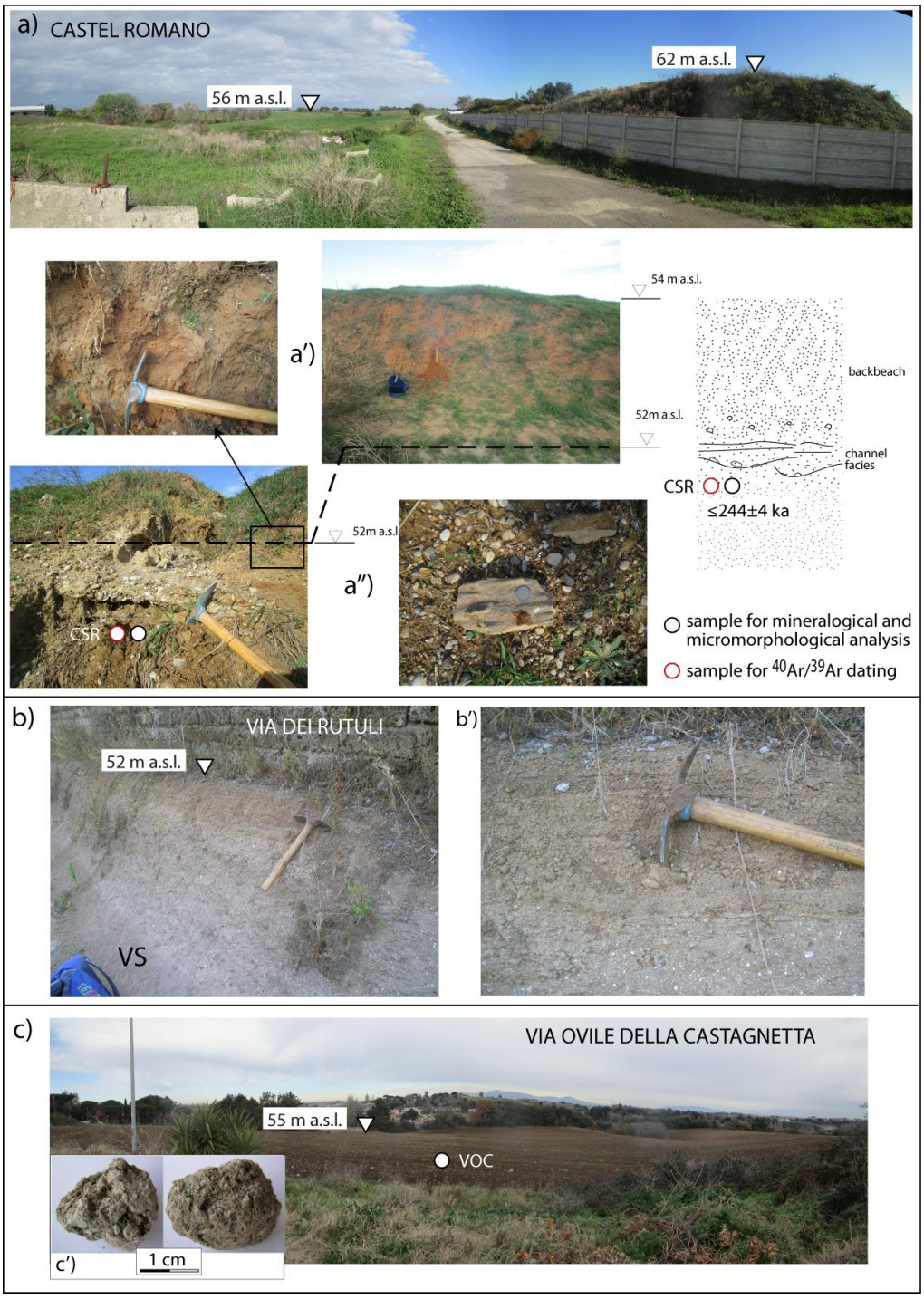

Figure 9 - Photographs and stratigraphic schemes showing the 51-57m a.s.l. paleo-surface and the sections from which samples analyzed in the present study were collected. See text for comments.

The 60-67 m terrace is not preserved between the two paleo-surfaces in this area, which are connected by a gentle incline degrading from ca. 70 m to 62 m a.s.l., behind the sub-vertical scarp. The 51-56 m paleo-surface at CSR is dissected by a gully exposing on its banks a reddened, massive sand deposit, 2 m thick (Figure 9a'), overlying a ca. 50 cm thick layer with gravel lenses and sandstone horizons with ripple marks (Figure 9a"). This braided channel facies overlies a massive sand deposit in which sample CSR for mineralogical analysis and $^{40}Ar/^{39}Ar$ dating was collected.

A different geologic substrate represented by the PL characterizes the 51-57 m paleo-surface within the Ardea Basin. However, exposure at Via dei Rutuli (VR, see Figure 3) provides evidence of a conglomeratic layer above the PL at 52 m a.s.l. (Figure 9b), which testifies the occurrence of a transgressive deposit that should be considered the coastal deposit associated with the 51-57 terrace in this area. It is a bedded, fining upward, 50 cm thick sand and gravel layer, containing well-rounded scoria clasts from the underlying pyroclastic deposit, which is erosionally truncated at the top (Figure 9b'). Evidence from another site within the Ardea basin (Via Ovile della Castagnetta -VOC, Figure 3) suggests that a fine-grained, lagoon deposit forms the upper portion of the 51-57 terrace in this area. Here, a wide paleo-surface around 55 m a.s.l. (Figure 9c) consits of a brown, mature paleosol in which one sample (VOC) was collected and analyzed for micromorphology. The occurrence of abundant, rounded calcareous concretions (Figure 9c'), which are uncommon in shallow soils developed directly upon the siliceous volcanic deposits, suggests the presence of a horizon of calcareous mud, as typically observed in the lagoon deposits of the MIS 7 Vitinia Formation (Karner and Marra, 1998) associated with the 51-57 paleo-surface in the northern coastal sector.

4.3 Micromorphological analyses

Results of thin section observations are summarized in Table 1.

TS[1]	Microstructure	Lithology	Groundmass[2]	c/f ratio	Rel Dist[3]	Pedofeatures
TML-CC	-	Matrix: 15 -20% fine sands (quartz; rare feldspar; chert; metamorphic rock fragments) Inside nodules: well sorted fine sands (±45%) (quartz; feldspar;	Orange (PPL) clay with SS and GS bfabric	20/80 (matrix) 50/50 (nodules)	OP (matr.) SSP (nod.)	Matrix: layered clay coatings and infillings, limpid and

		chert; metamorphic rock fragments; pyroxene)				silty clay, broad extinction lines, frequent.
CR1	Basic MS type: close porphyric	Fine sand (5%); Medium sand (60-65%) Lithology: quartz; feldspar; chert; pyroxene; metamorphic rock fragments; epidote. Sub-rounded and sub-angular grains.	Reddish (PPL) clays with SS and GS b-fabric	70/30	CP	Limpid clay coatings and infillings, 1st order yellow interference colors; broad extinction lines, occasional superimposed Fe coatings.
VDT	Subangular blocky, moderate	Very fine sand (5-10%); Fine sand (5%); Medium sand (5-10%) Lithology: quartz; chert; pyroxene (rare); Sub-rounded and sub-angular grains.	Orange (PPL) clay with CS and GS bfabric	20/80	OP	Limpid clay coatings, strongly deformed, frequent. Disorthic Fe/Mn nodules, typic and concentric, frequent, rounded.
VOC	Basic MS type: single-spaced porphyric	Very fine sand (±5%); Fine sand (15-20%); Medium sand (25-30%) Lithology: quartz; feldspar; chert; pyroxene; amphibole; volcanic scoria (rare); metamorphic rock fragments. Sub-rounded and sub-angular grains.	Yellowish (PPL) clays with GS bfabric	60/40	SSP	Limpid clay coatings, strongly deformed, frequent. Disorthic Fe/Mn nodules, typic and concentric, frequent, rounded.

Table 1 – Description of thin sections

[1] TS = Thin Section
[2] B-fabric: SS = Stipple speckled; PS = porostriated; GS = granostriated; CS = cross striated
[3] Rel Dist = Related distribution pattern: CP = close porphyric; SSP = single-spaced porphyric; OP = open porphyric

4.3.1 Concretionary layer from Tenuta Monte di Leva: sample TML-CC

Micromorophological analysis of this sample collected from the TML concretionary layer shows that the nodules are iron and manganese concretions that entrap sediments differing from those in the surrounding groundmass. The main differences between the sediments within the nodules and those in the matrix around them are as follows:

(a) The degree of sorting, which inside the nodules is good, with grains in the fine sand class, indicating that the nodules formed in aeolian or alluvial sands (e.g., channel facies).

(b) The lithology: the matrix consists only of weathering resistant species, whereas in the nodules some volcanic minerals (pyroxenes – Fig. S1) are preserved, and feldspar (e.g., microcline) is more abundant than in the surrounding matrix.

The matrix around the nodules shows the effects of marked pedogenesis. It is in fact very clay-rich and in the coarse fraction only weathering resistant material is preserved (quartz, chert,

metamorphic rock fragments – predominantly quartzite). Clay coatings, pertaining to several superimposed episodes of clay illuviation, are very strongly developed (Fig. S2). They occur as superimposed limpid and silty clay coatings or as coatings deformed due to shrink-swell phenomena.

Albeit that the nodules may be allochtonous (i.e., formed elsewhere and then transported and re-deposited after being eroded), observations attest that they contain remains of the former parent material on which pedogenesis has taken place, "preserving" it from successive weathering. Weathering and pedogenesis subsequently affected the groundmass but were impeded within the nodules.

4.3.2 Sand deposit from Colle Rotondo: sample CR-1

The sand fraction is composed of a mixture of siliciclastic and volcanoclastic (i.e. pyroxenes – augite) mineral species. The moderate sorting, the grainsize centered on the medium sand granulometric class, and the slight rounding of the grains are compatible with an aeolian (backbeach) sediment. There are no traces of reworking due to surface runoff or similar water and gravity-triggered slope processes. Pedogenesis is at an initial stage, especially compared to other samples from this study. Incipient reorganization of the groundmass, giving rise to a stipple-speckled b-fabric, is observed. Weak traces of incipient clay illuviation, such as thin clay coatings around skeletal grains, also point to an initial/moderate level of pedogenesis (Fig. S3). The weatherable minerals in the coarse fraction – especially pyroxenes – are abundant and do not show traces of weathering.

4.3.3 Paleosol from Via dei Tigli: sample VDT

This sample shows the highest degree of pedogenic weathering amongst the analyzed samples. The abundant clay in the groundmass shows orange-red colors resulting from the strong oxidation, and the clay are the outcome of repeated cycles of clay illuviation. Strong vertic processes (i.e.: internal turnover of soil material) led to the digestion of the illuvial clays in the fine mass and to the formation of strongly developed cross-striated and grano-striated b-fabric types (Fig. S4, S5). Also the nodules of iron and manganese owe their morphology to the strong shrink-swell phenomena in the sample (which led to the formation of concentric nodules with strong rounding). The coarse fraction is predominantly composed of weathering-resistant species (quartz and chert), albeit minor amounts of pyroxenes and unaltered volcanic glass are still present. The latter might derive from a 'fresher' or more recent input of volcaniclastic material into the soil during its formation. The poor sorting, sub-

angular morphology and medium-fine sand grain size of the siliciclastic fraction do not match the expected characteristics of an aeolian input, strongly suggesting an alluvial/colluvial origin.

4.3.4 Paleosol from Via Ovile della Castagnetta: sample VOC

The sorting of the coarse fraction is low. The sample has the highest percentage of volcanic mineral grains (pyroxenes and amphiboles – see Fig. S6) in the studied set, included the loose sand samples. The fine fraction derives from clay illuviation, which ultimately triggered vertic processes and the digestion of clay coatings within the groundmass, the development of a grano-striated b-fabric, and the formation of concentric iron and manganese nodules. Grains are predominantly in the fine and medium sand fraction, and show subrounded and rounded morphologies. The low sorting and the rounding of iron and manganese nodules indicate reworking and redeposition of the material. The presence of rare calcite infillings indicates re-carbonatation of the profile due to the effect of a dissolved carbonate-rich groundwater table (Fig. S6). Abundant, large (1-2 cm) carbonatic nodules also occur in the deposit.

4.4 Mineralogical analyses in thin section

4.4.1 sample TML-SA

Due to the granulometric bias introduced by sieving, it is not possible to ascertain the sedimentary environment in which the deposit formed through thin section observation. Nevertheless, it can be said that TML-SA is characterized by scanty medium and coarse sand fraction, and by fine material possibly indicating pedogenesis. Indeed, the fine material was observed before the sieving and also after it, especially in the form of "pseudosands" which survived the sieving procedure. The nature of the sand grains is essentially siliciclastic (Table 2), with a very minor volcanoclastic fraction and lack of volcanic scoriae. Grains have a subangular morphology.

Minerals	TML - SA	PC-SA	CSRM-SA
	%	%	%
Quartz	64	66	35
Metamporphic rock fragments	20	19	35
Chert	12	10	16
Feldspar	3	2	5
Pyroxene	1	3	8
Amphibole	1	0	0
Volcanic scoria	0	0	1

Total siliciclastic %	98	97	91
Total volcaniclastic %	2	3	9
Counted grains (n)	*152*	*156*	*154*

Table 2: results of petrographic determination of sands

Quartz, chert, metamorphic rock fragments (mainly quartzite with minor amounts of schist) and feldspar have been grouped under the "siliciclastic" category. Pyroxene (mostly augite and monocline pyroxene, diallagio), amphiboles (green and brown hornblende) and volcanic scoria belong to the "volcaniclastic" category.

4.4.2 Sand deposit at Podere Carafa: sample PC-SA

The sand displays strikingly similar grain composition (Table 1) and morphology as that of sample TML-SA.

4.4.3 Sand deposit at Castel Romano: sample CSR-SA

This sand sample is characterized by medium grain size with a subrounded morphology and no fine matrix. Mineralogical composition displays a higher percentage of volcanic species in comparison with the other sand samples (Table 1).

4.5 X-ray and SEM analysis

Results of diffractometric analyses are summarized in the diagrams of Figure 10.
Calcic clinopyroxene is ubiquitous in the pyroclastic rocks of the Colli Albani volcanic district. In addition, amorphous material derived from the weathering of volcanic glasses is typical of soils developed on pyroclastic rocks (generally, this soil component is identified in the RDX by the increase of counts in the region at lower 2Θ□□ Consequently, the height of clinopyroxene peak at 2Θ=29.85°, as well as that of amorphous material at 2Θ=4°, with respect to quartz peak at 2Θ=26.65° in the RDX can be assumed as an indicator of the abundance of volcanic components forming the soil. This provides an index (i.e. Qtz/(AM+Cpx) in Table 3) to distinguish the soils developed above a primary volcanic substrate (Index <6) from those overlying sedimentary deposits (Index >6).
Notably, quartz is present in all the soils developed above volcanic deposit and its abundance generally increases with decreasing depth as evidenced by magnitude of the peak at 2Θ=26.65° (Q1 Figure 10a). Quartz is practically absent closer to the base of the soil in VTB-1, and is scarce in the middle of the soil in VTB-2 and in Monte Migliore (MM). However, it is also abundant in the middle of VVL and VL, where the Q1 peak is comparable with that of all the surface samples. A marked quartz peak is present in sample VdT-2, from the soil developed

above the Villa Senni deposit on the 61-67 terrace, for which the siliciclastic fraction has been investigated in thin section for micromorphology on sample VdT-1. However, excluding the sample VCR-1, notably the closest one to the inferred sedimentary/volcanic transition in Figure 11, all the soils developed above volcanic deposit show higher amount of AM+Cpx (>12) in comparison with the others soils analyzed in this study (Table 3).

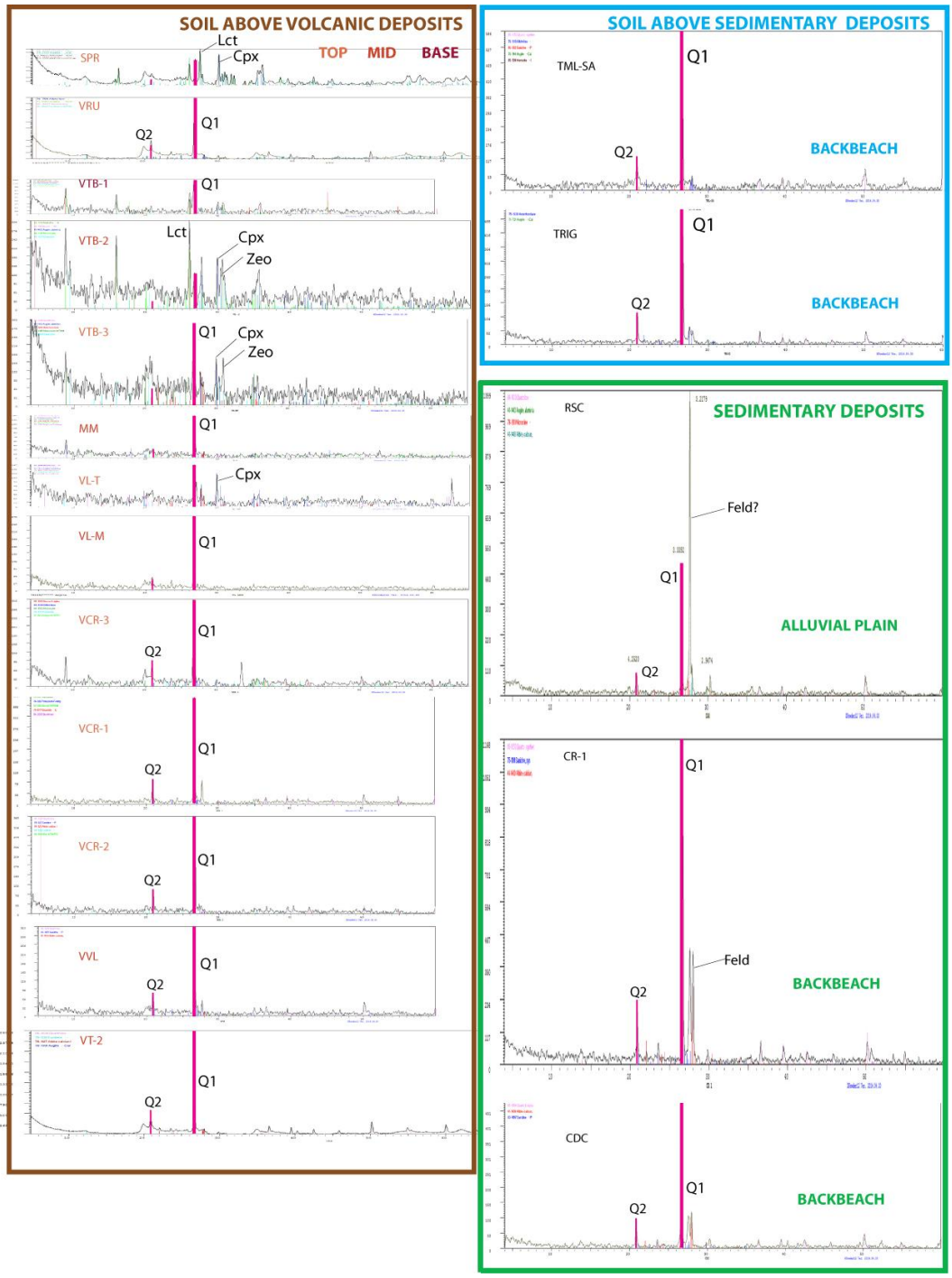

Figure 10 - Diffractograms of the soil and sediment samples. In inset a' diffractograms are... Vertical axes are normalized to the same scale; full-resolution original diagrams are provided in Suppl. Mat. #1B. See text for comments.

Moreover, quartz abundance decreases with the distance from the inferred paleo-shoreline in soils developed above the volcanic substrate. In order to verify this observation, we have collected two samples in the inland sector at the foot of the Colli Albani peri-caldera ring (SPR and RUT, Figure 11) and we have normalized results of diffractometric analyses peformed with a different equipment (see Methods in Supplementary Material #2) by re-analizing samples VTB-1 and VTB-3 with them (Table 3). As shown in Figure 10 and Tabkle 3, Q1 peaks and AM+Cpx/Qz are the highest one for thesec samples.

Apart for the discriminating AM+Cpx/Qz ratio, diffractograms of soils above sedimentary deposits differ from those above volcanic deposits only for the slightly larger magnitude of the main quartz peak Q1, and for the presence of a second quartz peak close to 10 (Q2). These peaks are much higher in the sediment samples which also display a remarkable peak corresponding to the pyroxene. Finally, the smaller magnitude of the quartz and pyroxene peaks in the fine sediment sample CDC suggests that magnitudes are also proportional to grainsize of the siliciclastic component.

Abundance, dimension and morphology of the Quartz and K-feldspar grains occurring in selected samples (VTB-1, TML-SA, VCR-1, CR1) have been analyzed at the SEM and discussed in section 5.1. Microphotographs are provided in Supplementaerty Material #2.

	SOILS ABOVE VOLCANIC DEPOSITS															SOILS ABOVE SEDIMEMNTARY DEPOSITS				
	VTB-1	VTB-2	VTB-1	VV	VL-M	VL-T	MM	VTB-1*	VTB-3*	VRU*	SPR*	VdT-2*	VCR-3	VCR-2	VCR-1	TRIG	TML-SA	RSC	CDC	CR-1
Amorphous	305	240	8000	58	54	121	45	68	9900	6100	8500	4750	80	70	30	52	59	55	45	110
Qtz	290	122	8000	320	270	147	150	0	20700	15977	6650	26343	316	349	394	520	586	1099	501	1168
Cpx	165	165	11500	0	10	118	15	40	9300	750	8000	550	25	0	10	20	20	40	20	0
TOT	760	527	27500	378	334	386	210	108	39900	22827	23150	31643	421	419	434	592	665	1194	566	1278
Amorphous	40	46	29	15	16	31	21	63	25	27	37	15	19	17	7	9	9	5	8	9
Qtz	38	23	29	85	81	38	71	0	52	70	29	83	75	83	91	88	88	92	89	91
Cpx	22	31	42	0	3	31	7	37	23	3	35	2	6	0	2	3	3	3	4	0
TOT	100	100	100	100	100	100	100	100	100	100	100	100	100	100	100	100	100	100	100	100
Qtz/Cpx+AM	0,6	0,3	0,4	5,5	4,2	0,6	2,5	0,0	1,1	2,3	0,4	5,0	3,0	5,0	9,9	7,2	7,4	11,6	7,7	10,6
Cpx+AM	62	77	71	15	19	62	29	100	48	30	71	17	25	17	9	12	12	8	11	9

Table 3 - X-ray powder diffraction (XRPD) data. Summary of absulte abundances of mineral phases in the analyzed samples (*samples analyzed with a different equipment, see Methods in Supplementary Material #2).

CR3	
Age (ka)	± 2σ (ka)
127,7	**± 11,3**
130,9	**± 11,2**
131,0	**± 9,6**
131,7	**± 9,7**
133,4	**± 13,7**
134,0	**± 14,3**
138,3	**± 6,3**
140,6	**± 12,5**
169,5	± 6,9
169,7	± 11,7
177,6	± 8,3
198,4	± 7,3
245,3	**± 6,6**
249,9	**± 7,2**
250,7	**± 6,5**
251,6	**± 6,6**
298,9	± 5,6
375,6	± 4,9
379,1	± 5,6
392,9	± 9,6
393,5	± 4,8
400,2	± 4,6
401,4	± 5,1
403,6	± 4,7
407,3	± 5,6
407,8	± 4,6
410,7	± 6,5
416,5	± 3,5
418,1	± 4,6
421,7	± 3,8
446,8	± 4,6
459,2	± 5,1
495,5	± 6,5
498,4	± 4,8
503,2	± 4,1
1289,3	± 6,5
1289,9	± 3,9
1293,0	± 6,9
1313,1	± 3,5
youngest population:	
134,2	**± 3,5**
249.3	**± 3.4**

TML-SA	
Age (ka)	± 2σ (ka)
151,1	**± 27,6**
165,5	**± 28,5**
166,6	**± 27,9**
171,0	**± 24,9**
181,7	**± 25,4**
189,3	**± 54,3**
216,5	± 6,0
239,9	± 4,7
246,2	± 17,8
250,0	± 6,6
252,3	± 7,1
257,6	± 5,1
262,8	± 22,7
266,0	± 20,0
287,5	*± 72,5*
316,8	± 18,7
329,8	± 20,8
335,5	± 96,7
351,5	± 15,7
361,0	± 40,6
368,2	± 32,7
369,5	± 20,0
371,2	± 21,5
372,6	± 18,7
382,2	± 23,2
389,6	± 23,0
398,9	± 16,2
409,6	± 5,9
422,9	± 63,3
430,5	± 10,9
435,7	± 8,7
446,4	± 5,6
504,4	± 5,6
541,7	± 5,0
549,4	± 5,4
551,8	± 4,3
557,0	± 40,2
589,3	± 4,4
600,0	± 6,4
1328,9	± 8,0
1339,3	± 15,9
youngest population:	
169	**± 11**

CSR-SA	
Age (ka)	± 2σ (ka)
232,3	**± 19,8**
240,9	**± 8,2**
244,5	**± 5,7**
246,8	**± 6,9**
263,1	± 4,6
263,7	± 29,1
310,1	± 16,3
395,5	± 5,0
407,9	± 4,4
476,6	± 7,1
488,3	± 5,3
494,5	± 4,7
500,8	± 6,8
508,5	± 3,5
542,1	± 17,2
552,1	± 9,0
563,1	± 6,2
597,3	± 3,7
625,7	± 6,7
805,2	± 9,7
youngest population:	
244.0	**± 3.8**

CAR-SA	
Age (ka)	±1σ (ka)
298,19	**± 3,50**
397,35	± 2,69
397,55	± 2,50
401,16	± 3,23
401,50	± 6,70
401,92	± 4,30
409,08	± 4,09
409,45	± 2,28
410,43	± 3,01
416,80	± 2,14
417,80	± 1,90
417,86	± 27,38
420,18	± 3,26
430,43	± 2,92
447,50	± 15,16
461,11	± 3,89
468,78	± 18,49
523,49	± 3,21
566,40	± 2,82
580,99	± 3,19

Table 4 - 40Ar/39Ar ages of dated samples

4.6 $^{40}Ar/^{39}Ar$ data

Single crystal age data for the three analyzed samples are reported in Table 4. Full analytical data are proved in Supplementary Material #3.

4.6.1 Sample CR3

Thirty-nine sanidine crystals extracted from the sand sample collected ca. 90 cm below the ground surface in Colle Rotondo provided a wide age spectrum, ranging 1.31 through 0.13 Ma. A youngest population of eight crystals yielded a weighted mean age of 134±3.5 ka.

4.6.2 Sample TML-SA

Forty-one sanidine crystals extracted from the sand sample collected ca. 60 cm below the ground surface in Tenuta Monte di Leva provided ages ranging 1.34 through 0.15 Ma. A youngest population of six crystals yielded a weighted mean age of 169±11 ka.

4.6.3 Sample CSR-SA

Twenty sanidine crystals extracted from the sample collected in the fluvial sand cropping out in Castel Romano provided ages ranging 0.80 through 0.23 Ma. A youngest population of four crystals yielded a weighted mean age of 244±4 ka.

4.6.4 Sample RSC-SA

Twenty sanidine crystals extracted from the sample collected in the fluvial sand cropping out in Riserva Carpineto provided one isolated, youngest crystal of 298±3.5 ka. The majority of the crystal ages are spread in the interval 398-468 ka, with three oldest crystals ranging 523 - 581 ka.

5. Discussion

5.1 Soils and paleo-surfaces

Analysis of soil samples for the present study has been conducted aimed at identifying their sedimentologic and petrographic features, in order to understand their origin and the paleogeographic conditions in which they formed. Pedologic considerations and a complete study of the processes involved the formation of these soils, as well as laboratory granulometric analyses are beyond the scope of the present work. Our main scope is to verify to what extent the present ground surfaces characterized by the same elevations range represented in Figure 2 and 3 can be considered indicative of the original paleo-surfaces representing the ancient coastal settings. In particular, we want to quantify the possible amount of later deposition, or erosion, which may have increased or decreased, respectively, the average elevation of these paleo-surfaces, therefore affecting our estimation of the sea-level related with the corresponding coastal terrace.

When studying the composition of the soils developed above the reconstructed paleo-surfaces, some preliminary considerations are necessary. In particular, when the paleo-surfaces of highest order are considered (i.e. those ranging 98-108, 80-89, and 71-79 m a.s.l., Figure 3), we must realize that the sub-horizontal attitude of these isolated, plateau-like sectors precludes alluvial sedimentation, almost completely. Furthermore, the whole catchment area drained by these paleo-surfaces is developed above volcanic deposits. Therefore, the siliciclastic component of the soils above the paleo-surfaces of this sector, which in the X-ray diagrams is sometimes predominant, can only have the following two origins:

i. it can be a back-beach to coastal plain sediment originally deposited above the volcanic substrate when the paleogeographic conditions allowed (i.e.: before the regional uplift, when the paleo-surface represented a coastal environmental setting) (BB and AL in Figure 11a);

ii. it can be an aeolian sediment (i.e., loess-like) accumulated above the volcanic deposits through air-fall emplacement and successively diffused within the soil by vertic processes (i.e.: internal turnover of soil material originated by pedogenetic processes).

Recognizing the origin of this siliciclastic sediment is therefore fundamental in order to reconstruct the paleogeographic setting of these paleo-surfaces, correctly, as shown in Figure 11, in which the paleogeographic scenario is illustrated. The dashed green line in Figure 11 separates the sampling sites where field observation have shown that the present soil overlies sedimentary sand deposits (to the southwest), from those where the soil is developed above the volcanic deposit of Pozzolanelle (to the northeast), as reported also in the cross-section of Figure 12. The oblique green lines indicate the area where the siliciclastic fraction in the analyzed soils is predominant.

Composition of the analyzed soils overlying the volcanic deposit of Pozzolanelle, with abundant quartz and feldspar, combined with micromorphological and SEM analyses which confirm the sedimentary origin of the quartz grains but rule out an aeolian (loess-like) origin, at least for the larger fraction (>200 μm; Figure S7), demonstrate that these soils affect thin (≤ 1 m) layers of alluvial and backbeach, predominantly siliciclastic deposits. In keeping with this interpretation, quartz abundance strongly decreases in soil samples collected in more inland locations (SPR, RUT), far from the inferred paleo-coastline (Figure 10).

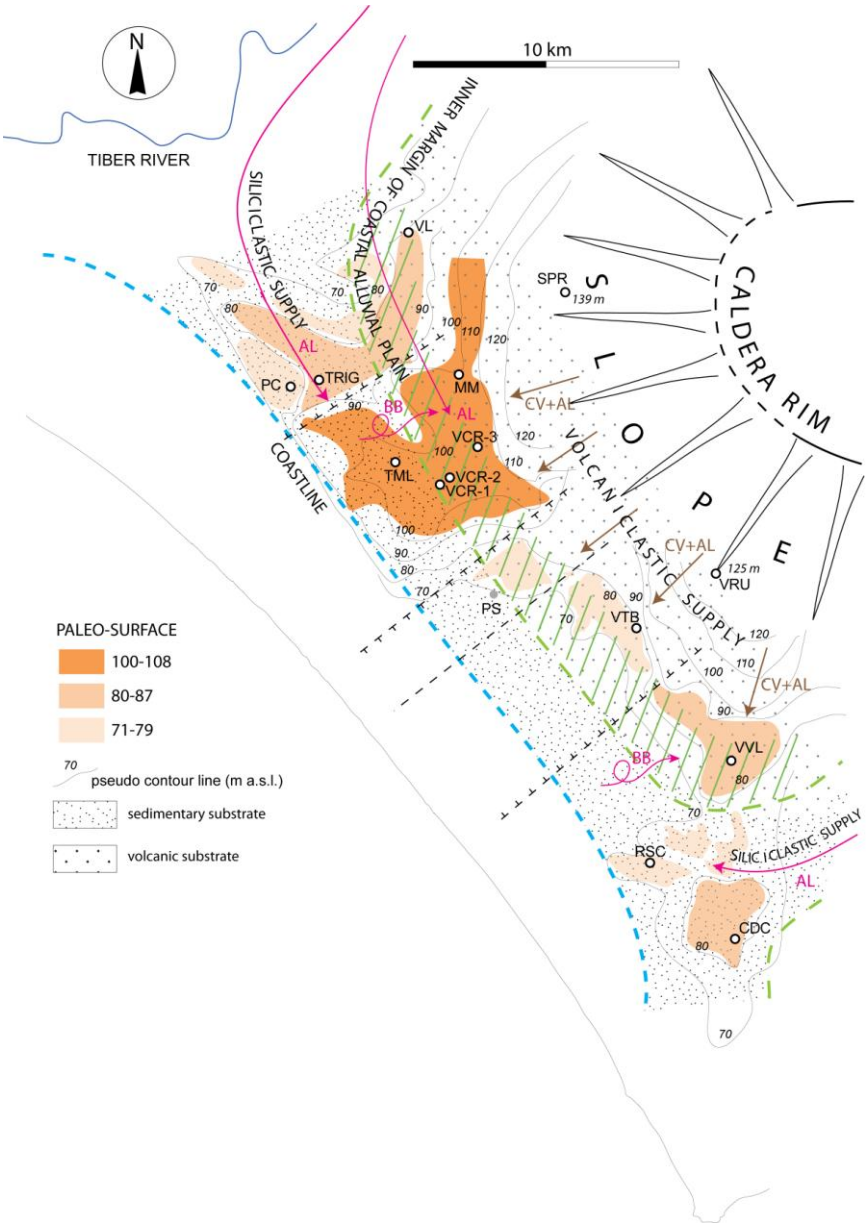

Figure 11- Paleogeographic reconstruction of the MIS 9 coastal setting. Stratigraphic investigations and sedimentologic, micromorphologic, mineralogic and petrographic analyses on sediment and soil samples have allowed to detect a transitional zone (oblique green dashes) corresponding with the inner margin of the coastal plain, where a thin horizon of backbeach to alluvial deposits overlaps the volcanic substrate. (see also cross-section in Figure 12a). This reconstruction evidences the occurrence of an original, homogeneous paleo-surface, subsequently disrupted and dislocated by tectonic movements, which gave rise to three main flat sectors at elevations ranging 100-108, 80-87, and 71-79 m a.s.l. (see text for comments).

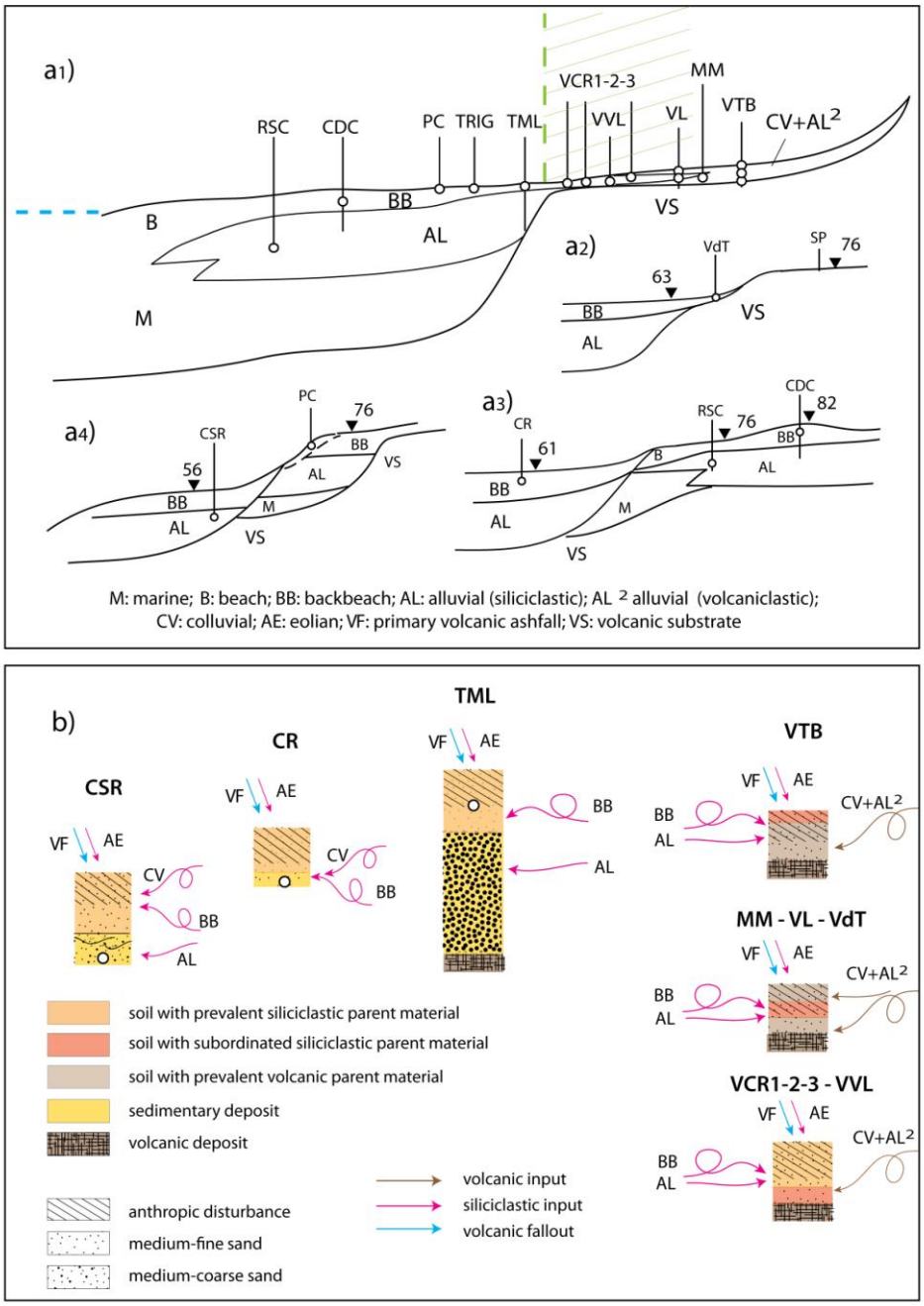

Figure 12 - a1-4) Cross-sections restored from tectonic dislocation showing the original paleogeographic and sedimentary settings reconstructed in the area where the soil and sediment samples were collected. b) Origin of the different sedimentary inputs contributing to the formation of the deposits and the related soils at the top of the paleo-surfaces reconstructed in the present study. See text for comments.

Alluvial/colluvial volcanic material (CV+AL in Figure 112b and 12), derived from the rocks cropping out at the inner margin of the coastal alluvial plain (green dashed area in Figure 11), were also continuously mixing with the alluvial and backbeach, predominantly siliciclastic deposits transported by the Tiber River and deposited in the coastal plain. Moreover, air-fall material including either loess-like sediment (AE in Figure 12b), or as primary air-fall volcanic ash (VF in Figure 12b), also progressively accumulated above this soils and was diffused by vertic processes into the sub-surface horizon. To this aeolian fraction must be ascribed part of the K-feldspar observed in this section and evidenced in the diffractograms, as well as part of the finest siliciclastic component.

Such an air-fall contribution must be extended to the soils developed above the sedimentary deposits, in which the volcanic component is also represented by re-deposited mineral species of the underlying sedimentary substrate, incorporated in the soil through colluviation, surface water and wind transport (CV in Figure 12b).

These mechanisms are envisaged in Figure 12, showing the different paleogeographic and sedimentary settings reconstructed in the area where the soil and sediment samples were collected. The age spectra provided by sanidine crystals extracted from the lowest portion (unaffected by agricultural disturbance) of the backbeach deposits above which the soils of the 98-108 and of the 61-67 paleo-surfaces have developed (TML-SA, CR3; Figure 13), compared to that of the "sealed" sedimentary deposit of the fluvial facies (RSC-SA, CSR-SA), provide further insights to the processes described above.

5.2 Age of the paleo-surfaces

Youngest crystal ages of 232±20 and 298±4 ka yielded by sedimentary samples collected in the alluvial facies (coastal plain) of the 51-57 m and of 71-79 m paleo-surfaces (CSR-SA and RSC-SA) support correlation with MIS 7 and MIS 9 for the corresponding coastal terraces, as discussed in the following sections.

Similarly, crystal ages of the samples collected from the backbeach facies at the top of the 98-108 m and 61-67 m paleo-surfaces provide time constraints on the sedimentary processes that acted in the time span following retreat of the coastline leading to progressive impoverishment of sediment supply.

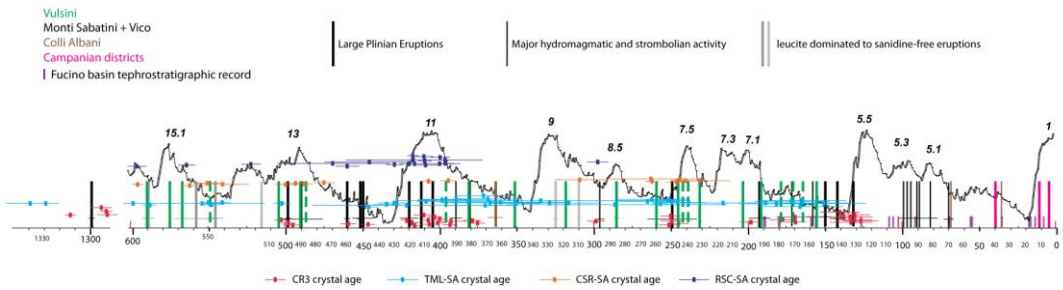

Figure 13 - Crystal age spectra for the four sedimentary samples dated in the present study. Each cross represents the age of one dated sanidine crystal with the associated analytical error at 2 σ. Comparison with the major eruptions occurred at the districts of the Roman Co-magmatic province is provided. Each bar represents one eruption age (see Suppl. Mat. for details and references). Comparison with the oxygen isotope curve (Lisiecki and Raymo, 2005) is also shown. See text for comments.

These age constraints are obtained by comparing the sample crystal ages with the eruptive histories of the volcanoes of the Latium Region, as provided in Figure 13. In considering the eruptive histories of the volcanic districts of Central Italy to compare age spectra yielded by the analyzed sedimentary samples reported in Figure 13, some preliminary considerations should be made.

i- These volcanoes are part of the "Roman Magmatic Province" (Conticelli and Peccerillo, 1992), characterized by a K-rich geochemistry which accounts for the diffuse presence of sanidine ($KAlSi_3O_8$) and leucite ($K[AlSi_2O_6]$) crystals, which also constitute the means of $^{40}Ar/^{39}Ar$ dating. However, while sanidine is a very resistant mineral species, leucite is highly sensible to weathering and easily alters to analcime ($NaAlSi_2O$): a process implying loose of K andcompromising $^{40}Ar/^{39}Ar$ dating. Indeed, fluvially transported and beach deposits of several hundred kyr lack pristine leucite crystals. Therefore, in Figure 13 we have not reported all the sanidine-free eruption units (i.e., most of those of the Colli Albani volcanic district, see Gaeta et al., 2016 and references therein), while we have indicated those dominated by leucite (for which a lesser statistical occurrence is expected).

ii- When incorporation of crystals derived from primary fallout deposits is considered, the overall eastward regional winds and a consequent dispersal axis should be considered, along with the distance from the source area. Therefore, the major source of fallout deposits are the MSVD and Vico, while deposits from the Colli Albani and the Campanian districts have a low probability of representation in the stratigraphic record. One exception is represented by the sanidine-bearing activity of the Albano Center spanning 70 through 36 ka (Giaccio et al., 2009, and ref.), for which the small vent distance should have led to a well-represented crystal population, as also evidenced by outcrops in the southeastern area of the CAVD (e.g., Cisterna

di Latina, Latina Plain; Gatta et al., 2018, Sevink et al., 2018). Moreover, huge explosive eruptions like the Campanian Ignimbrite (39 ka), Neapolitan Yellow Tuff (12 ka) and Avellino pumice (4 ka) have provided widespread tephrostratigraphic markers in Latium (e.g., Giaccio et al., 2017).

iii- The youngest eruptions should be better represented given the larger outcrop areas of the products in comparison with the older ones, which are buried under more recent cover. This reinforces the principle that a lack of crystals younger than the youngest population is evidence of deposition prior to the immediately following eruption.

Consistent with the considerations above, Figure 13 shows that the age spectra of sanidine crystals extracted from the four sand samples record a long eruptive history, ranging 0.60 - 0.13 Ma, plus one isolated cluster around 1.3 M. All crystal ages ≤0.6 Ma match known eruptions of the Monti Sabatini, Vico and Vulsini volcanoes (Palladino et al., 2010; Sottili et al., 2010; Marra et a., 2014, and ref. therein), while the oldest age matches that of early activity of the Cimini volcanic complex (Everdin and Curtis, 1965, Nicoletti, 1969), located in the upper Tiber Valley east of Vico. In contrast, all theeruption ages known from the literature that are missing in the dated crystal populations, besides the sanidine-free Colli Albani products, also correspond to sanidine-free or leucite-dominated products from Vico and Monti Sabatini volcanic districts (Cioni et al., 1987; Sottili et al., 2004; Perini et al., 2004; Masotta et al., 2010; Marra et al., 2014).

Based on these premises, in the following we discuss sample age implications on assessing the age of the related paleo-surfaces.

5.2.1 CSR-SA - 51-57 m paleo-surface

Based on the sedimentary features of the underlying deposits and the top elevation ranging 51-57 m a.s.l. (Figure 9a-a"), the Castel Romano paleo-surface is interpreted as a backbeach context, including the dune system superimposing the delta plain, developed during highstasnd of MIS 7.3/7.1. Loose sanidine crystals occurring in the sand deposit of the braided fluvial channel facies (Figure 9a'-a") yielded a youngest age of 232.3±19.8 ka, part of a statistically significant youngest population of 244.0±3.8 ka (Table 4). Such datum has to be considered a terminus post-quem which implies an age ≤ MIS 7.5 (Figure 13), excluding and age within MIS 9 and supporting correlation with highstand of the MIS 7.3/7.1.

5.2.2 RSC-SA - 71-79 m paleo-surface

The age spectrum of sample RSC-SA, collected within the alluvial plain deposit underlying the 71-79 paleo-surface at Riserva Carpineto, spans 581 - 398 ka, with a youngest crystal of 298±3.5 ka (Table 4). Most crystal ages are clustered between 460 and 390 ka, coincident with the large explosive phases emplacing sanidine-bearing products at Vico and Sabatini in this time span (Figure 13). In contrast, no crystal deriving from the Villa Senni eruption unit occurs in the dated sample, despite the sampled deposit overlies the Pozzolanelle eruption unit of 365±4 ka, consistent with the lack of sanidine phenocrystals in the Colli Albani products. The age of one single crystal yielding 298±3.5 ka has a poor statistical weight, and should be regarded as broadly indicative of the lack of crystals younger than 300 ka. However, it supports correlation with MIS 9 for the 71-79 m paleo-surface of Riserva Carpineto, suggesting that sedimentation in the alluvial plain was sealed in the late stages of the MIS 9 highstand, excluding an age within MIS 7, while an age within MIS 11 is also excluded by the fact that the sand deposit of Riserva Carpineto overlies the 365±5 ka Pozzolanelle pyroclastic-flow deposit.

5.2.3 CR3 - 61-67 m paleo-surface

Based on its sedimentologic features and the elevation ranging 61-67 m a.s.l., the Colle Rotondo paleo-surface is interpreted as a backbeach context, either part of a dune system or of a coastal alluvial plain, developed during highstasnd of MIS 7.5 (Figure 14a).
When the crystal ages from CR3 (red crosses in Figure 13) are compared to the eruptive histories of the volcanoes of the Latium Region, it is apparent that no eruption younger than 134±3.5 ka is recorded by the Colle Rotondo sand deposit. Indeed, given the large number of dated crystals (39) and the wide age spectrum observed, the lack of any crystal from the eruptive activity since 99 ka (see Figure 13) strongly suggests that the sample age should be constrained between 132 and 99 ka. In particular, a large hydromagmatic phase occurred in several volcanic centers of the MSVD, including Baccano, Stracciacappe, Le Cese, Acquarello, Piana dei Falliti and Martignano, 132±2 through 70±3 ka (Sottili et al., 2010; Marra et al., 2019b). While the earliest eruption that occurred at Baccano at 132±2 ka is evidently recorded by sample CR3, the lack of crystals from any later eruption strongly suggests a terminus ante-quem of ca. 99±3 ka (age of the products of the 2nd Baccano unit, erupted at the beginning of the multi-vented hydromagmatic activity that continued until 70±3 ka). Although this age boundary to the deposit is in conflict with the attribution to the Uluzzian for the lithic industry recovered at Colle Rotondo (Villa et al., 2018), we note that sample CR3 was not collected in the stratum in conjunction with the artifacts, but in a side excavation.

Therefore, its correspondence with the archaeological layer is not safely established and provenance may be from the immediately underlying older substrate. In this latter case, the occurrence of the Uluzzian lithic assemblage at ca. 80 cm depth suggests that the overlying package of sediment accumulated during the last 40 ky. Such an accelerated accumulation may be linked with recent anthropic activity (e.g., agriculture), triggering soil mobilization. In contrast, the apparent age of ~134 ka for the sand layer at 80 cm depth does not conflict with an inferred age of 250-200 ka within MIS 7 for the Colle Rotondo paleo-surface, as discussed hereby based on a detailed analysis of the $^{40}Ar/^{39}Ar$ dating results.

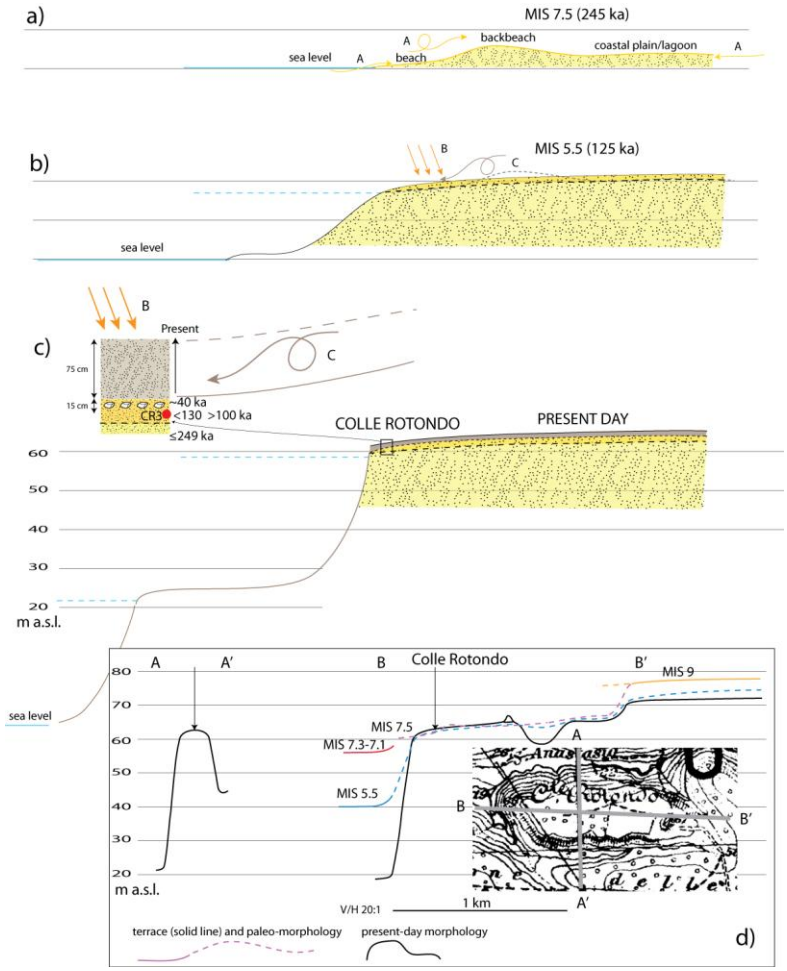

Figure 14 - Geomoprphological and paleogeographic evolution of the Collo Rotondo plateau (see text for step by step comment and explanation).

Like in the case of the sedimentary deposit sampled at Castel Romano which yielded a youngest crystal age of 232±20 ka, consistent with a deposition age corresponding to the highstand of MIS 7.3-7.1 (i.e. 220-200 ka), an age ≥245 ka is expected for the fluvial/beach

sedimentary deposit at Colle Rotondo (supply A in Figure 14a) incorporating crystals derived from erosion and re-deposition of the volcanic rocks erupted before that time, corresponding to highstand of MIS 7.5 (i.e., 245 ka, see Figure 13). However, a progressively younger age is expected for the backbeach deposit deriving from mixing of wind-blown sediment previously deposited (supply C in Figure 14b) with crystals deriving from primary eruptions occurring in the following time span (supply B in Figure 14b). Sample CR3 from Colle Rotondo yielded a statistically significant (8 crystals) youngest crystal population of 134.2±3.5 ka which is characterized by significantly larger associated errors in comparison with the older populations (see Table 5). In particular, these crystals yielded an average associated error of ±11 ka (corresponding to 8.2% when an age of 134 ka is considered) in comparison with an average associated error of ±5.4 ka for the 23 crystals yielding ages spanning 249.9 - 503.2 ka (corresponding to 2.2% - 1.1%). These larger errors are due to the systematically smaller dimensions of these crystals, evidencing their different means of transport in comparison with that affecting the oldest ones, i.e.: wind vs. water. When this distinction is taken into account, we find a second significant population age of 249.3±3.4 ka, along with a few crystal ages ranging 200-170 ka (Table 4 and Figure 13), consistent with an age within MIS 7.5 for the original beach/alluvial deposit. An age ≥134±3.5 ≤198.4±7.3 ka is established for the sampled backbeach deposit, showing that it accumulated above the MIS 7.5 paleosurface during ca. 110 ky (i.e., 245 through 134 ka). The lack of crystals deriving from the eruptions between 132 and 70 ka at the MSVD (see Figure 13), strongly suggests that the sampled layer cannot be younger. Indeed, accidental absence of crystal ages within this time span is statistically unlikely, given the eastern dispersal axis of the MSVD eruption (e.g. Sottili et al., 2004; Di Rita and Sottili, 2019) and the occurrence of large explosive eruptions 90 through 70 ka at a number of centers of the so-called "Hydromagmatic Phase" (De Rita et al., 1983; Sottili et al., 2010; Marra et al., 2019b). This fact also testifies that the depositional context progressively changed after 245 ka, consistent with continued uplift of the coast and isolation of the Colle Rotondo remnant paleo-surface, which was unaffected by deposition of water transported sediment, like that occurring in alluvial plain or beach contexts, while only eolian fallout deposits were emplaced, from then on. Since sample CR-1 occurs 90 cm below the present ground level (Figure 14c), we can infer that present elevation of 63 m is a close approximation of the MIS 7.5 paleo-surface, which is overlain by a thin eolian deposit accumulated since 245 ka (input B in Figure 14c). Indeed, it is likely that samples collected closer to the surface would yield progressively younger ages, consistent with incorporation of crystals deriving from the younger eruptions of 100 ka and 90 through 70 ka. However, the

strong anthropic disturbance of the upper 70 cm of sediment prevents any reliable analysis. Sample TML-SA from Tenuta Monte di Leva section provides further inferences on the formation process of this thin eolian cover of the paleo-surfaces.

CR3	
Age (ka)	± 2σ (ka)
134,0	**± 14,3**
133,4	**± 13,7**
140,6	**± 12,5**
169,7	± 11,7
127,7	**± 11,3**
130,9	**± 11,2**
131,7	**± 9,7**
131,0	**± 9,6**
392,9	± 9,6
177,6	± 8,3
198,4	± 7,3
249,9	± 7,2
169,5	± 6,9
1293,0	± 6,9
245,3	± 6,6
251,6	± 6,6
250,7	± 6,5
410,7	± 6,5
495,5	± 6,5
1289,3	± 6,5
138,3	**± 6,3**
298,9	± 5,6
379,1	± 5,6
407,3	± 5,6
401,4	± 5,1
459,2	± 5,1
375,6	± 4,9
393,5	± 4,8
498,4	± 4,8
403,6	± 4,7
400,2	± 4,6
407,8	± 4,6
418,1	± 4,6
446,8	± 4,6
503,2	± 4,1
1289,9	± 3,9
421,7	± 3,8
416,5	± 3,5
1313,1	± 3,5
youngest population:	
134,2	**±3,5**

TML-SA	
Age (ka)	± 2σ (ka)
335,5	± 96,7
287,5	± 72,5
422,9	± 63,3
189,3	**± 54,3**
361,0	± 40,6
557,0	± 40,2
368,2	± 32,7
165,5	**± 28,5**
166,6	**± 27,9**
151,1	**± 27,6**
181,7	**± 25,4**
171,0	**± 24,9**
382,2	± 23,2
389,6	± 23,0
262,8	± 22,7
371,2	± 21,5
329,8	± 20,8
266,0	± 20,0
369,5	± 20,0
316,8	± 18,7
372,6	± 18,7
246,2	± 17,8
398,9	± 16,2
1339,3	± 15,9
351,5	± 15,7
430,5	± 10,9
435,7	± 8,7
1328,9	± 8,0
252,3	± 7,1
250,0	± 6,6
600,0	± 6,4
216,5	± 6,0
409,6	± 5,9
446,4	± 5,6
504,4	± 5,6
549,4	± 5,4
257,6	± 5,1
541,7	± 5,0
239,9	± 4,7
589,3	± 4,4
551,8	± 4,3
youngest population:	
169	**±11**

CSR-SA	
Age (ka)	± 2σ (ka)
263,7	± 29,1
232,3	**± 19,8**
542,1	± 17,2
310,1	± 16,3
805,2	± 9,7
552,1	± 9,0
240,9	**± 8,2**
476,6	± 7,1
246,8	**± 6,9**
500,8	± 6,8
625,7	± 6,7
563,1	± 6,2
244,5	**± 5,7**
488,3	± 5,3
395,5	± 5,0
494,5	± 4,7
263,1	± 4,6
407,9	± 4,4
597,3	± 3,7
508,5	± 3,5
youngest population:	
244	**±4**

Table 5

5.2.4 TML-SA - 98-108 paleo-surface

Much caution should be used in interpreting results for the TML-SA sample because it was collected ca. 60 cm below the ground level within the soil horizon, in which both vertic processes and anthropic disturbance might have caused incorporation of younger crystals from the uppermost portion of the stratum.

However, the age spectrum of sample TML-SA, collected on the 98-108 paleosurface, is similar to that of CR3 but yields a youngest minimum age of 169±11 ka (Figure 13), evidencing a relative older age, with respect to the sample collected on the 61-67 paleosurface of Colle Rotondo.

These data suggest that the sampled sand deposit represents a sedimentary horizon that was sealed from air-fall input by 170 ka, supporting the notion that the uppermost portion of the reconstructed paleo-surfaces represents an accretionary horizon, built up mainly through accumulation of alluvially/colluvially transported and, subordinately, air-fallen material. Remarkably, also in this sample the youngest crystal population is characterized by larger associated errors (Table 5), supporting the different mean of transport for this sedimentary fraction which accumulated later, as an air-fall deposit above the underlying deposits of the alluvial plain.

The very low sedimentation rate and the limited thickness of these accretionary horizons overlying the "pristine" deposits forming the paleosurfaces, whose absolute age has been determined by $^{40}Ar/^{39}Ar$ dating on "in stratum" samples from Castel Romano and Riserva Carpineto, is consistent with the geomorphologic features of the TML and CR sectors, precluding significant alluvial/colluvial sedimentation.

5.3 The MIS 9 paleo-surface

Geomorphological, lithostratigraphic, paleo-environmental and geochronological constraints obtained for the deposits of the 71-79 m paleo-surface, and part of the 80-89 m and 98-108 m paleo-surfaces, allow the identification of these paleo-surfaces as the remnant coastal terrace of the MIS 9 highstand, tectonically dislocated (Figure 11 and 15). The subrounded morphology, the medium to coarse grain-size and the high degree of sorting of the sand deposits at Riserva Carpineto (RSC) clearly indicate that the flat sectors at elevations ranging 71-79 m a.s.l. represent remnant parts of an alluvial coastal plain, stretching NW to SE parallel to the present coastline (Figure 11 and 12a3). Crystal ages yielded by sample RSC-SA firmly constrain the formation of this coastal plain within MIS 9 (see also Figure 16). The bedded deposits of Campo di Carne (CDC), ranging from coarse sand to silty clay, are suggestive of a

coastal alluvial plain, overlain by a transgressive backbeach deposit forming a wide dune ridge system culminating at ca. 85 m a.s.l. in this area (Figure 11 and 12a3), and equivalent to that occurring in Trigoria (TRIG) at analogous elevations (Figure 11 and Figure 12a1). Evidence from the Tenuta Monte di Leva (TML) site shows that this backbeach setting homogeneously extends parallel to the paleo-coastline, but it is presently displaced to a ca. 20 m higher elevation in this sector (Figure 15). Micromorphological analysis of the concretionary layer observed in the TML indicates that this massive horizon formed in alluvial to backbeach environment characterized by a water table close to the surface, consistent with the reconstructed paleogeographic conditions, whichshow that it was part of the coastal plain. The geologic substrate at TML is indeed identical to that at TRIG, apart from the larger thickness of the upper, aeolian sand horizon above the concretionary layer at the latter location, consistent with a post-depositional tectonic displacement between these two sectors and limited erosion at TML.

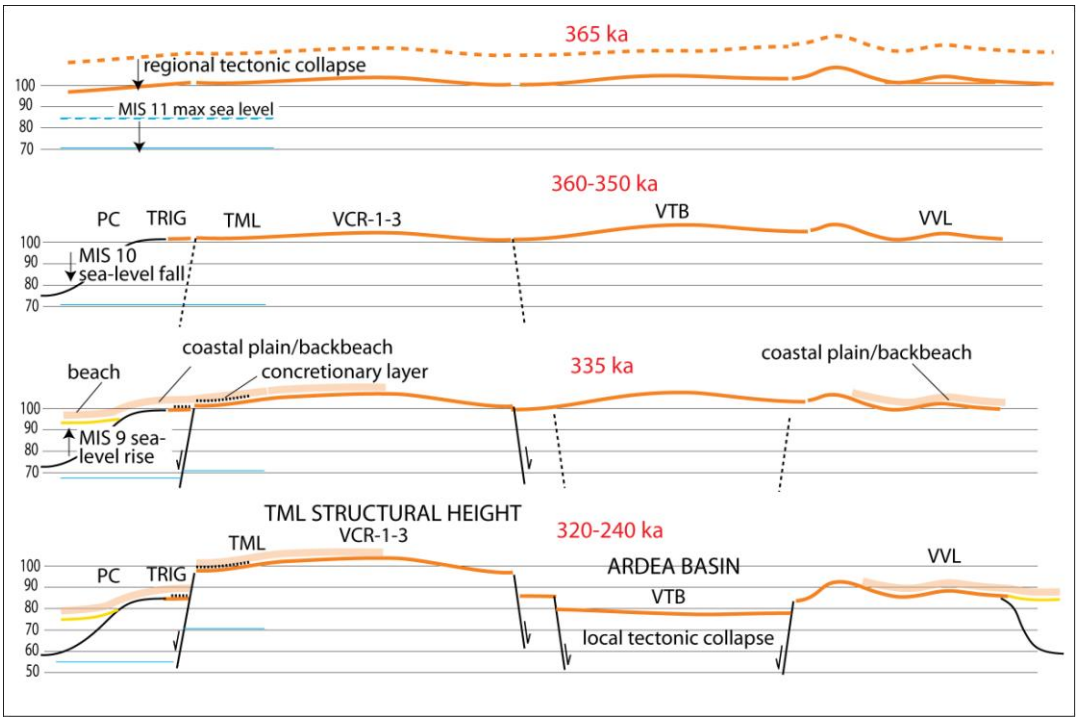

Figure 15 - Palinspastic reconstruction of the tectonic evolution of the coastal sector between the Tiber mouth and Anzio in the time span 365 ka (age of emplacement of the Villa Senni Eruption Unit during lowstand of MIS 10) and 240 ka (onset of MIS 7.5). a) A regional collapse immediately following emplacement of the pyroclastic flow-deposit is inferred from the elevation gain between the top surface of aggaddationasl successions of MIS 11 and MIS 9. MIS 11. b) Erosion of the original paleo-surface occurs during the lowstand of MIS 10, 360 through 350 ka. c) Fluvial and coastal incisions are filled by sediment-aggradation during glacial termination V (335 ka) at the onset of the sea-level rise during MIS 9, and a coastal

setting including a beach to backbeach and coastal plain environment forms during the MIS 9 highstand (325 ka). d) This homogeneous coastal setting is disrupted by fault displacement forming a structural heigh in the TML and a collapsed sector (Ardea basin) during the time span 320-240 ka (MIS 7.5 highstand) as indicated by the upper chrono-morphological constraint represented by the inner edges of MIS 7.5 coastal terrace (see text for further explanation).

On the other hand, the 98-108 paleo-surface represents a striking geomorphological anomaly bordering the Ardea Basin to the NW (see also Figure 4), and is clearly interpretable as the result of differential uplift at the footwall of a boundary fault of the half-graben structure (Figure 11 and 15). Also the different geologic substrate that characterizes the 71-79 m paleo-surface within the Ardea Basin (e.g., VTB), which is formed by volcanic deposits (i.e.: the same substrate as the inland portion of the 98-108 m paleo-surface in VCR 1-2), is suggestive of tectonic lowering following the formation of a homogeneous coastal platform during the highstand of MIS 9, throughout this region. In contrast, in the case of a pre-existing embayment in this area, the 71-79 m paleo-surface at VTB should have had the same sedimentary substrate as that occurring in PC and RSC, confirming a coastal environment. In particular, the tectonic collapse of the Ardea Basin is constrained between 320 ka (end of the MIS 9 highstand) and 240 ka (highstand of MIS 7.5) (Figure 15), as provided by the geometry of the 60-67 m and 51-57 m coastal terraces, indicating that an embayment formed by the time of establishment of the new coastline during MIS 7.5 through MIS 7.1 (see Figure 3 and 4). Remarkably, this time span is concident with the occurrence of the Monte delle Fate phase of activity at the Colli Albani Volcanic district (Gaeta et al., 2016, and references therein).

5.4 MIS 7.5 paleo-surface

The secure correlation with MIS 9 for the coastal plain deposits of the 71-79 m paleosurface, combined with previous geochronologic constraints that frame the 51-57m paleosurface within the broad MIS 7.5 - MIS 7.1 interval (Figure 16a), suggests that the intermediate 61-67 m surface should be correlated with the early interglacial 7.5, while the paleo-surface occurring a few meters below, at an elevation of 51-57 m, should be correlated with the later isotopic peaks 7.3/7.1 which are not separated by a marked sea-level fall (See Figure 16a), and can be regarded as a single eustatic event. Crystal age distribution yielded by sample CR3 from Colle Rotondo supports this correlation (Figure 16b). Based on the considerations reported above on the errors associated with the $^{40}Ar/^{39}Ar$ dating and their direct relation with grain-size, we can infer that an alluvial coastal plain formed by 249.3±3.4 ka, an age remarkably coincident with glacial termination III at the onset of MIS 7.5 (Figure 16b), at ca.

60 m a.s.l.. It was successively mantled by a wind-blown deposit derived from the nearby beach during the interval 200 - 170 ka, a time when the coastline rebounded to the elevation of 60 m a.s.l. during sea-level high stands linked with the double peak in the isotopes curve of MIS 7.3 and 7.1. Indeed, according to geomorphologic reconstruction, sedimentologic features, and micromorphologic analysis, the Colle Rotondo sand is a backbeach deposit. The sand grains originated mainly from very proximal aeolian transport from the beach, where the original sediment accumulated after being eroded and transported by the Tiber River and its tributaries (A in Figure 14a). Moreover, since formation of the dune ridge, more aeolian material, as well as primary, air-fallen volcanic deposits (including sanidine minerals, B in Figure 14a), accumulated above it. Eventually, this sector was isolated from the coastal environment by the continued uplift, and it was affected only by deposition of the syn-eruptive fallout deposit of the Baccano unit at 132±2 ka. If we consider the strong uplift of more than 50 m that occurred from 250 ka, the wind-blown depositional mechanism rapidly became ineffective, due to the increased elevation and distance from the coastline (e.g., by 125 ka, Figure 14b). The regional uplift, determining the deep incision of the coastal terrace through the action of fluvial erosion, also generated the canyon-like morphology that characterizes this area, isolating the Colle Rotondo plateau and preventing alluvial sedimentation on its top (Figure 14c-d). Therefore, it is reasonable to assume that a very limited thickness of sediment accumulated above the original paleo-surface representing the coastal terrace, mainly by the air-fall mechanism and only subordinately, as a consequence of re-mobilization of pre-existing sediment, through wind transport, or water run-off and colluviation from the upper part of the plateau towards the lower sectors (C in Figure 14b). If we consider that the elevation gain between the top and the margins of the Colle Rotondo plateau is less than 4 m (Figure 14d), the latter depositional mechanisms must have acted in a very limited way.

5.5 MIS 7.3-7.1 paleo-surface

The 51-57 m paleo-surface previously detected by Marra et al. (2016) has widespread expression at Ponte Galeria (Fig. 2), where chronostratigraphic constraints on the underlying aggradational deposits (Vitinia Formation, Luberti et al., 2017 and references therein) and their geometric/stratigraphic relationship with the 36 m terrace unambiguously provide correlation with the four-stepped sea-level rise that characterized MIS 7 (Marra et al., 2016b). In particular, an early aggradational phase of the Vitinia Formation around 269 ka matches the initial sea-level rise (A' in Fig. 16b) preceding the marked sea-level jump of glacial

termination III that occurred at 240 ka, with which in turn is associated the main aggradational succession of MIS 7.5, bracketed by post-quem ages of 253±8 ka and 248±4 ka (A in Fig. 16b).

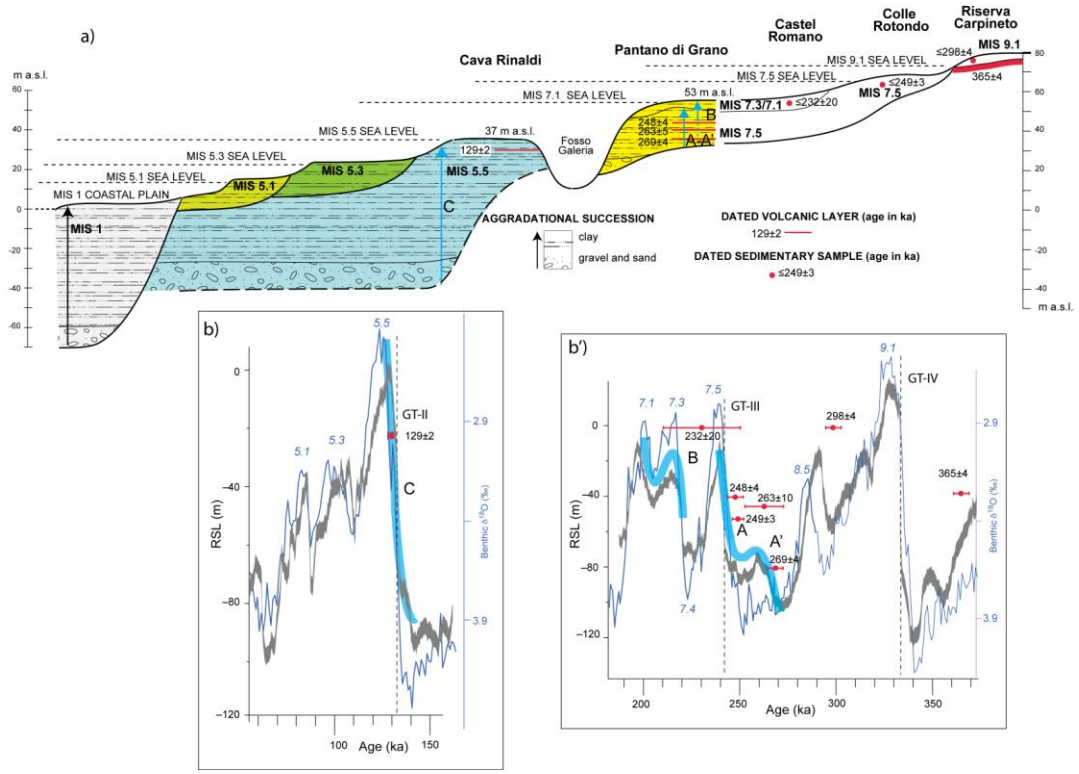

Figure 16 - a) Idealized cross-section reconstructing the terraced deposits and the corresponding aggradational successions in the investigated coastal sector, showing the geochronologic constraints providing correlation with MIS 9.1 through MIS 5.5. b-b') Ages of the dated volcanic deposits and reworked crystal populations (red dots, bars indicate the analytical error at 2σ) are compared with the Oxygen isotope curve (Lisiecki and Raymo, 2005) and the Relative Sea Level (RSL) curve (Grant et al., 2014). Correspondence of sediment aggradation with phases of rapid sea-level rise (thick blu lines) during glacial terminations (GT) is highlighted.

Finally, a marked unconformity cuts the deposits of MIS 7.5 aggradational succession and is overlain by a new aggradational succession that represents the deposit forming the flat top of the hills constituting the relict paleo-surface of 56-52 m a.s.l. The intervening erosional phase and the following sediment aggradation evidently match the sea-level fall of MIS 7.4 and the successive two-stepped sea-level rise of MIS 7.3 - MIS 7.1 (Marra et al., 2016b; B in Fig. 16b). This observation corroborates the new assessment of the 51-57 m paleo-surface, and its attribution to the later stages of MIS 7.3/7.1, rather than to MIS 7.5, as shown by correlation provided in cross-section of Figure 16a.

5.6 MIS 5.5 - 5.3 - 5.1 terraces

The occurrence of a suite of three lowest coastal terraces has been shown by geomorphologic reconstruction of their relict surfaces provided by Marra et al. (2016a, 2019a), who also demonstrated that three distinct successions of coastal plain sediments, corresponding to three coastlines at circa 34, 24 and 12 m a.s.l., are associated with these terraces (Figure 16a). The $^{40}Ar/^{39}Ar$ age of 129±1 ka on a pyroclastic-flow deposit intercalated within the aggradational succession forming the 36 m terrace at Cava Rinaldi (Epi-Tyrrhenian Formation, Marra et al., 2015) demonstrated correlation with the MIS 5.5 highstand of 125 ka (Figure 16b'). The two lower terraces at 26 and 16 m were therefore tentatively correlated with the sea-level highstands of MIS 5.3 and 5.1, respectively. However, an intervening tectonic collapse of ca. 10 around 100 ka, interrupting a steady uplift phase between 250 ka and the Holocene had to be invoked by Marra et al. (2016a), in order to reconcile elevation of the terrace at 26 m with absolute sea-level established for MIS 5.3 and 5.1 in the literature (e.g. Rohling t al., 2009). A discussion of the age of these terraces is beyond the scopes of the present paper, and further geochronologic and sedimentologic investigations of these youngest successions are in progress, aimed at verifying their exact correlation with the MIS timescale. However, in the present study we have found an excellent fit of the new geomorphological and statistical assessment of these paleo-surfaces with the previous results of Marra et al. (2016a, 2019a), and we maintain preliminary correlation with the three marine isotopes' sub-stages of MIS 5.5, 5.3, and 5.1 in the discussion of the tectonic uplift.

5.7 Tectonic implications

All the sea-level markers provided by the aggradational successions of the Paleo-Tiber River correlated with MIS 21 through MIS 1 from literature and from the present study are shown in Figure 17a. Differences in elevation among the different coastal deposits assumed as sea-level markers (green shading in Figure 17a) are the result of the intervening tectonic movement (uplift or collapse) combined with the difference in maximum sea-level at each interglacial (glacio-eustatic component). This latter element is estimated assuming a sea-level 10 m lower than present during MIS 21 through MIS 15 (blue crosses in Figure 17b') based on previous literature (Marra et al., 2016 and references therein), while values estimated in Rohling et al. (2009) are considered for MIS 13 through MIS 5.1 (green crosses).

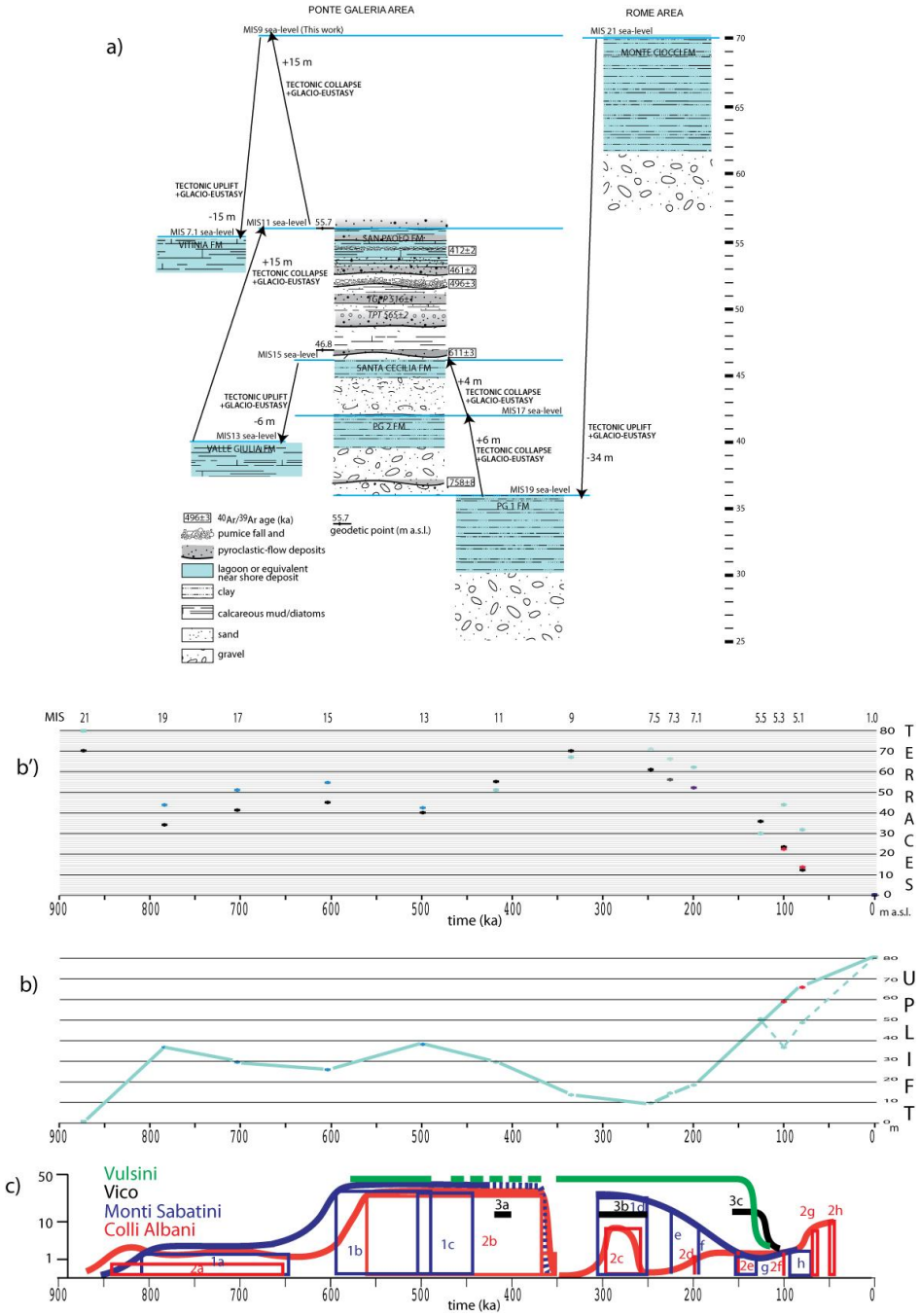

Figure 17 - a) Synoptic representation of the different sections from the Rome area indicating the aggradational successions and related sea-level indicators correlating with MIS 21 through MIS 7, integrating geochronologic and stratigraphic data from Karner and Renne, 1998; Karner and Marra, 1998; Karner et al., 2001b; Marra et al., 1998; 2016b; 2017a.

Alternative values for MIS 5.3 and 5.1 (red crosses) are also used to assess the uplift curve for the last 125 ka, based on the assumption of a more reliable uniform tectonic uplift in this time span, and on recently provided geochronologic and geomorphologic constraints on the related sea-level markers (Marra et al., 2016a, 2019a). Once the correction for the glacio-eustatic component is applied, the cumulative uplift curve of Figure 17b is obtained. Similar to previous work (Marra et al., 2016a, 2019b), comparison between the uplift curve and the eruptive histories of the volcanic districts of the Roman Province is also provided (Figure 17c). In comparison with previous reconstructions (e.g., Marra et al., 2016a) this refined uplift curve displays a marked subsidence phase between 500 and 300 ka, as provided by assessment of the MIS 9 sea-level markers at ca. 70 m a.s.l. established in the present work (Figure 17a). This fact reinforces the coupling already noted with the occurrence of two major phases of common volcanic activity at Colli Albani and Monti Sabatini 850 through 650 and 600 through 350 ka. In particular, uplift coincides with the onset of these phases, while subsidence characterizes the eruptive time spans. The subsidence phase continued until 250 ka and also encompasses the climax phase that, after a ca. 50 kyr dormancy, occurred at Vico, Monti Sabatini and Colli Albani, spanned the interval 320 - 250 ka, during which a rejuvenation of the volcanic activity occurred in all the districts of central Italy (Marra et al., 2004). The geochronologic constraints provided here for the MIS 7.5 and MIS 7.3/7.1 terraces allow a better definition of the beginning of the most recent uplift phase post-250 ka, which is characterized by an initial low gradient followed by a steady, steep increase 200 though 80 ka, and by a waning trend until the present (solid green curve in Figure 17b). As previously noted, this new uplift phase heralds and accompanies the latest volcanic phases during 90 - 70 ka at Monti Sabatini and 70-36 ka at Colli Albani, and it has been suggested to be related to the onset of a new magmatic phase extending from southern Latium to the Campanian districts of Phlegraean Fields and Vesuvius (Mara et al., 2016a). In contrast, volcanic activity seems to have been extinguished inthe districts of northern Latium (Vulsini, Vico) since 100 ka. However, Marra et al. (2019a) have shown that this recent uplift phase hs affected the whole coast of Latium homogeneously, in apparent conflict with the lack of a new magmatic phase at these volcanoes. In contrast, cessation of the activity at Vulsini and Vico matches the sudden tectonic collapse which is inferred when the current sea-level values for MIS 5.3 and 5.1 are assumed (dashed portion of the uplift curve in Figure 17c). However, a direct link between local volcanic activity in the northern sector and the global tectonic signal in this region is unlikely. Moreover, recent geochronologic and geomorphologic data strongly imply that anomalous sea-levels characterized the MIS 5.3 and MIS 5.1 highstands in the Mediterranean

region, suggesting the unforseen role played by Glacial Isostatic Adjustment (GIA) on regional tectonics during the the post-glacial period (Marra et al., 2019a).
Future investigation is needed in order to understand this complex framework of vertical movement, volcanic activity and glacio-eustasy affecting the Tyrrhenian Sea Margin during the last million years. Indeed, we note that beyond the common assumption of a interconnection between subduction, volcanism and regional uplift in the back-arc domain of the central Apennines (e.g., Conticelli and Peccerillo 1992), no dedicated study aimed at evaluating the geodynamic and isostatic forces responsible for the observed tectonic uplift has been undertaken so far.

6. Conclusions

Combined geomorphologic study and statistical analysis, together with review and re-analyses of previous published data, have allowed us to identify a set of paleo-surfaces defined by discrete classes of elevation for topographic culminations in the coastal Tyrrhenian Sea sector of central Latium.
We recognized eight such paleo-surfaces defined by the elevation ranges: 98-108, 80-89, 71-79, 61-67, 51-57, 30-43, 22-27, 11-17 m a.s.l..
The three lowest paleo-surfaces are narrowly elongated parallel to the coastline and were identified through definition of the corresponding sea-level markers and geochronologic constraints in previous studies as the marine terraces of MIS 5.5, 5.3 and 5.1, (Marra et al., 2016a, 2019a).
The highest five paleo-surfaces have been investigated here and their physical extension has been validated through DEM analyses, in order to compare the results of the geomorphological study on 1:25.000 topoghraphic maps.
The sedimentologic-stratigraphic features of the soils and of the sedimentary deposits forming these paleo-surfaces have been investigated in order to define their paleogeographic context and to identify the sea-level markers for those which have been interpreted as remnant portions of coastal terraces.
$^{40}Ar/^{39}Ar$ ages of detrital sanidine extracted from the sandy deposit of the recognized coastal terraces has allowed us to correlate the 71-79 m, the 61-67 m, and the 51-57 m paleo-surfaces with the coastal terraces formed during the MIS 9.1, MIS 7.5, and MIS 7.3/7.1 highstands, respectively.

Paleogeographic reconstrcution has allowed us to interpret the 71-79 m, 80-89 m, and 98-108 m paleo-surfaces as a sngle tectonically displaced, widespread coastal platform formed during the MIS 9.1 highstand.

Based on the combination of our refined dataset of terrace elevations with published data on relative elevation of maximum sea level during the highstands of MIS 21 through MIS 5.1, we assess the regional uplift curve in the last 900 ka and recognize the occurrence of a climactic extensional tectonic phase affecting this coastal sector between 320 and 240 ka, concident wirth occurrence of the Monte delle Fate phase of activity at the Colli albani Volcanic district.

Supplementary Material #1- 1:25.000 basemap with topographic culminations

Supplementary Material #2A: Micromorphology: Methods - Fig. S1-S6
#2B: X-Ray power diffraction methods **#2C**: SEM microphotographs - Fig. S7
Supplementary Material #2D - Diffractograms
Supplementary Material #3a, b: Full 40Ar/39Ar data.

REFERENCES

Barberi, F., Buonasorte, G., Cioni, R., Fiordelisi, A., Foresi, L., Iaccarino, S., Laurenzi, M.A., Sbrana, A., Vernia, L., Villa, I.M., 1994. Plio-Pleistocene geological evolution of the geothermal area of Tuscany and Latium. Mem. Descr. Carta Geol. d' It. 49, 77-134

Bridgland, D.R., Westaway, R., 2008. Climatically controlled river terrace staircases: a worldwide Quaternary phenomenon, Geomorphology 98, 285–315.

Cioni, R., Sbrana A., Bertagnini, A., Buonasorte G., Landi, P., Rossi, U., Salvati, L., 1987. Laurenzi, M.A., Tephrostratigraphic correlations in the Vulsini, Vico and Sabatini volcanic successions. Periodico di Mineralogia 56, 137-155.

Conticelli, S., Peccerilllo, A., 1992. Petrology and geochemistry of potassic and ultrapotassic volcanism in central Italy: petrogenesis and inferences on the evolution of the mantle sources, Lithos 28, 221-240.

De Rita, D., Funiciello, R., Rossi, U., Sposato, A., 1983. Structure and evolution of the Sacrofano-Baccano caldera, Sabatini Volcanic Complex, Rome: J. Volcanol. Geotherm. Res. 17, 219-236.

De Rita, D., Faccenna, C. Funiciello, R. Rosa, C., 1995. Stratigraphy and volcano-tectonics, in The Volcano of the Alban Hills, edited by R. Trigila, Università degli Studi di Roma "La Sapienza", Roma, 33–71.

Everdin, J.F., Curtis, G., 1965. The potassium-argon dating of Late Cenozoic rocks in East Africa and Italy. Current Anthrop., 6, 343-369.

Faccenna, C., Funiciello R., Bruni A., Mattei A., Sagnotti L., 1994. Evolution of a transfer-related basin: the Ardea Basin (Latium, Central Italy). Basin Research 5, 12-11.

Farr, T. G., Hensley, S., Rodriguez, E., Martin, J., Kobrick, M., 2000. The Shuttle Radar Topography Mission, Proceedings of a Conference held 26-29 October 1999, Toulouse, France. European Space Agency, 2000. ESA-SP vol. 450, ISBN: 9290926414, p.361.

Ferranti, L., Antonioli, F., Mauzc, B., Amorosi, A., Dai Pra, G., Mastronuzzi, G., Monaco, C., Orrù, P., Pappalardo, M., Radtke, U., Renda, P., Romano, P., Sansò, P., Verrubbi, V., 2006. Markers of the last interglacial sea-level high stand along the coast of Italy: Tectonic implications. Quaternay International 145/146, 30-54.

Freda, C., Gaeta, M., Palladino, D. M., Trigila, R., 1997. The Villa Senni Eruption (Alban Hills, Central Italy): the role of H_2O and CO_2 on the magma chamber evolution and on the eruptive scenario. Journal of Volcanology and Geothermal Research 78, 103-120.

Gaeta, M., Freda, C., Marra, F., Arienzo, I., Gozzi, F., Jicha, B., Di Rocco,T., 2016. Paleozoic metasomatism at the origin of Mediterranean ultrapotassic magmas: constraints inferred from time-dependent geochemistry of volcanic products from Colli Albani (Central Italy), Lithos, 244, 151-164. http://dx.doi.org/10.1016/j.lithos.2015.11.034

Gatta, M., Giaccio, B., Marra, F., Rolfo, M.F., 2017. Trace-element fingerprinting of the 69–36 ka Colli Albani eruptive units: A preliminary dataset for archaeological and tephra studies in central-southern Italy. Journal of Archaeological Science: Reports, 16, 330-340.

Giaccio, B., Marra, F., Hajdas, I., Karner D.B., Renne, P.R., Sposato A., 2009. $^{40}Ar/^{39}Ar$ and ^{14}C geochronology of the Albano maar deposits: implications for defining the age and eruptive style of the most recent explosive activity at the Alban Hills Volcanic District, Italy. Journal of Volcanology and Geothermal Research 185, 203-213.

Giaccio, B., Niespolo, E., Pereira, A., Nomade, S., Renne, P.R., Alber, P.G., Arienzo, I., Regattieri, Wagner, B., Zanchetta, G., Gaeta, M., Galli, P., Mannella, G., Peronace, E., Sottili , G., Florindo, F., Leicher, N., Marra, F., Tomlinson, E.L., 2017. First integrated tephrochronological record for the last ~190 kyr from the Fucino Quaternary lacustrine succession, central Italy. Quaternary Science Reviews 158, 211-234. http://dx.doi.org/10.1016/j.quascirev.2017.01.004

Giordano, G., De Benedetti, A.A., Diana, A., Diano, G., Gaudioso, F., Marasco, F., Miceli, M., Mollo, S., Cas, R.A.F., Funiciello, R., 2006. The Colli Albani mafic caldera (Roma, Italy): stratigraphy, structure and petrology, J. Volcanol. Geotherm. Res., 155, 49–80.

Grant, K.M., Rohling, E.J., Bronk Ramsey, C., Cheng, H., Edwards, R.L., Florindo, F., Heslop, D., Marra, F., Roberts, A.P., Tamisiea, M.E., Williams, F., 2014. Sea-level variability over five glacial cycles. Nature Communications 5, 5076. doi:10.1038/ncomms6076

Jicha, B.R., Singer, B.S., Sobol, P. 2016. Re-evaluation of the ages of 40Ar/39Ar sanidine standards and supereruptions in the western U.S. using a Noblesse multi-collector mass spectrometer. Chemical Geology 431, 54–66.

Karner, D.B., Marra, F., 1998. Correlation of fluviodeltaic aggradational sections with glacial climate history: A revision of the Pleistocene stratigraphy of Rome. Geological Society of America Bulletin 110, 748-758.

Karner, D.B., Marra, F., Florindo, F., Boschi, E., 2001a. Pulsed uplift estimated from terrace elevations in the coast of Rome: Evidence for a new phase of volcanic activity? Earth and Planetary Science Letters 188, 135-148.

Karner, D.B., Marra, F., Renne, P.R., 2001b. The history of the Monti Sabatini and Alban Hills volcanoes: groundwork for assessing volcanic-tectonic hazards for Rome. J. Volc. and Geoth. Res. 107: 185-215.

Lisiecki, L.E., Raymo, M.E., 2005. A Pliocene-Pleistocene stack of 57 globally distributed benthic $\delta^{18}O$ records. Paleoceanography 20, PA1003. doi:10.1029/2004PA001071.

Luberti, G.M., Marra, F., Florindo, F., 2017. A review of the stratigraphy of Rome (Italy) according to geochronologically and paleomagnetically constrained aggradational successions, glacio-eustatic forcing and volcano-tectonic processes. Quaternary International. http://dx.doi.org/10.1016/j.quaint.2017.01.044

Malinverno, A., Ryan, W.B.F., 1986. Extension in the Tyrrhenian sea and shortening in the Apennines as results of arc migration driven by sinking of the lithosphere. Tectonics 5, 227-245.

Mariucci, M.T., S. Pierdominici, F. Marra, P. Montone, L. Pizzino, 2008. Looking into a volcanic area: an overview on the 350m scientific drilling at Colli Albani (Rome, Italy). J. Volcanol. Geotherm. Res., doi:10.1016/j.jvolgeores.2008.04.007.

Marra, F., Florindo, F., Boschi E., 2008. The history of glacial terminations from the Tiber River (Rome): insights to glacial forcing mechanisms, Paleoceanography, 23, PA2205, doi:10.1029/2007PA001543.

Marra F., Karner, D.B., Freda, C., Gaeta, M., Renne, P.R., 2009. Large mafic eruptions at the Alban Hills Volcanic District (Central Italy): chronostratigraphy, petrography and eruptive behavior. Journ. of Volc. and Geoth. Res. 179, 217-232. doi:10.1016/j.jvolgeores.2008.11.009

Marra, F., Sottili, G., Gaeta, M., Giaccio, B., Jicha, B., Masotta, M., Palladino, D.M., Deocampo, D, 2014. Major explosive activity in the Sabatini Volcanic District (central Italy) over the 800-390 ka interval: geochronological - geochemical overview and tephrostratigraphic implications, Quaternary Science Reviews 94, 74-101.

Marra, F., Ceruleo, P., Jicha, B., Pandolfi, L. Petronio, Salari, L. , 2015. A new age within MIS 7 for the *Homo neanderthalensis* of Saccopastore in the glacio-eustatically forced sedimentary successions of the Aniene River Valley, Rome. Quaternary Science Reviews 129, 260–274. doi:10.1016/j.quascirev.2015.10.027

Marra, F., Florindo, F., Anzidei, M., Sepe, V., 2016a. Paleo-surfaces of glacio-eustatically forced aggradational successions in the coastal area of Rome: assessing interplay between tectonics and sea-level during the last ten interglacials. Quaternary Science Review, 148, 85-100. http://dx.doi.org/10.1016/j.quascirev.2016.07.003

Marra, F., Rohling, E.J., Florindo, F., Jicha, B., Nomade, S., Pereira, A., Renne., P.R., 2016b. Independent $^{40}Ar/^{39}Ar$ and 14C age constraints on the last five glacial terminations from the aggradational successions of the Tiber River, Rome (Italy). Earth Planet Sci Lett. in press.

Marra, F., Gaeta, M., Giaccio, B., Jicha, B., Palladino, D., Polcari, M., Sottili, G., Taddeucci, J., Florindo, F., Stramondo, S., 2016c. Assessing the volcanic hazard for Rome: $^{40}Ar/^{39}Ar$ and In-SAR constraints on the most recent eruptive activity and present-day uplift at Colli Albani Volcanic District, Geophys. Res. Lett. 43, 6898–6906. doi:10.1002/2016GL069518.

Marra, F., Florindo, F., Petronio, C., 2017. Quaternary fluvial terraces of the Tiber Valley: geochronologic and geometric constraints on the back-arc magmatism-related uplift in central Italy. Journal Scientific Reports 7: *2517*. DOI:10.1038/s41598-017-02437-1

Marra, F., Petronio, C., Salari, L., Florindo, F., Giaccio, B., Sottili, G., 2018a. A review of the Villafranchian fossiliferous sites of Latium in the framework of the geodynamic setting and paleogeographic evolution of the Tyrrhenian Sea margin of central Italy, Quaternary Science Reviews 191, 299-317. 10. 1016/ j. quascirev. 2018. 05. 011

Marra, F., Petronio, C., Ceruleo, P., Di Stefano, G., Florindo, F., Gatta, M., La Rosa, M., Rolfo, M.F., Salari, L., 2018b. The archaeological ensemble from Campoverde (Agro Pontino, central Italy): new constraints on the Last Interglacial sea level markers. Scientific Reports, SREP-18-23649, DOI : 10.1038/s41598-018-36111-x

Marra F., Nomade S., Pereira A., Petronio C., Salari L., Sottili G., Bahain J.J., Boschian G., Di Stefano G., Falgueres C., Florindo F., Gaeta M. Giaccio B., Masotta M., 2018c. A review of the geologic sections and the faunal assemblages of Aurelian Mammal Age of Latium (Italy) in the light of a new chronostratigraphic framework. Quaternary Science Reviews 181, 173-199. doi.org/10.1016/j.quascirev.2017.12.007

Marra, F., Bahain, J.-J., Jicha, B., Nomade, S., Palladino, D.M., Pereira, A., Tolomei, C., Voinchet, P., Anzidei, M., Aureli, D., Ceruleo, P., Falguères, C., Florindo, F., Gatta, M., Ghaleb, B., La Rosa, M., Peretto, C., Petronio, C., Rocca, R., Rolfo, M.F., Salari, L., Smedile, A., Tombret, O., 2019a. Reconstruction of the MIS 5.5, 5.3 and 5.1 coastal terraces in Latium (central Italy): a re-evaluation of the sea-level history in the Mediterranean Sea during the Last Interglacial, Quaternary International.

Marra, F., Florindo, F., Jicha, B.R., Nomade, S., Palladino, D.M., Pereira, A., Sottili, G., Tolomei, C., 2019b. Assessing volcano-tectonic hazard of the Monti Sabatini Volcanic District on the city of Rome (central Italy): evidence from new geochronologic constraints on the Tiber River MIS 5 terraces, Scientific Reports, in press.

Masotta, M., Gaeta, M., Gozzi, F., Marra, F., Palladino, D.M., Sottili, G., 2010. H_2O- and temperature-zoning in magma chambers: the example of the Tufo Giallo della Via Tiberina eruptions (Sabatini Volcanic District, central Italy). Lithos 118, 119-130.

Nicoletti, M., 1969. Datazioni argon-potassio di alcune vulcaniti dellew regioni vulcaniche Cimina e Vicana. Per. Mineral., 38, 1-20.

Nisi, M.F., Antonioli, F., Dai Pra, G., Leoni, G., Silenzi S., 2003. Coastal Deformation between the Versilia and the Garigliano plains (Italy) derived from the elevations of the Last Interglacial stage, Journal of Quaternary Science 18, 709-721.

Palladino, D, Simei, S., Sottili, G., and Trigila, R., 2010, Integrated approach for the reconstruction of stratigraphy and geology of Quaternary volcanic terrains: An application to the Vulsini Volcanoes (central Italy), in Stratigraphy and Geology of Volcanic Areas (eds. G. Groppelli, and L. Viereck-Goette), *The Geological Society of America Special Paper*, **464**, 63-84. doi: 10.1130/2010.2464(04).

Patacca, E., Sartori, R., Scandone, P., 1990. Tyrrhenian basin and apenninic arcs: kinematic relations since late Tortonian times. Mem. Soc. Geol. It. 45, 425-451.

Peccerillo, A., Frezzotti, M.L., 2015. Magmatism, mantle evolution and geodynamics at the converging plate margins of Italy. Journal of the Geological Society. http://dx.doi.org/10.1144/jgs2014-085

Pereira, A., Nomade, S., Falguères, C., Bahain, J-J., Tombret, O., Garcia, T., Voinchet, P., Bulgarelli, A.G., Anzidei, P., 2017. 40Ar/39Ar and ESR/U- series data for the La Polledrara di Cecanibbio archaeological site (Lazio, Italy). Journal of Archaeological Science: Reports, in press.

Perini, G., Francalanci, L., Davidson, J.P., and Conticelli, S., 2004, Evolution and genesis of magmas from Vico volcano, Central Italy: multiple differentiation pathways and variable parental magmas, *Journal of Petrology*, **45**, 139–182.

Rivera, T.A., Storey, M., Schmitz, M.D., Crowley, J.L., 2013. Age intercalibration of $^{40}Ar/^{39}Ar$ sanidine and chemically distinct U/Pb zircon populations from the Alder Creek Rhyolite Quaternary geochronology standard. Chemical Geology 345, 87-98.

Rohling E.J., Grant, K., Bolshaw, M., Roberts, A.P., Siddall, M. Hemleben, Ch., Kucera, M., 2009. Antarctic temperature and global sea level closely coupled over the past five glacial cycles. Nature Geoscience 2, 500-504. DOI: 10.1038/NGEO557

Serri, G., Innocenti, F., Manetti, P, 1993. Geochemical and Petrological evidence of the subduction of delaminated Adriatic continental lithosphere in the genesis of the Neogene-Quaternary magmatism of Central Italy, Tectonophysics 223, 117-147.

Sevink, J., Di Vito, M.A., Piochi, M., Mormone, A., Van Gorp, V., Bakels, C., 2018. A rare Mid-Würmian lithoid tuff in the Agro Pontino graben (Southern Lazio, Italy) and its identification as an Albano 5-7 related distal tephra deposit (41-36 kaBP): characteristics, provenance and palaeogeographical implications. Annals of Geophysics, 61, 1, S109. DOI: 10.4401/ag-7534

Sottili, G., Palladino, D.M., Marra, F., Jicha, B., Karner, D.B., Renne, P., 2010. Geochronology of the most recent activity in the Sabatini Volcanic District, Roman Province, central Italy, Journ. of Volc. and Geoth. Res. 196, 20-30. DOI:10.1016/j.jvolgeores.2010.07.003

Sottili G., Palladino D.M., Zanon V., 2004. Plinian activity during the early eruptive history of the Sabatini Volcanic District, Central Italy. J. Volcanol. Geotherm. Res. 135, 361-379.

Villa, P, Pollarolo, L., Conforti, I., Marra, F., Biagioni, C., Degano, I., Lucejko, J.J., Tozzi, C., Pennacchioni, M., Zanchetta, G., Nicosia, C., Panzeri, L., Martini, M., Sibilia, E., From Neandertals to modern humans: New data on the Uluzzian. Plos One 13(5): e0196786. https://doi.org/10.1371/journal.pone.0196786

Supplementary material for online publication only

Click here to download Supplementary material for online publication only: Suppl. Mat. #1 - topographic maps.jpg

Supplementary material for online publication only

Click here to download Supplementary material for online publication only: Suppl. Mat. #2 - methods.pdf

Supplementary material for online publication only

Click here to download Supplementary material for online publication only: Suppl. Mat. #2D - diffractograms.pdf

Supplementary material for online publication only

Click here to download Supplementary material for online publication only: Suppl. Mat. #3a - Ar-Ar dataset.xls

Supplementary material for online publication only

Click here to download Supplementary material for online publication only: Suppl. Mat. #3b - Ar-Ar dataset.xlsx